THE
PHYSICAL REVIEW
A journal of experimental and theoretical physics established by E. L. Nichols in 1893

VOL. 61, NOS. 3 AND 4 FEBRUARY 1 AND 15, 1942 SECOND SERIES

Transition Curves for Electron and Photon Produced Showers

NORRIS NERESON*
University of Denver, Denver, Colorado
(Received December 4, 1941)

An investigation has been made of the air-to-lead transition curves for electron and photon initiated showers. The results show that the maximum of the curve for photon-produced showers is displaced to the right with respect to the maximum for electron produced showers by a thickness of about 3 mm of lead. This is in agreement with the prediction of shower theory. It was also confirmed that the maximum for large showers lies at a greater thickness than that for small showers. The occurrence of a "second maximum" in the air-to-lead transition curve was checked and a negative result obtained.

INTRODUCTION

SINCE the discovery of cosmic-ray showers, the transition curve produced by these showers has been the subject of a large number of theoretical and experimental investigations. The best explanation of this curve at the present time is the cascade or multiplicative theory of showers as developed by several authors.[1] Although this theory has been confirmed in many respects, there are yet points where the consequences of the theory have not been conclusively tested and where various observers have obtained contradictory results. More experimental work appears to be desirable at these places.

The purpose of the present experiment was to investigate (a) the position of the maxima for showers initiated by photons and electrons, (b) the position of the maxima for showers of different sizes and (c) the existence of the so-called second maximum. The latter item is particularly important in connection with the cascade theory since its existence would indicate the existence of shower processes different from those predicted by this theory.

EXPERIMENTAL ARRANGEMENT

The experimental arrangement for investigating the first two points is shown in Fig. 1. The G-M counters employed were of the argon-air filled type having an average efficiency of about 97 percent. Counters designated by the same number are connected in parallel. The lead scatterer (S) was placed below counter group 5 so that all particles which produced showers in the scatterer would pass through this counter group. Lead walls 10 cm thick were placed at both sides of the arrangement to reduce the background count due to air showers. The effect of the lead shielding in eliminating the counts due to air showers was reduced to some extent by the production of knock-on showers by mesotrons in the lead itself.

Since it was desired to record various coinci-

* Now at Cornell University, Ithaca, New York.

[1] J. F. Carlson and J. R. Oppenheimer, Phys. Rev. **51**, 220 (1937); H. J. Bhabha and W. Heitler, Proc. Roy. Soc. **A159**, 432 (1937); L. Landau and G. Rumer, Proc. Roy. Soc. **A166**, 213 (1938); H. Snyder, Phys. Rev. **53**, 960 (1938); R. Serber, Phys. Rev. **54**, 317 (1938).

dence combinations simultaneously, a selective, multiple coincidence circuit[2] was developed for this purpose. Each of the counters (or counter groups) 1, 2, 3, 4, and 5 were coupled to the grid of a corresponding vacuum tube. The plates of the tubes coupled to 1, 2, and 3 were tied together in the usual manner and received their potential through a 50,000-ohm resistance R, while the plates of the tubes coupled to 4 and 5 were connected to R through extra resistances of

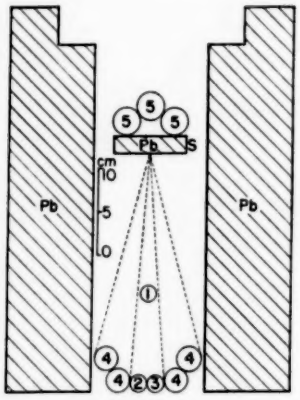

FIG. 1. Experimental arrangement for investigating the Rossi transition curve at thin thicknesses.

175,000 and 100,000 ohms, respectively. Pulses of various sizes were produced at the low potential side of R by different combinations of coincidences. The largest pulse produced was that due to a discharge of all the counters 12345 which will be designated as N_{12345}. The next largest pulse was produced by a discharge of only counters 1235 which will be represented by N_{1235-4}, and successively smaller pulses were produced by discharges of only counters 1234 and only 123 designated as N_{1234-5} and N_{123-45}, respectively. These different sized pulses were separated by feeding them onto the grids of four tubes differing in grid bias by the appropriate amounts and finally recorded by feeding the output of these tubes into four multi-vibrator recording circuits. Pulses due to coincidence combinations other than those mentioned above are very small and could easily be rejected.

It is evident from Fig. 1 that a coincidence N_{123-45} or N_{1235-4} requires a minimum of two particles, while a coincidence N_{1234-5} or N_{12345} requires a minimum of three particles. In general, the average size of shower discharging only counters 123 will be smaller than that discharging 1234 and therefore, N_{123-45} or N_{1235-4} may be called small showers and N_{1234-5} or N_{12345} large showers. The above shower types recorded with similar arrangements have been also referred to as "small angle" and "large angle" showers. This nomenclature is rather misleading, since except at small thicknesses the average angular distribution is the same for all showers from a given material. Since the density of shower particles is greatest at the center of a shower and decreases toward the edges, it is clear that as the number of shower particles is increased the particle density at the edges is also increased. Therefore, the probability that a counter placed at the edge of a shower will be discharged depends upon the number of particles in the shower rather than upon any "angle."

Counter group 5 was used to distinguish between electron and photon initiated showers. Apart from a small inefficiency of the counters, an electron would almost always discharge this group while a photon would not unless the Compton effect or pair production occurred in the walls of the counter. The probability of either of these events is small, but if either of the above processes occur in the upper walls of the counter the event would be recorded as an electron produced shower. Another disturbing effect would be the simultaneous arrival of electrons and photons, but this is a rare event.

With the above methods of distinguishing showers, the following types of showers were recorded: large (N_{12345}) and small (N_{1235-4}) electron initiated showers and large (N_{1234-5}) and small (N_{123-45}) photon initiated showers. Observations were made every twenty-four hours at

TABLE I. Results of the determination of transition curves for various shower types.

Thickness of Lead	Counts per Hour			
	N_{12345}	N_{1235-4}	N_{1234-5}	N_{123-45}
0.000 cm	0.0	0.0	0.0	0.0
0.318	0.30 ±0.02	0.28 ±0.03	0.26 ±0.02	0.55 ±0.03
0.635	0.55 ±0.02	0.50 ±0.03	0.56 ±0.02	1.00 ±0.03
0.953	0.78 ±0.03	0.46 ±0.04	0.91 ±0.03	1.38 ±0.04
1.270	0.94 ±0.04	0.40 ±0.04	1.29 ±0.03	1.34 ±0.04
1.588	0.99 ±0.04	0.31 ±0.03	1.59 ±0.04	1.12 ±0.04
1.905	0.94 ±0.03	0.28 ±0.03	1.71 ±0.04	0.68 ±0.03
2.222	0.87 ±0.03	0.22 ±0.02	1.61 ±0.03	0.43 ±0.02
2.540	0.79 ±0.03	0.15 ±0.02	1.51 ±0.02	0.34 ±0.02

[2] L. Janossy and B. Rossi, Proc. Roy. Soc. **A175**, 88 (1940).

thickness intervals of 0.318 cm up to a maximum thickness of 2.54 cm of lead.

The experimental arrangement for investigating the second maximum was identical to that employed by Bothe and Schmeiser[3] in their investigation of the second maximum. This particular arrangement was used since the above investigators have observed the most pronounced second maximum. Triple coincidences were observed as the thickness of the lead was varied at 4 cm intervals from 12 to 24 cm. Only the latter part of the transition curve was investigated since this range is sufficient to ascertain if any second maximum exists.

RESULTS

The data obtained in the first experiment are shown in Table I in which each reading represents an average of about 1000 coincidences observed over a period of about five months. The counting rate obtained with no lead for each shower type has been subtracted from the observed counting rate. This rate was different for each shower type but the average was about 2 counts per hour. The standard errors are given.

The transition curves produced by the total electron ($N_{12345}+N_{1235-4}$) and total photon ($N_{1234-5}+N_{123-45}$) showers are shown in Fig. 2. These curves bring out the significant fact that the maximum for photon initiated showers is shifted further to the right by 0.25 to 0.3 cm as compared to the electron initiated shower curve. This shift may be determined more accurately if each of these two curves is subdivided into transition curves for small and large showers such as has been done in Figs. 3 and 4, respectively. In these curves the errors are less and the maxima are better defined. The photon and electron maxima occur at 1.1 and 0.75 cm in Fig. 3 and at 1.9 and 1.6 cm in Fig. 4, showing a difference between the two maxima of 0.35 and 0.3 cm, respectively. A comparison of these curves also shows that the maximum for large showers occurs further to the right than that for small showers.

The data from the second experiment are given in Table II. It is evident that no second maximum is indicated but merely a straight line with perhaps a slight negative slope.

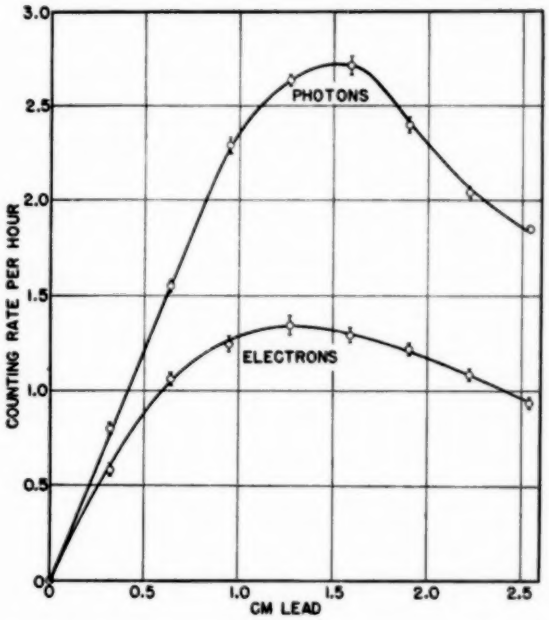

FIG. 2. Transition curves for total electron and total photon initiated showers.

DISCUSSION

The probability of recording a shower increases when the average number of particles is increased and it is safe to assume that the maximum coincidence rate is recorded when the average number of particles is a maximum. Now, the thickness of scatterer at which an electron of energy E_0 and a photon of energy W_0 produce a maximum number of particles has been calculated[4] from the multiplicative theory to be

$$T(E_0)=1.01[\log (E_0/\epsilon)-1]$$

for an electron, and

$$T(W_0)=1.01[\log (W_0/\epsilon)-\tfrac{1}{2}]$$

for a photon where ϵ is the critical energy. If ionization losses are neglected it can be shown[4] that the energy spectrum of photons and electrons is the same. Therefore, it follows from the above formulae that the maximum number of particles in a shower initiated by a photon should occur at a thickness of one-half a radiation length

[3] K. Schmeiser and W. Bothe, Ann. d. Physik **32**, 161 (1938).

[4] B. Rossi and K. Greisen, Rev. Mod. Phys. **13**, 240 (1941).

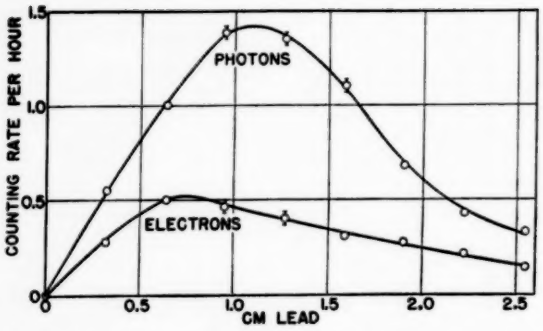

FIG. 3. Transition curves of small showers produced by electrons and photons.

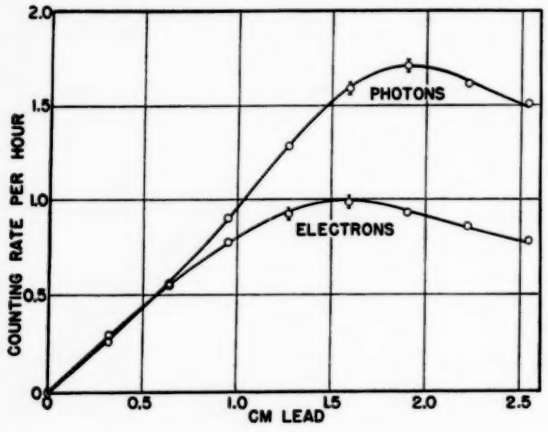

FIG. 4. Transition curves of large showers produced by electrons and photons.

greater than that for a shower initiated by an electron. This amounts to 0.3 cm in the case of lead. The experimental values as presented in the previous section are in good agreement with this figure.

Previous work on the transition curves produced by electrons and photons has been done by a few investigators without reaching any definite conclusion as to the positions of the maxima. Woodward's[5] results indicate a slight shift, but his experimental arrangement does not separate the two shower types sufficiently to verify the shift. The curves obtained by Starr[6] and by Regener[7] contain too few points in the region of the maxima to show any shift.

A number of investigators[8] have confirmed the theoretical expectation that the maximum for large showers should occur at greater thicknesses than that for small showers. The present investigation confirms these results by showing the maxima for small and large showers to be at 1.0 and 1.8 cm, respectively. Arley[9] has calculated the maximum for showers produced in lead by two or more particles to be at 1.3 cm and that for three or more particles at 1.6 cm. However, since the geometrical arrangement plays such a large part here, it is difficult to compare these values with the experimental ones.

The occurrence of a second maximum has continued to be a subject for investigation since it was first reported by Ackemann[10] and Hummel[11] in 1934. The continued interest in this subject is due to the facts that its occurrence is very important in regard to shower theory and that some investigators[12] have confirmed its existence while others[13] have not. Bothe and Schmeiser found the second maximum to be almost as high as the first in their experiments on narrow showers, but the present experiment with an identical arrangement fails to confirm this result.

TABLE II. Results of the investigation of the occurrence of a second maximum.

Thickness of Lead	Total Number of Counts Observed	Triple Coincidences per Hour
12 cm	4000	7.0±0.1
16	5000	6.9±0.1
20	5000	6.9±0.1
24	2500	6.9±0.1

[5] R. H. Woodward, Phys. Rev. **49**, 711 (1935).
[6] M. A. Starr, Phys. Rev. **53**, 6 (1938).
[7] V. H. Regener, Ric. Scient. **18**, 66 (1940).
[8] R. B. Brode and M. A. Starr, Phys. Rev. **51**, 1006 (1937); D. K. Froman and J. C. Stearns, Phys. Rev. **52**, 382 (1937); R. T. Young, Jr., Phys. Rev. **52**, 559 (1937); M. A. Starr, Phys. Rev. **53**, 6 (1938).
[9] N. Arley, Proc. Roy. Soc. **A168**, 519 (1938).
[10] M. Ackemann, Naturwiss. **22**, 169 (1934).
[11] J. N. Hummel, Naturwiss. **22**, 170 (1934).
[12] A. Drigo, Ric. Scient. **5**, 88 (1934); H. Kulenkampff, Physik. Zeits. **36**, 785 (1935); H. Maass, Ann. d. Physik **27**, 507 (1936); J. A. Priebsch, Akad. Wiss. Wien. Ber. **145**, 101 (1936); J. Clay, A. van Gemmert, and J. T. Wiersma, Physica **3**, 627 (1936); R. H. Woodward, Phys. Rev. **49**, 711 (1936); J. Clay and K. H. J. Jonker, Rev. Mod. Phys. **11**, 287 (1939); W. F. G. Swann and W. F. Ramsey, Phys. Rev. **58**, 477 (1940); P. J. G. De Vos, Nature **145** 387 (1940).
[13] A. Schwegler, Zeits. f. Physik **101**, 93 (1936); K. Z. Morgan and W. M. Nielsen, Phys. Rev. **52**, 564 (1937); P. Auger, R. Maze, P. Ehrenfest, and A. Freon, J. de phys. et rad. **10**, 1 (1939); B. Rossi and L. Janossy, Rev. Mod. Phys. **11**, 281 (1939); P. Auger and T. Grivet, Rev. Mod. Phys. **11**, 232 (1939); G. O. Altmann, H. N. Walker, and V. F. Hess, Phys. Rev. **58**, 1011 (1940); L. Janossy, M. McCaig, and E. P. George, in print; W. M. Nielsen, J. E. Morgan, and K. Z. Morgan, Phys. Rev. **55**, 995 (1939).

This is in agreement with the findings of Altmann, Walker, and Hess[13] who have carried out an experiment similar to the one described here.

A final point may be brought out from the fact that the counting rate is practically the same at 12 as at 24 cm of lead. In consideration of the error in these readings, one can conclude that the maximum decrease in this counting rate could be only 3 to 4 percent, while the total decrease in the number of mesotrons brought about by 12 cm of lead is about 8 percent.[14] This difference may be explained by considering that only mesotrons of high energy are capable of producing knock-on showers. By considering the experimentally determined mesotron energy spectrum, Lovell[15] has calculated that the probability of observing knock-on showers is highest when the energy of the mesotron lies between 3 and 6×10^9 ev. If 5×10^9 ev is taken as the most probable mesotron energy for observing a knock-on shower with the present experimental arrangement, it can be shown that the energy spectrum above 5×10^9 ev is decreased by only 3 percent by 12 cm of lead. The slight decrease of this energy spectrum compared with the slight decrease in the counting rate indicates that only mesotrons above energies of the order of 5×10^9 ev produce knock-on showers.

In conclusion, the author wishes to thank especially Professor J. C. Stearns for his suggestion and direction of the experiment and also Professor D. K. Froman for helpful comments. To Professor Bruno Rossi and Mr. Kenneth Greisen of Cornell University the author is deeply grateful for valuable discussions on the interpretation of the results.

[14] B. Rossi and D. Hall, Phys. Rev. **59**, 223 (1941).
[15] A. C. B. Lovell, Proc. Roy. Soc. **A172**, 568 (1939).

FEBRUARY 1 AND 15, 1942 PHYSICAL REVIEW VOLUME 61

Frequency of Proton and Alpha-Tracks in Cosmic-Ray "Stars"

MAURICE M. SHAPIRO
Ryerson Physical Laboratory, University of Chicago, Chicago, Illinois
(Received December 4, 1941)

To obtain data concerning the multiple nuclear disintegrations produced by the cosmic radiation, special photographic plates were left on Mt. Evans for nearly eight months. From a statistical investigation of 365 tracks in 142 cosmic-ray "stars" found in one of these emulsions, it is estimated that more than 90 percent of the tracks were produced by protons. Most of the remaining star tracks are probably due to alpha-particles of energy less than 9 Mev.

INTRODUCTION

EVIDENCE of multiple nuclear disintegrations associated with the cosmic radiation has been provided by cloud chambers,[1] by photographic emulsions,[2] and indirectly by proportional counters.[3]

Of 20,500 counter-tripped cloud-chamber photographs of cosmic rays obtained by Brode and Starr[1a] at sea level, ten showed nuclear disintegrations produced by the cosmic radiation with the emission of heavy[4] particles. Even at an altitude of 4300 m[1b] only a few such disintegrations were observed in thousands of photographs. Because of the rare occurrence of these events, the continuously sensitive photographic emulsion has proved a useful tool in their investigation.

In the photographic emulsion a multiple nuclear disintegration produces a "fork," or group of microscopic tracks emanating from a common center. Each track consists of a row of discrete silver grains spaced several microns apart, the spacing being greater for protons than for alpha-

[1] (a) R. B. Brode and M. A. Starr, Phys. Rev. **53**, 3 (1938); (b) C. D. Anderson and S. H. Neddermeyer, Phys. Rev. **50**, 263 (1936); (c) J. Crussard and L. Leprince Ringuet, J. de phys. et rad. [7] **8**, 216 (1937).
[2] References 6–10 are to photographic emulsion studies of cosmic rays. Résumé and bibliography, M. M. Shapiro, Rev. Mod. Phys. **13**, 58 (1941).
[3] S. A. Korff, Phys. Rev. **59**, 949 (1941).
[4] The word "heavy" will be used here to describe particles at least as massive as protons.

particles of the same energy. Forks can also be produced by radioactive contamination of the plate, resulting in the step-wise disintegration of a single nucleus and its descendents, or in the emission of particles from several contiguous nuclei.[5] It is convenient to designate as "stars" those forks arising from multiple nuclear disintegrations associated with the cosmic radiation.

From studies of these stars by Blau and Wambacher,[6] Schopper and Schopper,[7] Wambacher,[8] Filippov, Jdanov, and Gurevich,[9] and Stetter and Wambacher,[10] there emerges the following picture of nuclear "evaporations." A nucleus of light or medium weight excited by the cosmic rays to multiple disintegration usually emits between two and five heavy charged particles, and infrequently as many as six to fourteen. (While neutrons are probably released in similar numbers, they do not produce visible tracks; nor do any electrons which may be emitted possess a sufficiently high specific ionization to leave tracks in the emulsion.) A large sample of star tracks shows random distribution in direction.

The energy and frequency of stars increase rapidly, and the multiplicity (average number of tracks per star) slightly, with altitude. Star frequency has an altitude dependence similar to those of large cosmic-ray showers, bursts, and neutrons. The energy of a typical star registered at a depth of 6 to 8 m water equivalent below the top of the atmosphere is of the order of 70 Mev. As for the mechanism whereby a star is produced, the available data are not inconsistent with the Bohr model of a nuclear excitation, according to which several particles may be evaporated in succession from an activated compound nucleus.[10a]

Blau and Wambacher,[6] and Stetter and Wambacher,[10] indicated that most star tracks can probably be ascribed to protons by comparison with recoil-proton tracks produced in collisions with neutrons. For the purpose of calculation they assumed that all the tracks were made by protons, recognizing, however, the possibility that some of them might in fact be due to alpha-particles. On the other hand, Schopper and Schopper,[7] and Filippov, Jdanov, and Gurevich,[9] attributed certain of their star tracks to alpha-particles, basing this identification on measurements of grain spacing and track length.

The average grain spacing of alpha-ray and proton tracks serves as a means of distinguishing between them, provided that the alpha-particles in question have energies which do not exceed those in the natural radioactive region. This was demonstrated by Wilkins and St. Helens,[11] who registered alpha-particles from ThC and ThC′, and protons and deuterons from cyclotrons, on separate plates. They measured about 260 tracks of each type, and plotted the number of grains against the length of each track. Their distributions of alpha- and proton tracks are shown in Figs. 3 and 5 of reference 11. These show a fairly clear separation.

We have here applied the grain-spacing technique in an effort to compare statistically the occurrence of alpha-particles and protons in cosmic-ray stars.

MEASUREMENTS

To obtain sufficient star data, several kinds of plates were sent into the stratosphere in a number of unmanned balloon flights,[12] and others were exposed for many months at various mountain altitudes. Because of their relatively short duration, the stratosphere flights did not yield a sufficient concentration of data on any single plate to render its inspection worth while for our purpose. An Agfa "K-plate," which had been left vertically oriented for 239 days at an altitude of 4300 m,[13] was selected for this investigation. The emulsion, 43 microns thick, was developed for 5 minutes in a fine-grain

[5] For photomicrographs of such "forks," see references 7–9; or Shapiro, reference 2, p. 60.

[6] M. Blau and H. Wambacher, Akad. Wiss. Wien [IIa] **146**, 469 and 623 (1937).

[7] E. Schopper and E. M. Schopper, Physik. Zeits. **40**, 22 (1939).

[8] H. Wambacher, Physik. Zeits. **39**, 883 (1938).

[9] A. Filippov, A. Jdanov, and I. Gurevich, J. Phys. U.S.S.R. **1**, 51 (1939).

[10] G. Stetter and H. Wambacher, Physik. Zeits. **40**, 702 (1939).

[10a] N. Bohr and F. Kalckar, K. Danske Vid. Sels., Math.-fys. Med. **14**, No. 10 (1937).

[11] T. R. Wilkins and H. J. St. Helens, Phys. Rev. **54**, 783 (1938).

[12] These flights were conducted by Dr. W. P. Jesse, whose generous cooperation is acknowledged.

[13] Professor J. C. Stearns, of the University of Denver, very kindly arranged for storage of plates in the cosmic-ray station at Mt. Evans.

Plate No. 55a Date 8/10/40 Page 13

Type of plate Ilford D, Tilt Evans, 3 months, vertical.

Position	Sketch		Measurements					
			l_d	l_μ	d	L	n-1	s
No. 61		A	9.5	21.6	26	33.8	10	3.38
x 37.5		B	12.5	28.4	10	30.1	7	4.30
y 120.0		C	10.0	22.7	13	26.2	9	2.91
		D	9.0	20.4	16	25.9	6	4.31
		E						
No. 62		A	20.2	45.9	19	49.6	14	3.54
x 37.7		B	5	11.35	13	17.3	8	2.16
y 118.8		C						
		D						
		E						
No. 63	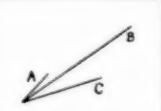	A	5.0	11.35	—	11.35	5	2.27
x 42.4		B	18.0	40.9	9	41.9	9	4.65
y 122.15		C	11.0	25.0	—	25.0	7	3.57
		D						
		E						
No. 64	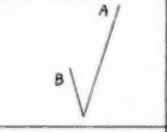	A	25.2	57.2	9	58.0	14	4.14
x 43.2		B	10.3	23.4	9	25.1	10	2.51
y 124.6		C						
		D						
		E						
No. 65	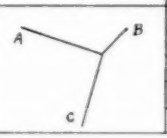	A	14.2	32.2	—	32.2	9	3.58
x 55.5		B	6.0	13.6	23	26.7	7	3.81
y 116.9		C	11.0	25.0	12	27.7	10	2.77
		D						
		E						

FIG. 1. A page of representative data. l_d is the projection of the track-length on the surface of the emulsion, measured in divisions of the eyepiece scale. l_μ denotes the same quantity in microns. (1 division = 2.27μ.) d, L, and s denote, respectively, the depth, length, and mean grain spacing of the track in microns. n is the number of grains in the track.

developing solution; and examined under a binocular microscope[14] equipped with mechanical stage, eyepiece scale, objective with variable iris diaphragm, and dark-field condenser.

Many single tracks, as well as groups of tracks radiating from a common center were observed. In order to exclude from the data forks due to radioactive contamination, only those were studied which contained at least one track attributable to either an alpha of energy >9 Mev or to a proton. In practice this was accomplished by considering as cosmic-ray stars only those forks which have at least one track with a mean grain spacing ≥ 2.4 microns. (The choice of this minimum value is explained in footnote 18.) If only one track in a fork conformed to this description, it was further required that this track include at least five silver grains, so that the determination of grain spacing governing the identification of the fork as a star be based upon at least four spacings. A track with equivalent air range greater than 10 cm would have qualified its fork as a star even if it possessed alpha-spacing. No track with such length and spacing occurred, however. It should be noted that the application of these criteria restricts the generality of the conclusions to be drawn from this study; for it is quite possible that some of the forks containing *only* alpha-tracks of energies within the radioactive range are also of cosmic-ray origin.

Of 200 stars satisfying these requirements, 58 were rejected from this study because one or more of their tracks could not be measured accurately. In such cases either a part of the track was obscured by background silver grains, or else the track sloped too steeply into the emulsion to permit an accurate count of the number of grains in it. For the remaining stars, the following criterion was used to prevent the inclusion of fortuitous collineations of silver grains as tracks. A row of grains emanating from a star center was counted as a track only if it comprised at least four grains.

For each track of the 142 stars constituting the data, the following measurements were made at a magnification of 750 diameters. The projection l of the length upon the surface of the emulsion was measured with an eyepiece scale. The depth d was determined from scale readings on the fine-adjustment head of the microscope when the two ends of a track were successively brought into sharp focus. The refractive index (1.5) of the emulsion was taken into account. During such focusing the iris diaphragm of the objective was opened wide for minimum depth of field.

From l and d the actual length L of the track was deduced; and by counting the number n of silver grains in it, the average spacing $s=L/(n-1)$ between grains was determined. Many of the L values corresponded to incomplete ranges, the tracks in such instances running out of the emulsion. Along with these measurements, the coordinates (x, y) of each star, given by the mechanical stage of the microscope, were

[14] For the loan of this microscope, the writer is indebted to Professor W. H. Taliaferro, Dean of the Division of Biological Sciences, University of Chicago.

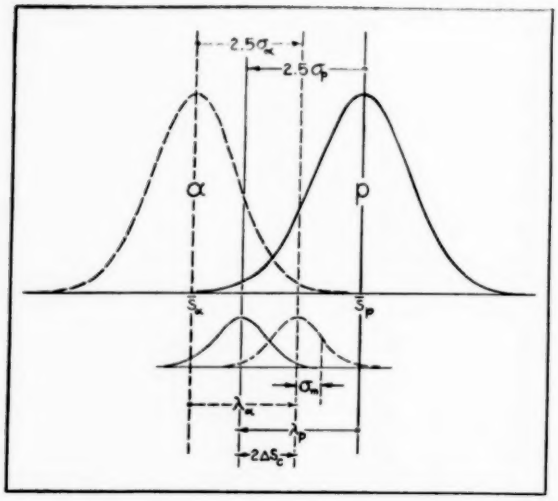

FIG. 2. Diagram illustrating choice of Δs_c. Track frequency is plotted against average grain-spacing. In the comparison data the alpha-group extends to an upper limit $\bar{s}_\alpha+2.5\sigma_\alpha$, and the proton group to a lower limit $\bar{s}_p-2.5\sigma_p$. Because of our error in measurement, σ_m, the upper limit is increased to $\bar{s}_\alpha+\lambda_\alpha$, and the lower one decreased to $\bar{s}_p-\lambda_p$, where $\lambda_\alpha=[(2.5\sigma_\alpha)^2+\sigma_m^2]^{\frac{1}{2}}$ and $\lambda_p=[(2.5\sigma_p)^2+\sigma_m^2]^{\frac{1}{2}}$. The extent of overlapping of λ_α and λ_p determines the interval of uncertainty $2\Delta s_c$.

recorded together with a sketch of the star to insure that it would not be counted twice. Figure 1 shows a representative page of data.

RESULTS

The 142 stars studied, comprising between two and five tracks each, contained a total of 365 tracks, with s values ranging from 1.36 to 5.52 microns. An estimate of the relative numbers of proton and alpha-tracks occurring in the stars can be obtained by deducing a critical value s_c of s such that tracks with $s>s_c$ may be attributed to protons, and those with $s<s_c$ to alpha-particles. In a tabular summary, Wilkins and St. Helens[11] give an average spacing 1.74μ for the group of alphas with greatest s values, and an average 2.68μ for the group of protons with shortest spacing. It would appear easy, then—if we are dealing with alphas which are not more energetic than those from ThC′—to separate alphas from protons. It must be remembered, however, that these s values are *averages* for many tracks. Actually, the mean spacings for proton and alpha-tracks overlap because of inhomogeneities in the distribution of AgBr grains in the emulsion and fluctuations due to errors in measurement.[15]

This overlapping gives a band of s values lying within an interval $s_c\pm\Delta s_c$ such that tracks with s values in this interval cannot be identified on the basis of spacing alone. The half-width Δs_c of this interval determines the error in the estimate of the proportion of alpha-particles and protons. To evaluate Δs_c for the population of cosmic-ray tracks, it is necessary to consider (a) the "spread" of s values in the most energetic alpha-group and that in the least energetic proton group of the comparison data (of Wilkins and St. Helens[16]), and (b) the additional spread arising from experimental error in our measurements of the cosmic-ray tracks. (See Fig. 2.)

(a) Let D_α be the total spread (difference between the largest and smallest s values) for the most energetic alpha-group, and D_p the spread for the least energetic proton group. Denote the standard deviations of these groups by σ_α and σ_p; and the mean s values by $\bar{s}_\alpha$ and $\bar{s}_p$, respectively. To a sufficiently close approximation, the standard deviations are $\sigma_\alpha=D_\alpha/6$ and $\sigma_p=D_p/6$. From the data in Figs. 3 and 5 of reference 11,

$$\bar{s}_\alpha=1.70\mu \qquad \bar{s}_p=2.40\mu$$
$$\sigma_\alpha=0.17\mu \qquad \sigma_p=0.20\mu.$$

Now, for the alpha-group, $\bar{s}_\alpha+2.5\sigma_\alpha$ may be taken[17] as an upper limit for the range of s values; similarly, $\bar{s}_p-2.5\sigma_p$ is a reasonable lower limit for the proton group in the comparison data.

(b) If we take into account the standard error $\sigma_m=0.1\mu$,[18] in our measurement of s for the

[15] The overlapping is much more serious if the population of tracks in question includes alphas with energies exceeding 9 Mev. This case will be discussed separately below.

[16] These authors do not give explicitly the standard deviations in the spacings within these groups of tracks. This information was obtained from the frequency distributions shown in their graphs (cf. Figs. 3 and 5 of their paper).

[17] For a normal frequency distribution with standard deviation σ, approximately 99 percent of the total area is included between the ordinates at $\pm2.5\sigma$.

[18] Taken as one-third the estimated maximum error in measurement of s. σ_m is combined with $2.5\sigma_\alpha$ as follows: $\lambda_\alpha\equiv[(2.5\sigma_\alpha)^2+\sigma_m^2]^{\frac{1}{2}}=0.45\mu$ (see Fig. 2).

We may now explain the choice of $s=2.4\mu$ for at least one track in a fork as a minimum value for the latter's admission to the star data: $\bar{s}_\alpha+2.5\sigma_\alpha+2.5\sigma_m=2.4\mu$. Thus the probability that a track with $s\geq2.4\mu$ was produced by an alpha of radioactive origin is vanishingly small. The application of this cautious criterion virtually eliminates error due to radioactive contamination.

cosmic-ray tracks, we arrive at the following limits:

Upper limit for the α-group: $\bar{s}_\alpha+0.45\mu=2.15\mu$
Lower limit for the p group: $\bar{s}_p-0.50\mu=1.90\mu$

i.e., the "interval of uncertainty" within which tracks cannot be identified with confidence is given by $1.9<s<2.15\mu$. We may put $s_c=2.02\mu$ and $\Delta s_c=0.12\mu$.

The star tracks may now be classified as in Table I.

One-half of the number of tracks in this borderline group lies within the half-interval Δs_c. Thus in our sample population of star tracks, the percentage of protons in stars containing at least one proton is 93.7 ± 3.2 percent. The standard error 3.2 percent in the relative frequency is increased only to 3.4 percent if we take into account the error due to sampling, which is estimated as 1.3 percent.[19]

In Table II the stars are divided into two groups—those having at least one alpha-track, and those containing only protons—and these in turn are classified according to track multiplicity.

DISCUSSION

Our statistical separation of protons from alphas based on the criterion of grain spacing is valid for a population of tracks in which the alpha-energies do not exceed 9 Mev. It was shown by Schopper and Schopper[7] that to alpha-energies greater than this there correspond s values higher than those in the less energetic group of alphas from natural radioactive substances. These higher values are in fact as large as those of less energetic protons. Thus to each s value of an energetic[20] alpha there corresponds a proton with the same grain spacing. If, then, an unknown population of tracks contain an appreciable number of energetic alphas, it becomes necessary to know the complete range r of a particle, as well as its grain spacing. From these data and Schopper's curves plotting grain spacing against length for protons and alphas, one can identify the track.

Many of the tracks in our experiment, however, are incomplete, either because the emulsion was not sufficiently thick to record their entire length, or because they originated too close to one of its surfaces. It might seem arbitrary to classify such tracks as protons. It can be shown, however, that in the plate investigated the number of energetic alpha-tracks, if any, was negligible. In the first place, no clear evidence for such alphas was found on the plate. Very few tracks with air-equivalent lengths greater than 10 cm were observed, and of these, those which lay completely in the emulsion could be identified as protons by reference to Schopper's curves. There was not a single complete track with $l>7$ cm air equivalent which fitted on Schopper's alpha-curve. It remains to be shown, however, that only a negligible number of the incomplete tracks with $s>2.15\mu$ can be due to alphas.

Consider the probability $P(l)$ that a track with range r which originates in an emulsion of thickness k has a length l in the emulsion between l_1 and l_2. From geometrical considerations it can be shown that when $r>k$, and l ranges over the intervals indicated below, then for a population of tracks with isotropic[20a] distribution, $P(l)$ has the following values:

$$k\leq l_1\leq l\leq r \qquad P(l_1\leq l\leq r)=k/2l_1$$

$$l<r \qquad P(l_1\leq l\leq l_2)=1-\frac{k}{2l_2}-\frac{l_1}{2k}.$$

TABLE I.

	Number of tracks	Percentage
$s>2.02\mu$	342	93.7
$s\leq2.02\mu$	23	6.3
Total	365	100.0
$1.90<s<2.15$	23	6.3

TABLE II. Numbers of "alpha-stars" (those containing at least one alpha) and "proton stars" (those with protons only).

Multiplicity	p stars	α-stars	Totals
2-fold	63	10	73
3-fold	50	9	59
4-fold	7	1	8
5-fold	1	1	2
Totals	121	21	142

TABLE III. Expected number of long tracks for several values of f.

f	1	0.5	0.1	0.05
$0.455fN$	86	43	9	4

[19] This is combined with the error 3.2 percent by computing the square root of the sum of their squares.

[20] We shall use "energetic" to describe alphas with energy exceeding 9 Mev.

[20a] The directional distribution of star tracks is very nearly isotropic, according to Stetter and Wambacher, reference 10.

Suppose that in the stars investigated all tracks whose spacing satisfies the relation $2.15<s<4.0\mu$ were alphas. From Schopper's alpha-curve it is found that for all such tracks $r\geq 140\mu$. Compare the probability P_a that such a track have an emulsion length $\geq 140\mu$ with the probability P_b that such a track have a length between 20μ and 50μ. For the emulsion used here ($k=43\mu$),

$$\frac{P_a(140\leq l\leq r)\mu}{P_b(20\leq l\leq 50)\mu}=0.455.$$

Thus, if in a given plate area we find a group G of N tracks with l satisfying $20\leq l\leq 50\mu$ and s in the interval $2.15<s<4.0\mu$, then we should expect to find $0.455N$ tracks in the same spacing interval with $l\geq 140\mu$, provided that all the N tracks are alphas. If only a fraction f of the tracks are alphas, we should expect $0.455fN$ tracks with $2.15<s<4.0\mu$ and $l\geq 140\mu$. The experimental data give $N=190$ tracks between 20 and 50μ. Table III shows the expected number of long tracks for several values of f. Actually, *no* tracks were observed satisfying $2.15<s<4.0\mu$ and $l\geq 140\mu$. It is thus improbable that an appreciable number of the tracks in group G are due to alphas.

If we assume, on the other hand, that group G consists of protons, then from Schopper's proton curve we find that the maximum range for such tracks is 140μ, and we should expect to find *no* tracks within the s interval of G longer than 140μ. This agrees with the observations. A similar investigation for the tracks with $s>4.0\mu$ leads to the same conclusion: there is very little evidence for the presence of energetic alphas in the plate studied.

We should expect—and this has been confirmed[11] in the case of deuterons—that the grain spacings of H^2, H^3, or He^3 particles will have values lying between those of alphas and protons. It seems possible, therefore, that a few of our star tracks were produced by particles of mass intermediate between those of proton and alpha-particle. However, the emission of an H^2, H^3, or He^3 is improbable compared with the competitive processes of proton or alpha-emission, since the binding energies of the former—especially in nuclei of medium weight—are large compared with those of the latter. We cannot exclude the possibility that protons of double charge[21] are responsible for some of the tracks with alpha-spacing. Taylor, Fraser, and Dabholkar[22] have concluded that the detection of doubly charged protons with the photographic method is not possible.

Finally, we might inquire whether any of the dense tracks identified as alphas are really due to heavier nuclei. This is possible; but even the smallest average grain spacings in our group of alphas lie within the maximum spread of s values in the comparison group of alphas. Hence it is not necessary to ascribe any of our star tracks to recoil nuclei.

An investigation of the nature of the star-producing radiation is now in progress, and will be reported in another paper.

ACKNOWLEDGMENTS

The author is grateful to Dr. M. Schein, Dr. H. W. Norton, Mr. G. W. Brier, and other members of the staff at Ryerson Laboratory for helpful suggestions. He is particularly indebted to Professors Arthur H. Compton and George S. Monk for their inspiring counsel and generous interest.

[21] H. J. Bhabha, Phys. Rev. **59**, 100 (1941).
[22] H. J. Taylor, D. Fraser, and V. D. Dabholkar, Nature **146**, 777 (1940).

Origin of the Soft Component of Cosmic Rays

BRUNO ROSSI AND KENNETH GREISEN
Cornell University, Ithaca, New York

(Received December 1, 1941)

The number of electrons arising from the decay of mesotrons has been calculated with the multiplication theory. A comparison with experimental data indicates the existence of an electron component having a sharper maximum in the vertical direction and increasing with altitude more rapidly than the decay electrons.

1. INTRODUCTION

THE question as to the origin of the soft component of cosmic rays in the atmosphere has been the subject of much discussion in the last years.[1-7] Until recently the general belief was that the soft component is produced partly by incoming primary electrons, partly by electrons arising from the decay of mesotrons and from collision processes of mesotrons in air. Lately Schein, Jesse, and Wollan[6] have suggested that practically all of the soft component may be a secondary product of mesotrons, the bulk of it being produced by the decay.

In the present paper the above hypothesis is developed quantitatively and the results are compared with experimental data. The main theoretical problem is to calculate the intensity of the soft component arising from the disintegration of mesotrons and the subsequent multiplication of the decay electrons in air. It has been shown by one of us[2] that this calculation can be carried out in a very elementary way, without making use of the multiplication theory of showers, if one assumes that the rate of production of the decay electrons does not change appreciably over a distance in which the showers generated by these electrons are completely absorbed. Bernardini and his collaborators[4] have found that the intensity of the soft component calculated by this method increases with height more slowly than the observed intensity. However, the assumption on which the above method of calculation is based represents only a very rough approximation. It is therefore desirable to treat the problem more accurately, and the use of the multiplication theory then becomes essential.

2. THEORETICAL PROBLEM

We want to determine the number of electrons at a certain point in the atmosphere arising from the decay of mesotrons in the upper layers. We shall consider mesotrons and electrons coming in a given direction and neglect scattering.

Let us denote by t the depth below the top of the atmosphere in radiation lengths, measured in the direction of the incoming particles, and by $f(t_1, p)dp$ the number of mesotrons with momentum between p and $p+dp$ present at the depth t_1. In general, only those mesotrons are recorded which go through a certain thickness x_0 of absorber and have, therefore, momenta larger than a certain value p_0. Hence the observed number of mesotrons at t_1 is given by

$$N(t_1)=\int_{p_0}^{\infty} f(t_1, p)dp. \qquad (1)$$

For an absorber of 15 cm of lead, for instance, $p_0=3\times10^8$ ev/c. Let us further indicate by N_1 the number of mesotrons with momentum smaller than p_0. N_1 is not measured directly, but can be evaluated approximately and is always small compared with N.

The number of mesotrons in the momentum interval (p, dp) which disintegrate in the air layer between t_1 and t_1+dt_1 is given by

$$\frac{\mu}{\tau_0}X_0\frac{f(t_1, p)dp}{p}\frac{dt_1}{\rho(t_1)},$$

where μ is the rest mass, τ_0 the proper lifetime of

[1] W. Heisenberg and H. Euler, Ergeb. d. exact. naturwiss. **17**, 1 (1938).
[2] B. Rossi, Phys. Rev. **57**, 469 (1940).
[3] E. Nelson, Phys. Rev. **58**, 771 (1940).
[4] G. Bernardini, B. N. Cacciapuoti, B. Ferretti, O. Piccioni, and G. C. Wick, Phys. Rev. **58**, 1017 (1940).
[5] L. W. Nordheim, Phys. Rev. **59**, 554 (1941).
[6] M. Schein, W. P. Jesse, and E. O. Wollan, Phys. Rev. **59**, 614 (1941).
[7] G. Cocconi, Phys. Rev. **60**, 532 (1941).

mesotrons, X_0 the radiation length in g/cm² of air, $\rho(t_1)$ the density of air at the depth t_1.[8] We shall assume that each mesotron disintegrates into an electron and a neutrino and that, in the frame of reference of the mesotron, the electron is emitted with equal probability in any direction. It follows that, in the frame of reference of the earth, the probability of an electron of energy (E, dE) being produced by the decay of a mesotron of momentum p is given by dE/p.[9]

The electrons produced in the layer (t_1, dt_1) multiply into a shower which can conveniently be described by a function $k(t_1, t)$ where $k(t_1, t)dt_1dt$ represents the energy dissipated by the shower electrons in the layer dt at a distance t from t_1. If we then indicate by $K(t_2)dt_2$ the energy dissipated by all shower electrons in the layer between t_2 and t_2+dt_2, $K(t_2)$ is given by

$$K(t_2)=\int_0^\infty k(t_2-t, t)dt. \tag{2}$$

The upper limit of the integral can be taken as infinity if the depth at which the measurements are made is larger than the maximum penetration of showers.

3. METHOD OF CALCULATION FOR HIGH ENERGY MESOTRONS

We shall consider, for the moment, only the electrons arising from the decay of mesotrons with momentum larger than p_0, and we shall assume that p_0^2 is large compared with μ^2. We indicate by $z(t_1)dt_1$ the total amount of energy given to electrons by the mesotrons disintegrating in the layer (t_1, dt_1). In consequence of the formulae above, $z(t_1)$ is given by the following integral:

$$z(t_1)=\frac{\mu}{\tau_0}\frac{X_0}{\rho(t_1)}\int_{p_0}^\infty \frac{f(t_1, p)dp}{p^2}\int_{E_{\min}}^{E_{\max}} EdE, \tag{3}$$

where $E_{\min}$ and $E_{\max}$ are given by Eqs. (26) (see Appendix). If we neglect μ^2 with respect to p^2, the limits become practically 0 and p, and Eq. (3) yields

$$z(t_1)=\frac{1}{2}\frac{\mu}{\tau_0}X_0\frac{N(t_1)}{\rho(t_1)}. \tag{3a}$$

[8] See, for instance, B. Rossi, Rev. Mod. Phys. **11**, 296 (1939). For the system of units used in the present article, see B. Rossi, Phys. Rev. **57**, 660 (1940).

[9] See B. Ferretti, Nuovo Cimento **15**, 421 (1938).

$z(t_1)$ represents also the area under the "shower curve"; i.e., the curve giving $k(t_1, t)$ as a function of t:

$$z(t_1)=\int_0^\infty k(t_1, t)dt, \tag{4}$$

because the whole energy of the decay electrons is eventually dissipated by the particles of the shower to which they give rise.

Most of the electrons present at any particular depth t_2 arise from the decay of mesotrons not very far above t_2, say between $t_2-\Delta t$ and t_2. If one neglects the change in the shape of the energy spectrum of mesotrons over the distance Δt, one can put in Eq. (2)

$$\begin{aligned} k(t_2-t, t)&=\frac{z(t_2-t)}{z(t_2)}k(t_2, t)\\ &=\frac{N(t_2-t)}{\rho(t_2-t)}\frac{\rho(t_2)}{N(t_2)}k(t_2, t). \end{aligned} \tag{5}$$

In fact, Eq. (5) gives a good approximation even if the energy spectrum of mesotrons, and consequently that of the decay electrons, undergoes an appreciable change. This is so because the *shape* of the shower curve depends only slightly on the energy of the particles which produce the shower. On the other hand, the *area* under the shower curve is correctly given by (5), according to Eqs. (3a) and (4).

The quantity $N(t_2-t)/\rho(t_2-t)$ can be developed in a Taylor series:

$$\frac{N(t_2-t)}{\rho(t_2-t)}=\left(\frac{N}{\rho}\right)_{t_2}-t\left[\frac{\partial(N/\rho)}{\partial t}\right]_{t_2}+\frac{1}{2}t^2\left[\frac{\partial^2(N/\rho)}{\partial t^2}\right]_{t_2}+\cdots \tag{6}$$

Substitution of (5) in (2) then gives

$$\begin{aligned} K(t_2)=&\int_0^\infty k(t_2, t)dt\\ &-\frac{\rho(t_2)}{N(t_2)}\left[\frac{\partial(N/\rho)}{\partial t}\right]_{t_2}\int_0^\infty tk(t_2, t)dt\\ &+\frac{1}{2}\frac{\rho(t_2)}{N(t_2)}\left[\frac{\partial^2(N/\rho)}{\partial t^2}\right]_{t_2}\int_0^\infty t^2k(t_2, t)dt+\cdots \end{aligned} \tag{7}$$

or, recalling (3a) and (4),

$$K(t_2)=\frac{1}{2}\frac{\mu}{\tau_0}X_0\left\{\left(\frac{N}{\rho}\right)_{t_2}-\bar{t}\left[\frac{\partial(N/\rho)}{\partial t}\right]_{t_2}+\frac{1}{2}\langle t^2\rangle_{Av}\left[\frac{\partial^2(N/\rho)}{\partial t^2}\right]_{t_2}+\cdots\right\}, \quad (7a)$$

where $\bar{t}$, $\langle t^2\rangle_{Av}$, $\cdots$, are the average values of t, t^2, etc.; i.e.,

$$\bar{t}=\frac{\int_0^\infty tk(t_2,t)dt}{\int_0^\infty k(t_2,t)dt},$$

$$\langle t^2\rangle_{Av}=\frac{\int_0^\infty t^2k(t_2,t)dt}{\int_0^\infty k(t_2,t)dt}.$$

(7a) can be written also as follows:

$$K(t_2)=\frac{1}{2}\frac{\mu}{\tau_0}X_0\left\{\left(\frac{N}{\rho}\right)_{t_2-\bar{t}}+\tfrac{1}{2}[\langle t^2\rangle_{Av}-(\bar{t})^2]\left[\frac{\partial^2(N/\rho)}{\partial t^2}\right]_{t_2}+\cdots\right\}. \quad (8)$$

Thus the problem is reduced to the determination of the quantities $\bar{t}$, $\langle t^2\rangle_{Av}$, $\langle t^3\rangle_{Av}$, etc.

4. EVALUATION OF $\bar{t}$ AND $[\langle t^2\rangle_{Av}-(\bar{t})^2]$

We indicate by $k_E(t)$ the function describing the shower produced by a single incident electron of energy E. An expression for $k_E(t)$ has been given by Serber in the form of a complex integral, and can be written as follows:

$$k_E(t)=\frac{\epsilon}{2\pi i}\int_{\delta-i\infty}^{\delta+i\infty}\frac{ds}{s}\frac{\sigma_0+\lambda_1(s)}{\lambda_1(s)-\lambda_2(s)}\times K_1(s,-s)\left(\frac{E}{\epsilon}\right)^s\exp[\lambda_1(s)t]-\frac{\epsilon}{2\pi i}\int_{\delta-i\infty}^{\delta+i\infty}\frac{ds}{s}\frac{\sigma_0+\lambda_2(s)}{\lambda_1(s)-\lambda_2(s)}\times K_2(s,-s)\left(\frac{E}{\epsilon}\right)^s\exp[\lambda_2(s)t]. \quad (9)$$

The function $k_E(t)$ is equal to ϵ times the function $\Pi(E_0, 0, t)$ defined by Eq. (2.103) in the article "Cosmic-ray theory" by Rossi and Greisen.[10] ϵ is the critical energy, σ_0 is the absorption coefficient of high energy photons, s is a complex variable and $\lambda_1(s)$, $\lambda_2(s)$, $K_1(s,-s)$ and $K_2(s,-s)$ are the functions of s defined in (CRT) by Eqs. (2.19) and (2.76).

We consider the Laplace integral of $k_E(t)$ with respect to t; i.e., the function

$$L_E(\lambda)=\int_0^\infty k_E(t)e^{-\lambda t}dt. \quad (10)$$

For $E\gg\epsilon$, $L_E(\lambda)$ can be evaluated by the method of residues, and the result is [see CRT, Eqs. (2.106)]

$$L_E(\lambda)=-\frac{\epsilon}{s}\frac{K_1(s,-s)}{\lambda_1'(s)}\frac{\sigma_0+\lambda_1(s)}{\lambda_1(s)-\lambda_2(s)}\left(\frac{E}{\epsilon}\right)^s, \quad (11)$$

where s is defined as a function of λ by the equation

$$\lambda_1(s)=\lambda. \quad (12)$$

It follows immediately from the definition of the Laplace integral that

$$\int_0^\infty k_E(t)dt=L_E(0), \quad (13a)$$

$$\int_0^\infty tk_E(t)dt=-(\partial L_E/\partial\lambda)_{\lambda=0}, \quad (13b)$$

$$\int_0^\infty t^2k_E(t)dt=(\partial^2L_E/\partial\lambda^2)_{\lambda=0}, \quad (13c)$$

etc.

The function L_E and its derivatives can be calculated with Eq. (11). The result is [see CRT, Eqs. (2.106)]

$$\int_0^\infty k_E(t)dt=E, \quad (14a)$$

$$\int_0^\infty tk_E(t)dt=E(b\log E/\epsilon+a), \quad (14b)$$

$$\int_0^\infty t^2k_E(t)dt=E(b^2\log^2E/\epsilon+d\log E/\epsilon+c), \quad (14c)$$

[10] B. Rossi and K. Greisen, Rev. Mod. Phys. **13**, 233 (1941). In what follows we shall refer to this article as (CRT).

where $b=-1/\lambda_1'(1)=1.01$, $a=0.40$, $d=2ab-\lambda_1''(1)/[\lambda_1'(1)]^3=2.42$, and $c=-0.1$. The primes denote differentiation with respect to s.

The approximations made in the deduction of the above formulae are only valid when E is large compared with ϵ; moreover the mathematical procedure becomes meaningless for $E<\epsilon$. Nevertheless, Eq. (14a) happens to be rigorously correct for every value of E because it expresses the obvious fact that the energy dissipated by all shower particles equals the energy of the electron which has produced the shower.

Let $k_p(t_1, t)dpdt_1$ be the function representing the shower produced by the decay of mesotrons with momentum (p, dp) in the layer (t_1, dt_1). According to Section 2, k_p is given by

$$k_p(t_1, t)=\frac{\mu}{\tau_0}\frac{X_0}{\rho(t_1)}\frac{f(t_1, p)}{p^2}\int_{E_{\min}}^{E_{\max}} k_E(t)dE, \quad (15)$$

Consequently,

$$\int_0^\infty k_p(t_1, t)dt=\frac{\mu}{\tau_0}\frac{X_0}{\rho(t_1)}\frac{f(t_1, p)}{p^2}\times\int_{E_{\min}}^{E_{\max}}dE\int_0^\infty k_E(t)dt, \quad (16a)$$

$$\int_0^\infty tk_p(t_1, t)dt=\frac{\mu}{\tau_0}\frac{X_0}{\rho(t_1)}\frac{f(t_1, p)}{p^2}\times\int_{E_{\min}}^{E_{\max}}dE\int_0^\infty tk_E(t)dt, \quad (16b)$$

$$\int_0^\infty t^2k_p(t_1, t)dt=\frac{\mu}{\tau_0}\frac{X_0}{\rho(t_1)}\frac{f(t_1, p)}{p^2}\times\int_{E_{\min}}^{E_{\max}}dE\int_0^\infty t^2k_E(t)dt. \quad (16c)$$

The expression (16a) can be evaluated from (14a) and yields, if one neglects terms of the order of $(\mu/p)^2$,

$$\int_0^\infty k_p(t_1, t)dt=\frac{1}{2}\frac{\mu}{\tau_0}\frac{X_0}{\rho(t_1)}f(t_1, p). \quad (17a)$$

In the expression (16b) one can use (14b) for $E>\epsilon$. On the other hand, since $\epsilon\ll p$ the integral with respect to E from $E_{\min}$ to ϵ is certainly negligible with respect to the integral from ϵ to $E_{\max}$, both because comparatively few electrons are emitted with energy smaller than ϵ and because these electrons have a very small range. Hence one can extend the integral from ϵ to $E_{\max}$ rather than from $E_{\min}$ to $E_{\max}$. The same conclusion applies to (16c). Neglecting terms of the order of $(\epsilon/p)^2$, one obtains

$$\int_0^\infty tk_p(t_1, t)dt=\frac{1}{2}\frac{\mu}{\tau_0}\frac{X_0}{\rho(t_1)}f(t_1, p)\times\left(B\log\frac{p}{\epsilon}+A\right), \quad (17b)$$

$$\int_0^\infty t^2k_p(t_1, t)dt=\frac{1}{2}\frac{\mu}{\tau_0}\frac{X_0}{\rho(t_1)}f(t_1, p)\times\left(B^2\log^2\frac{p}{\epsilon}+D\log\frac{p}{\epsilon}+C\right), \quad (17c)$$

where, if a, b, c and d are as given above, $A=a-\frac{1}{2}b=-0.10$, $B=b=1.01$, $C=c-\frac{1}{2}d+\frac{1}{2}b^2=-0.8$, and $D=2AB-\lambda_1''(1)/[\lambda_1'(1)]^3=1.40$.

The function $k(t_1, t)$ describing the shower produced by the decay of mesotrons of all momenta larger than p_0 in the layer (t_1, dt_1) is given by

$$k(t_1, t)=\int_{p_0}^\infty k_p(t_1, t)dp. \quad (18)$$

It follows that

$$\int_0^\infty k(t_1, t)dt=\frac{1}{2}\frac{\mu}{\tau_0}\frac{X_0}{\rho(t_1)}\int_{p_0}^\infty f(t_1, p)dp=\frac{1}{2}\frac{\mu}{\tau_0}\frac{X_0}{\rho(t_1)}N(t_1), \quad (19a)$$

$$\int_0^\infty tk(t_1, t)dt=\frac{1}{2}\frac{\mu}{\tau_0}\frac{X_0}{\rho(t_1)}\times\left[B\int_{p_0}^\infty f(t_1, p)\log\frac{p}{\epsilon}dp+AN(t_1)\right], \quad (19b)$$

$$\int_0^\infty t^2k(t_1, t)dt=\frac{1}{2}\frac{\mu}{\tau_0}\frac{X_0}{\rho(t_1)}\times\left[B^2\int_{p_0}^\infty f(t_1, p)\log^2\frac{p}{\epsilon}dp+D\int_{p_0}^\infty f(t_1, p)\log\frac{p}{\epsilon}dp+CN(t_1)\right]. \quad (19c)$$

Equation (19a) is identical with Eq. (3a). Equations (19b) and (19c) give, from the definitions of $\bar{t}$ and $\langle t^2\rangle_{Av}$, and by inserting the values of the constants, the following results:

$$\bar{t}=1.01(\log p/\epsilon)_{Av}-0.10, \tag{20}$$

$$\langle t^2\rangle_{Av}-(\bar{t})^2=1.02\left[\left(\log^2\frac{p}{\epsilon}\right)_{Av}-\left(\log\frac{p}{\epsilon}\right)^2_{Av}\right]+1.61\left(\log\frac{p}{\epsilon}\right)_{Av}-0.8, \tag{21}$$

where

$$(\log p/\epsilon)_{Av}=\frac{\int_{p_0}^{\infty}f(t_1,p)\log\frac{p}{\epsilon}dp}{\int_{p_0}^{\infty}f(t_1,p)dp}$$

and

$$(\log^2 p/\epsilon)_{Av}=\frac{\int_{p_0}^{\infty}f(t_1,p)\log^2\frac{p}{\epsilon}dp}{\int_{p_0}^{\infty}f(t_1,p)dp}$$

represent the average values of $\log p/\epsilon$ and $\log^2 p/\epsilon$ over the momentum spectrum of mesotrons from p_0 to infinity.

5. LOW ENERGY MESOTRONS

We have considered so far only mesotrons with momentum larger than p_0. The average energy of the electrons arising from the decay of mesotrons with momentum less than p_0 is small and we may assume that it is completely dissipated in a short distance from the place of production. Therefore the function $K_1(t_2)dt_2$ representing the energy dissipated in the layer (t_2, dt_2) by the shower arising from the decay of mesotrons with momentum smaller than p_0 (but different from zero) can be regarded as equal to the energy of the decay electrons produced in the same layer. This energy has already been calculated by one of us,[2] assuming that the absorption curve for mesotrons has a constant slope for thicknesses less than x_0, the range of mesotrons of momentum p_0. Since the whole term is very small compared with the contribution of the mesotrons with momentum above p_0, the error introduced by this assumption is negligible. The result is

$$K_1(t_2)=\frac{1}{2}\frac{\mu}{\tau_0}\frac{\dot{X_0}}{\rho(t_2)}\frac{N_1(t_2)}{ax_0}\times[p_0-\mu\tan^{-1}(p_0/\mu)], \tag{22}$$

where a is the momentum loss per g/cm² of the absorber used for mesotrons of momentum p_0, and N_1 is the number of mesotrons stopped in the absorber; i.e., the number of mesotrons with momentum smaller than p_0.

The contribution of mesotrons which disintegrate after having been stopped by collision losses is small and moreover uncertain, because part of the mesotrons may be captured by the nuclei before disintegrating. Therefore this contribution will be neglected.

Should the mesotrons disintegrate each into an electron and a photon, rather than an electron and a neutrino, the intensity of the soft component would be approximately twice as large as that given by these calculations.

6. COMPARISON WITH EXPERIMENTS

We shall compare our theoretical results with some recent measurements by one of us[11] on the intensity of the hard and of the soft component as a function of altitude and of zenith angle. The measurements were performed by counting coincidences between Geiger-Müller tubes arranged in a straight line. For the measurements on the hard component the tubes were shielded by a total absorber thickness equivalent to 167 g/cm² of lead. In this condition the counting rate is a measure of the number N of mesotrons with momentum larger than about 3.0×10^8 ev/c ("fast" mesotrons). Measurements were taken at altitudes of 259, 1616, 3240 and 4300 m above sea level. The values of N in the vertical direction are plotted in Fig. 1 as solid dots against atmospheric depth in radiation lengths. The curve connecting the dots represents therefore the number of "fast" mesotrons as a function of depth. This curve has been extrapolated to small depths by means of the results of Schein, Jesse and Wollan.[12]

[11] K. Greisen, to be published shortly.
[12] M. Schein, W. P. Jesse and E. O. Wollan, Phys. Rev. 57, 847 (1940).

The difference n between the counting rates with and without the absorber is taken as a measure of the intensity of the "soft" component. The values of n in the vertical direction are plotted as open dots in Fig. 1. The soft component includes mesotrons below 3.0×10^8 ev/c and electrons of sufficient energy to penetrate the counter walls; i.e., in the present experiments, 2.3 g/cm² of brass. The number of "slow" mesotrons has been indicated by N_1. Let us denote by D, D_1 and C the numbers of electrons arising from the decay of "fast" mesotrons, from the decay of "slow" mesotrons and from collision processes of mesotrons in air, respectively. If no electrons of different origin are present,

$$n=N_1+D+D_1+C. \tag{23}$$

The various terms in Eq. (23) are evaluated as follows:

(*a*) *"Slow" mesotrons, N_1.* The values of N_1/N at 1616 m and at 3240 m have been obtained by extrapolating to zero thickness differential absorption curves measured recently with an anticoincidence method. The value of the same ratio at 259 m can easily be calculated from the absorption curve at Echo Lake or at Denver, by taking into account the decay, and the result obtained is in agreement with direct measurements. The value taken for N_1/N at 4300 m is a liberal estimate. The results are listed in Table I. No claim of accuracy is laid on the figures for N_1/N. However, it may be noted that an error in the evaluation of N_1 does not affect the final results seriously because N_1 itself is a small fraction of the total number of soft particles.

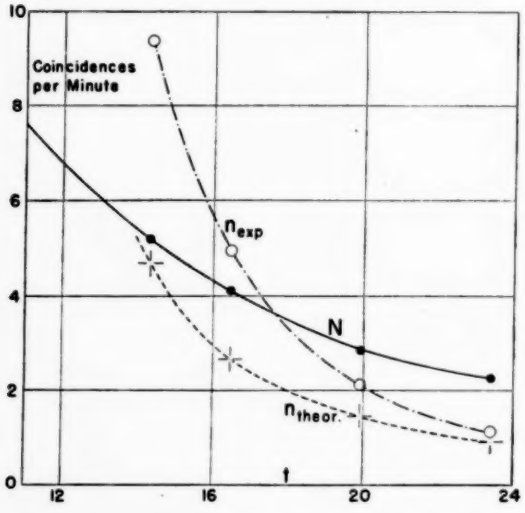

FIG. 1. The number of "fast" mesotrons N, the calculated number of "soft" particles $n_{theor.}$, and the observed number of "soft" particles n_{exp}, as functions of depth in radiation lengths.

(*b*) *Electrons arising from the decay of "fast" mesotrons, D.* This number, which is the dominant term in Eq. (23), may be regarded as proportional to the quantity K given by Eq. (8). In the evaluation of K we may take $X_0=43$ g/cm², $\epsilon=10^8$ ev, $\tau_0/\mu=9\times10^{-4}$.[13] $N(t)$ is given by Fig. 1 and $\rho(t)=t\rho_0/t_0$, where ρ_0 and t_0 are the values of ρ and t at sea level. The quantities $\bar{t}$ and $\langle t^2\rangle_{Av}-(\bar{t})^2$ can be calculated at sea level, where direct measurements of the momentum spectrum of mesotrons are available. Using Blackett's results[14] one obtains for $p>3\times10^8$ ev/c [see Eqs. (20) and (21)]: $(\log p/\epsilon)_{Av}=3.11$, and $(\log p/\epsilon)_{Av}=10.78$, hence $\bar{t}=3.04$ rad. lengths, $\langle t^2\rangle_{Av}-(\bar{t})^2=5.3$ (rad. lengths)². No direct measurements of the momentum spectrum of mesotrons at high elevation have been reported so far. Probably the values of $\bar{t}$ and $\langle t^2\rangle_{Av}-(\bar{t})^2$ decrease slightly with increasing altitude. If we neglect this decrease we slightly overestimate the increase of K with altitude, although the error is probably small. Numerical calculations show that already the second term in Eq. (8) is negligible with respect to the first one. Hence, in the vertical direction the expression for K reduces to

$$K(t)=4.44\times10^8N(t-3.04)/(t-3.04). \tag{24}$$

If the walls of the counters were infinitely thin, one would have $D=K/\epsilon$, since ϵ represents the energy loss of electrons per radiation length. Because of the finite thickness of the counter walls, electrons with energy below a certain limit are not recorded and D has a smaller value. We may write $D=\beta K/\epsilon$, with $\beta<1$. In the present case, the value of β probably lies between 0.8 and 0.9. Some values of D/N, calculated with $\beta=0.85$, are listed in Table I.[15]

[13] B. Rossi and D. B. Hall, Phys. Rev. **59**, 223 (1941). This value of τ_0/μ has been confirmed by recent experiments to be published shortly.

[14] P. M. S. Blackett, Proc. Roy. Soc. **159**, 1 (1937).

[15] It may be noted that the values of D thus calculated are considerably larger in absolute value and increase with height at a faster rate than the values calculated by previous, less accurate methods (see references 2 and 4).

TABLE I. Calculated and observed numbers of "soft" particles per "fast" mesotron at various altitudes.

Altitude (meters)	Depth (rad. lengths)	N_1/N	D/N	D_1/N	C/N	$\frac{N_1+D+D_1+C}{N}$	n/N observed
259	23.41	0.07	0.22	0.010	0.10	0.40	0.50±0.020
1616	19.93	0.09	0.31	0.014	0.10	0.51	0.74±0.053
3240	16.47	0.13	0.39	0.025	0.10	0.65	1.20±0.050
4300	14.33	0.27	0.47	0.060	0.10	0.90	1.81±0.058

(*c*) *Electrons arising from the decay of "slow" mesotrons,* D_1. We may take $D_1=\beta_1 K_1/\epsilon$, where K_1 is given by Eq. (22) and β_1 is a constant dependent on the thickness of the walls of the counters. β_1 is somewhat smaller than β because the average energy of electrons arising from the decay of "slow" mesotrons is smaller than that of electrons arising from the decay of "fast" mesotrons. Using $\beta_1=0.8$ we obtain for D_1/N the values listed in Table I.

(*d*) *Electrons produced by collision processes,* C. The number C can be regarded as proportional to the number N of fast mesotrons because low energy mesotrons cannot transfer any large fraction of their energy to electrons. The actual value of C depends again on the thickness of the counter walls. A rough estimate gives, for the present case, $C=0.1N$ (see, for instance, reference 5).

The above results yield for the total numbers of soft particles the values plotted in Fig. 1 as crosses. The ratios of these numbers to N are listed in Table I. In particular, at 4300 m the ratio between soft and hard particles is

$$(n/N)_{\text{theor}}=0.90\pm0.30,$$

where the error corresponds to a generous estimate of the maximum uncertainty of the various quantities which enter in the calculation. On the other hand, the observed value for n/N at the same altitude is

$$(n/N)_{\text{exp}}=1.81\pm0.06$$

and is therefore much larger than the calculated one. We conclude that *not all the electrons observed at 4300* m *can be accounted for by disintegration or collision processes of mesotrons.* It may be added that if the scattering of the electrons had been taken into account, the disagreement between the experimental and theoretical values of n/N would have been even more pronounced.

Inspection of Fig. 1 shows that not only the absolute values of the observed number n, but also the rate of variation of n with altitude differs strongly from what one would expect under the assumption that all electrons are secondaries of mesotrons. This conclusion is independent of any particular assumption about the values of the constants which enter into the calculations. It would also be valid if each mesotron decayed into an electron and a photon, instead of into an electron and a neutrino. In fact, the terms N_1, D_1 and C cannot account for more than a small fraction of the number n of soft particles observed at high altitude, for any reasonable assumption about the value of N_1. On the other hand, the rate of increase of the dominant term D with altitude depends only on $\bar{t}$ and on $N(t)$, since

$$\frac{D(t_1)}{D(t_2)}=\frac{N(t_1-3.04)}{N(t_2-3.04)}\times\frac{t_2-3.04}{t_1-3.04}.$$

In Table II we list the ratios of the values of N, n and D at various altitudes to the values at 259 m. It is seen that the calculated number of decay electrons increases with altitude more rapidly than the number N of fast mesotrons, but much less rapidly than the observed number n of soft particles.

The conclusion that not all electrons are secondaries of mesotrons is further strengthened by a consideration of the variation of the intensities with zenith angle. In Table III we list

TABLE II. Variation with height of the numbers of "fast" mesotrons (N), "soft" particles (n), and electrons arising from the decay of "fast" mesotrons (D).

Altitude (meters)	N/N_{259}	n/n_{259}	D/D_{259}
259	1.00	1.00	1.00
1616	1.26±0.026	1.86±0.15	1.73
3240	1.82±0.032	4.38±0.24	3.17
4300	2.29±0.037	8.27±0.41	4.83

TABLE III. Variation with zenith angle of the numbers of "fast" mesotrons (N), "soft" particles (n), and electrons arising from the decay of "fast" mesotrons (D).

Altitude (meters)	N^0/N^{46}	n^0/n^{46}	D^0/D^{46}
259	2.10±0.043	3.7±0.67	2.4
1616	2.15±0.062	2.7±0.36	2.5
3240	2.10±0.055	4.0±0.47	2.4
4300	2.05±0.048	3.2±0.22	2.5

the ratios between the observed intensities at 0° and at 46° for the hard and soft components at various altitudes, along with the theoretical ratios for electrons arising from the decay of "fast" mesotrons. Here the soft component was measured with a permanent thickness of 15 g/cm² between the Geiger-Müller tubes so as to eliminate electrons of very small energy, which undergo considerable scattering. It is seen that the ratios for D are only slightly larger than the corresponding ratios for N and are considerably smaller than those for n.

CONCLUSION

The comparison of the theoretical results with experimental data, summarized in Fig. 1 and Tables I, II and III, indicates the existence of an electron component which increases more rapidly with altitude and has a sharper maximum in the vertical direction than the electrons arising from the decay or from collision processes of mesotrons. These electrons are probably the product of cascade processes of primary electrons. At a depth of about two-thirds of an atmosphere, they form a large fraction of the total electron intensity, while near sea level they seem to be not very abundant in comparison with the electrons produced by mesotrons (see Fig. 1). It is possible that at very high altitudes the decay electrons may again be responsible for most of the total electron intensity because the maximum in the number of decay electrons should occur at a higher altitude than the maximum in the number of electrons from primary cascade showers.

APPENDIX

The following relation between the energy of the decay electron and the angle at which it is emitted can be obtained from the conservation of energy and momentum, if one neglects the rest energy of the particles arising from the decay:

$$E=\tfrac{1}{2}\mu^2/[(p^2+\mu^2)^{\frac{1}{2}}-p\cos\theta] \tag{25}$$

where p is the momentum, μ the rest mass of the mesotron, E the energy of the decay electron and θ its angle of emission with respect to the path of the mesotron. It follows from (25) that the maximum and minimum energies of the decay electron are, respectively,

$$E_{\max}=\tfrac{1}{2}[(p^2+\mu^2)^{\frac{1}{2}}+p]$$
$$E_{\min}=\tfrac{1}{2}[(p^2+\mu^2)^{\frac{1}{2}}-p], \tag{26}$$

or, if $p^2\gg\mu^2$,

$$E_{\max}=p+\mu^2/4p$$
$$E_{\min}=\mu^2/4p. \tag{26'}$$

Equation (25) shows that no appreciable error is made by neglecting the finite angle of emission of the decay electrons, in the calculation of the soft component arising from the decay. In fact, the contribution to the soft component of decay electrons with energy smaller than μ is negligible. The angle of emission of electrons of energy μ, if $p\gg\mu$, is given by

$$1-\cos\theta=\mu/2p$$

and is therefore small.

Elastic and Inelastic Scattering of Fast Neutrons*

H. H. BARSCHALL† AND RUDOLF LADENBURG
Palmer Physical Laboratory, Princeton University, Princeton, New Jersey

(Received July 14, 1941)

The scattering of the 2.5 Mev $d-d$ neutrons by C, Al, Fe, Cu, Zn, and Pb was investigated by analyzing the distribution in energy of recoiling α-particles in an ionization chamber. Measurements were carried out for scattering angles of the neutrons of 45° and 100°. The differential cross section for elastic scattering was measured, and the amount of inelastic scattering could be estimated. The elastic scattering showed a strong anisotropy whereas the inelastic scattering was roughly the same for the two scattering angles. The ratio of elastic to inelastic scattering was found to be appreciably larger in C, Al, and Pb than in Fe and Cu.

I. INTRODUCTION

THE scattering of fast neutrons by nuclei is at least partly inelastic in the case of medium and heavy masses like Fe, Ag, and Pb. This was first shown by Danysz *et al.*[1] and then confirmed by Fermi and collaborators[2] and by other authors.[3] Using a radon-beryllium neutron source one finds a change in the radioactivity induced in various detectors when different substances are interposed between the source and the detector. Detectors sensitive to slow neutrons (of a few ev energy) like Ag and Rh show an increase in activity, whereas detectors such as Si and Al sensitive to fast neutrons of some Mev energy show a decrease. A similar effect produced by light nuclei such as carbon and silicon can be explained perhaps by the energy loss in elastic collisions, which in a scatterer of mass A may produce an energy loss of $4A/(A+1)^2$ times the initial neutron energy. But the slowing down by heavy nuclei must be due to inelastic collisions, that is, excitation of the nucleus to some excited state while the neutron loses the corresponding amount of kinetic energy. The excited nucleus may lose its energy by emitting γ-rays or internally converted electrons, going down to its normal state. Such γ-rays from the "non-capture" excitation of nuclei by fast neutrons have actually been found by Lea,[4] by Kikuchi, Aoki, and Husimi[5] and by others.[6]

Using the neutrons from a Po-Be source which may have an average energy of about 5 Mev Lea found appreciably more γ-rays from Pb than from Fe, and many less from carbon. Kikuchi, Aoki, and their collaborators used the homogeneous neutrons of 2.5 Mev energy from the $d-d$ reaction and got fewer γ-rays from Al and Pb than from Fe and Cu. A similar result was obtained by Kallmann and Kuhn.[6] Grahame and Seaborg[3] concluded from their experiments with different detectors that high energy neutrons of more than 4 Mev produce relatively more γ-rays in Pb, compared for example with Fe and Cu, than do "medium" fast neutrons of about 1 Mev. Hudspeth and Bonner[7] analyzed in a Wilson cloud chamber the neutrons from the $d-d$ reaction scattered by 3 cm of Pb, by measuring the distribution in energy of the protons in the forward direction. They concluded from their results that only 10–15 percent of the initial neutrons of 2.5 Mev made inelastic collisions in the lead with energy losses of from

* A preliminary report of the experiments has been given at the Washington meeting, 1941, see Phys. Rev. **59**, 917 (1941).

† Now at the University of Kansas, Lawrence, Kansas.

[1] M. Danysz, J. Rotblat, L. Wertenstein, and M. Zyw, Nature **134**, 970 (1934).

[2] Amaldi, d'Agostino, Fermi, Pontecorvo, Rasetti, and Segrè, Proc. Roy. Soc. **A149**, 533 (1935).

[3] W. Ehrenberg, Nature **136**, 870 (1935); J. Rotblat and M. Zyw, Nature **137**, 185 (1936); P. I. Lukirsky and T. Careva, Comptes rendus Acad. des sci. de l'U.R.S.S. **3**, 411 (1936); C. H. Collie and J. H. E. Griffith, Proc. Roy. Soc. **A155**, 434 (1936); G. T. Seaborg, G. E. Gibson, and D. C. Grahame, Phys. Rev. **52**, 408 (1937); D. C. Grahame and G. T. Seaborg, Phys. Rev. **53**, 795 (1938); E. T. Booth and C. Hurst, Proc. Roy. Soc. **A161**, 248 (1937); W. D. Allen and C. Hurst, Proc. Phys. Soc. **52**, 501 (1940). See also Bethe's report, Rev. Mod. Phys. **9**, 156 (1937), containing the complete literature and its critical discussion up to that time.

[4] D. E. Lea, Proc. Roy. Soc. **A150**, 637 (1935).

[5] S. Kikuchi, K. Husimi, and H. Aoki, Proc. Phys. Math. Soc. Japan **18**, 188 (1936); **19**, 369 (1937).

[6] R. Fleischmann, Zeits. f. Physik **97**, 242 (1935); H. Kallmann and E. Kuhn, Naturwiss. **26**, 106 (1938); Grahame and Seaborg, reference 3; I. Nonaka, Phys. Rev. **59**, 681 (1941).

[7] E. Hudspeth and T. W. Bonner, Phys. Rev. **53**, 928 (1938).

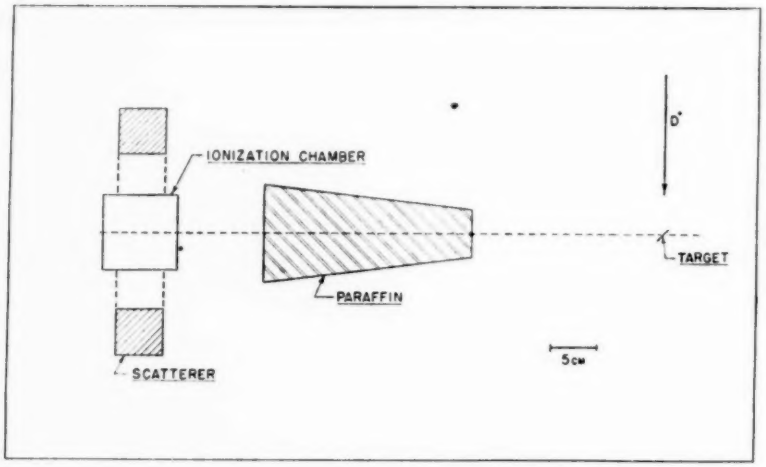

FIG. 1. Experimental arrangement for investigating the neutrons scattered through 100°.

0.5 to 1.3 Mev. Kikuchi, Aoki, and Wakatuki[8] have studied the angular distribution of monoenergetic neutrons of about 3 Mev scattered in C, Al, Fe, Cu, Sn, Pb, Bi, and found a large anisotropy increasing with atomic mass. The scattering was much stronger in the forward direction than at larger scattering angles, but their experiments do not enable one to distinguish whether the scattered neutrons have lost energy or not. We shall come back to these results in the discussion. Bacher[9] concluded from his experiments that neutrons of high energy from a Be target bombarded by deuterons, and detected by the radioactivity of Al were "elastically" scattered to an appreciable extent by C, Cu, and Pb in the forward direction only, but no quantitative data on the relative amounts of elastic and inelastic scattering were given.

It was hoped that more quantitative information could be obtained by using the experimental arrangement in this laboratory which allows one to analyze the distribution in energy of neutrons in a large pressure ionization chamber.[10]

II. EXPERIMENTAL METHOD

In order to distinguish between elastically and inelastically scattered neutrons the distribution in energy of recoil particles in an ionization chamber was analyzed. Baldinger, Huber, and Staub[11] first pointed out that the distribution in energy of fast neutrons could be determined by this method provided that the maximum range of the recoil particles is small compared with the size of the chamber. The relation between the two distributions is particularly simple if the angular distribution of the neutrons scattered by the gas in the chamber is isotropic in the center of mass system. Since this condition is known[10] to hold in hydrogen and deuterium for 2.5-Mev neutrons over a wide range of angles, it would appear that either of these gases would be appropriate for filling an ionization chamber if one wants to determine the distribution in energy of fast neutrons. Previous measurements[10] have shown, however, that considerable difficulties arise if one increases the stopping power of the gas to values at which the range of the recoil protons or deuterons from 2.5-Mev neutrons is small compared to the size of the chamber. γ-rays occurring when neutrons are scattered inelastically may produce electrons which give rise to ionization pulses indistinguishable from those due to low energy recoil particles. A further difficulty is the relatively long time it takes to collect the ions in the chamber even with very high collecting fields. The long collecting times reduce the resolving power for different neutron energies to such an extent that it cannot be hoped to obtain a clear analysis of the neutron energies.

The present experiments were carried out, therefore, by observing recoiling helium nuclei. The use of helium had, however, other disadvantages. The angular distribution of 2.5-Mev neutrons scattered by helium is known[10] to be

[8] S. Kikuchi, H. Aoki, and T. Wakatuki, Proc. Phys. Math. Soc. Japan, **21**, 232, 410, 656 (1939).
[9] R. F. Bacher, Phys. Rev. **57**, 352 (1940).
[10] H. H. Barschall and M. H. Kanner, Phys. Rev. **58**, 590 (1940).
[11] E. Baldinger, P. Huber, and H. Staub, Helv. Phys. Acta **11**, 245 (1938).

anisotropic (cf. Fig. 2), and it is to be expected that the scattering will be anisotropic also for lower neutron energies. Unfortunately the angular distribution is so far known only for neutrons between 2- and 3-Mev energy. Furthermore, the neutron-helium scattering cross section varies strongly with neutron energies between 0.5 and 2 Mev. These circumstances make it impossible to give a quantitative analysis of the inelastically scattered neutrons, but the present experiments enable one to estimate the amount of inelastic scattering and to determine the differential cross section for elastic scattering for different scattering angles.

In all the experiments the 2.5-Mev neutrons emitted at right angles to the deuteron beam in the $d-d$ reaction were used. The deuterons were accelerated by voltages of 200 to 300 kv. The target consisted of D_2O ice. The various kinds of ions in the deuteron beam were not separated.

The recoiling α-particles were produced in an ionization chamber with multiple collecting electrodes.[10] The chamber was filled with 5.5 atmos. of helium. The collecting field was 1700 volts/cm. The chamber was 8 cm high and 8 cm in diameter.

The ionization pulses were amplified by means of a linear amplifier with strong inverse feedback. In some of the experiments the pulses were recorded on photographic paper with a torsion type oscillograph. In other experiments pulses above a definite size were selected by a thyratron relaxation oscillator with long time constants and counted by a scale-of-two circuit connected to a mechanical counter.

The gain of the amplifier and its linearity were checked with the help of artificial pulses of variable size as described before.[12] The calibration of the pulses recorded by the oscillograph in terms of ionization was accomplished by measuring the maximum recoil pulses from 2.5-Mev neutrons. These pulses were compared with standard pulses so that no new calibration was necessary when the gain of the amplifier was changed.

Since the frequency response of the mechanical oscillograph was not exactly the same as that of the selector stage of the counting circuit this comparison was not valid when the pulses were counted by the scaling circuit. For these experiments the grid bias setting of the selector tube was calibrated in terms of ionization energy by the following procedure. Both recoil pulses and artificial pulses were photographed and counted simultaneously. By coupling the two circuits the breakdown of the selector stage was recorded simultaneously with the acting pulses. The coupling was arranged so that the pulses counted by the selector stage were recorded considerably larger than the maximum recoil pulses which were not counted. It was noted at which voltage setting of the pulse generator a part, for instance half, of the artificial pulses were counted. On the photographic record the maximum size of recoil pulses which were not counted was measured and compared with the photographed standard pulses. In this way the minimum energy to which a pulse had to correspond in order to be counted was determined. During the measurements this value was checked frequently by the use of standard pulses. Variations in the standard pulse voltage at which half the pulses were rejected by the selector did not exceed 2 percent during a measurement.

The protons from the $d-d$ reaction were used for monitoring the number of neutrons. The protons emitted at a right angle with respect to the deuteron beam into a known solid angle entered an ionization chamber connected to a linear amplifier. The pulses were counted by means of a scale-of-eight and a mechanical counter.

The experimental arrangement for the scattering experiments is shown schematically in Fig. 1. The scatterers had the form of rings with square cross sections. They had an inner diameter of 16.4 cm and were 5 cm thick. The rings were castings except in the case of carbon where graphite was used. A truncated cone of paraffin, 22 cm long, was interposed between the target and the ionization chamber in order to reduce the number of neutrons not scattered in the ring, but detected in the chamber. The paraffin was placed so that all the neutrons coming from the target, which could reach the chamber directly, had to pass through it. The neutrons could get to

[12] M. H. Kanner and H. H. Barschall, Phys. Rev. **57**, 372 (1940).

the scatterer, however, without passing through the paraffin. When the scatterer was in the position shown in Fig. 1 the mean scattering angle of the neutrons was 100°. By moving both the scatterer and the paraffin closer to the target the scattering angle could be reduced to 45°. Since the scatterer subtended a finite angle at the target there was a spread in energy of the neutrons on account of the variation of the angle of emission of the neutrons with respect to the deuteron beam. This uncertainty in neutron energy amounted to about ±0.10 Mev for the distant position of the ring scatterer and to ±0.15 Mev for the close position of the scatterer. The large dimensions of the scatterer and the detector also introduced an appreciable uncertainty in the scattering angles of the neutrons, approximately ±20° for the position in which the mean scattering angle was 100°, and ±10° for the position corresponding to a mean scattering angle of 45°.

In the first part of the experiments the distribution in energy of the recoiling α-particles due to scattered neutrons was measured. Photographic records were taken alternately with and without the ring scatterer, the number of protons counted being the same in the two cases. The records were evaluated by counting the number of pulses ending in each of about twenty deflection intervals. The difference in the numbers in each interval obtained with and without scatterer, gives the distribution of α-particles due to neutrons scattered by the ring.

If one assumes that the α-particles of highest energies are due to elastically scattered neutrons, the cross section $\sigma(\vartheta)$ for elastic scattering through an angle ϑ per unit solid angle is given by[13]

$$\sigma(\vartheta)=\frac{A\cdot E_m}{\sigma_{\mathrm{He}}Nn_1n_2\Delta E\int dV_1dV_2/r^2},$$

A being the number of α-particles in the energy interval between $E_m-\Delta E$ and E_m, E_m the maximum recoil energy due to 2.5-Mev neutrons, σ_{He} the total scattering cross section of helium (4π times the differential cross section per unit solid angle) for backward scattering of 2.5-Mev neutrons, N the number of neutrons impinging upon 1 cm² of the scatterer, n_1 the number of nuclei per cm³ of the scatterer, n_2 the number of nuclei per cm³ in the ionization chamber, r the distance between a volume element dV_1 of the scatterer and a volume element dV_2 of the chamber. The number N can be computed from the number of protons counted, the known[14] yield of protons and neutrons in the $d-d$ reaction and the geometry of the apparatus. It should be pointed out, however, that errors in the previous measurement[10] of σ_{He} and in the present measurement of N can be expected to cancel, since a very similar experimental set-up was used in both experiments.

In the second part of the experiments three quantities were measured: the number of recoil particles N_1 counted without paraffin and without scatterer (due to direct neutrons), the number of recoil particles N_2 with the paraffin interposed, but without scatterer, and the number of recoil particles N_3 with both the paraffin and the scatterer present. The three numbers were reduced to the same number of protons. The background of the chamber due to natural radioactivity of the chamber was subtracted from these numbers. If only recoil particles of highest energies are counted, $\sigma(\vartheta)$ may be obtained similarly as in the preceding formula by

$$\sigma(\vartheta)=\frac{V_2\cdot r_1^2}{R^2n_1\int dV_1dV_2/r^2}\cdot\frac{N_3-N_2}{N_1},$$

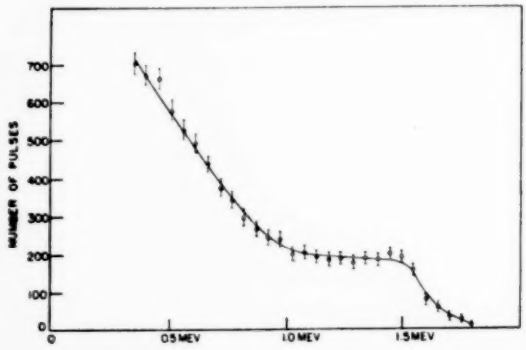

FIG. 2. Distribution in energy of recoiling α-particles knocked on by 2.5-Mev neutrons from the $d-d$ reaction.

[13] We are much indebted to Professor J. A. Wheeler and Mr. P. Olum for numerical evaluation of the integral appearing in the above formula. The calculation was accomplished by expanding $1:r^2$ into spherical harmonics on a four-dimensional sphere, and using the zero- and second-order terms in the expansion (the odd members of the expansion vanish upon integration).

[14] R. Ladenburg and M. H. Kanner, Phys. Rev. **52**, 911 (1937).

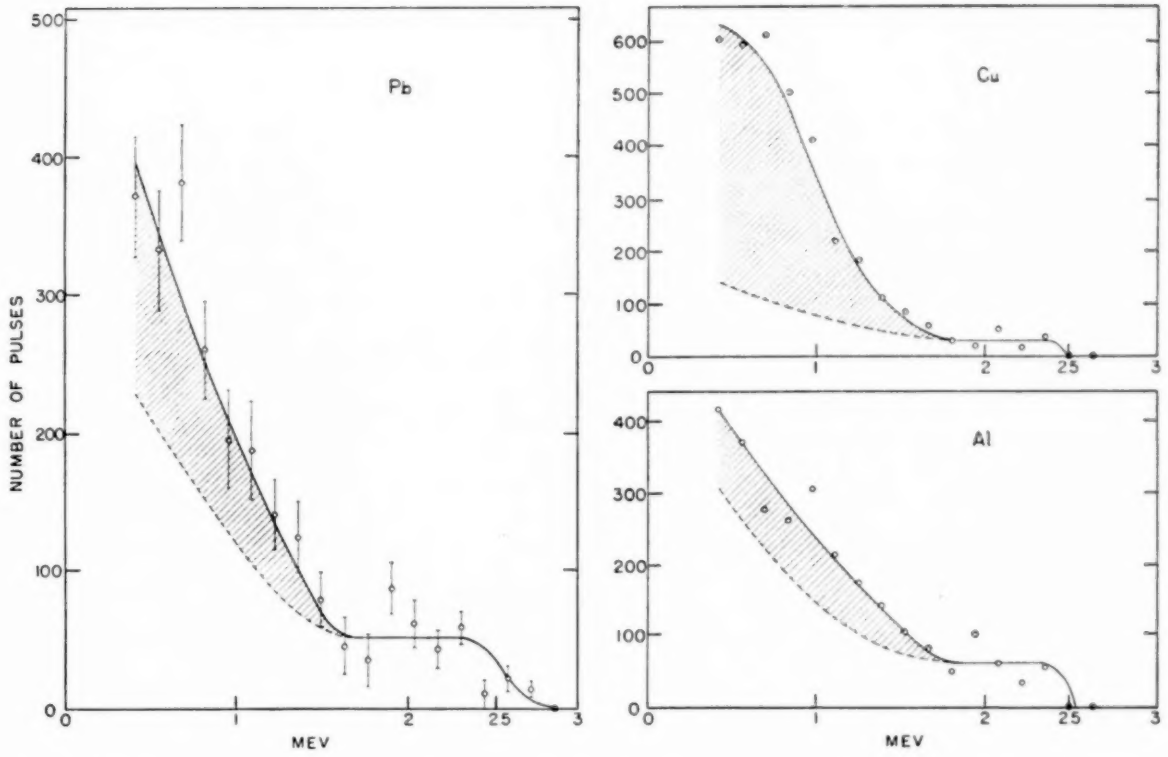

FIG. 3. Distribution in energy of recoiling α-particles knocked on by neutrons which were scattered through 100° by Al, Cu, and Pb. The cross-hatched areas are a measure of inelastic scattering.

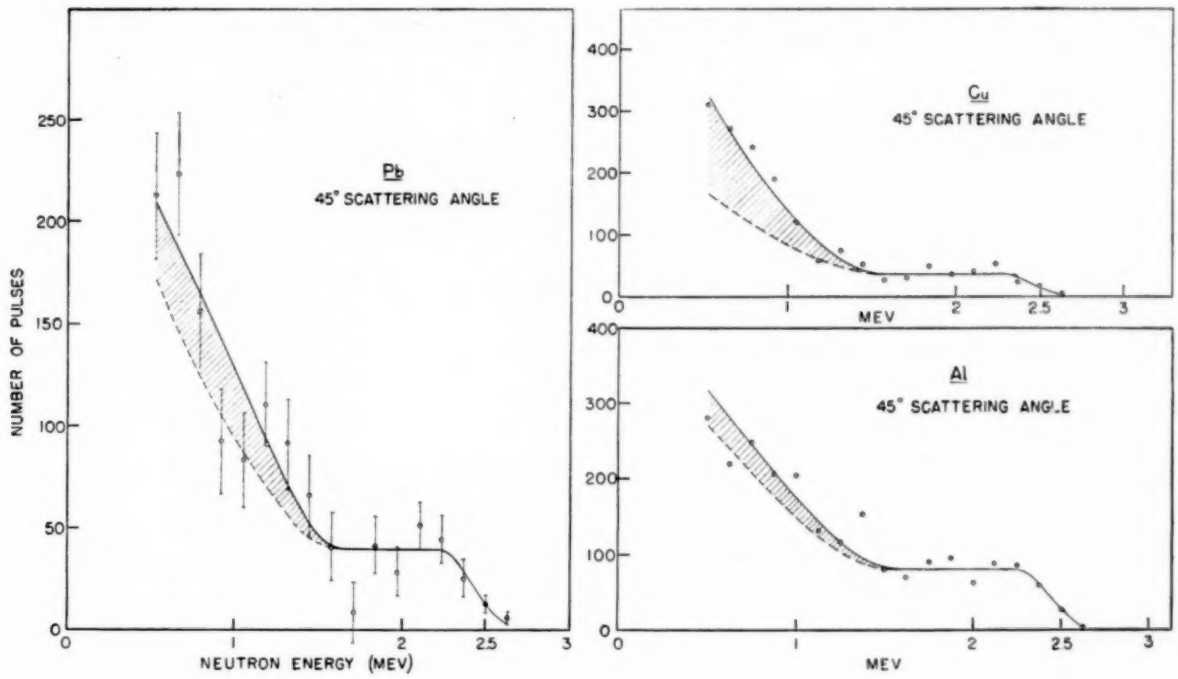

FIG. 4. Distribution in energy of recoiling α-particles from neutrons which were scattered through 45° by Al, Cu, and Pb.

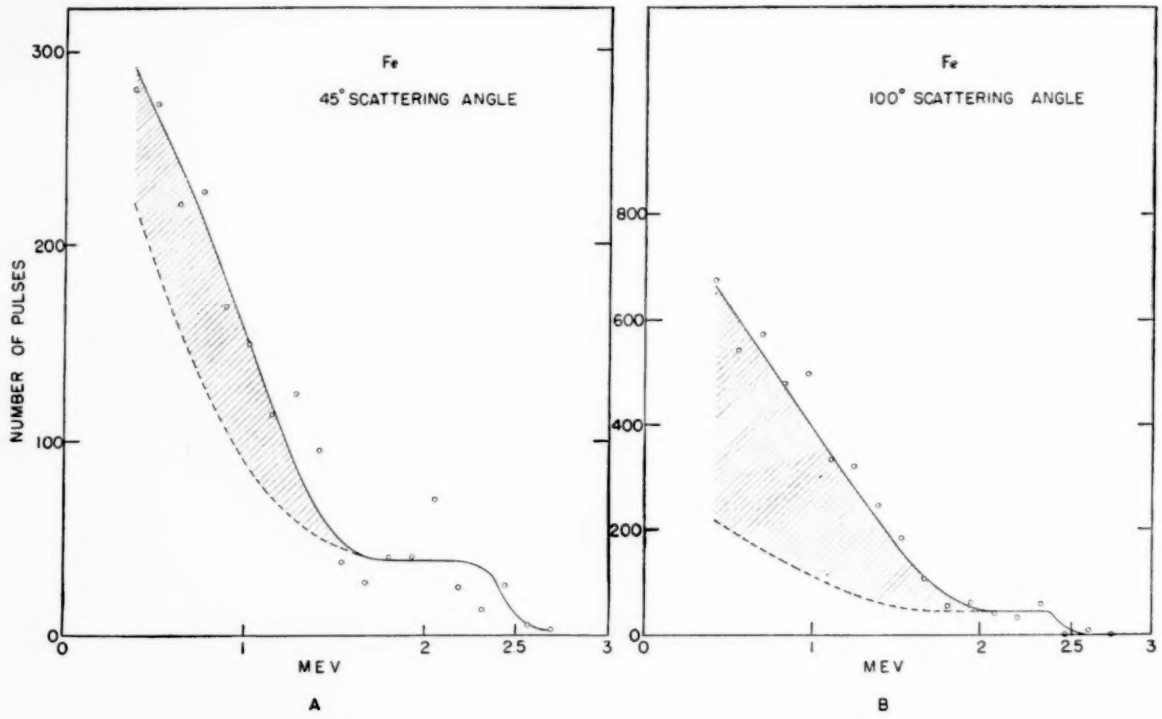

FIG. 5. Distribution in energy of recoiling α-particles from neutrons scattered by Fe through (A) 45° and (B) 100°.

V_2 being the volume of the chamber, r_1 the distance between the scatterer and the target, R the distance between the chamber and the target.

In this calculation it is assumed that the elastically scattered neutrons have the same energy and therefore the same scattering cross section σ_{He} as the primary neutrons, although a fraction ϵ of the original energy is lost even in an elastic collision. The corresponding change of σ_{He} can be neglected for our measurements,[15] but a correction has to be applied because the distribution in energy of the α-particles extends to different energies for the direct and the scattered neutrons. As can be shown easily the cross section should therefore be increased by $100\cdot\epsilon(E_m-\Delta E)/\Delta E$ percent, ΔE being the interval of recoil energy used in the experiment and E_m the maximum energy of an α-particle knocked on by a direct neutron. This correction holds if $\epsilon E_m/\Delta E$ is small compared to 1 and is therefore not valid for very light nuclei.

[15] H. Staub and H. Tatel, Phys. Rev. **58**, 820 (1940).

III. RESULTS

When the paraffin cone was introduced in the path of the direct neutrons it was found that the number of recoils was reduced to about 9 percent in the range of high recoil energies and to 20 to 25 percent at the low values of recoil energy. A considerable fraction of the recoils which were observed in the presence of the paraffin was due to neutrons which passed through the paraffin with or without loss of energy. This was concluded from the fact that the number of recoils counted was reduced to 6 and 14 percent, respectively, if a longer paraffin block was used instead of the cone. Some of the remaining neutrons may have been produced in places where parts of the deuteron beam hit the walls of the target chamber. Some neutrons may have been scattered by the floor or parts of the apparatus. The large background at low recoil energies is mostly due to the very high sensitivity of the chamber for neutrons of lower energies.

In view of this large background the scatterer had to be large in order to make its effect at all

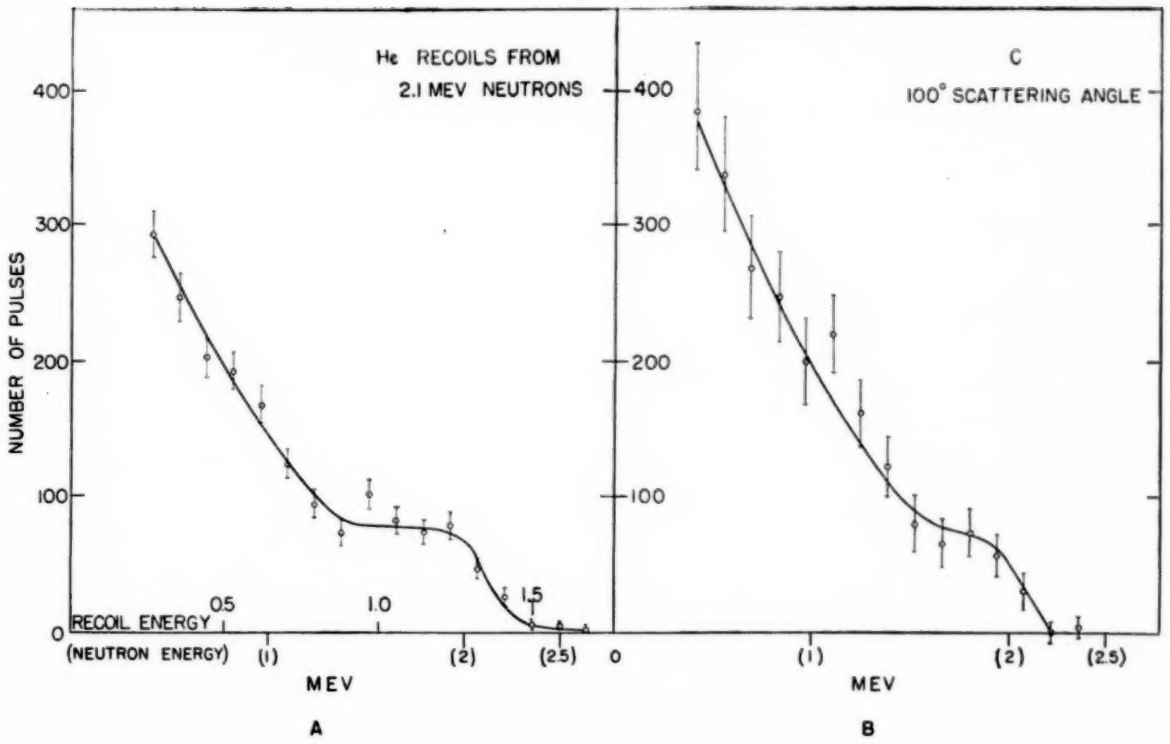

FIG. 6A. Distribution in energy of recoiling α-particles knocked on by 2.1-Mev neutrons from the $d-d$ reaction. B. Distribution in energy of recoiling α-particles from neutrons scattered by carbon through 100°.

observable. But even with a big scatterer the effect was always smaller than the background. Consequently, it was not possible to obtain results with great statistical accuracy although in every measurement more than 10,000 pulses were evaluated. The statistical error given for all the present measurements is the square root of the sum of the numbers, the difference of which is the experimental value.

Measurements of the distribution in energy of recoil α-particles were carried out for scattering angles of 45° and 100° in aluminum, iron, copper and lead, and for 100° in carbon. The results are plotted in Figs. 3, 4, 5, and 6. The circles represent the measured numbers of recoil particles per energy interval. The vertical bars show the statistical errors involved. The energy values given are the energies of neutrons which would produce recoils from zero energy up to the indicated value. For instance "2.5 Mev" corresponds to a recoil energy of 1.6 Mev, and if neutrons of 2.5 Mev are present the distribution curve shows a break at this energy (see Fig. 2).

In order to interpret the curves in Figs. 3, 4, and 5 they should be compared with the distribution obtained for the direct 2.5-Mev neutrons. The latter distribution is reproduced in Fig. 2. It shows an almost flat portion at high recoil energies. All the distributions in recoil energy shown in Figs. 3, 4, and 5 exhibit a similar feature. This indicates that—within the rather large statistical uncertainty—there are no scattered neutrons present of energies between 1.8 and 2.3 Mev. All the neutrons of more than 2.3 Mev will be referred to hereafter as "elastically" scattered neutrons. It should be emphasized, however, that some of these neutrons may have lost energy by inelastic collision, since the resolving power of the apparatus is not sufficient to distinguish neutrons, which have lost less than 10 percent of their energy in an inelastic collision, from those which are elastically scattered. It should be pointed out also that α-particles of less than 300-kev energy were not counted at all so that neutrons which have lost more than about 2 Mev of their energy in inelastic collisions would not have been detected.

Assuming that all the recoils in the flat portion

of the curves in Figs. 3, 4, and 5 are due to elastically scattered neutrons one can find the effect of the elastically scattered neutrons at lower recoil energies by extrapolating according to the graph in Fig. 2. The extrapolated distributions are shown by dashed curves in Figs. 3, 4, and 5. The differences between the dashed curves and the experimental curves are measures of the inelastic scattering. The areas corresponding to inelastic scattering are cross-hatched. Figure 3 shows the distribution curves obtained when neutrons were scattered through 100° by Al, Cu, and Pb. In the plot the indicated ordinates give the actually measured numbers. The scales were chosen, however, in such a way that they correspond to equal numbers of nuclei per cm^3 for the three elements. Therefore the ordinates are direct measures of the scattering cross sections. Corresponding plots are given in Fig. 4 for a scattering angle of 45°. Since the geometry is different for different scattering angles the plots in Fig. 3 and Fig. 4 are not directly comparable. The scales of the ordinates in Fig. 4 should be multiplied by a factor of 2.4 to reduce them to the same solid angle as the one at 100°. Figure 5A shows the scattering by Fe at 45°, Fig. 5B at a scattering angle of 100°. In these figures the plots are reduced to the same solid angle. In all cases the cross section for elastic scattering is obviously considerably larger at 45° than at 100°. Furthermore, the figures show differences in the amount of inelastic scattering. The inelastic scattering is very much greater compared with the elastic scattering in Fe and Cu than in Al and Pb. If one measures the cross-hatched areas for any one element at the two scattering angles one finds that they agree within 15 percent when reduced to the same solid angle. In spite of the fact that these areas are obtained as second differences of quantities involving considerable statistical uncertainties, one may conclude that within the accuracy of these experiments the amount of inelastic scattering does not differ appreciably for the scattering angles of 45° and 100°. Thus, our experiments show that the elastic scattering is anisotropic and the inelastic scattering isotropic within the accuracy of our measurements.

In the case of the scattering of neutrons by carbon through 100° the energy loss of a neutron even in an elastic collision is quite appreciable (17 percent). The distribution in energy of the recoil α-particles from neutrons scattered by carbon should therefore be compared with that due to neutrons of about 2.1 Mev energy. Such neutrons were obtained from the $d-d$ reaction by placing the ionization chamber above the target, i.e., by observing in the backward direction. A distribution curve of this kind is shown in Fig. 6A. In Fig. 6B the results for neutrons scattered by carbon are plotted. The breaks in the two curves occur roughly at the same energy so that one can assume that the distribution in energy of the fastest neutrons is about the same in the two cases. Although the distribution curve of the recoils due to neutrons scattered by carbon rises somewhat faster towards lower recoil energies than the curve due to the direct neutrons, the difference is not outside the statistical uncertainty. The experiments do not show any inelastic scattering of 2.5-Mev neutrons in carbon. A comparison of Figs. 6A and B shows once more the difficulty in obtaining good statistical accuracy in these scattering experiments even if large numbers of pulses are counted.

In order to obtain a somewhat better statistical accuracy for the determination of the elastic scattering cross section, experiments were carried out in which only the pulses above 1.1-Mev recoil energy were counted. The method used is described in the second section of this paper. The results of these experiments are given in the second and third columns of Table I. The values are averages both of the results obtained from the photographic records and of those obtained by counting directly, except in the case of Zn, where no records were photo-

TABLE I. Data on scattering cross section $4\pi\sigma(\vartheta)\times10^{24}$ cm^2.

1 Element	2 Elastic scattering (B and L) $\vartheta=100°\pm20°$	3 Elastic scattering (B and L) $45°\pm10°$	4 Total scattering (Kikuchi *et al.*) 100°	5 Total scattering (Kikuchi *et al.*) 45°	Total cross section from transmission experiments
6 C	1.2 ±0.2	—	—	2.0±0.2	1.6±0.3
13 Al	1.1 ±0.2	3.4±0.5	(2.5)	3.8±0.2	2.4±0.3
26 Fe	0.60±0.15	1.7±0.3	2.0±0.4	4.3±0.3	3.1±0.3
29 Cu	0.38±0.1	1.4±0.3	—	3.5±0.3	2.7±0.3
30 Zn	0.68±0.2	1.7±0.3	—	—	3.0±0.3
82 Pb	2.5 ±0.4	5.0±0.6	3.1±0.8	9.2±0.6	6.0±0.7

graphed, and in the case of carbon where only the records were used. The error given is the statistical uncertainty.

According to whether one computes the mean free path from the elastic or the total cross section, one obtains values greater or less than the dimensions of the scatterer. An experiment was carried out therefore with a Pb scatterer which had half the thickness of the scatterer used before. The measurement gave the same value for the elastic scattering cross section which was obtained with the thicker scatterer.

One may object that some of the neutrons scattered by the scatterer and detected in the chamber did not come direct from the target but were scattered by the paraffin. This point was investigated by removing the scatterer and placing the paraffin in such a position that both the direct neutrons and those scattered by the paraffin could reach the chamber. With this arrangement it is possible to measure the distribution in energy of the neutrons which reach the scatterer in the main experiments. No change in the shape of the distribution curve with and without the paraffin could be detected.

IV. DISCUSSION

Columns 2 and 3 of Table I show definitely that for all nuclei investigated the cross section for elastic scattering is appreciably larger for a scattering angle of 45° than for 100°. This is in agreement with the wave mechanical picture of the collision of neutrons with nuclei.[16] A quantitative comparison of the present experiments with a more detailed theory[17] is not possible, as the theory applies only to neutrons of such high energy that the de Broglie wave-length is small compared with the nuclear radius. (For 2.5-Mev neutrons $\lambda/2\pi = 2.9\times10^{-13}$ cm.)

The anisotropy of the scattering of neutrons was established experimentally for the first time by Kikuchi, Aoki, and Wakatuki[8] (see columns 4 and 5 of Table I), but their experiments do not enable one to distinguish between elastic and inelastic scattering. These authors measured the total ionization due to hydrogen and carbon nuclei knocked on by $d-d$ neutrons which were scattered in different materials. Both the scattering cross section of the gas in the chamber and the ionization produced by the recoiling particles depend on the energy of the neutrons. Only if these effects just canceled, would the results be independent of the energy of the neutrons and give the total scattering cross sections of the materials investigated. Therefore it is not possible to draw definite conclusions from the comparison of their results with ours. If one takes the difference between the two results at 100° (column 4 and column 2 of Table I), one finds that the ratio of inelastic to elastic scattering is much larger for Fe than for Al and Pb. For a scattering angle of 45° this conclusion is not quite so definite since the elastic scattering increases so much for smaller scattering angles.[18]

Above we drew the conclusion that Fe and Cu show relatively more inelastic scattering than Al and Pb already directly from the distribution in energy of the recoiling α-particles. This result agrees also with the measurements of Aoki[5] and of Nonaka[6] who investigated the secondary γ-rays due to excitation of nuclei by $d-d$ neutrons. For obtaining relative values of the inelastic scattering at two angles we believe that the cross-hatched areas in the figures give the most reliable results, while for estimates of the absolute value of the inelastic scattering one has to take differences in Table I.*

It is a pleasure to thank Dr. C. C. Van Voorhis for his cooperation throughout the experiments. We wish also to express our appreciation to Mr. W. A. Hane and Mr. R. L. Kramer for their help in evaluating some of the photographic records.

[16] I. I. Rabi, Phys. Rev. **43**, 838 (1933).

[17] N. Bohr, R. Peierls, and G. Placzek, Proc. Copenhagen Academy, to appear shortly; G. Placzek and H. A. Bethe, Phys. Rev. **57**, 1075 (1940).

[18] From the difference in the cross sections for Pb in columns 5 and 3 it would appear that the inelastic scattering by Pb is much larger at 45° than at 100°, but this is not in agreement with our direct measurements.

* *Note Added in Proof (January 8, 1942).*—In the meantime a paper of Dunlap and Little on the scattering of $d-d$ neutrons by lead has appeared (Phys. Rev. **60**, 639 (1941). Their somewhat indirect conclusion that the anisotropic distribution of scattered neutrons is due to elastic scattering is corroborated by our experiments. Also their relatively small value of the cross section for inelastic scattering of the $d-d$ neutrons by lead agrees with our results.

On Tensor Forces and the Theory of Light Nuclei

EDWARD GERJUOY AND JULIAN SCHWINGER*
Department of Physics, University of California, Berkeley, California
(Received December 1, 1941)

The quadrupole moment of the deuteron indicates the existence of non-central tensor forces in nuclei which destroy the constancy of the total orbital angular momentum. With simple operational representations of the wave functions, the influence of two-body tensor forces on the ground state eigenfunctions of the light nuclei H^3 and He^4 has been calculated. In H^3, the tensor forces directly couple to the fundamental $^2S_{\frac{1}{2}}$ state a $^4D_{\frac{1}{2}}$ state, which in turn interacts with $^2P_{\frac{1}{2}}$ and $^4P_{\frac{1}{2}}$. To the fundamental $^1S_0$ state of He^4 is admixed a $^5D_0$ state which is coupled by the tensor forces with $^3P_0$. All states consistent with the total angular momentum and parity conservation rules occur in the ground state eigenfunctions, and these nuclei therefore constitute the simplest examples of the complete breakdown of spin and orbital angular momentum conservation laws. Rarita and Schwinger have satisfactorily accounted for the properties of the deuteron by including the tensor force in a simple interaction represented by a rectangular well potential. With this interaction to describe the forces between all pairs of nuclear particles, the binding energies of H^3 and He^4 have been estimated by a variation method The trial functions are of the form $^2S_{\frac{1}{2}}+^4D_{\frac{1}{2}}$ for H^3 and $^1S_0+^5D_0$ for He^4, with Gaussian radial functions. The calculations yield 32 and 50 percent of the binding energy for H^3 and He^4, respectively, while a similar test calculation for the deuteron gives 54 percent of the binding energy. The probability that these nuclei are in a D state is found to be 4 percent for all three nuclei, in agreement with the exact deuteron computations. Improvement of the radial dependence of the trial functions increases the estimated binding energy of the deuteron to 76 percent of the known value but does not materially affect either the estimated binding energies of H^3 and He^4, or the amount of D state admixture of the three nuclei. An analysis of the results shows that the tensor forces, which produce all the binding in the deuteron, are relatively ineffective in binding H^3 and He^4. This apparently indicates that the assumption of ordinary and tensor forces of the same range is not adequate to represent the properties of H^3 and He^4.

I. INTRODUCTION

THE theory of nuclei attempts to interpret nuclear properties in terms of two-body forces. Current nuclear theories further postulate equal interactions between all pairs of nuclear particles, and until very recently it has been customary in the theory of light nuclei to construct the interaction as a linear combination of Majorana, Heisenberg, Wigner, and Bartlett forces operating through similar potentials of the same range. That this is insufficient was, however, demonstrated by Rarita and Present,[1] and their conclusions substantiated by the analysis of proton-proton scattering data.[2] An interaction of the sort described, when fitted to represent the experimental binding energies of H^2 and H^3, as well as the cross section for slow neutron-proton scattering, will predict a binding energy of He^4 which is about 20 percent too large. The existence of the quadrupole moment of the deuteron has established that the neutron-proton interaction must involve tensor spin-orbit coupling terms of the form

$$S_{12}=\frac{3(\boldsymbol{\sigma}_1\cdot\mathbf{r}_{12})(\boldsymbol{\sigma}_2\cdot\mathbf{r}_{12})}{r_{12}^2}-\boldsymbol{\sigma}_1\cdot\boldsymbol{\sigma}_2$$

and spin dependent forces of this character are predicted by various current mesotron field theories of the neutron-proton interaction. More recently Rarita and Schwinger[3] have examined the possibility of representing the properties of the deuteron by means of the interaction operator

$$V=-\{1-\tfrac{1}{2}g+\tfrac{1}{2}g\boldsymbol{\sigma}_1\cdot\boldsymbol{\sigma}_2+\gamma S_{12}\}J(r_{12}). \quad (1)$$

For the ground state of the deuteron, which is of even parity, the omission of space exchange operators from (1) is of no consequence, and therefore, for this state, V is equivalent to the most general linear combination of Majorana, Heisenberg, Wigner, Bartlett, and tensor operators. Indeed, it has been shown that, with $J(r_{12})$ a square well of range $r_0=2.80\times10^{-13}$ cm and depth $V_0=13.89$ Mev, and $g=0.0715$ and

* Now at Purdue University, Lafayette, Indiana.
[1] William Rarita and R. D. Present, Phys. Rev. **51**, 788 (1937).
[2] G. Breit, H. M. Thaxton, and L. Eisenbud, Phys. Rev. **55**, 1018 (1939).
[3] William Rarita and Julian Schwinger, Phys. Rev. **59**, 436 and 556 (1941).

$\gamma=0.775$, (1) will account for all the properties of the neutron-proton system which depend only on the neutron-proton forces.

The operator S_{12} couples the spin and orbital motion of the particles, and is not invariant under separate rotation of space or spin coordinates. Its inclusion in the Hamiltonian therefore results in leaving as constants of the motion, available for the description of stationary states, in general only the parity, the total angular momentum J, and the total magnetic quantum number m. The eigenfunction of the ground state of a many-particle system will consequently contain terms corresponding to higher spins and orbital angular momenta than predicted in the absence of spin-orbit coupling, or, in other words, including S_{12} in the neutron-proton interaction implies a breakdown of the previously assumed nuclear Russell-Saunders coupling. The extent of this breakdown is of immediate interest with reference to the magnetic dipole moments and other multipole moments of nuclei, as well as to the problem of selection rules in nuclear transmutations. In this paper we investigate the influence of interaction terms of the type S_{12} on the eigenfunctions of the ground states of the light nuclei H^3 and He^4 by first, in Section II below, determining the types of states which may appear in these eigenfunctions, and then, in the last section, using the operator (1) with the constants determined by Rarita and Schwinger to estimate by a variational method the amount of admixture and binding which may be expected. As described in more detail below, our calculations indicate that only the D state has an appreciable probability of being included in the ground states of H^3 and He^4 along with the S state, and that the probability of finding either of these nuclei in a D state is about four percent. Our variational estimates of the binding energies of H^3 and He^4 are rather low, and an analysis of our results shows that, with respect to their influence on the binding, the tensor forces are, in H^3 and He^4, relatively ineffective when compared with the deuteron. In the deuteron the tensor force is so effective that its introduction in sufficient quantity to give the known quadrupole moment of the deuteron reduces the magnitude of the ordinary interaction necessary to fit the binding energy with the range 2.80×10^{-13} cm from 21.22 Mev to 13.89 Mev. This reduction in the magnitude of the ordinary interaction greatly diminishes the amount of S state binding, and since the tensor forces do not seem to compensate for this diminution in H^3 and He^4, it follows that our low estimates of the binding energies of these nuclei probably indicate real deficiencies. In other words, the simple introduction of the S_{12} coupling in a symmetric Hamiltonian in which all the forces are of equal range is apparently not yet adequate to reconcile the known properties of the two-particle system with the experimental mass defects of H^3 and He^4. The validity and limitations of these conclusions are discussed more fully in the last section.

II. GENERAL FORMULAE

With the breakdown of spin and orbital angular momentum conservation, an eigenfunction of definite total angular momentum J is most conveniently regarded as a mixture of many states classified in terms of their total spin and total orbital angular momentum. The classifications possible are just those consistent with the rules for compounding angular momenta, limited however by a definite maximum total spin. Thus in H^3 the ground state is $J=\frac{1}{2}$ and the maximum spin $\frac{3}{2}$, and therefore the eigenfunction is a mixture of $^2S_{\frac{1}{2}}$, $^2P_{\frac{1}{2}}$, $^4P_{\frac{1}{2}}$ and $^4D_{\frac{1}{2}}$ states. Similarly in He^4 the ground state eigenfunction is composed of $^1S_0$, $^3P_0$ and $^5D_0$ states. In a many particle system it is generally possible to form states of either parity and any total orbital angular momentum, so that in H^3 and He^4 the parity selection rule merely reduces the number of states in the eigenfunction included in any particular classification such as $^2P_{\frac{1}{2}}$ or $^3P_0$, but does not completely eliminate any classification. These nuclei are consequently more complicated than the simple deuteron system, in which the ground state, as in H^3 and He^4, is of even parity and the odd $^3P_1$ state is therefore absent from the eigenfunction. A further simplification in the deuteron which does not appear in H^3 and He^4 is the conservation of total spin which, for a two-particle system only, is a consequence of the symmetry of S_{12} in the operators σ_1 and σ_2.

The elucidation of these statements and the

more detailed consideration of the states which actually appear in the eigenfunctions necessitate actually obtaining the wave functions of the states in question. These can be readily written down in an operational representation such as developed by Rarita and Schwinger[3] in the theory of the deuteron. We first introduce the usual relative coordinate systems for H^3 and He^4, defined by:

In H^3 $\quad \boldsymbol{\varrho}=\mathbf{r}_2-\mathbf{r}_1, \quad \mathbf{r}=\mathbf{r}_3-(\mathbf{r}_1+\mathbf{r}_2)/2.$

In He^4 $\quad \boldsymbol{\varrho}_1=\mathbf{r}_2-\mathbf{r}_1, \quad \boldsymbol{\varrho}_2=\mathbf{r}_4-\mathbf{r}_3,$

$$\mathbf{r}=\frac{\mathbf{r}_4+\mathbf{r}_3}{2}-\frac{\mathbf{r}_1+\mathbf{r}_2}{2}.$$

In both nuclei the subscripts 1 and 2 refer to neutrons, and 3 and 4 to protons. With the abbreviation $\boldsymbol{\sigma}_{ij}=(\boldsymbol{\sigma}_i-\boldsymbol{\sigma}_j)/2$, the wave functions of the states that can occur in the ground state eigenfunctions of H^3 and He^4 are, as explained below:

H^3:

$$^2S_{\frac{1}{2}}{}^m: \frac{1}{4\pi}\frac{1}{\sqrt{2}}(\chi_1{}^+\chi_2{}^- - \chi_1{}^-\chi_2{}^+)\chi_3{}^m=\psi, \tag{2}$$

$$^2S_{\frac{1}{2}}{}^m: \frac{1}{\sqrt{3}}(\boldsymbol{\sigma}_{12}\cdot\boldsymbol{\sigma}_3)\psi, \tag{3}$$

$$\left.\begin{aligned} &^2P_{\frac{1}{2}}{}^m: \left(\frac{3}{2}\right)^{\frac{1}{2}}\frac{\boldsymbol{\sigma}_3\cdot\mathbf{r}\times\boldsymbol{\varrho}}{r\rho}\psi, \\ &^2P_{\frac{1}{2}}{}^m: \frac{1}{\sqrt{2}}\frac{1}{r\rho}[(\boldsymbol{\sigma}_1+\boldsymbol{\sigma}_2+\boldsymbol{\sigma}_3)\cdot\mathbf{r}\times\boldsymbol{\varrho}](\boldsymbol{\sigma}_{12}\cdot\boldsymbol{\sigma}_3)\psi=\frac{1}{\sqrt{2}}\frac{1}{r\rho}\{\boldsymbol{\sigma}_{12}\cdot\mathbf{r}\times\boldsymbol{\varrho}+i\boldsymbol{\sigma}_3\times\boldsymbol{\sigma}_{12}\cdot(\mathbf{r}\times\boldsymbol{\varrho})\}\psi, \end{aligned}\right\} \tag{4}$$

$$^4P_{\frac{1}{2}}{}^m: \frac{1}{r\rho}\left\{\boldsymbol{\sigma}_{12}\cdot\mathbf{r}\times\boldsymbol{\varrho}-\frac{i}{2}\boldsymbol{\sigma}_3\times\boldsymbol{\sigma}_{12}\cdot(\mathbf{r}\times\boldsymbol{\varrho})\right\}\psi, \tag{5}$$

$$\left.\begin{aligned} &^4D_{\frac{1}{2}}{}^m: \left(\frac{3}{2}\right)^{\frac{1}{2}}\left\{\frac{(\boldsymbol{\sigma}_{12}\cdot\mathbf{r})(\boldsymbol{\sigma}_3\cdot\mathbf{r})}{r^2}-\frac{1}{3}(\boldsymbol{\sigma}_{12}\cdot\boldsymbol{\sigma}_3)\right\}\psi, \\ &^4D_{\frac{1}{2}}{}^m: \left(\frac{3}{2}\right)^{\frac{1}{2}}\left\{\frac{(\boldsymbol{\sigma}_{12}\cdot\boldsymbol{\varrho})(\boldsymbol{\sigma}_3\cdot\boldsymbol{\varrho})}{\rho^2}-\frac{1}{3}(\boldsymbol{\sigma}_{12}\cdot\boldsymbol{\sigma}_3)\right\}\psi, \\ &^4D_{\frac{1}{2}}{}^m: \frac{3}{2(5)^{\frac{1}{2}}}\frac{1}{r\rho}\{(\boldsymbol{\sigma}_{12}\cdot\mathbf{r})(\boldsymbol{\sigma}_3\cdot\boldsymbol{\varrho})+(\boldsymbol{\sigma}_{12}\cdot\boldsymbol{\varrho})(\boldsymbol{\sigma}_3\cdot\mathbf{r})-\tfrac{2}{3}(\mathbf{r}\cdot\boldsymbol{\varrho})(\boldsymbol{\sigma}_{12}\cdot\boldsymbol{\sigma}_3)\}\psi, \end{aligned}\right\} \tag{6}$$

$$^4D_{\frac{1}{2}}{}^m: \frac{15}{4(5)^{\frac{1}{2}}}\frac{1}{r^2\rho^2}\{(\boldsymbol{\sigma}_{12}\cdot\mathbf{r}\times\boldsymbol{\varrho})(\boldsymbol{\sigma}_3\cdot\mathbf{r}\times\boldsymbol{\varrho})-\tfrac{1}{3}(\mathbf{r}\times\boldsymbol{\varrho})^2(\boldsymbol{\sigma}_{12}\cdot\boldsymbol{\sigma}_3)\}\psi. \tag{7}$$

He^4:

$$^1S_0: \frac{1}{(4\pi)^{\frac{1}{2}}}\tfrac{1}{2}(\chi_1{}^+\chi_2{}^- - \chi_1{}^-\chi_2{}^+)(\chi_3{}^+\chi_4{}^- - \chi_3{}^-\chi_4{}^+)=\varphi$$

$$^1S_0: \frac{1}{\sqrt{3}}(\boldsymbol{\sigma}_{12}\cdot\boldsymbol{\sigma}_{34})\varphi,$$

$$\left.\begin{aligned} &^3P_0: \left(\frac{3}{2}\right)^{\frac{1}{2}}\frac{(\boldsymbol{\sigma}_{12}\cdot\mathbf{r}\times\boldsymbol{\varrho}_1)}{r\rho_1}\varphi \\ &^3P_0: \left(\frac{3}{2}\right)^{\frac{1}{2}}\frac{(\boldsymbol{\sigma}_{34}\cdot\mathbf{r}\times\boldsymbol{\varrho}_1)}{r\rho_1}\varphi \\ &^3P_0: \left(\frac{3}{4}\right)^{\frac{1}{2}}\frac{\boldsymbol{\sigma}_{12}\times\boldsymbol{\sigma}_{34}\cdot(\mathbf{r}\times\boldsymbol{\varrho}_1)}{r\rho_1}\varphi \end{aligned}\right\} \text{etc.}$$

$$\left.\begin{aligned} {}^5D_0\colon\ & \left(\frac{3}{2}\right)^{\frac{1}{2}}\left\{\frac{(\boldsymbol{\sigma}_{12}\cdot\mathbf{r})(\boldsymbol{\sigma}_{34}\cdot\mathbf{r})}{r^2}-\tfrac{1}{3}(\boldsymbol{\sigma}_{12}\cdot\boldsymbol{\sigma}_{34})\right\}\varphi, \\ {}^5D_0\colon\ & \frac{3}{2(5)^{\frac{1}{2}}}\frac{1}{r\rho_1}\{(\boldsymbol{\sigma}_{12}\cdot\mathbf{r})(\boldsymbol{\sigma}_{34}\cdot\boldsymbol{\rho}_1)+(\boldsymbol{\sigma}_{12}\cdot\boldsymbol{\rho}_1)(\boldsymbol{\sigma}_{34}\cdot\mathbf{r})-\tfrac{2}{3}(\mathbf{r}\cdot\boldsymbol{\rho}_1)(\boldsymbol{\sigma}_{12}\cdot\boldsymbol{\sigma}_{34})\}\varphi, \end{aligned}\right\}\text{etc.} \tag{8}$$

$$^3P_0\colon\ \frac{3}{\sqrt{2}}\frac{1}{r^2\rho_1\rho_2}(\boldsymbol{\rho}_1\times\boldsymbol{\rho}_2\cdot\mathbf{r})(\boldsymbol{\sigma}_{12}\cdot\mathbf{r})\varphi,\ \text{etc.} \tag{9}$$

The symbolic representations listed above may be derived with the aid of a systematic procedure. Thus, in H^3, we wish to describe states of even parity and $J=\frac{1}{2}$. In terms of the spin functions χ of the particles, a $^2S_{\frac{1}{2}}$ wave function of this character can at once be written down, and is just ψ defined by Eq. (2). The magnetic quantum number m of this state is, as indicated, determined by the magnetic quantum number assigned to χ_3. All other wave functions of total angular momentum $J=\frac{1}{2}$ and the same m can now be obtained by operating on ψ by means of scalar functions of the spin vector operators and space vectors of the system, for such operators commute with $\mathbf{J}$. Such rotation invariant functions can only be formed by combining the scalars, vectors, and tensors formed from the spin operators with similar forms built from the position vectors, and because of the commutation properties of the spin operators, the number of independent invariants is actually quite limited. Since the total spin and total orbital angular momentum classification of any state are determined by its rotational properties with respect to spin and space separately, the representation of the wave functions of the even $J=\frac{1}{2}$ states of H^3 becomes a straightforward and simple problem. More specifically, as a consequence of the antisymmetry of ψ in the neutron spins, $(\boldsymbol{\sigma}_1+\boldsymbol{\sigma}_2)\psi=0$, so that, with respect to operations on ψ, there are only two independent linear combinations of $\boldsymbol{\sigma}_1$, $\boldsymbol{\sigma}_2$ and $\boldsymbol{\sigma}_3$, which we may choose symmetrically as $\boldsymbol{\sigma}_{12}$ and $\boldsymbol{\sigma}_3$. Therefore, with the exception of the identity operator, the only independent scalar spin operator will be $\boldsymbol{\sigma}_{12}\cdot\boldsymbol{\sigma}_3$, and since this operator is also invariant with respect to space rotations, the wave function (3) will have the same transformation properties as ψ, that is, it will represent a $^2S_{\frac{1}{2}}$ state. In the same way there are three independent spin vectors, namely $\boldsymbol{\sigma}_{12}$, $\boldsymbol{\sigma}_3$, and $\boldsymbol{\sigma}_3\times\boldsymbol{\sigma}_{12}$, which may be combined with the vector $\mathbf{r}\times\boldsymbol{\rho}$ to form the rotation invariant operators $\boldsymbol{\sigma}_{12}\cdot\mathbf{r}\times\boldsymbol{\rho}$, $\boldsymbol{\sigma}_3\cdot\mathbf{r}\times\boldsymbol{\rho}$, and $\boldsymbol{\sigma}_3\times\boldsymbol{\sigma}_{12}\cdot(\mathbf{r}\times\boldsymbol{\rho})$. These operators transform like vectors, in other words, like the spherical harmonics of the first order, under space rotations, and, consequently, when applied to ψ, produce P wave functions which, however, in general represent combinations of $^2P_{\frac{1}{2}}$ and $^4P_{\frac{1}{2}}$ states. To determine then the representations of the pure $^2P_{\frac{1}{2}}$ and $^4P_{\frac{1}{2}}$ states we employ the device of operating on the two $^2S_{\frac{1}{2}}$ wave functions, (2) and (3), with the operator $(\boldsymbol{\sigma}_1+\boldsymbol{\sigma}_2+\boldsymbol{\sigma}_3)\cdot\mathbf{r}\times\boldsymbol{\rho}$ which commutes with $(\boldsymbol{\sigma}_1+\boldsymbol{\sigma}_2+\boldsymbol{\sigma}_3)^2$. We obtain in this way the two wave functions (4) which must have the same total spin as (2) and (3) and can therefore only describe pure $^2P_{\frac{1}{2}}$ states. The wave function (5) of the $^4P_{\frac{1}{2}}$ state is the linear combination of $\boldsymbol{\sigma}_{12}\cdot\mathbf{r}\times\boldsymbol{\rho}$ and $\boldsymbol{\sigma}_3\times\boldsymbol{\sigma}_{12}\cdot(\mathbf{r}\times\boldsymbol{\rho})$ which is orthogonal to (4). That (5) really represents a quartet state may be verified by demonstrating that $\boldsymbol{\sigma}_1\cdot\boldsymbol{\sigma}_3$ has the eigenvalue 1 when operating on (5). The $^4D_{\frac{1}{2}}$ wave functions can be derived by combining the spin tensor $\boldsymbol{\sigma}_{12}\boldsymbol{\sigma}_3$ with the various tensors formed from the space vectors and applying the resultant rotation invariant operators to ψ. As before, this will in general furnish a mixture of the $J=\frac{1}{2}$ wave functions of H^3, but after the subtraction of the known (2) through (5), the remainder can only represent pure $^4D_{\frac{1}{2}}$ states. The necessity for this subtraction may, however, be avoided by making use of the principle that the components of the symmetric traceless tensor $x_iy_j+x_jy_i-\frac{2}{3}\delta_{ij}\sum_k x_ky_k$, $i, j, k=1$ to 3, transform like the spherical harmonics of the second order, if $\mathbf{x}$ and $\mathbf{y}$ are vectors. Consequently, since (6) and (7) represent D states of $J=\frac{1}{2}$ they are necessarily $^4D_{\frac{1}{2}}$, and again it is easy to verify

that $(\boldsymbol{\sigma}_1+\boldsymbol{\sigma}_2+\boldsymbol{\sigma}_3)^2$ has the eigenvalue 15 in the states (6) and (7) and that (6) and (7) are all orthogonal to the wave functions (2) through (5).

Any of the wave functions (2) through (7) may be multiplied by a scalar function of $\mathbf{r}$ and $\boldsymbol{\varrho}$ to give a new wave function of the same spectral classification, and it is possible to obtain additional orthogonal wave functions in this fashion. This possibility corresponds to the fact that in H^3, as in all many particle systems, there are many different ways of compounding any given value of the total orbital angular momentum out of the orbital angular momenta of the constituent particles. For example, ψ represents a state in which the neutron system and the proton are both in s states. $(\mathbf{r}\cdot\boldsymbol{\varrho})\psi$ is a ${}^2S_{\frac{1}{2}}$ wave function in which the neutrons and the proton are both in p states. In the eigenfunction ψ will of course be multiplied by a scalar function whose angular dependence will determine the relative contribution of each different possible combination of neutron and proton motions to the singlet (in the neutron spins) ${}^2S_{\frac{1}{2}}$ state of H^3. Since in the H^3 relative coordinate system there are only three independent vectors, $\mathbf{r}$, $\boldsymbol{\varrho}$, and $\mathbf{r}\times\boldsymbol{\varrho}$, of which only $\mathbf{r}\times\boldsymbol{\varrho}$ is invariant under spatial mirroring, it is quite evident from the foregoing discussion that, except for a multiplicative scalar factor, we have listed all the wave functions of H^3 of $J=\frac{1}{2}$ and even parity. As written, the wave functions (2) through (7) are normalized to unity with respect to the summation over all spin coordinates and integration over all angles in the relative coordinate system. Considerations very similar to the above pertain to the derivation of the wave functions of He^4 of $J=0$ and even parity. There is only the complication that several independent vectors of even parity are now available, thereby greatly increasing the number of different types of states. We have therefore only listed examples of the kinds of spin dependence possible, indicating by "etc." that additional wave functions may be obtained merely by substituting new vectors for those in the functions listed (i.e., by replacing $\boldsymbol{\varrho}_1$ by $\boldsymbol{\varrho}_2$, etc.). A further consequence of the increased number of space vectors is the existence of a pseudoscalar $\mathbf{r}\cdot\boldsymbol{\varrho}_1\times\boldsymbol{\varrho}_2$ which converts wave functions of odd parity into even and vice versa. Thus the wave function (9) is a perfectly acceptable even ${}^3P_0$ state formed from the odd $(\boldsymbol{\sigma}_{12}\cdot\mathbf{r})\varphi$, and we could of course include in our list one such wave function corresponding to every odd state of $J=0$ of He^4. However, states of this character, involving the pseudoscalar $\mathbf{r}\cdot\boldsymbol{\varrho}_1\times\boldsymbol{\varrho}_2$, in no way enter into the calculations of the following section, so that we have deemed it sufficient to write down the single example (9) and again indicate by "etc." that the list, for He^4, is not exhaustive. As in H^3 the wave functions are normalized to unity with respect to spin summation and angular integration.

In the absence of spin-orbit coupling the ground state of H^3 is ${}^2S_{\frac{1}{2}}$. The new term in the Hamiltonian is $\sum_{i>j}J(r_{ij})S_{12}(\mathbf{r}_{ij})$ summed over all pairs of particles. Applying this operator to a ${}^2S_{\frac{1}{2}}$ wave function will obviously produce only ${}^4D_{\frac{1}{2}}$ wave functions, and it is readily calculated that in H^3 $\sum_{i>j}J(r_{ij})S_{12}(\mathbf{r}_{ij})\psi$ or $\sum_{i>j}J(r_{ij})\times S_{12}(\mathbf{r}_{ij})(\boldsymbol{\sigma}_{12}\cdot\boldsymbol{\sigma}_3)\psi$ is a linear combination of the wave functions (6). The further application of $\sum_{i>j}J(r_{ij})S_{12}(\mathbf{r}_{ij})$ to the wave functions (6) produces a complicated mixture of terms among which are included the P states (4) and (5), as well as the remaining D state (7). In other words, in the ground state of H^3, to the first approximation of the perturbation theory, the effect of introducing S_{12} coupling in the neutron-proton interaction is to admix the simpler ${}^4D_{\frac{1}{2}}$ states defined by (6) with the fundamental ${}^2S_{\frac{1}{2}}$ states. In second approximation all possible types of states appear. Once more very similar statements may be made concerning the ground state of He^4. The first effect of the S_{12} coupling is to combine ${}^5D_0$ wave functions of the type (8), bilinear in the vectors $\mathbf{r}$, $\boldsymbol{\varrho}_1$ and $\boldsymbol{\varrho}_2$ with the fundamental ${}^1S_0$ wave functions. All other states with the exception of those which, like (9), involve the pseudoscalar $\mathbf{r}\cdot\boldsymbol{\varrho}_1\times\boldsymbol{\varrho}_2$, are included in the eigenfunction through their interaction with the ${}^5D_0$ states. The states involving the pseudoscalar only appear in still higher approximation. Thus (9) is produced by the application of the Hamiltonian to the ${}^3P_0$ wave functions of the usual type, such as $(\boldsymbol{\sigma}_{12}\cdot\mathbf{r}\times\boldsymbol{\varrho}_1)\varphi$. It is in performing the calculations implied by the statements of this paragraph and Section III below that the advantages of the operational representations we have given for the wave functions become apparent. The evaluation of any matrix

element of the interaction becomes merely an exercise in the combination of spin operators, and it is never necessary to make use of the complicated reduction formulas of the rotation group.

III. VARIATION CALCULATION

As stated in the introductory section, we have employed the interaction (1) with the constants determined by Rarita and Schwinger to estimate by a variational method the binding energies and the amount of admixture of the ground states of H^3 and He^4. The smallness of g in (1) and the fact that only the states (6) are directly coupled to ψ by S_{12} then suggest that only the states (2) and (6) have an appreciable probability of being represented in the ground state of H^3. A suitable normalized, antisymmetric in the neutron coordinates, trial function for the variation calculation in H^3 is consequently

$$\Phi_1=\frac{N_S}{(1+C^2)^{\frac{1}{2}}}\exp[-\tfrac{1}{2}\mu(r_{12}^2+r_{13}^2+r_{23}^2)]\psi+\frac{CN_D}{(1+C^2)^{\frac{1}{2}}}\exp[-\tfrac{1}{2}\nu(r_{12}^2+r_{13}^2+r_{23}^2)]$$
$$\times(3(\boldsymbol{\sigma}_1\cdot\boldsymbol{\tau})(\boldsymbol{\sigma}_3\cdot\boldsymbol{\varrho})+3(\boldsymbol{\sigma}_1\cdot\boldsymbol{\varrho})(\boldsymbol{\sigma}_3\cdot\boldsymbol{\tau})-2(\boldsymbol{\tau}\cdot\boldsymbol{\varrho})(\boldsymbol{\sigma}_1\cdot\boldsymbol{\sigma}_3))\psi$$

with

$$N_S=\frac{2(2\mu)^{3/4}(3/2\mu)^{3/4}}{\Gamma(3/2)},\quad N_D=\frac{2(2\nu)^{5/4}(3/2\nu)^{5/4}}{(20)^{\frac{1}{2}}\Gamma(5/2)},$$

$$r_{12}^2+r_{13}^2+r_{23}^2=2r^2+\tfrac{3}{2}\rho^2.$$

The energy is minimized, using (1), with respect to the parameters μ, ν and C. This choice of trial function limits the orbital angular momenta of the constituent neutron and proton motions in the S and D waves to as small values as possible. That is, the S wave, as stated in the previous section, represents a state in which the neutron system and the proton are both in s states, in the D wave the neutrons and the proton are in p states. These are the states whose energies would be expected to lie lowest in a Hartree approximation. Similarly, in He^4 we choose the trial function

$$\Phi_2=\frac{N_S}{(1+C^2)^{\frac{1}{2}}}\exp[-\tfrac{1}{2}\mu(2\rho_1^2+2\rho_2^2+4r^2)]\varphi-\frac{CN_D}{(1+C^2)^{\frac{1}{2}}}\exp[-\tfrac{1}{2}\nu(2\rho_1^2+2\rho_2^2+4r^2)]$$
$$\times(3(\boldsymbol{\sigma}_1\cdot\boldsymbol{\varrho}_1)(\boldsymbol{\sigma}_3\cdot\boldsymbol{\varrho}_2)+3(\boldsymbol{\sigma}_1\cdot\boldsymbol{\varrho}_2)(\boldsymbol{\sigma}_3\cdot\boldsymbol{\varrho}_1)-2(\boldsymbol{\varrho}_1\cdot\boldsymbol{\varrho}_2)(\boldsymbol{\sigma}_1\cdot\boldsymbol{\sigma}_3))\varphi,$$

$$N_S=\frac{2^{3/2}(2\mu)^{3/4}(2\mu)^{3/4}(4\mu)^{3/4}}{[\Gamma(3/2)]^{\frac{3}{2}}},\quad N_D=\frac{2^{3/2}(2\nu)^{5/4}(2\nu)^{5/4}(4\nu)^{3/4}}{(20)^{\frac{1}{2}}\Gamma(5/2)[\Gamma(3/2)]^{\frac{1}{2}}},$$

$$2\rho_1^2+2\rho_2^2+4r^2=r_{12}^2+r_{13}^2+r_{14}^2+r_{23}^2+r_{24}^2+r_{34}^2.$$

As demanded by the exclusion principle, Φ_2 is antisymmetric with respect to the interchange of neutron or proton coordinates. It is readily verified that, in both Φ_1 and Φ_2, with our symmetric choice of Gaussian radial functions, the D wave function must be restricted to the particular form we assumed in order that the exclusion principle be satisfied.

In order that we may have some estimate of the validity of our results, we have also performed a similar variation calculation for the deuteron, using as a trial wave function for the ground state

$$\Phi_3=\frac{N_S}{(1+C^2)^{\frac{1}{2}}}\exp(-\tfrac{1}{2}\mu\rho^2)\chi+\frac{CN_D}{(1+C^2)^{\frac{1}{2}}}\exp(-\tfrac{1}{2}\nu\rho^2)(3(\boldsymbol{\sigma}_N\cdot\boldsymbol{\varrho})(\boldsymbol{\sigma}_P\cdot\boldsymbol{\varrho})-\rho^2(\boldsymbol{\sigma}_N\cdot\boldsymbol{\sigma}_P))\chi,$$

$$N_S=\frac{\sqrt{2}(\mu)^{3/4}}{[\Gamma(3/2)]^{\frac{3}{2}}},\quad N_D=\frac{\nu^{7/4}}{2[\Gamma(7/2)]^{\frac{1}{2}}},\quad \boldsymbol{\varrho}=\boldsymbol{\tau}_P-\boldsymbol{\tau}_N.$$

χ is the fundamental normalized ${}^3S_1$ state of the deuteron, defined analogously to ψ and φ. The details of the calculation of the binding energies of these wave functions are quite standard and it is therefore sufficient to write down just the expressions for the binding energies in terms of the variational parameters:

$$\begin{aligned}
\mathrm{H}^3\text{:}\quad (1+C^2)\frac{E}{E_0} &= -3.662x^2+35.654m_2(x)-6.1033C^2y^2+9.60C^2m_2(y)-1.632C^2m_4(y)\\
&\quad -5.2800C^2m_6(y)+737.66C\frac{x^3y^5}{(x^2+y^2)^4}m_4\left[\left(\frac{x^2+y^2}{2}\right)^{\frac{1}{2}}\right],\\
\mathrm{He}^4\text{:}\quad (1+C^2)\frac{E}{E_0} &= -5.4932x^2+71.3088m_2(x)-7.9346C^2y^2+32C^2m_2(y)-3.264C^2m_4(y)\\
&\quad -3.52C^2m_6(y)+2409.16C\frac{x^{9/2}y^{13/2}}{(x^2+y^2)^{11/2}}m_4\left[\left(\frac{x^2+y^2}{2}\right)^{\frac{1}{2}}\right],\\
\mathrm{H}^2\text{:}\quad (1+C^2)\frac{E}{E_0} &= -1.8310x^2+12.80m_2(x)-4.2725C^2y^2-7.0400C^2m_6(y)\\
&\quad +245.89C\frac{x^{3/2}y^{7/2}}{(x^2+y^2)^{5/2}}m_4\left[\left(\frac{x^2+y^2}{2}\right)^{\frac{1}{2}}\right].
\end{aligned} \tag{10}$$

In H^3: $x=r_0(3\mu)^{\frac{1}{2}}$, $y=r_0(3\nu)^{\frac{1}{2}}$. In He^4: $x=r_0(4\mu)^{\frac{1}{2}}$, $y=r_0(4\nu)^{\frac{1}{2}}$. In H^2: $x=r_0(2\mu)^{\frac{1}{2}}$, $y=r_0(2\nu)^{\frac{1}{2}}$.

Here E_0 is the binding energy of the deuteron, 2.17 Mev, and E the binding energy of the system associated with the wave function under consideration.[4] The expression on the right side of the equation, consequently, is positive when there is binding, and must be maximalized with respect to C, x, and y. This part of the computations must of course be performed numerically, and is greatly facilitated by the introduction of the functions $m_n(u)$, the incomplete normal moment functions, defined, for n even, as[5]

$$m_n(u)=\frac{1}{2}\frac{\int_0^u dv v^n \exp(-\frac{1}{2}v^2)}{\int_0^\infty dv v^n \exp(-\frac{1}{2}v^2)}.$$

From (10), the best values of the binding energy, expressed for each of the nuclei in units of the binding energy of the deuteron, and the corresponding values of the parameters, are given in Table I. We have included in Table I the percent of actual binding to which our extremal energies correspond, assuming the binding energies of H^3 and He^4 to be 8.3 Mev and 28 Mev, respectively. The correct value of C in the ground state of the deuteron is, according to the exact computations of Rarita and Schwinger, $C=0.197$. The calculations were performed by finding the best value of C for any pair of values of x and y, which measure the effective ranges of the S and D radial functions, and it is noteworthy that in all three nuclei

TABLE I.

	E	x	y	C	Percent binding
H^3	1.216	1.6	2.5	0.168	32
He^4	6.518	1.8	2.3	0.193	50
H^2	0.536	1.5	3.0	0.195	54

[4] We may remark that the forms of the expressions (10) show that with the introduction of tensor forces it is no longer possible to use the "equivalent" two-body method to estimate the binding energy.

[5] These functions are tabulated in the *Tables for Statisticians and Biometricians*, edited by Karl Pearson, Cambridge University Press (1914). With the aid of these tables it is possible to combine, in calculations of the sort described here, the advantages of Gaussian radial functions and square well potentials.

this best value of C was almost independent of the choice of x and y in the neighborhood of the extremum, and differed surprisingly little from the extremal value for even quite bad choices of x and y. Thus in H^3 for $x=2.2$ and $y=2.7$ the best value of C is 0.222, although this set of values fails to give any binding by 1.156 deuteron energies. By actually evaluating the analytical expressions for $\partial E/\partial x$, $\partial E/\partial y$ and $\partial E/\partial C$ from (10) and showing that these derivatives passed through zero in the immediate neighborhood of the extremal points given in Table I, it was possible to establish definitely that we had found the extremum. The variation of E with x or y is, as might be expected, a good deal more rapid than its variation with respect to C.

We have also attempted to estimate the effect on the extremal value of C of improving the radial dependence of the trial functions. That is, in the trial functions Φ_1, Φ_2, and Φ_3, we replace the single Gaussian radial function of the S terms by a sum of two Gauss functions of the form $\exp(-\frac{1}{2}\mu(\sum r_{ij}^2))+A\exp(-\frac{1}{2}\tau(\sum r_{ij}^2))$, suitably normalized, and then, retaining the previous values of x and y from Table I in the trial function, varying with respect to A, τ, and C. The new positions of the extremum, with the values of x and y fixed as in Table I, are listed in Table II. z is defined like x and y; $z=r_0(3\tau)^{\frac{1}{2}}$ in H^3, $z=r_0(4\tau)^{\frac{1}{2}}$ in He^4, $z=r_0(2\tau)^{\frac{1}{2}}$ in H^2. Finally, in the deuteron, we replaced the D radial function by the normalized form $\exp(-\frac{1}{2}\nu(\sum r_{ij}^2))+B\exp(-\frac{1}{2}\omega(\sum r_{ij}^2))$ and, with x, y, z, and A as in Tables I and II, varied with respect to B, C, and ω. The extremal values were $E=0.759$, $C=0.19$, $B=0.01$.

The results of this section seem to indicate that, as a result of the tensor spin-orbit forces S_{12}, the probability of finding either of the nuclei H^3 or He^4 in a D state is about four percent. This conclusion is supported by the very good agreement between the calculated and exact value of C in the deuteron, and by the small variation of the extremal value of C either with improvement of the trial functions or changes in x and y. We may note, however, that our attempts to improve the radial functions were much more effective in the deuteron than in either of the other two nuclei. These "radial" functions are, as we have pointed out,

TABLE II.

	E	C	A	z	Percent binding
H^3	1.477	0.15	0.05	0.8	39
He^4	6.653	0.18	0.01	1.0	52
H^2	0.742	0.17	0.10	0.6	74

angular dependent in H^3 and He^4, and the lack of comparable (to the deuteron) improvement in these nuclei is apparently due to our not having taken this angular dependence into account. As a matter of fact, it is actually true that in the deuteron a sum of two Gauss functions is a very good approximation to the S radial function, whereas in view of its omission of angular terms, such a form must be inadequate in H^3 and He^4. This inadequacy is probably more important, in explaining the relatively low binding obtained for these nuclei, than our failure to include in the trial functions those states interacting only with the D waves, and, in He^4, the states like (9) involving the pseudoscalar. Because of the smallness of the D state probability, these other states will appear with still smaller probabilities, and their neglect will not be a bad approximation. We have nevertheless quite a lot of binding to account for, in H^3 and He^4, and it is questionable whether improvement in the trial functions is all that is necessary. In this connection we may list the relative amounts of binding produced by the various terms in C in (10). That is, we may rewrite (10) as

$$\frac{E}{E_0}=\frac{S}{1+C^2}+\frac{DC^2}{1+C^2}+\frac{IC}{1+C^2},$$

where, for each nucleus, $S/(1+C^2)=S'$ is the binding of the S wave, $DC^2/(1+C^2)=D'$ the binding of the D wave, and $IC/(1+C^2)=I'$ the interaction energy of the two waves. Then, for the parameters given in Table I, with E as usual in units of E_0 we have the values given in Table III.

Table III clearly shows that the D wave, which by its interaction with the S wave, produces all the binding in the deuteron, is much less effective in binding the heavier H^3 and He^4. The 35 percent reduction in the depth of the ordinary potential well which the presence of the tensor force requires in the deuteron, reduces

TABLE III.

	S'	D'	I'	E
H^3	0.166	−0.983	2.033	1.216
He^4	4.976	−1.076	2.618	6.518
H^2	−1.022	−1.508	3.066	0.536

by an even larger percentage the S wave binding in H^3 and He^4, because this binding is the small difference between the kinetic and potential energies of the S state. Consequently, unless the variation approximation is, in H^3 and He^4, very much worse for the D than for the S wave, the binding energies of these nuclei predicted by (1) must be less than the known experimental values. All these results have of course been obtained with the interaction in the form (1); the justifications for its use are its success in the deuteron system and its simplicity, which reduces the amount of calculation required. This simplicity consists largely in the omission of space exchange operators, a matter which is of no consequence in the deuteron, but can influence the energies of the states in H^3 and He^4. However, the substitution of exchange forces for the ordinary forces in (1) can only reduce the binding. Furthermore, the neglected forces are known to be principally of the Majorana type, and because of the symmetry of the S waves in our trial functions, the substitution of Majorana forces for the ordinary forces in (1) can only cause a reduction in the D wave binding of our trial function, i.e., a decrease in D' in Table III. These considerations just correspond to the well-known fact that in the calculation of the binding energies of H^3 and He^4 in the absence of spin-orbit coupling forces, the substitution of Majorana for ordinary forces is a good approximation. In other words, while the omission of space exchange forces in (1) may affect our numerical value of the amount of D state admixture in H^3 and He^4, it seems to be a justifiable conclusion from our calculations that a simple linear combination of the S_{12}, Majorana, Heisenberg, Wigner, and Bartlett forces operating through similar potentials of the same range in a symmetric Hamiltonian probably cannot account for slow neutron-proton scattering, the properties of the deuteron, and the binding energies of H^3 and He^4.

We wish to stress that, because of the incomplete character of the variation calculation, the conclusions of this section must be considered somewhat speculative. These conclusions could have been made more precise by carrying the variation to a definite completion, but in view of the fundamental theoretical uncertainty in the very form of the neutron-proton interaction, the amount of computational labor which such a calculation would require would scarcely be justified. Our results support the view that the successful introduction of the tensor forces into the two-body interaction will require the assumption of different ranges for the spin-orbit coupling and conservative forces. There exist, however, limitations on the range of the tensor force,[6] and the possibility that many-body forces may be necessary cannot be overlooked. We should like finally to express our thanks to Professor J. R. Oppenheimer for his interest in this work.

[6] J. Schwinger, Phys. Rev. **60**, 164A (1941).

Precise Determination of the Fine Structure Constant from X-Ray Spin Doublet Splitting[1]

R. F. CHRISTY[2] AND J. M. KELLER[3]
Department of Physics, University of California, Berkeley, California

(Received December 17, 1941)

Corrections to the Sommerfeld formula for the L_{II}–L_{III} x-ray spin doublet splitting, to take into account departures from a pure Coulomb field for heavy elements caused by interactions between electrons, are calculated by using Dirac wave functions for a Coulomb field and calculating, with all relativistic corrections, the terms in the electron interaction of order e^2, i.e., of relative order $1/Z$, compared to the Sommerfeld splitting. The result is applied to experimental data for elements varying from $Z=60$ to $Z=92$, to obtain a direct experimental value for the fine structure constant. By the method of least squares, we find $1/\alpha=\hbar c/e^2=136.93$ with an estimated *limit* of error of 0.18.

INTRODUCTION

IN view of the discrepancy that has existed between different determinations of the various fundamental atomic constants, as well as because of the interest attached to the value of the fine structure constant, $\alpha=e^2/hc$, it has again seemed desirable to attempt a precise determination of this quantity from experimental data. One might hope to use for this purpose a measurement of the fine structure of the hydrogen atom spectrum. But as is well known, difficulties of resolving the small splitting, of the same order as the line breadths, as well as theoretical uncertainties in its interpretation, do not permit a precise evaluation. The splitting, however, becomes very much greater for the heavier atoms, varying roughly as the fourth power of the atomic number; and, as we shall see, the uncertainties of quantum electrodynamics do not here play a decisive role.

The well-known relativistic formula for the energy levels of an electron in a Coulomb field of charge Ze, where e is the charge on the proton, is

$$E=mc^2/[1+(\alpha Z)^2/(n'+\gamma)^2]^{\frac{1}{2}}, \qquad (1)$$

where E is the total energy (including rest energy), n' is the radial quantum number, $\gamma=[k^2-(\alpha Z)^2]^{\frac{1}{2}}$, $|k|=j+\frac{1}{2}$, j is the total angular momentum, and m and c have their usual meanings. Thus the difference in energy of the L shell levels ($2p_{1/2}$ and $2p_{3/2}$) is

$$E(2p_{3/2})-E(2p_{1/2})=mc^2\{\tfrac{1}{2}[4-(\alpha Z)^2]^{\frac{1}{2}} -\tfrac{1}{2}[2+2[1-(\alpha Z)^2]^{\frac{1}{2}}]^{\frac{1}{2}}\} \qquad (2)$$
$$=mc^2S(\alpha Z),$$

which we shall refer to as "the Sommerfeld formula."[4]

About two years ago, R. T. Birge[5] suggested that one could take advantage of this greatly magnified "fine structure" in the heavier elements to determine an accurate value for the fine structure constant. At that time he assembled data on the splitting of the x-ray spin doublets (L_{II} and L_{III} levels) as obtained from several different x-ray lines, and from elements varying in atomic number from $Z=29$ to 92. He showed that these data formed a body of material of sufficient accuracy and consistency for such a determination.

However, in interpreting the experiments, it was clearly not adequate to consider the field in which one of the electrons of a heavy atom finds itself as just the Coulomb field of the nucleus. One could get around this difficulty in a rather unsatisfactory manner by introducing a screening constant s, defined in such a way that the level splitting is given by $S[\alpha(Z-s)]$. One

[1] A brief report of this work has been given previously—R. F. Christy and J. M. Keller, Phys. Rev. **58**, 658 (1940). Certain additions and corrections to the original calculations have been made in the present paper.

[2] Now at Illinois Institute of Technology, Chicago, Illinois.

[3] Now at Washington University, St. Louis, Missouri.

[4] First derived by Sommerfeld from the Bohr theory. See A. Sommerfeld, *Atomic Structure and Spectral Lines* (Methuen, 1934).

[5] R. T. Birge, Phys. Rev. **55**, 1119 (1939).

expects that the electrons in the K shell will be quite efficient at screening the nucleus from the L shell, that the electrons of the L shell will partially screen the nuclear field from each other, and that electrons of the outer shell will be successively less significant, until a point is reached beyond which the addition of further outer electrons has no appreciable effect. The value of the screening constant calculated from the experiments was about 3.5 for the heaviest atoms, and did not vary appreciably with atomic number above about $Z=60$. The value of s, and its dependence on Z, were altered when one used different values of α in the determination of $S[\alpha(Z-s)]$. This was roughly what one would expect.

But this approach is unsatisfactory for several reasons. In the first place, the field that acts on electrons in a heavy atom is certainly not a pure Coulomb field, and use of an uncalculable screening constant to correct for this circumstance is unsatisfactory. Furthermore, an increase in the nuclear charge itself produces a distortion in the charge and current distribution of the electrons, and not just a change of scale. This is true even if the field is considered as that of a Coulomb potential, provided one takes into account relativistic effects. (The Sommerfeld splitting is a manifestation of this distortion in the $2p$ electrons alone.) The wave functions of the several states are functions of αZ, entirely apart from any screening.

The essential point is that we must distinguish between two distinct parameters which occur in the problem. One is the atomic number Z; this parameter tells us the number of electrons in an atom, rough values of the mean radii, and energies of the several states, and in general it may appear in connection with those aspects of the problem that are essentially non-relativistic. In the present calculation, $1/Z$ will be treated as a small number. The other parameter involved is $\alpha Z=Ze^2/\hbar c$. This quantity indicates the extent to which relativistic effects are significant; for the present problem, it cannot be considered small, for it is actually of order $\frac{1}{2}$.

To illustrate this point, we make an expansion of $S[\alpha(Z-s)]$ in terms of these two parameters

$$
\begin{aligned}
&S[\alpha(Z-s)] \\
&=\left[\frac{1}{32}(\alpha Z)^4+\frac{5}{256}(\alpha Z)^6+\frac{53}{4096}(\alpha Z)^8+\cdots\right] \\
&\quad-\frac{s}{Z}\left[\frac{4}{32}(\alpha Z)^4+\frac{30}{256}(\alpha Z)^6\right. \\
&\qquad\qquad\left.+\frac{424}{4096}(\alpha Z)^8+\cdots\right] \qquad (3) \\
&\quad+\left(\frac{s}{Z}\right)^2\left[\frac{6}{32}(\alpha Z)^4+\frac{75}{256}(\alpha Z)^6+\cdots\right] \\
&\quad-\left(\frac{s}{Z}\right)^3\left[\frac{4}{32}(\alpha Z)^4+\cdots\right]+\cdots.
\end{aligned}
$$

The first line of Eq. (3) is just the Sommerfeld formula $S(\alpha Z)$. The supposition that s approaches a constant value, as one approaches the larger values of Z, imposes an unnecessary restriction on the form of the higher order terms as functions of αZ.

We wish to make a theoretical calculation to replace Eq. (3) for the spin doublet splitting in elements of large atomic number. The effect of the electrons in the atom on the splitting will be of order $1/Z$ compared to that of the nuclear charge Ze. Hence we can calculate this effect by perturbation theory. The first-order term will correspond to the second line in Eq. (3). But we may obtain this term to an arbitrary accuracy, both in magnitude and in its functional dependence on αZ. In the higher order terms in $1/Z$, only the lowest term in αZ could in principle be determined by higher order perturbation calculation. Further terms in αZ cannot be so determined because of fundamental limitations of present quantum-electrodynamic theory. But these terms are of order α^2 times the splitting and are negligible. Actually we shall not calculate the coefficient even of the leading terms in αZ of the second and higher order perturbation terms, but consider it sufficient to introduce coefficients that will be determined by fitting the experimental data.

CALCULATION OF THE FIRST-ORDER PERTURBATION

For unperturbed wave functions, we consider the individual electrons each in a Coulomb potential of charge Ze, independent of the presence of the other electrons. This leads to the well-known Dirac wave functions for a Coulomb field. The effect of the interactions of the electrons among themselves we consider as a perturbation and calculate to first order. For this purpose we use the Breit Hamiltonian interaction

$$\frac{e_i e_j}{|r_{ij}|}-\frac{1}{2}\left[\frac{\boldsymbol{\alpha}_i\cdot\boldsymbol{\alpha}_j}{|r_{ij}|}+\frac{(\boldsymbol{\alpha}_i\cdot\mathbf{r}_{ij})(\boldsymbol{\alpha}_j\cdot\mathbf{r}_{ij})}{|r_{ij}|^3}\right], \tag{4}$$

where r_{ij} is the displacement between points i and j, and the $\boldsymbol{\alpha}$'s are the Dirac current operators. The Breit Hamiltonian was originally derived from classical electrodynamics[6] as a quasi-static approximation, by keeping terms in the energy of order $(v/c)^2$. The two terms in Eq. (4) correspond, of course, to the electrostatic repulsion, and to magnetic and retardation effects, respectively. (When the divergence of the current vanishes, the second term reduces to the Biot-Savart law.)

The Breit Hamiltonian can also be obtained from quantum electrodynamics.[7] The magnetic contribution results from a second-order perturbation calculation involving the emission and absorption of (virtual) quanta. The energy denominators that occur contain the energy of the quanta and the difference in energy between the interacting states of the electrons involved. Again, to obtain a quasi-static approximation, the latter energy difference is neglected. This results in an expression that can be represented as an interaction in configuration space, as above. For any *particular* pair of states, the magnetic interaction can be expressed in configuration space without this approximation, but it contains explicitly the energy difference involved. One can make an expansion in powers of $\epsilon r/\hbar c \sim v/c \sim \alpha Z$, where ϵ is this energy difference. The first term gives the magnetic interaction as in the Breit formula. Higher terms have been neglected in the main part of the calculations, and their effect is subsequently introduced as a correction and in the estimate of error.

We have both direct and exchange interactions to consider. As we are interested not in the actual energy levels of the (excited) atoms, but only in the difference in energies for atoms in the cases of a $2p_{1/2}$ electron or a $2p_{3/2}$ electron missing, it is not necessary to calculate the interaction energies of all pairs of electrons, but only of a $2p$ electron with other electrons. We take advantage of the spherical symmetry of subshells to calculate the interaction on a $2p$ electron of complete subshells. (By a subshell we mean all those electrons of a particular orbital and total angular momentum in a particular shell—for example the two $2s$ electrons.) We do this even in calculating the interaction of, for instance, three $2p_{3/2}$ electrons on the fourth (missing) electron of that subshell. Including this "phantom" electron in the calculations actually makes no difference, as the addition to the direct integral will just be cancelled by the addition to the exchange integral.

The Dirac wave functions are products of spherical harmonics, exponentials in the radius, and polynomials in powers of the radius. Using the expansions of $1/|r_{ij}|$ and $1/|r_{ij}|^3$ in terms of r_s/r_g and spherical harmonics of the angular coordinates of the separate electrons (where r_s and r_g are, respectively, the smaller and greater of r_1, r_2), we can reduce the integrals to products of angle and radial integrals. The former are just products of spherical harmonics. Taking the polynomials in the wave functions term by term, we can evaluate the radial integrals in terms of gamma-functions and hypergeometric functions. The resulting expressions are, however, very complicated and unilluminating, and in order to use them, we have calculated their value numerically for six values of αZ, including $\alpha Z=0$. The values of αZ were chosen rather arbitrarily, to simplify the numerical work as much as possible, and to cover fairly smoothly the region in which data exist.

The numerical results for the largest value of αZ used are given in Table I. All numerical values given are energies of interaction of a $2p_{1/2}$ or a $2p_{3/2}$ electron with a complete subshell, and in units $Ze^2/a=mZe^4/\hbar^2$ where a is the Bohr radius. Electrostatic and magnetic parts of the

[6] G. Breit, Phys. Rev. **34**, 553 (1929).
[7] J. R. Oppenheimer, Phys. Rev. **35**, 461 (1930).

TABLE I. Interaction energies (in units $Ze^2/a = mZe^4/\hbar^2$) between various subshells and a $2p_{1/2}$ or $2p_{3/2}$ electron, for $[1-(\alpha Z)^2]^{\frac{1}{2}} = 0.76$, $(\alpha Z \sim 0.65)$.

Subshell	$2p_{1/2}$	$2p_{3/2}$	Difference
Electrostatic direct interaction			
$1s$	0.64192	0.51552	0.12640
$2s$	0.39988	0.36876	0.03112
$2p_{1/2}$	0.46014	0.41311	0.04702
$2p_{3/2}$	0.82623	0.76061	0.05562
$3s$	0.20613	0.19861	0.00752
$3p_{1/2}$	0.22651	0.21640	0.01011
$3p_{3/2}$	0.41345	0.39792	0.01553
$3d_{3/2}$	0.46181	0.45312	0.00869
$3d_{5/2}$	0.66454	0.65408	0.01046
Electrostatic exchange interaction			
$1s$	−0.01796	−0.01498	−0.00298
$2s$	−0.03227	−0.03426	0.00199
$2p_{1/2}$	−0.23007	−0.01716	−0.03890
$2p_{3/2}$	−0.03432	−0.20833	
Magnetic exchange interaction			
$1s$	0.02773	0.00998	0.01776
$2s$	0.00192	−0.00095	0.00287
$2p_{1/2}$	0.00725	0.00170	0.00556
$2p_{3/2}$	0.00339	0.00960	−0.00621
Total			0.30256

interaction are treated separately. Magnetic direct integrals all vanish identically. This corresponds to the fact that there is no net current from a closed subshell. The values for $\alpha Z = 0$ (non-relativistic limit) are just those calculable from Schroedinger wave functions. One sees, even though the electrostatic interactions are larger than the energies due to currents by order $(c/v)^2$, that the contributions to the differences for the two cases of a missing $2p_{1/2}$ or $2p_{3/2}$ electron are *roughly* of the same order of magnitude. This is of course due to the complete cancellation in the non-relativistic limit of the electrostatic terms.

Nevertheless, one sees that the dominant effects are the contributions of the electrostatic direct integrals. Furthermore, these contributions are always in a direction to decrease the splitting predicted by the Sommerfeld formula. Except in the case of the $2p$ subshells, the electrostatic exchange energies are of the order of a twentieth of the direct terms. Because the exchange effects for the $2p$ subshells involve the interaction of these subshells with electrons missing from one of the states of the same subshell, we expect their contribution to be large and of the same order as the direct integrals. Current effects are also small, being roughly a tenth of the corresponding electrostatic direct terms.

It is not practicable to carry to completion an asymptotic calculation of this type, where effects of successive shells of electrons are taken into account one by one. One continues the calculation to the point beyond which the remainder seems negligible. Accordingly, we have included direct interactions of the K, L, and M shells, and exchange interactions of the K and L shells. The numerical values of these interactions suggest that the still uncalculated contributions are perhaps one percent of the total first-order term. Actually, a fairly careful estimate of the contribution of the N shell direct integrals leads to a value about 0.2 percent of the previously calculated interaction. A comparison of the non-relativistic values of the M shell electrostatic exchange with the corresponding direct integrals indicates that the contribution of the former is ~ 0.5 percent of the total first-order term.

In any case, the neglect of these outer shell electrons certainly will not alter significantly the shape of the first-order term as a function of αZ: at most this value will slightly change its magnitude. Hence we will take for the total first-order perturbation term W the sum of the parts already calculated. W is tabulated in Table II. We later consider the error produced by multiplying W by a factor to allow for its estimated error.

There is also a correction to the calculations due to the approximate nature of the Breit Hamiltonian. As mentioned above, the Breit Hamiltonian actually represents just the first term of an expansion in powers of $\epsilon r/hc \approx v/c$. To determine the magnitude of the error introduced, we have calculated the effect of the next term in the interaction of the $1s$ electrons with a $2p_{1/2}$ or $2p_{3/2}$ electron. This should be by far the largest part of the neglected effect, because of the large kinetic energy of the K shell electrons. For $\gamma = 0.76$, $(\alpha Z \sim 0.65)$ we thus find a change in the original calculation of energy difference by 0.00317 in units $mZe^4/\hbar^2$.

TABLE II. Calculated correction to the Sommerfeld formula, $W(\alpha Z)$, in units $Ze^2/a = mZe^4/\hbar^2$.

$[1-(\alpha Z)^2]^{\frac{1}{2}}$	Z (approx.)	$W(\alpha Z)$
1.00	0	0.00000
0.96	38	0.03995
0.91	57	0.09508
0.86	70	0.15666
0.82	78	0.21110
0.76	89	0.30256

DETERMINATION OF α FROM EXPERIMENTAL DATA

We now wish to compare our calculation with the observed x-ray spin doublet splittings ($\Delta\nu$), and from this to obtain a value for α. To do this, we write in analogy with Eq. (3)

$$h\Delta\nu = mc^2 S(\alpha Z) - W(\alpha Z) + O(1/Z^2). \quad (5a)$$

$S(\alpha Z)$ is the Sommerfeld formula, Eq. (2), for the splitting in a pure Coulomb field. $W(\alpha Z)$ is the correction of order $1/Z$ that we have calculated. The dependence of the $1/Z^2$ and higher terms as functions of (αZ) is as $(\alpha Z)^4$ and higher powers. The present state of quantum-electrodynamic theory does not justify an attempt to calculate functional dependence of these higher order terms. But their effect must be small, and we shall include just the term $(mc^2/Z^2)(\alpha Z)^4$, multiplied by an arbitrary constant. We can write

$$W(\alpha Z) = (mZe^4/h^2)(\alpha Z)^2 f(\alpha Z) = (mc^2/Z)(\alpha Z)^4 f(\alpha Z). \quad (6)$$

$f(\alpha Z)$ is a quantity that approaches a constant value, as αZ approaches zero. To eliminate the quantities h, e, and m, where they occur explicitly in this relation, we introduce the Rydberg constant R. The value of R is known experimentally to a precision considerably higher than the uncertainties in h, e, and m, and there seems to be no reason to doubt the correctness of the relation

$$R = 2\pi^2 me^4/h^3 = \alpha^2 mc^2/2h. \quad (7)$$

Hence we reformulate the connection between the doublet splitting $\Delta\nu$ and the fine structure constant α by the expression

$$\Delta\nu/R = (2/\alpha^2) S(\alpha Z) - 2\alpha^2 Z^3 f(\alpha Z) + B_1 \alpha^2 Z^2. \quad (5b)$$

α appears in this expression in several ways. In the third term of the right-hand side, α^2 appears multiplied by an undetermined constant. We can absorb our ignorance of the precise value for α in that of the constant, writing as a single constant to be determined, $B = B_1\alpha^2$. α also appears in the argument of the first two terms on the right-hand side of Eq. (5b). These terms we treat in the familiar way, by expanding about an approximate value of α and neglecting second and higher derivatives. We use the value $1/\alpha_0 = 137$. Finally

$$\frac{\Delta\nu}{Z^4 R} - \frac{2}{\alpha_0^2 Z^4} S(\alpha_0 Z) + \frac{2\alpha_0^2}{Z} f(\alpha_0 Z) = \left[\frac{4}{\alpha_0 Z^4} S(\alpha_0 Z) - \frac{2}{\alpha_0 Z^3}\frac{d}{dZ} S(\alpha_0 Z) + \frac{4\alpha_0^3}{Z} f(\alpha_0 Z) + 2\alpha_0^3 \frac{d}{dZ} f(\alpha_0 Z)\right] \Delta\left(\frac{1}{\alpha}\right) + \frac{B}{Z^2}. \quad (8)$$

Equation (8) differs from Eq. (5b) by a factor of $1/Z^4$. This makes the two sides of Eq. (8) roughly independent of Z, and gives the observations of $\Delta\nu/R$ for different elements and the same *a priori* weights roughly equal influence in determining the best value of $\Delta(1/\alpha)$. $W(\alpha Z)$, and hence $f(\alpha Z)$, was obtained by fitting a power series in (αZ) to the six calculated values (Table II). A correction was then applied to W for terms of order $(v/c)^4$ in the interaction energy between electrons. This correction to the Breit Hamiltonian contributes to Eq. (5b) a term of order $(mc^2/Z)(\alpha Z)^6$. Thus such a term, whose magnitude calculated for the K shell is 0.0178 $(mc^2/Z)(\alpha Z)^6$, was added to the initially calculated value of W.[8]

Professor Birge kindly supplied us with his

TABLE III. Experimental data. (These data were compiled, and kindly given to us, by R. T. Birge. They are based on the value, $R = 109737$.)

Z	$\Delta\nu/R$ (grating scale)	Weight	Z	$\Delta\nu/R$ (grating scale)	Weight
60	37.74799	148	74	98.34305	228
62	43.91743	92	75	104.68251	216
63	47.11417	90	76	111.06647	126
64	50.55852	90	77	118.30763	208
65	54.28796	90	78	125.67344	198
66	58.20409	110	79	133.39571	228
67	62.15851	110	80	141.73230	106
68	66.66333	110	81	150.07457	228
69	71.14493	110	82	159.21877	198
70	76.08290	110	83	168.48213	216
71	81.23862	142	90	249.60507	208
72	86.71362	110	91	263.14925	120
73	92.30472	228	92	277.73164	228

[8] Another effect that alters the splitting of the $2p$ levels is the modification of a Coulomb field at distances from the nucleus of order $\hbar/mc$, due to virtual creation of positrons (polarization of the vacuum). This correction to the energy difference is approximately $(1/160\pi)(mc^2/Z)(\alpha Z)^7$, and is too small to alter appreciably our calculated value of α. The interaction between atomic electrons is not affected by negative energy states to this order of perturbation ($1/Z$ or α).

values of $\Delta\nu/R$ compiled from experiments on the doublets from many different x-ray lines, and weighted according both to the number of lines entering into the determination of each value of $\Delta\nu/R$, and to the *a posteriori* consistency of each line used. Values of $\Delta\nu/R$, and of the corresponding weights, are compiled in Table III for the range of atomic number used (26 elements, running from $Z=60$ to $Z=92$). These values have been converted from the conventional Siegbahn scale, on which all experimental results are published, to the presumably true values of the so-called grating scale of wave-lengths, by the use of the factor $\lambda_g/\lambda_s=1.002034$.

Finally, the values of $\Delta(1/\alpha)$ and of B were found from these data by a least-square calculation, based directly on Eq. (8). The values obtained are $\Delta(1/\alpha)=-0.072$, $B=4.858\times10^{-4}$. The statistical probable error in the determination of $\Delta(1/\alpha)$ is 0.034. These results give $1/\alpha=136.928\pm0.034$.

The determination of the $f(\alpha Z)$, the correction of order $1/Z$ to the spin splitting, is incomplete due to our neglect of outer shells. We have estimated that this incompleteness might falsify the magnitude of f by not more than one percent, which would produce a change in $1/\alpha$ of 0.081. Adding three times the statistical probable error to this gives a figure of 0.18 for the limit of error on $1/\alpha$. Hence we conclude that the value of $1/\alpha$ is 136.93, correct to within 0.18.

We gratefully acknowledge our indebtedness to Professor J. R. Oppenheimer for suggesting this problem, and for pointing out the method of calculation. We also wish to express our gratitude to the National Youth Administration for furnishing assistance in the numerical calculations.

FEBRUARY 1 AND 15, 1942 PHYSICAL REVIEW VOLUME 61

The Mean Life of Neutrons in Water and the Hydrogen Capture Cross Section

J. H. MANLEY, L. J. HAWORTH, AND E. A. LUEBKE
Department of Physics, University of Illinois, Urbana, Illinois

(Received September 22, 1941)

Direct observations of the time variation of slow neutron density in a large volume of water during and after irradiation by neutrons from the D−D reaction have been made. An exponential growth and decay is found. From an analysis of these data and data on the spatial density distribution which determines the effect of diffusion, the mean life of neutrons in water was found to be 205 ± 10 microseconds. This leads to a cross section of 0.33×10^{-24} cm² for the capture of slow neutrons by hydrogen.

CONTROL of the ion beam responsible for neutron production from an artificial neutron source makes it possible to observe transient neutron phenomena. One such phenomenon is the time rate of change of neutron density in hydrogenous material. In water, for example, this depends on the probability of neutron escape from the surfaces, the loss by capture and the distribution of sources. For pure water, in which the capture is chiefly due to hydrogen nuclei, suitable measurements will lead to the capture probability and hence to the hydrogen capture cross section.

Baker and Bacher[1] have observed the mean life of neutrons emerging from a paraffin block after the source has been removed. The effect of diffusion, however, complicates considerably the proper interpretation of such data. The analysis is more straightforward if the time variation of neutron density is obtained in a region where the effect of diffusion can be evaluated.

Previous results on the mean life of neutrons in paraffin and water vary from 170 to 270 microseconds[2,3] although the hydrogen density, which is the important factor, varies by only about 30 percent. Such a fundamental quantity as the cross section for the $n+p\rightarrow d$ reaction

[1] C. P. Baker and R. F. Bacher, Phys. Rev. **59**, 332 (1941).

[2] E. Amaldi and E. Fermi, Phys. Rev. **50**, 899 (1936).

[3] O. R. Frisch, H. v. Halban, and J. Koch, Proc. Danske Vidensk. Selskab **15**, 10 (1938).

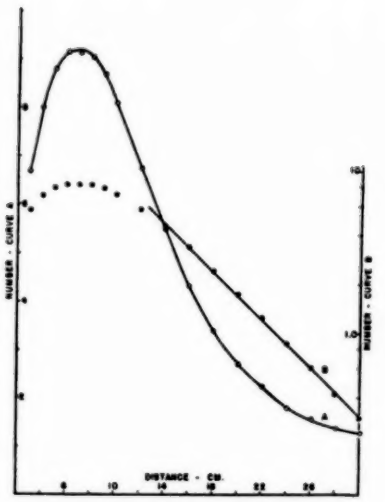

FIG. 1. Neutron density as a function of distance from target side of the tank. The center of the tank is at 22 cm. Curve A is an ordinary plot to show the point of inflection at 12 cm. Curve B is a logarithmic plot of the same data. The solid line is the function $n=n_0e^{-0.173x}$. Approximately 20,000 counts were taken for each point.

warrants more precise determination. An investigation with an intermittent neutron source was, therefore, undertaken.

The neutron source, method of control, and recording circuits have been described previously.[4,5] Bursts of fast neutrons from the D−D reaction were used to irradiate a cylindrical tank of water 44 cm in diameter by 54 cm high. The tank was located so that the center of its vertical axis was approximately 60 cm from the target of the accelerating tube and in the same horizontal plane. A cylindrical BF_3 proportional counter (sensitive volume 2 cm in diameter by 5 cm long) was supported with its axis vertical by a small copper tube so that it could be moved in the median plane of the tank. The total absorption of the counter itself was measured and found to be equivalent to 90 cc of water, only slightly more than the displacement of the counter. The amplified pulses from this counter, appearing on an oscilloscope screen[5] with a suitable time scale, were photographed in order to record their time distribution. The tank, which was paraffin-lined to prevent solution of metallic ions, contained 85.6 liters of distilled water.

[4] J. H. Manley, L. J. Haworth, and E. A. Luebke, Rev. Sci. Inst. **12**, 587 (1941).
[5] L. J. Haworth, J. H. Manley, and E. A. Luebke, Rev. Sci. Inst. **12**, 591 (1941).

In order to obtain the effect of diffusion, neutron densities at different points in the tank must be known. Measurements of this distribution were made for the steady state case. The neutron density along a line from the target to the center of the tank is shown by curve A of Fig. 1. Distances are measured from the side of the tank nearest the target. Curve B is a logarithmic plot of the same data to indicate that near the center of the tank, $x=22$ cm, the experimental points follow the curve $N=N_0e^{-0.173x}$. Measurements in planes perpendicular to this line reveal that over several diffusion lengths from it the density is essentially constant. It will, therefore, be possible to apply the one-dimensional diffusion equation to the data of Fig. 1.

It is possible to obtain the desired information on the effect of capture and diffusion by observation at a single space point of either the growth of neutron density during irradiation or the decay after irradiation. The size of the oscilloscope screen and considerations of ease of counting the recorded neutron pulses made it more feasible to observe the growth and decay in separate experiments with an overlap for correlation. Since this was done at three space points, $x=12$, 14, and 22 cm, there are six independent observations. Irradiation occurred cyclically with a time of irradiation sufficient to reach saturation and a lapse long enough to eliminate any measurable carry-over of neutrons to the next cycle. The number of counts in each 50-microsecond time interval was summed over a large number of cycles. A typical composite growth and decay curve is shown in Fig. 2.

Determination of the saturation value neces-

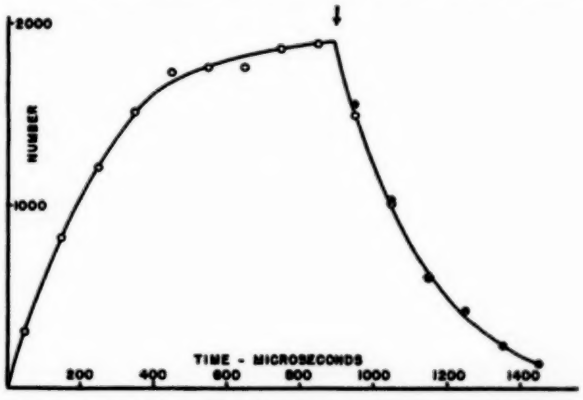

FIG. 2. A typical growth-decay curve. The arrow indicates the end of irradiation.

sary for the analysis of the growth curve introduced additional error which does not enter the analysis of the decay curve. Even though the statistical accuracy was good on the points near saturation the high density of pulses on the recording film increased the probability of missing them in the counting process. The decay data were, therefore, considered more reliable even though growth data are in satisfactory agreement. Exponential plots[6] of the decay data at three different space points are shown in Fig. 3. For the reason mentioned above the highest points were not given as much weight in determining the best straight line representing the data. As is to be expected, the observed mean life as given by the curves of Fig. 3 depends on the position at which the measurements were made. If the effect of diffusion at these positions can be evaluated, the mean life due to capture alone can be obtained from each set of data.

Reduction of the diffusion problem to one dimension has already been experimentally justified. For the general case of a neutron density $N(x, t)$ resulting from a distribution of sources producing $\rho(x, t)$ neutrons per second

$$dN/dt - Dd^2N/dx^2 + N/\tau = \rho(x, t). \quad (1)$$

τ is the mean life for capture and D the diffusion coefficient. A solution of this equation appropriate to the case in which the source is removed at $t=0$ leaving a spatial distribution $N(x)$ is

$$N(x, t) = \frac{e^{-t/\tau}}{2(\pi Dt)^{\frac{1}{2}}} \int_{-\infty}^{\infty} dx' N(x') \times \exp\left[-\frac{(x'-x)^2}{4Dt}\right]. \quad (2)$$

In order to investigate the behavior of $N(x, t)$ for a general $N(x')$ we note that the integrand has a saddle point for a particular x'

$$x'_0 = 2Dtf' + x \quad \text{where} \quad f = \log N.$$

Then

$$N(x, t) = Ne^{-t/\tau - Dtf'^2}/(1-2Dtf'')^{\frac{1}{2}} \quad (3)$$

in which N and its derivatives are to be evaluated at x'_0. The result is valid if

$$f'''(2Dt)^{\frac{1}{2}}/(1-2Dtf'')^{\frac{1}{2}} \ll 1$$

and if higher derivatives of f are negligible at x'_0.

[6] Similar plots were obtained for the growth.

It is clear that for sufficiently long times the error function in (2) will be of so great a width as to make higher derivatives of f important; under these conditions (3) will be only approximately valid. The observations actually included points for which (3) could not be used; for these cases numerical integration of (2) gave results which differed appreciably from the approximate ones obtained by the saddle point method.

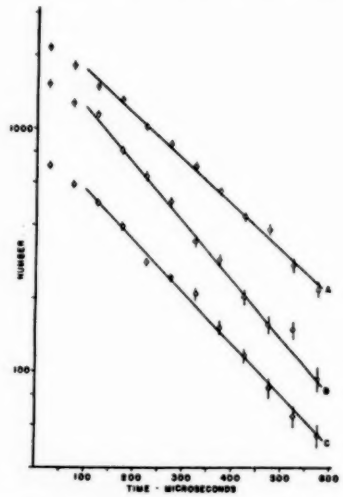

FIG. 3. Exponential decay curves after irradiation. Curve A was taken at $x=22$ cm; Curve B at $x=12$ cm; Curve C at $x=14$ cm.

Since x enters (3) only implicitly through x'_0 we expand $N(x'_0)$ and its derivatives, and again neglect higher orders than the second. Then

$$N(x, t) = \frac{N(x)}{(1-2Dtf'')^{\frac{1}{2}}} \times \exp\left\{-t/\tau - Dt\left[f'^2 - \frac{2f'^2}{1-2Dtf''}\right]\right\}$$

$$\simeq N(x) \exp\{-[1/\tau - D(f'^2+f'')]t\}$$

$$= N(x) \exp\left\{-\left[1/\tau - D\frac{N''}{N}\right]t\right\} \quad (4)$$

if $2Dtf'' \ll 1$. $N(x)$ is the observed spatial distribution at $t=0$. As would be expected, diffusion effects would vanish if the time dependence of $N(x, t)$ were observed at a point for which N'' and all higher derivatives vanish.

This analysis applies equally well to the rise of neutron density during irradiation. Let us consider a steady-state spatial distribution resulting from distributed sources which are con-

stant in time. Then it can be shown in a very general way, including the effects of diffusion and capture, that the rise to this steady state as a function of space and time is the same as the fall from the steady state when the sources are removed.

To correct the observations for the effect of diffusion, the coefficient D must be known. This may be computed from the kinetic theory value, $D=\frac{1}{3}\lambda\bar{v}$. A value of 2.2×10^5 cm/sec. for $\bar{v}$ has been chosen although there is some indication that this may be too low. Different experiments on the mean free path, λ, are not in complete agreement. Goldhaber and Briggs[7] give $\lambda=2.5$ mm in paraffin and find the scattering per hydrogen atom to be the same in water within 2 percent. This would lead to $\lambda=3.0$ mm for H_2O. Brickwedde, Dunning, Hoge, and Manley[8] have measured the scattering of H_2O directly with a geometrical arrangement very similar to that of Goldhaber and Briggs. Their results give $\lambda=3.35$ mm. With 3.2 mm as an average of these two results, $D=2.4\times10^4$ cm^2/sec. The effect of diffusion on the observed time dependence of the neutron density at various positions may be found by application of Eq. (2) or (4).

At the 12-cm position for which $N''=0$, Eq. (4) predicts no diffusion correction. However, since $f''\backsimeq-0.01$ cm^{-2}, (4) is not valid for times after irradiation greater than 200 μsec. Numerical integration of (2) for different values of t reveals that, in the range of measurement, $e^{-t/\tau}$ is multiplied by a slowly varying linear function of time. This function may accordingly be represented by e^{at}. For this position, $a=-200$ sec.$^{-1}$ rather than zero as predicted by (4). A similar situation exists at $x=14$ cm except that $a=50$ sec.$^{-1}$.

Since the spatial distribution on either side of $x=22$ cm is rather accurately given by $N=N_0e^{-0.173x}$ for which $f''=0$, Eq. (4) would yield $a=DN''/N=720$ sec.$^{-1}$ for this position. A check numerical integration of (2), however, gives $a=600$ sec.$^{-1}$. This integration reveals that for $t=500$ μsec. the width of the error function of (2) is such that values of $N(x)$ outside the region of validity of the exponential contribute to the integral. The experimental points in this region lie below the exponential and, therefore, a lower value of a is obtained. This means that this deviation which starts at $x=14$ cm affects the observations at $x=22$ cm through higher derivatives at this point which are not negligible. The saddle point integration used in obtaining (4) is, therefore, a poor approximation for such times. The complete results are summarized in Table I.

TABLE I. Data on mean life of neutrons.

Position (x) cm	12	14	22
Observed mean life (growth), μsec.	180	195	214
Observed mean life (decay), μsec.	182±9	202±12	240±9
Reciprocal mean life, observed, sec.$^{-1}$	5500	4950	4180
Diffusion correction a, sec.$^{-1}$	−200	50	600
Corrected mean life, μsec.	189±10	200±12	209±9

The maximum diffusion correction is 15 percent, and errors in the coefficient are, therefore, relatively unimportant. They show that for $x=14$ cm there is almost no net diffusion while at 12 cm diffusion removes neutrons from this position and at 22 cm there is an inflow. From the geometrical arrangement the small, neglected curvature in other directions would be negative, corresponding to a removal of neutrons, and more important at smaller x. This may account for the trend in the results for the mean life, in which case the 22-cm value of $\tau=209$ μsec. would be more reliable. However, to within 5 percent we may take $\tau=205$ μsec. as a weighted mean.

The capture cross section is related to the mean life or the reciprocal capture probability by

$$1/\tau=P=n\sigma\bar{v}.$$

It may be assumed that σ is proportional to $1/v$ so the capture probability becomes independent of velocity. The average cross section, when we take $\bar{v}=2.2\times10^5$ cm/sec. and the above mean life, is 0.33×10^{-24} cm^2, the largest uncertainty being in $\bar{v}$. The capture cross section of oxygen which is less than 3 percent of this value has been neglected.

Financial assistance from the Graduate School Research Board of the University is gratefully acknowledged. We are indebted to Professor R. Serber and Dr. S. M. Dancoff for discussion of several aspects of this problem.

[7] M. Goldhaber and G. H. Briggs, Proc. Roy. Soc. **162**, 127 (1937).

[8] F. G. Brickwedde, J. R. Dunning, H. J. Hoge, and J. H. Manley, Phys. Rev. **54**, 266 (1938).

Rydberg Corrections for *D*-Terms in He I

LEO PINCHERLE
King's College, London, England
(Received August 11, 1941)

The interaction between the normal $1snd$- and the $2p2p$-configuration in He I is evaluated, and its contribution to the difference between the Rydberg corrections of the ortho- and para-terms is found to be very large. As a consequence the theoretical values for these differences result too small.

(1) INTRODUCTION

THE Rydberg corrections for the terms of He I have been calculated by H. Bethe,[1] who has studied the polarization of the inner electron in the field of the outer one. These calculations have been completed by E. Ludwig,[2] and a similar treatment has also been given by E. A. Hylleraas.[3] The same results should be obtained by a complete treatment of the second and higher orders of Schrödinger perturbation theory (configuration interaction), but this calculation has not yet been carried out.

The theoretical values are in agreement with experiment except for *D*-terms, for which the theory gives a value too high for the difference $\delta_p-\delta_o$ between the Rydberg corrections of the para- and of the ortho-term. This theoretical value is determined only by the exchange integral, as the polarization has very little effect on $\delta_p-\delta_o$, even in the approximation considered by Ludwig.

It is suggested here that this discrepancy is due to the electrostatic configuration interaction between the $1snd$ and the $2p2p$ configuration. In fact the latter includes a ^1D-term, but does not include a ^3D-one; so that, while $1snd\,^3D$ is unaffected, the singlets are displaced nearer to the triplets.

This effect, as shown in Section (2), is very large, and makes the new theoretical values for $\delta_p-\delta_o$ to be now too small. Of course the complete calculation of the interaction of $1snd$-D with all possible configurations would be necessary, as stated above, to find the exact theoretical value of $\delta_p-\delta_o$. Such a calculation would require the eigenfunctions of many doubly excited states to be evaluated, and the many approximations which should be introduced would lead to a result which was not very accurate. However we may observe that the other configurations which can interact with $1snd$ include both the ^1D- and the ^3D-terms, so that their interaction does not affect $\delta_p-\delta_o$ appreciably. Also configurations of the type $npnp$ or $ndnd$, which include only ^1D, are found to have a negligible effect; so that it is not necessary to carry out the complete calculation, as only the treated interaction with $2p2p$ gives an effective contribution.

(2) APPROXIMATION AND RESULTS

The interaction between $1snd\,^1D$ and $2p2p\,^1D$ is determined by the matrix element:[4]

$$R=\left(\frac{4}{15}\right)^{\frac{1}{2}}\int\int_0^\infty R_{1s}(r_1)R_{nd}(r_2)\times\frac{e^2r_<}{r_>^2}R_{2p}(r_1)R_{2p}(r_2)r_1^2r_2^2dr_1dr_2$$

TABLE I. Values of R, the displacements of δE of the singlets and contributions to δ_p.

Term	R (cm^{-1})	δE (cm^{-1})	Contribution to δ_p
$3D$	1213	+4.83	−0.00059
$4D$	860	+2.47	−0.00072
$5D$	633	+1.35	−0.00077

(where $r_<$ is the smaller and $r_>$ the larger between r_1 and r_2, and R_{1s}, etc., are the radial eigenfunctions of the various electrons).

As this interaction is very small compared with the distance of the interacting terms, we can

[1] H. Bethe, Article in *Handbuch der Physik*, Vol. 24/I, p. 339. Results summarized in Table 6, p. 347.
[2] E. Ludwig, Helv. Phys. Acta **7**, 273 (1934).
[3] E. A. Hylleraas, Zeits. f. Physik **88**, 108 (1934).
[4] See an analogous calculation carried out for Mg I by R. Bacher, Phys. Rev. **43**, 264 (1933).

consider separately the interaction of each of the $1snd$-terms, and have a secular equation of the second degree for each term.

For $1snd$ we can assume the experimental term values and hydrogen eigenfunctions with a nuclear charge equal to 2 for the inner and equal to 1 for the outer electron.

The position of the negative $2p2p\,^1D$-term is not known experimentally: we shall assume the value calculated by W. S. Wilson,[5] namely -2.6624 Rydberg with respect to the He I limit. A calculation by Ta-You Wu[6] gives the near value -2.680. An observation by P. G. Kruger[7] gives the $2p2p\,^3P$-term at -282894 cm^{-1}: with this value, an evaluation of the difference $6F_2$ between the energies of $(2p)^2\,^3P$ and $(2p)^2\,^1D$ gives for ^1D a value in good agreement with Wilson's.

The eigenfunction evaluated by W. S. Wilson and R. B. Lindsay[8] with the method of the self-consistent field has been used for the $2p$ electron.

The results are reported in Table I, which gives the values of R, the displacements δE of the singlets, and the contributions to δ_p for $3D$, $4D$, $5D$.

Evaluation of R in which for $2p$ a hydrogen eigenfunction is used with an effective nuclear charge $Z=1.66$, corresponding to Wilson's value of the term, gives about the same values, as an example for $3D$: $R=1182$ cm^{-1}.

Table II gives the values of $\frac{1}{2}(\delta_p-\delta_o)$ for $3D$, $4D$, ∞D.

[5] W. S. Wilson, Phys. Rev. **48**, 536 (1935).
[6] Ta-You Wu, Phys. Rev. **46**, 239 (1934).
[7] P. G. Kruger, Phys. Rev. **36**, 855 (1930).
[8] W. S. Wilson and R. B. Lindsay, Phys. Rev. **47**, 681 (1935).

As stated before, the theoretical values are now too low.

I have tried to improve the approximation by using for the $1s$ electron the first-order eigenfunction which takes into account the effect of its polarization in the field of the $3d$ electron; but, for $3D$, this correction decreases the integral R of only 17 cm^{-1}.

As the interaction with other configurations does not improve the results, it seems that some other cause must be looked for.

TABLE II. Contributions to $\frac{1}{2}(\delta_p+\delta_0)$.

Term	Exchange	Interaction with $2p2p$	Total	Experimental
$3D$	$+0.00034$	-0.00030	$+0.00004$	$+0.00020$
$4D$	$+0.00048$	-0.00036	$+0.00012$	$+0.00027$
∞D	$+0.00066$	-0.00045	$+0.00021$	$+0.00036$*

* Value given by Bethe, reference 1. Experimental values are not concordant.

For higher values of n the experimental values are not concordant. According to the data reported by Kayser and Konen,[9] $\delta_p-\delta_o$ decreases when n increases, and becomes negative for $n=9$. This phenomenon cannot be explained by the present theory, because, for high values of n, the relative importance of the exchange integral A and of the displacement δE due to the configuration interaction does not vary when n varies; in fact the part of the (not normalized) d radial eigenfunction which contributes to the integrals is the same for all values of n, and so both A and δE are proportional to the square of the normalization coefficient of R_{nd}.

[9] Kayser and Konen, *Handbuch der Spektroscopie*, Vol. 7 (Leipzig, 1934) p. 622.

The Temperature Diffuse Scattering of X-Rays by Potassium Chloride and Potassium Bromide Crystals

JANE HAMILTON HALL*
Ryerson Physical Laboratory, The University of Chicago, Chicago, Illinois
(Received September 22, 1941)

The temperature diffuse scattering of x-rays by KCl and KBr crystals has been investigated with Cu $K\alpha$ radiation. The displacements of the temperature diffuse maxima from the Bragg scattering angle have been obtained experimentally for various settings of the crystal near the 400, 420 and 440 Bragg reflections. The theoretical displacement curve for the special case of KCl has been accurately calculated by considering the relative effects of the α_1 and α_2 wavelengths at the different angles of incidence used. The experimental results are found to be in good agreement with the theory when this is done. The half-widths and relative intensities have been noted experimentally and suitable corrections applied for the vertical divergence of the slit system. An attempt has been made to determine the elastic constants of KBr from diffuse scattering data.

INTRODUCTION

THE present existence of three widely differing theories[1–6] concerning the diffuse scattering of x-rays has led to many experimental studies of this phenomena. Three recent papers in particular have appeared which made it desirable to carry out further investigations in greater detail. The first of these papers[5] treated very rigorously the theory of the temperature diffuse scattering of x-rays and led to results which had been found previously by experimental workers. The second of these articles[7] reported that the observed displacements of the diffuse maxima from the Bragg scattering angle did not agree with the temperature diffuse theory. These displacements had been calculated, however, from an approximate formula to be found in an earlier publication.[8] Re-calculation of the published data by the more rigorous formula appearing in the theoretical paper mentioned above resulted in excellent agreement with the theory.[9] These data were for sodium chloride. The third paper[10] mentioned above reported an agreement in the half-widths calculated and observed for potassium chloride. The half-widths in this case had been calculated by the approximate formula. The more exact theory predicts considerably smaller half-widths. It was therefore decided to carry out further work on potassium chloride to check the half-widths of the diffuse maxima and to measure the displacements of these maxima from the Bragg angle of scattering. Potassium chloride is a convenient substance to use because it may be treated as a simple cubic crystal and because the elastic constants which enter directly into the theory are well known from other sources. If it is assumed that the Cauchy relation is satisfied for KBr, the ratio of the elastic constants should be obtainable from diffuse scattering data. An attempt was made to determine these constants. The only partial success will be discussed in a latter section of the paper.

THE THEORY OF THE TEMPERATURE DIFFUSE SCATTERING OF X-RAYS

The x-radiation scattered by a normal crystal may be divided into three components. The first (and coherent) part is the Laue-Bragg scattering which exhibits sharp maxima in the Laue directions and is zero elsewhere. The incoherent part consists of the Compton diffuse scattering and the temperature diffuse scattering. From

* Now at the University of Denver.
[1] C. V. Raman and P. Nilakantan, Proc. Indian Acad. Sci. **11**, 379, 389, 398 (1940); Nature **147**, 805 (1941); Phys. Rev. **60**, 63 (1941); Current Science **5**, 241 (1941).
[2] W. H. Bragg, Nature **146**, 509 (1940); **148**, 112 (1941).
[3] G. D. Preston, Nature **143**, 76 (1939); **147**, 358 (1941); **147**, 467 (1941).
[4] M. Born, Nature **147**, 674 (1941).
[5] W. H. Zachariasen, Phys. Rev. **59**, 860 (1941).
[6] M. Born and K. Sarginson, Proc. Roy. Soc. **179**, 69 (1941).
[7] G. E. M. Jauncey and O. J. Baltzer, Phys. Rev. **59**, 699 (1941).
[8] W. H. Zachariasen, Phys. Rev. **57**, 597 (1940).
[9] W. H. Zachariasen, Phys. Rev. **59**, 909 (1941).
[10] S. Siegel, Phys. Rev. **59**, 371 (1941).

considerations of the equilibrium positions of the atoms in a simple cubic lattice and of the vibrations of the atoms in this lattice it has been shown[5] that the temperature diffuse scattering intensity may be written as

$$J=\frac{NI_a}{4\pi^2 m_a \tau_0^2}\sum_j \frac{(\boldsymbol{s}\cdot\boldsymbol{A}_j)^2}{v_j^2}Q_j, \qquad (1)$$

where $\boldsymbol{\tau}_0=\boldsymbol{B}_H-\boldsymbol{k}-\boldsymbol{k}_0$ and is the wave vector of a vibrational mode of the lattice, I_a is the intensity of coherent scattering from one atom, N is the number of atoms, m_a is the atomic mass, $\boldsymbol{k}_0$ is the incident wave vector, $\boldsymbol{k}$ is the scattered wave vector, $\boldsymbol{B}_H$ a reciprocal lattice vector, $\boldsymbol{s}=2\pi(\boldsymbol{k}-\boldsymbol{k}_0)$, A_j is the jth polarization direction associated with the wave vector $\boldsymbol{\tau}_0$, v_j the propagation velocity corresponding to the jth polarization direction.

$$Q_j=\frac{h\nu_j}{\exp(h\nu_j/kT)-1}+\frac{h\nu_j}{2}.$$

It has been shown[5, 11, 12] that the equations of motion of a simple cubic lattice which consider only the atomic interaction between nearest and next nearest neighbors may be written as a set of linear homogeneous equations from which the frequency and polarization direction may be obtained. The equations may be written as:

$$[\boldsymbol{\phi}(\tau)-v^2\mathbf{1}]\cdot\boldsymbol{A}=0, \qquad (2)$$

where $\mathbf{1}$ is the unit tensor and $\boldsymbol{\phi}$ a symmetrical tensor. In the Cartesian system which has its coordinate axes along the cube edges,

$$\phi_{11}=\frac{a+2b-[a+b(\cos 2\pi\tau_2+\cos 2\pi\tau_3)]\cos 2\pi\tau_1}{\tau^2},$$

$$\phi_{12}=\frac{b\sin 2\pi\tau_1\sin 2\pi\tau_2}{\tau^2}.$$

τ_1, τ_2, τ_3 are components of τ in the reciprocal lattice.

$$a=\alpha/2\pi^2 m_a, \quad b=\gamma/\pi^2 m_a.$$

α and γ are the force constants for nearest and next nearest neighbors and are equal to[11]

$$\alpha=a_0(c_{11}-c_{12}-c_{44}),$$

$$4\gamma=a_0(c_{12}+c_{44}),$$

where a_0 is the edge of the unit cell. It is seen that the three real roots of the secular equation

$$|\boldsymbol{\phi}-v^2\mathbf{1}|=0$$

will be the propagation velocities v_j^2. Furthermore, if the vibrational wave number is small so that $\sin 2\pi i=2\pi i$, the tensor may be expanded to

$$\boldsymbol{\phi}=2\pi^2 a_0^2 b[\mathbf{1}+2\boldsymbol{nn}]$$

$$+2\pi^2 a_0^2(a-b)\begin{bmatrix}\alpha_1^2 & 0 & 0\\ 0 & \alpha_2^2 & 0\\ 0 & 0 & \alpha_3^2\end{bmatrix}. \qquad (3)$$

Here $\boldsymbol{\tau}=\tau\boldsymbol{n}$ and α_1, α_2, α_3 are the direction cosines of $\boldsymbol{n}$ relative to the cube edges, $\boldsymbol{n}$ being the unit vector along the propagation direction.

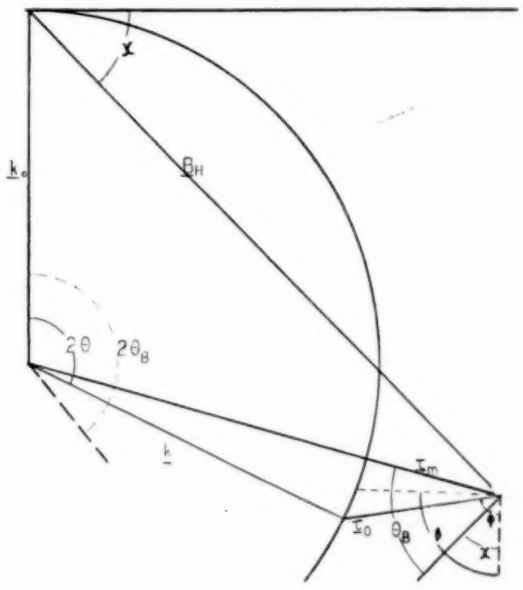

FIG. 1. A section of the reciprocal lattice drawn for an *HKO* reflection, Δ being negative.

Before developing the general theory further it will be convenient to discuss Fig. 1 which shows the reciprocal lattice construction for the scattering process. It will be valuable in geometrically interpreting the equations to follow.

[11] M. Born and Th. v. Kármán, Physik. Zeits. **13**, 297 (1912).
[12] M. Blackman, Proc. Roy. Soc. **148**, 365, 384, (1935); **159** 416 (1937).

The general case is drawn in which the plane of reflection does not lie along a cube face as in the case of an *HOO* reflection but is at an angle with the cube face. This will correspond to an *HKO* reflection. 2θ is the scattering angle for the diffuse radiation; $2\theta_B$ is the Bragg scattering angle; and $\boldsymbol{B}_H$ is a reciprocal lattice vector corresponding to an *HKO* plane. $\boldsymbol{k}_0$ is the wave vector of the incident x-rays, while $\boldsymbol{k}$ is the wave vector of the scattered x-rays. τ_0 is the wave vector of an elastic wave and is given by the relation $\boldsymbol{k}-\boldsymbol{k}_0+\tau_0=\boldsymbol{B}_H$. τ_m is the minimum value which τ_0 will assume as $\boldsymbol{k}$ varies. θ_B is in reality $\theta_B-\Delta\cos 2\theta_B$ ($\theta_B-\Delta$) is the actual glancing angle of incidence) but the second term may be neglected when Δ is small. The angle ϕ is the angle between the cube edge and the varying τ_0. For each plane of reflection there will be a different value of ϕ for which the intensity of scattering is a maximum. The dotted line shown is the direction of polarization of the quasi-longitudinal wave which makes an angle β with the wave vector. In general, none of the three polarization directions will coincide with the propagation directions. This means that none of the three waves is purely longitudinal or purely transverse.

Returning now to the intensity expression of Eq. (1) and the tensor $\boldsymbol{\phi}$ [Eq. (3)] it is seen that the first term of $\boldsymbol{\phi}$ is a tensor with rotational symmetry about the propagation direction $\boldsymbol{n}$. (It has been stated that $\tau=\tau\boldsymbol{n}$.) If in Eq. (3) $c_{11}=3c_{12}$ the second term becomes zero and the three waves resulting will be one longitudinal and two transverse. This is a special case but is rather closely approximated by sodium chloride.

The most general case of a cubic crystal for which the Cauchy relation holds will be treated in the following discussion. Not all crystals showing cubic symmetry will fulfill the Cauchy relation which demands that the elastic constant c_{12} equal the constant c_{44}.[6] For the alkali halides at room temperature the condition is, in general, satisfied. The elastic constants for KCl have the values[7] $c_{11}=3.76\times10^{11}$ dynes/cm^2; $c_{12}=0.64\times10^{11}$ dynes/cm^2; $c_{44}=0.63\times10^{11}$ dynes/cm.[2] When the tensor $\boldsymbol{\phi}$ is expanded the result

$$\boldsymbol{\phi}=\frac{c_{12}V}{m_a}\begin{pmatrix}1+2\alpha_1^2 & 2\alpha_1\alpha_2 & 2\alpha_1\alpha_3\\ 2\alpha_2\alpha_1 & 1+2\alpha_2^2 & 2\alpha_2\alpha_3\\ 2\alpha_3\alpha_1 & 2\alpha_3\alpha_2 & 1+2\alpha_3^2\end{pmatrix}+(c_{11}-3c_{12})\frac{V}{m_a}\begin{pmatrix}\alpha_1^2 & 0 & 0\\ 0 & \alpha_2^2 & 0\\ 0 & 0 & \alpha_3^2\end{pmatrix} \quad (4)$$

is obtained. If K is allowed to equal c_{11}/c_{12}

$$\boldsymbol{\phi}=\frac{c_{12}V}{m_a}\begin{pmatrix}1+(K-1)\alpha_1^2 & 2\alpha_1\alpha_2 & 2\alpha_1\alpha_3\\ 2\alpha_2\alpha_1 & 1+(K-1)\alpha_2^2 & 2\alpha_2\alpha_3\\ 2\alpha_3\alpha_1 & 2\alpha_3\alpha_2 & 1+(K-1)\alpha_3^2\end{pmatrix}.$$

If $\boldsymbol{k}_0$ and $\boldsymbol{k}$ lie in a cube face and if $\boldsymbol{B}_H$ is of the type $\boldsymbol{B}_{H_1H_2O}$, it follows that $\alpha_3=0$. When one sets $\alpha_3=0$ and substitutes for α_1 and α_2 the values of the sin or cos function of the angle ϕ (Fig. 1) he finds that the tensor reduces immediately to one of second order of the form

$$\boldsymbol{\phi}=\frac{c_{12}V}{m_a}\begin{pmatrix}1+(K-1)\cos^2\phi & 2\cos\phi\sin\phi & 0\\ 2\cos\phi\sin\phi & 1+(K-1)\sin^2\phi & 0\\ 0 & 0 & 1\end{pmatrix}.$$

Hence, $v_3^2=c_{12}V/m_a$ while $\boldsymbol{A}_3$ becomes the third Cartesian coordinate vector $\boldsymbol{k}$. From Eq. (2) two linear homogeneous equations are obtained by substituting the expression for $\boldsymbol{\phi}$. Here $\boldsymbol{A}$ is equal to $A_x\boldsymbol{i}+A_y\boldsymbol{j}+A_z\boldsymbol{k}$ and v^2 is set equal to $(V/m_a)c_{12}x$

$$(1+\cos^2\phi(K-1)-x)A_x+(2\cos\phi\sin\phi)A_y=0.$$
$$(2\cos\phi\sin\phi)A_x+(1+(K-1)\sin^2\phi-x)A_y=0.$$

Solving these for x results in

$$x=\frac{K+1}{2}\pm\left\{1+\cos^2 2\phi\left[\left(\frac{K-1}{2}\right)^2-1\right]\right\}^{\frac{1}{2}}. \quad (5)$$

It is seen from Fig. 1 that A_x will be $A\cos\beta$, A_y will be $A\sin\beta$. The tangent of β becomes

$$\tan\beta=\frac{x-\sin^2\phi-K\cos^2\phi}{\sin^2\phi}, \quad (6)$$

where $\beta_2=\beta_1+\frac{1}{2}\pi$. The tangent of β_1 corresponds to the positive sign before the radical in Eq. (5); tan β_2 corresponds to the negative sign before the radical.

Substituting in Eq. (1) for

$$\tau_0^2=\tau_m^2/\cos^2(\theta_B+\phi-\chi)$$

and setting $Q_j=kT$ (which is justified unless the temperature T is very small compared to the characteristic temperature of the crystal) one gets

$$J=C'\cos^2(\theta_B+\phi-\chi)\sum_j\frac{(\boldsymbol{s}\cdot\boldsymbol{A}_j)^2}{v_j^2},$$

where C' may be treated as a constant for given $\boldsymbol{B}_H$, λ and Δ. The summation is now composed of two terms only because of $A_3=k$.

$$(\boldsymbol{s}\cdot\boldsymbol{A}_j)^2=s\cdot(\boldsymbol{A}_j\cdot\boldsymbol{u})^2$$

where $\boldsymbol{u}$ is along the vector $\boldsymbol{B}_H$. Thus,

$$J=C\cos^2(\theta_B+\phi-\chi)\left[\frac{\sin^2(\beta_1-\chi)}{x_1}+\frac{\sin^2(\beta_2-\chi)}{x_2}\right]$$

or, more conveniently for purposes of calculation

$$J=C\cos^2(\theta_B+\phi-\chi)\times\left[\frac{\sin^2(\beta_1-\chi)}{x_1}+\frac{\cos^2(\beta_1-\chi)}{x_2}\right]. \quad (7)$$

It will be discussed later that an additional factor comes into the intensity expression when the α_1 and α_2 radiations are considered.

Referring again to Fig. 1, it is seen that $\lambda\tau_m=\lambda\tau_0\cos(\theta_B+\phi-\chi)$. This also equals $-\Delta\sin 2\theta_B$ and from the figure

$$2\theta=2\theta_B+\Delta\sin 2\theta_B[\tan\theta_B-\tan(\theta_B+\chi-\phi)].$$

This reduces to the more simple expression

$$2\theta=2\theta_B+\frac{2\Delta}{1+\cot\theta_B\cot(\phi-\chi)}, \quad (8)$$

which gives then the scattering angle 2θ in terms of ϕ and Δ.

EXPERIMENTAL DISCUSSION

The data were obtained with a carefully aligned Bragg spectrometer, nickel filtered Cu $K\alpha$ radiation, and x-ray plates which were covered with a 16-micron thick nickel foil to eliminate air-scattered radiation and thus reduce the background of the photographic plate. The slit system was arranged for a horizontal divergence of the incident beam on the crystal face of 9′ of arc for most of the exposures although 18′ divergence was used in two cases. To avoid corrections for horizontal divergence it is only necessary that the horizontal divergence be small compared to the half-width at half-maximum of the pattern or effect being observed. Even with the 18′ divergence the half-widths measured were still much larger. The vertical divergence must, however, be considered. This will be discussed later.

Because the transformer used had only one kilowatt output and the tube was self-rectified, very long exposure times were necessary. The exposures ranged from 20 hours for small displacements to 100 hours for larger displacements.

In the selection of a crystal to be used for these measurements difficulty was encountered in getting a specimen for which the Bragg reflection of a particular plane would not persist over many minutes of arc. If the surface of a crystal is rough, striated, or contains strains from internal stresses it will be found that even upon turning the crystal many minutes or even a degree away from the Bragg angle of incidence the Bragg reflections of α_1 and α_2 will be present after long exposures. This was overcome by using a freshly, and very smoothly cleaved crystal section of an excellent artificial crystal of KCl. Observations were taken down to $|\Delta|=17'$ without the Bragg radiation being present on long exposures. For observations on the 440 plane a crystal was ground at an angle of 45° to eliminate absorption and to produce a focusing effect. To get rid of the Bragg persistence here it was necessary to polish the 45° face with optical rouge on an optical block and carefully etch the surface with alcohol and water. Because KCl and KBr are very soluble in water excessive etching may make the Bragg persistence worse. Each of the crystals finally used had a half-width at half-maximum of the Bragg reflection of the order of 2 minutes of arc. If the shape of the Bragg reflection follows a simple error function it is to be expected that the reflec-

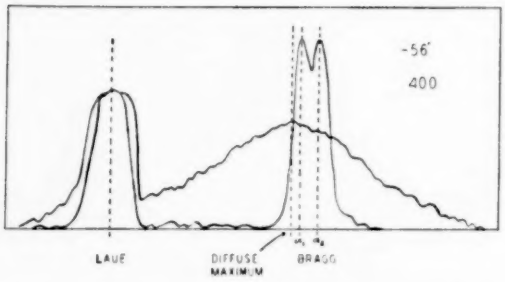

FIG. 2. Photometer tracings of the diffuse maximum for $\Delta = -56'$ with the Bragg $\alpha_1\alpha_2$ super-imposed to demonstrate the displacement of the diffuse from the Bragg angle. The backgrounds which are due to air-scattered radiation have been adjusted to coincide for purposes of comparison.

tion will be completely gone for long exposures at approximately five times its half-width.

A blackening *versus* intensity curve for the $\alpha_1\alpha_2$ radiations was obtained by first taking a series of exposures varying the angle of incidence around the Bragg angle and keeping the time of exposure constant. The resultant curve gave the ratio of the integrated intensity of the $\alpha_1\alpha_2$ sum to the integrated intensity at any crystal setting. Because of the narrow half-width $\alpha_1\alpha_2$ appeared together, fully resolved, however, at only three one-minute interval settings of the crystal. The exposure time was varied for the second curve keeping the crystal fixed at an angle where the intensity of α_1 equaled the intensity α_2. The combination of the two curves gave then the integrated intensity of the $\alpha_1\alpha_2$ combination as a function of the blackening of the photographic plate in terms of the deflections of a microphotometer.

In taking the exposures of the diffuse radiation the following procedure was adopted. The position of the crystal was determined for α_1 intensity equal to α_2 intensity. A short exposure of the order of magnitude of five seconds was made of this Bragg reflection. The crystal was then turned to the selected displacement Δ from the Bragg angle of incidence and an exposure of approximately two hours made to obtain the Laue spot for that particular plane. Another plate was put on the spectrometer without changing the crystal setting or the position of the plate-holder arm and the long exposure for the diffuse radiation made. The first plate thus gave accurately the displacements of α_1 and α_2 from the Laue spot and served as an accurate measurement of the crystal displacement from the Bragg angle of incidence. The second plate gave the displacement of the diffuse radiation from the Laue. The difference, of course, resulted in the displacement of the diffuse line from the $\alpha_1\alpha_2$ positions. The plates were measured by a microphotometer which had a magnification of about 50. Five sets of tracings were taken on the plates to rule out any variations in the microphotometer sensitivity, and to average the shrinkage of the recording paper. The tracings were then reduced to an intensity scale and the displacements, half-widths and intensities measured. Figure 2 is a composite of two photometer tracings. One is the Laue-diffuse plate tracing, the other is the Laue-Bragg plate tracing. The centers of the two Laues are super-imposed as are the backgrounds. The displacement of the maximum of the diffusely scattered radiation

TABLE I. Comparison of theoretical and experimental displacements for various values of delta. (Potassium chloride.) Δ_{α_1} = displacement of crystal from α_1 angle of incidence ($29^\circ\ 18'$). δ_{α_1} = displacement of diffuse maximum from the Bragg scattering angle of the α_1 wave-length and is equal to $2\theta_m - 2\theta_{B\alpha_1}$.

HKL	Δ_{α_1} (min.)	Theor. 1* δ_{α_1}	Exper. δ_{α_1}	Theor. 2 δ_{α_1}	Theor. 3 δ_{α_1}
400	−92	− 9.5		−10.3	−44.3
	−56	− 4.75	− 5.0±0.5	− 6.25	−28.0
	−37	− 3.0	− 3.3±0.5	− 4.1	−17.8
	−28	− 2.25	− 2.5±0.5	− 3.1	−13.5
	−17	− 1.5	− 1.0±0.5	− 1.9	− 8.2
	−10	− 1.0		− 1.0	− 4.8
	− 5†	-0.5^{α_1} 8.75^{α_2}		− 0.6	− 1.2
	0†	0.0^{α_1} 9.5^{α_2}		0.0	0.0
	5†	0.5^{α_1} 10.0^{α_2}		0.6	1.2
	10†	1.0^{α_1} 10.5^{α_2}		1.0	4.8
	15†	3.5^{α_1} 10.0^{α_2}		1.7	7.2
	23	8.0	8.0±0.5	2.6	11.1
	31	7.0	6.7±0.5	3.5	14.9
	62	10.5		6.9	29.8
	92	13.5		10.3	44.3
420	−36	− 5.0	−10.0±1.0	−16.0	−21.6
440	−33	−28.0	−25.0±0.5	−30.0	−31.7

* The theoretical results given here under 1 have been calculated from the equations developed in the text with the effect of α_1 and α_2 considered. Column theory 2 has been calculated from the same equations but the mean radiation is used instead of considering the relative effects of α_1 and α_2. Theor. 3 column has been calculated from the less rigorous formula and is inserted here to demonstrate the large difference existing between the two formulae. The equation used here was $2\theta = 2\theta_B + 2\Delta \sin^2 \theta_B$. $\theta_B = 29°22'$.

† At small displacements of the crystal the diffusely scattered radiation will resolve into an α_1 diffuse peak and an α_2 diffuse peak. The superscript indicates the displacement of the α_1 diffuse maximum from the Bragg scattering angle of α_1. The α_2 superscript indicates the displacement of the α_2 diffuse maximum from the Bragg scattering angle of α_1.

from the Bragg scattering angle is well illustrated. The slit divergence in this case was 18′ so the α_1 and α_2 are not well-resolved. The displacements measured on these tracings will be found in Table I.

All probable errors indicated on the drawings or in the tables were calculated by the usual method of taking the square root of the sum of the squares of the individual errors.

THE DISPLACEMENTS OF THE DIFFUSE MAXIMA FROM THE BRAGG ANGLE OF SCATTERING

In analyzing the data obtained it was found necessary to consider the effect of the combination of α_1 and α_2 rather than to take the arithmetical average as is usually done. Thus it is to be seen that the diffuse maximum at, say, $-20'$ will be more strongly affected by the α_1-radiation than $+20'$ will be. In this case of $+20'$ the α_2 will play a more important part.

In making the calculations for the shapes, displacements, and half-widths of the diffuse maxima the equations which resulted from the expansion of the tensor were used. K which was set equal to c_{11}/c_{12} has the value of 6 for KCl. The expression for x (Eq. (5)) was solved by using values of ϕ ranging from $-30°$ to $+90°$. The angle β for each value of ϕ was determined from Eq. (6), and the intensity calculated from Eq. (7). In the case of the 400 reflection χ of course is equal to 0. For the 440 $\chi=45°$, for the 420 $\chi=26°34'$. The factor C for the α_1 radiation is proportional to a factor $2/\Delta^2_{\alpha_1}$, where Δ_{α_1} is the displacement of the crystal from the Bragg angle for α_1. The factor C for α_2 is proportional to $1/\Delta^2_{\alpha_2}$ where Δ_{α_2} is the displacement of the crystal from the Bragg angle for α_2. (The relative intensities of α_1 and α_2 in the incident beam are in the ratio of 2 : 1.) If one considers, then, this additional factor in the computations the intensity of the diffuse line is obtained as a function of ϕ. This is then reduced to a function of 2θ by means of Eq. (8), where $\theta_B=\theta_{\alpha_1}$ or θ_{α_2}, depending on the line radiation being considered. These calculations result in a theoretical diffuse radiation curve for a particular value of Δ considered for either α_1- or α_2-radiation. The analogous curve is then calculated for the other component of the α-radiation and the two curves are combined by adding ordinates. The final curve will then be the theoretical diffuse radiation curve for particular values of Δ_{α_1} and Δ_{α_2}, the difference in the two deltas being, of course, the separation of α_1 and α_2 glancing angles, and for the 400 equal to 5′. From this curve the position and intensity of the maximum is found and the half-width at half-maximum is measured. Each value of Δ is treated in the same manner. Figure 3 demonstrates the displacement δ_{α_1} of the combined diffuse maxima

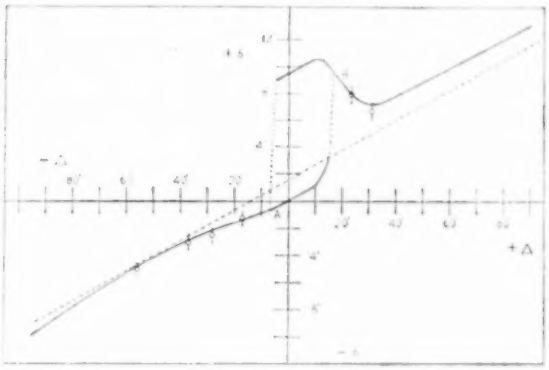

FIG. 3. Theoretical displacement curve for the temperature diffuse maxima. Δ is the displacement of the crystal from the Bragg angle of α_1. δ is the displacement of the diffuse scattering angle from the Bragg scattering angle of α_1. The experimental points with the probable errors are indicated.

from the Bragg scattering angle of α_1. The choice of α_1 as a reference point is purely arbitrary. The displacement δ_{α_2} of the combined diffuse maximum from the Bragg scattering angle of α_2 would be $-10'+\delta_{\alpha_1}$.

In the region of the point A indicated on the drawing the diffuse radiation begins to resolve into an α_1 diffuse maximum and an α_2 diffuse maximum. This condition will exist until at the region of the point B on the + side the effect of the α_2 is small enough to keep the two diffuse maxima from resolving. At the minimum portion of the curves the effect of α_1 is becoming much larger than α_2 and the curve approaches a straight line. The dotted line indicates roughly the effect of the mean radiation on the displacement of the resultant diffuse maximum. If the displacement from the α_1 scattering angle is measured relative to the average Bragg scattering angle (58°44′) the theory predicts a line running through the origin parallel to the dotted

line. Table I gives the numerical values of the experimental results, the theoretical values calculated considering the two component radiations separately, the theoretical values calculated by considering only the mean radiation, and the theoretical values calculated by the less exact formula to be found in an earlier publication.[8]

Also included in Table I are values for the 420 and 440 planes. As has been previously

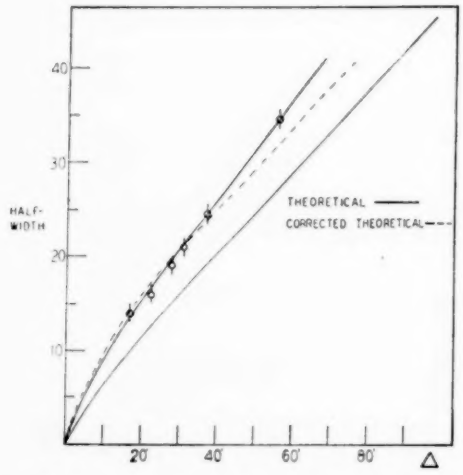

FIG. 4. Half-widths of the diffuse maxima *versus* Δ, the displacement of the crystal from the Bragg angle of α_1. The dotted line represents the correction to the theoretical curve to account for slit divergence.

mentioned the crystal was ground at an angle of 45° to reflect the 440. This procedure eliminated absorption and produced a focusing effect. In the case of the 420 this was not done. The effect of reflecting from an internal plane was to produce large divergence of the reflected beam, this producing, in turn, the same results as if the slits had been very wide. Consequently, the measurements on the 420 are not comparable in accuracy to the 400 and 440. The diffuse radiation of the 420 extended well into the Laue spot which would further destroy the accuracy of the measurements.

THE HALF-WIDTHS OF THE TEMPERATURE DIFFUSE RADIATION MAXIMA

The manner in which the theoretical diffuse maxima curves have been obtained was explained in the preceding section. The theoretical half-widths at half-maxima are measured directly from these curves. Table II gives the numerical values of the experimental and theoretical values and also the corrected theoretical values. Figure 4 demonstrates the relation between these values.

If a' = the theoretical half-width obtained from the theoretical diffuse maximum curve and z = the factors upon which the intensity near a maximum depends, it can be shown that[13]

$$\frac{\frac{1}{2}\tan^{-1}(\phi/a')}{a'} = \frac{\tan^{-1}[\phi/(a'^2+z^2)^{\frac{1}{2}}]}{(a'^2+z^2)^{\frac{1}{2}}}$$

and if $y=z/a'$, $\phi/a=k'$

$$\frac{1}{2}\tan^{-1}(k') = \frac{\tan^{-1}[k'/(1+y^2)^{\frac{1}{2}}]}{(1+y^2)^{\frac{1}{2}}},$$

where ϕ is the vertical divergence of the slit and $=l/2R$. l = height of the slit and R is the distance of the plate from the crystal. In this case $\phi = 58'$. By solving this for various values of a', y is obtained equal to a constant multiplied by a'. For a' equal to 10′ the correction factor y becomes 1.5, for a' equal to 20′ y equals 1.35, for a' equal to 40′ y is 1.2. These values are applied to the theoretical curve and the resultant corrected curve is shown in the drawing by the broken line.

It has been reported[10] that the observed half-widths for KCl agreed with the theoretical half-widths as calculated by the less rigorous expression which has been mentioned before. The values which the more exact formula requires are

TABLE II. Comparison of theoretical* and experimental values of the half-widths of the diffuse radiation. (Potassium chloride.)

HKL	$\Delta\alpha_1$ (min.)	Theoretical half-width (minutes)	Theoretical half-width (corrected)	Experimental half-width
400	92	43.5		
	62	28.5	33.5	
	56	27.0	31.0	34.5±1.0
	37	19.0	23.0	24.5±1.0
	31	15.8	19.7	21.0±1.0
	28	15.0	19.0	19.0±1.0
	23	12.5	16.5	16.0±1.0
	17	10.0	13.7	14.0±1.0
420	36	45.0	55.0	50.0±2.0
440	33	20.0	25.0	25.5±1.0

* The theoretical values were corrected by the method described in the text. The effect of the vertical slit divergence is demonstrated in Fig. 4.

[13] S. Siegel and W. H. Zachariasen, Phys. Rev. **57**, 795 (1940).

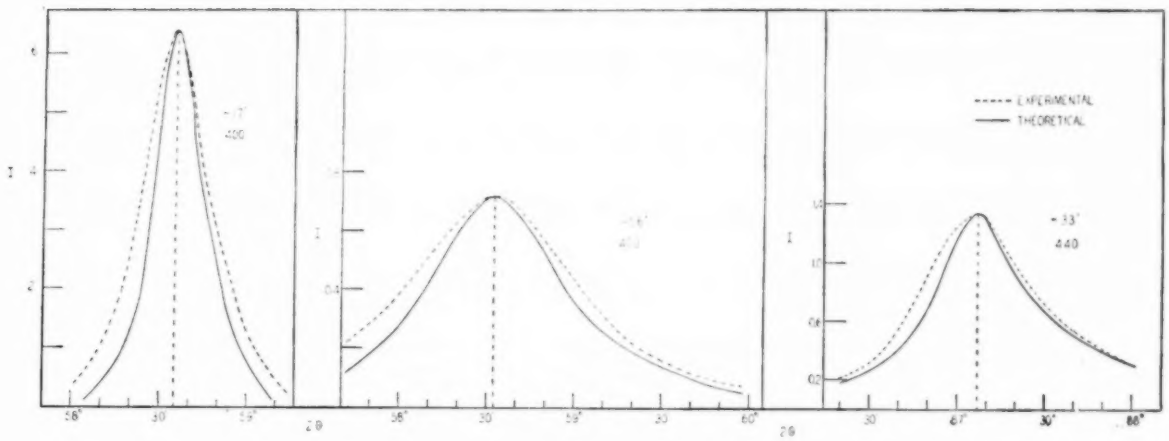

FIG. 5. Experimental and theoretical shapes of the temperature diffuse maxima for three values of Δ.

much smaller than the ones reported in this paper. This discrepancy may be explained by the fact that the plates which the investigator took were rather heavily fogged by air-scattered radiation and consequently, this scattered radiation superimposed upon the diffuse radiation gave half-widths too wide. Another explanation might be that the reduction curve of blackening *versus* intensity was not correct. In any event it is probably safe to assume that the experimental values found by the first mentioned investigator may not be correct.

Figure 5 illustrates the differences in the shapes of the theoretical and experimental diffuse maxima curves. These curves are not corrected for vertical divergence of the slit. The maxima have been adjusted to coincide by means of a constant factor and this factor then applied to the ordinates of the entire experimental curve. For $\Delta_{\alpha_1} = -17'$ it may be noticed that an asymmetry in the curve exists on the right side of the maximum. This is the effect of the α_2-radiation and would be more pronounced if Δ were smaller.

It should be mentioned here that the values for the half-widths are slightly different for + and − values of Δ because of the effect of the two radiations. The differences being so small it was thought unnecessary to include them on the curve.

THE RELATIVE INTENSITIES OF THE DIFFUSE MAXIMA

In any intensity measurement it is the absolute intensity of the effect which is most desired rather than the relative intensities. Because photographic methods in x-ray analyses do not lend themselves to absolute measurements the relative intensity measurements of the diffuse intensity are not to be given great weight in interpreting the phenomena. For this reason no especial care was taken to keep the x-ray tube factors entirely constant over the entire exposure time, particularly in view of the length of exposure. To obtain the experimental relative intensities of the diffuse maxima the maxima were reduced from the blackening to the intensity scale and this divided by the time of exposure. The intensities were then on a relative scale. The theoretical and experimental values were made to agree for $\Delta = -28'$ and the same reduction factor used in reducing the other experimental values. Figure 6 demonstrates the theoretical curve with the experimental points indicated in the usual manner. The dotted line again indicates the theoretical curve corrected for the vertical divergence. Here the corrected intensity will be proportional to

$$\frac{\tan^{-1}(\phi/\Delta \sin 2\theta)}{\Delta}.$$

The corrected theoretical curve is joined to the theoretical curve in the region of $\Delta = 10'$. It is seen that the effect of the vertical divergence is to cause the intensity to approach zero more slowly.

Table III contains the theoretical and experimental relative intensities. The differences in the

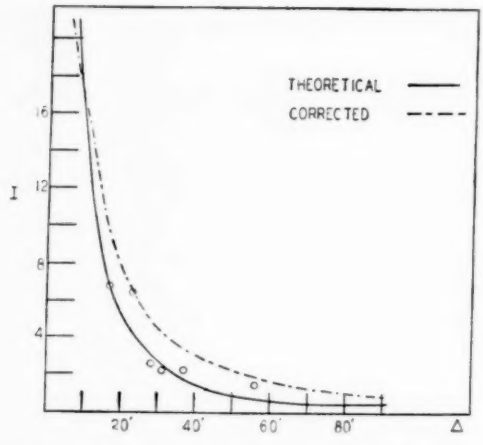

FIG. 6. Theoretical curve for the intensities of the diffuse maxima as a function of Δ. Experimental points indicated by circles.

intensities for + and − values of Δ have been observed but because they are rather small have not been included in the curve, the average being taken instead.

The ratio of the intensity of the temperature diffuse maximum to the integrated intensity of the sum of α_1 and α_2 is found to be of the order of 5×10^{-5} for $\Delta=20'$.

DETERMINATION OF ELASTIC CONSTANTS FROM DIFFUSE SCATTERING DATA

If the present theory concerning the diffuse scattering of x-rays is correct within the limitations it imposes upon itself, namely, that only the forces of the nearest and next nearest neighboring atoms are considered and not the electrostatic forces or the forces due to all the atoms, then from this theory it should be possible to obtain directly the elastic constants of cubic crystals. With enlargement upon the theory to include all symmetry types it should be possible to obtain the elastic constants of crystals having symmetry lower than the cubic arrangement.

With this in mind, diffuse scattering data were obtained for KBr for $\Delta_{\alpha_1}=-35'$ and $\Delta_{\alpha_1}=-17'$. Positive values of the displacement were not considered because of the behavior of the displacement curve in regions close to the Bragg angle.

The experimental results were:

$\Delta_{\alpha_1}=-35'$ $\delta_{\alpha_1}=-6'\pm0.5'$ Half-width $=18'$.
$\Delta_{\alpha_1}=-18'$ $\delta_{\alpha_1}=-5'\pm0.5'$ Half-width $=11'$.

If the diffuse maximum were due to one wavelength instead of two whose relative effects vary with changing Δ, it would be possible to obtain ϕ directly from Eq. (8) for the half-width at half-maximum and for the maximum. Having, then, these two values of ϕ which would correspond to J and $J/2$, it would be possible to solve rather conveniently by trial for the value of $K=c_{11}/c_{12}$ which would satisfy the experimental data. This not being the case because of the two line radiations α_1 and α_2, various values of K were selected and for each value the diffuse maxima plotted for α_1 and α_2 and combined as described before. This was done for $\Delta_{\alpha_1}=-35'$ and $\Delta_{\alpha_1}=-18'$. For $K=3$ the following theoretical values were obtained.

$\Delta_{\alpha_1}=-35'$ $\delta_{\alpha_1}=-7'$ Half-width $=23.5'$,
$\Delta_{\alpha_1}=-18'$ $\delta_{\alpha_1}=-4'$ Half-width $=13'.0$.

The agreement here is not very good, but appears to be the best trial solution. It may only be said then that from preliminary measurements with the method of diffuse scattering the ratio of the constant c_{11} of KBr to c_{12} is very close to 3. $c_{11}=3c_{12}$ is the ideal isotropic case for a cubic crystal, and here x_1, which equals $v_1^2m_a/Vc_{12}$ will equal 3, $x_2=1$, $x_3=1$. The three waves of propagation in the crystal will then be one longitudinal and two transverse. It would seem then, that if $c_{11}/c_{12}\approx3$ for KBr as the diffuse

TABLE III. Comparison of the theoretical and experimental values* of the relative intensities of the diffuse maxima.

HKL	Δ_{α_1} (min.)	Theoretical J/constant	Theoretical (corrected)	Experimental
400	10	16.0	16.3	
	17	6.4	8.9	6.8
	23	4.4	6.2	6.4
	28	2.6	4.8	2.5
	31	2.5	4.2	2.2
	37	1.5	3.3	2.2
	56	0.7	1.8	1.4
	62	0.65	1.5	
	92	0.3	0.8	
440	33	2.9	3.6	3.0

* The experimental values for the intensities were all corrected by the factor which was needed to reduce the experimental value for $\Delta=-28'$ to the uncorrected theoretical value. The theoretical corrected column was calculated by the method discussed in the text which takes into account the vertical divergence of the slits. The theoretical corrected curve and the theoretical curve were joined in the region of 10'.

scattering data would indicate KBr would be a very good substance for using in further investigations. If a monochromatized beam of x-rays were used the complicating factor due to the $\alpha_1\alpha_2$ radiations would be eliminated, at the expense of the intensity of the incident beam, however.

ACKNOWLEDGMENT

The author wishes to thank Professor William H. Zachariasen for his valuable aid and criticism throughout this investigation. We also wish to thank Mr. Paul C. Weyrich of the University of Michigan for the gift of the excellent artificial potassium chloride crystals.

FEBRUARY 1 AND 15, 1942 PHYSICAL REVIEW VOLUME 61

First Spark Spectrum of Neodymium—Preliminary Classification and Zeeman Effect Data

WALTER E. ALBERTSON, GEORGE R. HARRISON, AND J. RAND MCNALLY, JR.
George Eastman Research Laboratories of Physics, Massachusetts Institute of Technology, Cambridge, Massachusetts

(Received November 29, 1941)

Classification by means of the combination principle of 367 lines of Nd II as arising from 30 lower and 57 upper levels has been checked by Zeeman effect measurements at fields up to 87,180 oersteds, and by other data from the M.I.T.-W.P.A. wave-length project. Quantum numbers have been assigned to those levels which have approximate *LS* coupling, and *g* values of all known levels have been determined. The lowest term is $4f^4(^5I)6s-a^6I$. All of the low terms found arise from $4f^46s$ and $4f^45d$, while all identified upper terms are believed to arise from $4f^46p$. The strongest lines in the spectrum belong to the sextet and quartet supermultiplets arising from the transition $4f^4(^5I)6p-6s$, but these show perturbations which give rise to important intensity anomalies which affect the selection of *raies ultimes*. Curves are given which show the variation, in the progression La II, Ce II, Pr II, and Nd II, of the binding of terms arising from the configurations f^ns, f^np, f^nd and, where known, f^{n+1}.

NEODYMIUM ($Z=60$) is third in order of the 14 elements in the Periodic Table called the "rare earths." It gives rise to extremely complex spectra, the normal atom being characterized, according to the Bohr-Stoner theory, by six outer electrons of which several are *f* electrons. No previous known attempt at classification of any of the Nd spectra has met with success, and only by making extensive Zeeman effect studies at high magnetic fields, and by using new determinations of the wave-lengths of lines between 2000 and 11,000A from the neodymium arc, have we succeeded in determining the basic regularities in Nd II.

Some 2700 intense lines of neodymium are listed in the *M.I.T. Wavelength Tables*,[1] while the M.I.T.-W.P.A. card catalog contains a total of 6000 lines believed to arise from this element. Most of these lines can readily be ascribed to the normal atom or the first or second stages of ionization, on the basis of King's[2] studies with the electric furnace. In the present paper 367 Nd II lines are classified as arising from 30 lower and 57 upper levels, to the majority of which quantum numbers have been assigned. Zeeman effect data are included for such of the lines as show resolvable patterns at fields up to 87,180 oersteds. These data suffice to determine the Landé splitting-factors (*g* values) of all terms.

The only Zeeman determinations on Nd lines which we were able to find in the literature were those of Van de Vliet,[3] who reported the separations of a large number of unresolved triplets and resolved patterns for 16 Nd II lines. Van de Vliet used magnetic fields of 38,500 oersteds. Since we had available fields more than twice as strong in

[1] *M.I.T. Wavelength Tables* (John Wiley & Sons, New York, 1939).

[2] A. S. King, Astrophys. J. **78**, 9 (1933).

[3] H. J. Van de Vliet, Thesis Amsterdam (1939).

TABLE I. Classified lines of Nd II.

λ	Int.	Combination	Type	Sep.	p	n	g_1	g_2
8643.48	2	$a^6H_{3\frac{1}{2}}-z^6H^\circ_{2\frac{1}{2}}$	—	—	—	—	—	—
7982.090	4	$a^6G_{4\frac{1}{2}}-z^6H^\circ_{3\frac{1}{2}}$	—	—	—	—	—	—
7825.20	2	$b^4I_{3\frac{1}{2}}-25{,}235$	—	—	—	—	—	—
7796.42	2	$b^4I_{4\frac{1}{2}}-z^6H^\circ_{3\frac{1}{2}}$	—	—	—	—	—	—
7792.24	2	$b^4I_{5\frac{1}{2}}-z^6H^\circ_{4\frac{1}{2}}$	5	55	—	1290	1.05	1.00
7766.86	2	$b^4I_{4\frac{1}{2}}-z^6H^\circ_{3\frac{1}{2}}$	—	—	(0)	800	0.8	0.8
7603.75	2	$b^4I_{3\frac{1}{2}}-1^\circ_{4\frac{1}{2}}$	5	302	—	1842	0.482	0.784
7587.66	2	$a^6H_{2\frac{1}{2}}-z^6I^\circ_{3\frac{1}{2}}$	5	308	(150)	1520	0.444	0.752
7513.77	5	$b^4I_{3\frac{1}{2}}-20{,}830$	6	214	(751)	588	0.479	0.693
7432.20	2	$b^4I_{4\frac{1}{2}}-21{,}871$	—	—	—	—	—	—
7288.56	10	$b^4I_{3\frac{1}{2}}-z^6H^\circ_{2\frac{1}{2}}$	5	170	(84)	920	0.493	0.321
7285.29	10	$a^6H_{2\frac{1}{2}}-6^\circ_{3\frac{1}{2}}$	5	390	(190)	1828	0.459	0.849
7261.64	2	$(b^4I_{3\frac{1}{2}}-z^6H^\circ_{3\frac{1}{2}})$ $(b^6I_{4\frac{1}{2}}-z^6H^\circ_{4\frac{1}{2}})$	—	—	—	—	—	—
7243.23	2	$b^4I_{3\frac{1}{2}}-z^6H^\circ_{2\frac{1}{2}}$	7	—	(0)	1090	1.09	1.09
6968.35	5	$b^4I_{3\frac{1}{2}}-21{,}871$	—	—	—	—	—	—
6816.02	10	$a^6K_{4\frac{1}{2}}-1^\circ_{4\frac{1}{2}}$	6	238	(1076)	—	(0.552)	0.790
6782.50	2	$b^6I_{4\frac{1}{2}}-z^6H^\circ_{5\frac{1}{2}}$	—	—	—	—	—	—
6780.61	5	$b^6I_{4\frac{1}{2}}-13^\circ_{5\frac{1}{2}}$	—	—	—	—	—	—
6765.786	2	$b^6I_{5\frac{1}{2}}-z^6I^\circ_{4\frac{1}{2}}$	—	—	—	—	—	—
6743.57	1	$a^6K_{4\frac{1}{2}}-20{,}830$	—	—	—	—	—	—
6725.26	2	$b^6I_{2\frac{1}{2}}-3^\circ_{3\frac{1}{2}}$	—	—	—	—	—	—
6681.12	2	$b^6I_{5\frac{1}{2}}-10^\circ_{4\frac{1}{2}}$	—	—	—	—	—	—
6671.117	2	$b^6I_{3\frac{1}{2}}-24^\circ_{3\frac{1}{2}}$	—	—	—	—	—	—
6669.647	3	$b^6I_{4\frac{1}{2}}-7^\circ_{4\frac{1}{2}}$	—	—	—	—	—	—
6553.070	8	$a^6K_{5\frac{1}{2}}-z^6H^\circ_{4\frac{1}{2}}$	—	138	—	—	(0.842)	0.980
6539.937	10w	$a^6K_{4\frac{1}{2}}-z^6H^\circ_{3\frac{1}{2}}$	4	276	(130)	−414	0.550	0.826
6523.151	10	$b^6I_{3\frac{1}{2}}-z^6I^\circ_{2\frac{1}{2}}$	6	273	(952)	—	0.489	0.762
6504.463	10	$a^6H_{2\frac{1}{2}}-y^6I^\circ_{3\frac{1}{2}}$	5	363	(182)	1731	0.458	0.821
6483.445	5h	$a^6L_{6\frac{1}{2}}-2^\circ_{4\frac{1}{2}}$	—	—	—	—	—	—
6476.201	3	$b^6I_{4\frac{1}{2}}-8^\circ_{5\frac{1}{2}}$	—	160	(79)	—	(0.840)	1.000
6464 99	4	$a^6H_{2\frac{1}{2}}-25{,}138$	—	—	—	—	—	—
6439.86	3	$a^6K_{5\frac{1}{2}}-4^\circ_{4\frac{1}{2}}$	—	—	—	—	—	—
6394.80	4	$b^6I_{4\frac{1}{2}}-9^\circ_{4\frac{1}{2}}$	6	133	(598)	—	(0.840)	0.973
6385.196	100l	$b^6I_{5\frac{1}{2}}-25{,}014?$	—	—	—	—	—	—
6365.554	15	$b^6I_{3\frac{1}{2}}-z^6K^\circ_{4\frac{1}{2}}$	5	293	(144)	1810	0.489	0.782
6362.093	10	$b^6I_{4\frac{1}{2}}-z^6I^\circ_{5\frac{1}{2}}$	5	175	—	1802	0.841	1.016
6358.391	2	$b^6I_{5\frac{1}{2}}-13^\circ_{5\frac{1}{2}}$	—	—	—	—	—	—
6341.507	15	$a^6K_{5\frac{1}{2}}-5^\circ_{4\frac{1}{2}}$	—	—	—	—	—	—
6300.970	5	$a^6K_{4\frac{1}{2}}-21{,}871$	—	—	—	—	—	—
6298.418	20	$b^6I_{3\frac{1}{2}}-6^\circ_{3\frac{1}{2}}$	6	362	(1269)	665	0.485	0.847
6287.207	5	$b^6I_{4\frac{1}{2}}-10^\circ_{4\frac{1}{2}}$	6	(56)	(249)	—	(0.840)	0.896
6284.726	3	$a^6K_{4\frac{1}{2}}-8^\circ_{4\frac{1}{2}}$	7b	—	(0)	1060	(1.015)	1.007
6264.34	5	$b^6I_{4\frac{1}{2}}-z^6K^\circ_{3\frac{1}{2}}$	—	—	—	—	—	—
6257.834	25	$a^6L_{5\frac{1}{2}}-1^\circ_{4\frac{1}{2}}$	—	168	—	—	(0.620)	0.788
6243.349	4	$b^6I_{3\frac{1}{2}}-z^6I^\circ_{4\frac{1}{2}}$	5	454	(237)	—	0.484	0.938
6238.499	20	$b^6I_{4\frac{1}{2}}-z^6K^\circ_{5\frac{1}{2}}$	5	80	(40)	1245	(0.840)	0.92
6183.907	20	$b^6I_{5\frac{1}{2}}-z^6K^\circ_{6\frac{1}{2}}$	7b	—	(0)	1039	1.039	1.039
6170.486	30	$a^6H_{2\frac{1}{2}}-y^6H^\circ_{2\frac{1}{2}}$	6	188	(467)	545	0.454	0.642
6150.431	10	$b^6I_{5\frac{1}{2}}-15^\circ_{5\frac{1}{2}}$	—	—	—	—	—	—
6133.964	5	$a^6K_{5\frac{1}{2}}-z^6K^\circ_{4\frac{1}{2}}$	5	—	—	1140	(0.842)	0.776
6108.410	20	$a^6H_{2\frac{1}{2}}-26{,}041$	—	—	—	—	—	—
6106.75	2	$b^6I_{7\frac{1}{2}}-27{,}744$	—	—	—	—	—	—
6094.98	2	$b^6I_{4\frac{1}{2}}-12^\circ_{5\frac{1}{2}}$	—	—	—	—	—	—
6082.96	2	$b^6I_{6\frac{1}{2}}-21^\circ_{5\frac{1}{2}}$	—	—	—	—	—	—
6077.39	2	$a^6K_{4\frac{1}{2}}-4^\circ_{4\frac{1}{2}}$	6	450	(2028)	770	0.550	1.000
6051.875	4	$b^6I_{5\frac{1}{2}}-17^\circ_{4\frac{1}{2}}$	5	60	—	1343	(1.034)	0.964
6048.44	2w	$b^6I_{3\frac{1}{2}}-9^\circ_{4\frac{1}{2}}$	—	—	—	—	—	—
6034.239	20	$b^6I_{5\frac{1}{2}}-29{,}027$	6	81	(678)	—	1.281	1.200
6031.266	25	$b^6I_{5\frac{1}{2}}-z^6K^\circ_{7\frac{1}{2}}$	7b	—	(0)	1086	1.141	(1.133)
6000.564	2	$b^6I_{4\frac{1}{2}}-13^\circ_{5\frac{1}{2}}$	—	—	—	—	—	—
5989.341	15	$a^6K_{4\frac{1}{2}}-5^\circ_{5\frac{1}{2}}$	—	—	—	—	—	—
5942.063	2	$b^6I_{5\frac{1}{2}}-26{,}182$	6	(9)	(48)	1024	1.029	1.020
5934.747	10	$a^6K_{4\frac{1}{2}}-z^6I^\circ_{3\frac{1}{2}}$	4	201	(105)	0	(0.552)	0.753
5932.140	3	$b^6I_{5\frac{1}{2}}-18^\circ_{4\frac{1}{2}}$	5	—	—	1497	(1.034)	1.105
5924.313	2	$b^6I_{4\frac{1}{2}}-14^\circ_{5\frac{1}{2}}$	—	—	—	—	—	—
5918.035	2	$a^6K_{6\frac{1}{2}}-12^\circ_{5\frac{1}{2}}$	—	—	—	—	—	—
5909.874	10	$b^6I_{4\frac{1}{2}}-y^6I^\circ_{5\frac{1}{2}}$	7b	—	(0)	1031	1.031	1.031
5906.646	6	$a^6K_{5\frac{1}{2}}-8^\circ_{4\frac{1}{2}}$	6	164	(897)	929	0.844	1.008
5900.430	5	$b^6I_{3\frac{1}{2}}-11^\circ_{4\frac{1}{2}}$	6	465	(1627)	710	0.480	0.945
5891.528	20	$b^6I_{4\frac{1}{2}}-y^6I^\circ_{4\frac{1}{2}}$	6	188	—	937	0.843	1.031
5890.503	5	$b^6I_{6\frac{1}{2}}-22^\circ_{5\frac{1}{2}}$	—	—	—	—	—	—
5865.057	15	$b^6I_{7\frac{1}{2}}-z^6K^\circ_{6\frac{1}{2}}$	4	—	(0)	1036	1.227	(1.202)
5842.391	25	$b^6I_{6\frac{1}{2}}-y^6I^\circ_{5\frac{1}{2}}$	6	(18)	(116)	1150	1.141	1.159
5835.89	2	$a^6K_{6\frac{1}{2}}-13^\circ_{5\frac{1}{2}}$	—	—	—	—	—	—
5825.872	25	$a^6G_{4\frac{1}{2}}-y^6H^\circ_{3\frac{1}{2}}$	5	634	(316)	1598	0.009	0.643
5811.572	15	$a^6K_{5\frac{1}{2}}-z^6I^\circ_{4\frac{1}{2}}$	6	173	(948)	928	0.844	1.017
5804.020	100	$a^6K_{4\frac{1}{2}}-z^6K^\circ_{4\frac{1}{2}}$	6	225	(1014)	666	0.553	0.778
5770.500	20	$a^6G_{4\frac{1}{2}}-26{,}041$	—	—	—	—	—	—
5761.695	10	$b^6I_{4\frac{1}{2}}-16^\circ_{4\frac{1}{2}}$	6	142	(639)	915	0.842	0.984
5748.154	4	$a^6K_{4\frac{1}{2}}-6^\circ_{3\frac{1}{2}}$	4	294	(150)	−462	0.566	0.860
5744.766	25	$a^6K_{5\frac{1}{2}}-15^\circ_{5\frac{1}{2}}$	—	—	—	—	—	—
5744.138	8	$a^6K_{4\frac{1}{2}}-7^\circ_{4\frac{1}{2}}$	—	—	—	—	—	—
5743.196	20wh	$b^6I_{6\frac{1}{2}}-27{,}744$	6	(62)	(405)	—	(1.144)	1.082
5740.862	35	$b^6I_{5\frac{1}{2}}-21^\circ_{5\frac{1}{2}}$	6	—	(20)	1023	1.03	1.02
5726.825	25	$b^6I_{4\frac{1}{2}}-17^\circ_{4\frac{1}{2}}$	6	116	(526)	903	0.847	0.963
5718.120	35	$b^6I_{7\frac{1}{2}}-y^6I^\circ_{7\frac{1}{2}}$	6	68	(508)	—	1.229	(1.161)
5708.280	60	$a^6K_{5\frac{1}{2}}-z^6K^\circ_{5\frac{1}{2}}$	6	70	(387)	—	(0.842)	0.912
5706.206	40	$b^6I_{3\frac{1}{2}}-y^6I^\circ_{3\frac{1}{2}}$	6	337	—	663	0.490	0.827
5702.244	25	$a^6K_{4\frac{1}{2}}-z^6I^\circ_{4\frac{1}{2}}$	6	387	(1742)	760	0.553	0.940
5698.927	10	$b^6I_{3\frac{1}{2}}-z^6K^\circ_{3\frac{1}{2}}$	4	—	(0)	1110	1.286	(1.267)
5688.525	150	$a^6K_{6\frac{1}{2}}-z^6K^\circ_{5\frac{1}{2}}$	6	(16)	(107)	1027	1.019	1.035
5675.76	6	$b^6I_{2\frac{1}{2}}-25{,}138$	6	703	(2460)	837	0.477	1.180
5668.868	15	$a^6K_{3\frac{1}{2}}-29{,}027$	5	—	(0)	1679	1.253	(1.203)
5645.240	2	$a^6L_{6\frac{1}{2}}-5^\circ_{5\frac{1}{2}}$	—	—	—	—	—	—
5632.15	1	$a^6L_{5\frac{1}{2}}-z^6H^\circ_{4\frac{1}{2}}$	—	—	—	—	—	—
5625.722	10	$b^6I_{3\frac{1}{2}}-14^\circ_{3\frac{1}{2}}$	6	552	(1929)	760	0.483	1.035
5620.6	—	$b^6I_{5\frac{1}{2}}-y^6I^\circ_{5\frac{1}{2}}$	6	63	(525)	—	1.278	1.215
5614.303	10	$b^6I_{4\frac{1}{2}}-19^\circ_{4\frac{1}{2}}$	6	208	(930)	944	0.839	1.047
5603.651	5	$a^4I_{5\frac{1}{2}}-2^\circ_{5\frac{1}{2}}$	6	89	(491)	—	0.975	0.886
5599.48	1	$b^6I_{4\frac{1}{2}}-y^6I^\circ_{5\frac{1}{2}}$	—	—	—	—	—	—
5594.425	150	$a^6K_{7\frac{1}{2}}-z^6K^\circ_{7\frac{1}{2}}$	6	(11)	(79)	1133	1.127	1.138
5581.601	3	$a^6K_{5\frac{1}{2}}-12^\circ_{5\frac{1}{2}}$	6	128	(707)	904	0.843	0.971
5548.474	10	$a^6L_{5\frac{1}{2}}-4^\circ_{4\frac{1}{2}}$	4	383	(188)	−1367	0.617	1.000
5539.26	10	$a^6K_{4\frac{1}{2}}-9^\circ_{4\frac{1}{2}}$	—	—	—	—	—	—
5533.396	15	$b^6I_{5\frac{1}{2}}-23^\circ_{4\frac{1}{2}}$	—	—	—	—	—	—
5526.143	5	$b^6I_{5\frac{1}{2}}-y^6I^\circ_{6\frac{1}{2}}$	5	131	(66)	—	1.035	1.166
5508.398	15	$a^6K_{5\frac{1}{2}}-13^\circ_{5\frac{1}{2}}$	6	146	(798)	912	0.840	0.986
5487.026	2	$b^6I_{4\frac{1}{2}}-20^\circ_{3\frac{1}{2}}$	4	136½	(71)	361	0.840	0.976
5485.699	20	$a^6K_{6\frac{1}{2}}-z^6K^\circ_{5\frac{1}{2}}$	7b	—	(0)	1203	1.203	1.203
5483.09	2h	$a^6K_{6\frac{1}{2}}-26{,}182$	7b	—	(0)	1009	(1.015)	1.016
5474.734	3	$a^6K_{6\frac{1}{2}}-18^\circ_{6\frac{1}{2}}$	6	88½	(581)	1054	1.012	1.101
5473.083	6	$a^6K_{7\frac{1}{2}}-22^\circ_{6\frac{1}{2}}$	5	—	(0)	1360	1.122	(1.087)
5455.815	30	$a^6K_{5\frac{1}{2}}-y^6I^\circ_{4\frac{1}{2}}$	4	—	(0)	957	(1.015)	1.026
5447.556	8	$b^6I_{4\frac{1}{2}}-21^\circ_{5\frac{1}{2}}$	5	173	—	—	(0.840)	1.013
5447.556	8	$b^6I_{3\frac{1}{2}}-y^6H^\circ_{2\frac{1}{2}}$	4	161	—	—	0.480	0.642
5442.274	25	$a^6L_{6\frac{1}{2}}-8^\circ_{5\frac{1}{2}}$	4	152	(74)	0	0.852	1.004
5432.360	3	$a^6K_{7\frac{1}{2}}-24^\circ_{7\frac{1}{2}}$	6	(10)	(80)	1110	1.11	1.11
5431.526	25	$a^6K_{7\frac{1}{2}}-y^6I^\circ_{6\frac{1}{2}}$	—	—	—	—	—	—
5421.559	15	$a^6K_{4\frac{1}{2}}-z^6K^\circ_{3\frac{1}{2}}?$	—	—	—	—	—	—
5416.381	15	$a^6K_{5\frac{1}{2}}-y^6I^\circ_{4\frac{1}{2}}$	4	187	(91)	0	0.843	1.030
5414.819	3	$a^6K_{4\frac{1}{2}}-11^\circ_{3\frac{1}{2}}$	4	392	(196)	−824	0.551	0.943
5399.109	2	$b^6I_{3\frac{1}{2}}-26{,}041$	—	—	—	—	—	—
5371.935	20	$a^6K_{3\frac{1}{2}}-z^6K^\circ_{3\frac{1}{2}}$	7b	—	(0)	1255	1.243	(1.267)
5361.474	25	$a^6L_{4\frac{1}{2}}-z^6I^\circ_{3\frac{1}{2}}$	4	161½	(82)	−31	0.852	1.014
5361.174	3	$a^4I_{6\frac{1}{2}}-z^6H^\circ_{5\frac{1}{2}}$	—	—	—	—	—	—
5356.976	15	$a^6K_{3\frac{1}{2}}-y^6I^\circ_{2\frac{1}{2}}$	5	60	(30)	1515	1.204	(1.161)
5345.709	6	$a^6K_{7\frac{1}{2}}-27{,}744$	5	—	(0)	1360	(1.127)	1.091
5336.552	8	$a^6L_{5\frac{1}{2}}-23{,}171$	4	460	(232)	−1458	0.617	1.077
5319.818	60	$a^6L_{5\frac{1}{2}}-z^6K^\circ_{4\frac{1}{2}}$	4	159	(79)	−80	0.620	0.779
5311.461	15	$a^6K_{6\frac{1}{2}}-21^\circ_{4\frac{1}{2}}$	7b	—	(0)	996	(1.015)	1.019
5308.42	2	$a^6K_{3\frac{1}{2}}-29{,}027$	7b	—	(0)	1220	1.22	1.22
5306.472	4	$a^6K_{5\frac{1}{2}}-16^\circ_{4\frac{1}{2}}$	4	138	(70)	220	0.843	0.981
5302.279	12	$a^6K_{3\frac{1}{2}}-y^6I^\circ_{3\frac{1}{2}}$	5	—	(0)	1530	1.253	(1.220)
5293.168	60	$a^6L_{7\frac{1}{2}}-z^6K^\circ_{6\frac{1}{2}}$	4	—	(0)	837	(0.998)	1.023
5276.879	10	$a^6K_{5\frac{1}{2}}-17^\circ_{4\frac{1}{2}}$	4	114½	(57)	323	0.840	0.954
5273.431	25	$a^6L_{6\frac{1}{2}}-z^6K^\circ_{5\frac{1}{2}}$	4	61	(29)	519	0.841	0.902
5255.510	50	$a^4I_{4\frac{1}{2}}-1^\circ_{4\frac{1}{2}}$	6	(31)	(141)	772	0.757	0.788

TABLE I. Classified lines of Nd II.—*Continued.*

λ	Int.	Combination	Type	Sep.	p	n	g_1	g_2
5250.816	10	$a^6K_{4\frac{1}{2}}-y^6I^\circ_3$	4	268	(135)	−390	0.549	0.817
5249.585	60	$a^6L_{3\frac{1}{2}}-z^6K^\circ_{2\frac{1}{2}}$	4	—	(0)	915	1.107	(1.133)
5234.195	50	$a^6L_{5\frac{1}{2}}-z^6I^\circ_{4\frac{1}{2}}$	4	320	(160)	−814	0.620	0.940
5228.427	6	$a^4I_{3\frac{1}{2}}-z^6H^\circ_{4\frac{1}{2}}$	7b	—	(0)	977	0.977	0.977
5225.045	5	$a^6K_{4\frac{1}{2}}-25{,}138$	4	635	(317)	−1667	0.553	1.188
5212.365	30	$a^4I_{4\frac{1}{2}}-20{,}830$	5	—	(0)	942	(0.754)	0.700
5192.621	40	$a^6L_{5\frac{1}{2}}-z^6K^\circ_{3\frac{1}{2}}$	4	—	(0)	1058	1.187	(1.202)
5191.448	40	$a^4I_{4\frac{1}{2}}-2^\circ_{3\frac{1}{2}}$	5	131	(67)	1476	0.756	0.887
5182.603	8	$a^6K_{4\frac{1}{2}}-14^\circ_{3\frac{1}{2}}$	4	480	(238)	−1130	0.553	1.033
5181.165	5	$a^6K_{3\frac{1}{2}}-19^\circ_{4\frac{1}{2}}$	4	203	(101)	—	0.841	1.044
5167.923	5	$a^4I_{6\frac{1}{2}}-8^\circ_{5\frac{1}{2}}$	5	103	(52)	1676	1.115	1.012
5165.140	10	$a^6L_{6\frac{1}{2}}-12^\circ_{5\frac{1}{2}}$	4	117	(59)	206	0.850	0.967
5143.332	8	$a^6I_{5\frac{1}{2}}-2^\circ_{5\frac{1}{2}}$	6	136	(747)	958	1.024	0.888
5130.596	40	$a^6L_{10\frac{1}{2}}-z^6K^\circ_{9\frac{1}{2}}$	4	—	(0)	1050	1.247	(1.267)
5127.10	—	$a^6K_{6\frac{1}{2}}-y^6I^\circ_{6\frac{1}{2}}$	—	—	—	—	—	—
5119.58	2	$a^6L_{6\frac{1}{2}}-25{,}014$	—	—	—	—	—	—
5107.585	20	$a^6L_{7\frac{1}{2}}-18^\circ_{6\frac{1}{2}}$	4	99	(52)	362	1.001	1.100
5106.637	8	$a^6L_{8\frac{1}{2}}-24^\circ_{7\frac{1}{2}}$	7b	—	(0)	1073	1.107	(1.112)
5102.393	15	$a^6L_{6\frac{1}{2}}-13^\circ_{5\frac{1}{2}}$	4	135	—	112	0.852	0.987
5096.524	8	$a^6L_{5\frac{1}{2}}-9^\circ_{4\frac{1}{2}}$	4	352	(175)	−968	0.619	0.971
5092.797	20	$a^4I_{5\frac{1}{2}}-5^\circ_{4\frac{1}{2}}$	6	(7)	(39)	970	0.977	0.963
5089.837	10	$a^4I_{4\frac{1}{2}}-z^6H^\circ_{3\frac{1}{2}}$	4	69	—	507	0.749	0.818
5033.517	6	$a^6L_{9\frac{1}{2}}-29{,}027$	4	—	(0)	1065	(1.187)	1.202
5027.852	4	$a^6L_{5\frac{1}{2}}-10^\circ_{4\frac{1}{2}}$	4	278	(142)	−636	0.618	0.896
4972.67	2h	$a^4I_{3\frac{1}{2}}-23{,}171$	—	—	—	—	—	—
4970.922	5	$a^6I_{6\frac{1}{2}}-5^\circ_{5\frac{1}{2}}$	5	184	(92)	2171	1.154	0.970
4961.396	15	$a^6I_{5\frac{1}{2}}-25{,}235$	5	183	(93)	2650	1.291	1.108
4959.130	35	$a^6I_{4\frac{1}{2}}-1^\circ_{4\frac{1}{2}}$	6	(13)	(56)	795	0.802	0.788
4958.139	5	$a^4I_{5\frac{1}{2}}-z^6K^\circ_{4\frac{1}{2}}$	5	199	(103)	—	0.983	0.784
4943.901	10	$a^4I_{4\frac{1}{2}}-21{,}871$	5	115	(57)	1159	0.754	0.639
4942.961	5	$a^4I_{7\frac{1}{2}}-18^\circ_{6\frac{1}{2}}$	5	89	—	1770	1.192	1.103
4930.729	5	$a^6L_{7\frac{1}{2}}-z^6K^\circ_{7\frac{1}{2}}$	6	135	(999)	1077	1.001	1.136
4920.692	60	$a^6I_{4\frac{1}{2}}-20{,}830$	5	107	(53)	1175	0.802	0.695
4914.385	15	$a^4I_{3\frac{1}{2}}-7^\circ_{4\frac{1}{2}}$	4	—	(0)	835	(0.979)	1.011
4902.041	15	$a^6I_{4\frac{1}{2}}-2^\circ_{3\frac{1}{2}}$	—	82	—	—	(0.803)	0.885
4876.112	3	$a^4I_{6\frac{1}{2}}-25{,}014$	7b	—	(0)	1080	(1.109)	1.115
4867.839	6	$a^4I_{4\frac{1}{2}}-z^6H^\circ_{4\frac{1}{2}}$?	—	—	—	—	—	—
4859.030	60	$a^6I_{6\frac{1}{2}}-z^6H^\circ_{5\frac{1}{2}}$	5	88	(44)	1639	1.156	1.068
4835.982	15	$a^6I_{3\frac{1}{2}}-1^\circ_{4\frac{1}{2}}$	5	341	(170)	1983	0.447	0.788
4830.82	2h	$a^6L_{6\frac{1}{2}}-26{,}182$	—	—	—	—	—	—
4825.482	100	$a^6I_{3\frac{1}{2}}-z^6H^\circ_{4\frac{1}{2}}$	5	—	(0)	1216	(1.027)	0.985
4824.185	10	$a^4I_{6\frac{1}{2}}-25{,}235$	7b	—	(0)	1091	(1.109)	1.107
4820.336	40	$a^4I_{4\frac{1}{2}}-3^\circ_{3\frac{1}{2}}$	7b	—	(0)	759	0.759	0.759
4811.343	60	$a^6I_{4\frac{1}{2}}-z^6H^\circ_{3\frac{1}{2}}$	4	—	(0)	736	(0.803)	0.822
4809.45	2h	$a^4L_{6\frac{1}{2}}-y^6I^\circ_{5\frac{1}{2}}$	—	—	—	—	—	—
4805.103	6	$a^4I_{4\frac{1}{2}}-4^\circ_{4\frac{1}{2}}$	6	250	(1120)	—	0.761	1.011
4799.423	15	$a^6I_{3\frac{1}{2}}-20{,}830$	6	249	(870)	574	0.448	0.697
4797.157	30	$a^4I_{6\frac{1}{2}}-15^\circ_{5\frac{1}{2}}$	4	40	(20)	925	(1.109)	1.144
4763.865	20	$a^6I_{5\frac{1}{2}}-4^\circ_{4\frac{1}{2}}$	5	—	(0)	1080	(1.027)	1.01
4763.624	10	$a^4I_{5\frac{1}{2}}-9^\circ_{4\frac{1}{2}}$	7b	—	(0)	1059	(0.979)	0.961
4750.020	4	$a^4I_{4\frac{1}{2}}-5^\circ_{5\frac{1}{2}}$	—	—	—	—	—	—
4724.88	3	$a^6L_{5\frac{1}{2}}-29{,}027$	—	—	—	—	—	—
4715.589	30	$a^4I_{4\frac{1}{2}}-z^6I^\circ_{5\frac{1}{2}}$	7b	—	(0)	755	0.755	0.755
4709.714	30	$a^6I_{5\frac{1}{2}}-5^\circ_{5\frac{1}{2}}$	6	53	(292)	990	1.020	0.967
4706.542	50	$a^6I_{3\frac{1}{2}}-z^6H^\circ_{2\frac{1}{2}}$	5	138½	(70)	795	0.447	0.308
4703.576	20	$a^4I_{5\frac{1}{2}}-10^\circ_{4\frac{1}{2}}$	5	74	(30)	1314	0.983	0.909
4699.719	1	$a^6I_{6\frac{1}{2}}-8^\circ_{5\frac{1}{2}}$	—	—	—	—	—	—
4689.002	2	$a^6G_{4\frac{1}{2}}-30{,}037$	—	—	—	—	—	—
4680.734	50	$a^6I_{4\frac{1}{2}}-21{,}871$	5	164	(78)	1380	0.804	0.640
4676.262	2	$a^4I_{5\frac{1}{2}}-z^6K^\circ_{5\frac{1}{2}}$	—	—	—	—	—	—
4647.759	8	$a^4I_{4\frac{1}{2}}-z^6H^\circ_{3\frac{1}{2}}$	5	305	(150)	2447	0.766	1.071
4639.377	10	$a^6I_{6\frac{1}{2}}-z^6I^\circ_{5\frac{1}{2}}$	5	140	—	1930	1.145	1.005
4632.688	12	$a^4I_{4\frac{1}{2}}-z^6K^\circ_{4\frac{1}{2}}$	6	(20)	(88)	760	0.750	0.770
4612.473	12	$a^6I_{4\frac{1}{2}}-z^6H^\circ_{4\frac{1}{2}}$	6	174	(770)	888	0.800	0.974
4609.148	1	$a^6I_{5\frac{1}{2}}-z^6H^\circ_{5\frac{1}{2}}$	—	—	—	—	—	—
4607.381	25	$a^4I_{6\frac{1}{2}}-18^\circ_{6\frac{1}{2}}$	7b	—	(0)	1105	1.105	1.105
4602.242	10	$a^4I_{7\frac{1}{2}}-z^6K^\circ_{6\frac{1}{2}}$	—	—	—	—	—	—
4597.52	2h	$a^6L_{5\frac{1}{2}}-26{,}182$	—	—	—	—	—	—
4597.013	25	$a^4I_{4\frac{1}{2}}-6^\circ_{3\frac{1}{2}}$	4	89	—	438	0.747	0.836
4594.447	10	$a^4I_{4\frac{1}{2}}-7^\circ_{4\frac{1}{2}}$	6	259	(1167)	883	0.753	1.012
4590.905	4	$a^4I_{5\frac{1}{2}}-12^\circ_{5\frac{1}{2}}$	7b	—	(0)	971	(0.979)	0.963
4569.849	8	$a^4I_{4\frac{1}{2}}-3^\circ_{3\frac{1}{2}}$	—	—	—	—	—	—
4567.606	20	$a^4I_{4\frac{1}{2}}-z^6I^\circ_{4\frac{1}{2}}$	6	183	(828)	848	0.757	0.940
4556.735	15	$a^6I_{5\frac{1}{2}}-7^\circ_{4\frac{1}{2}}$	7b	—	(0)	1046	(1.027)	1.023
4556.136	20	$a^6I_{4\frac{1}{2}}-4^\circ_{4\frac{1}{2}}$	6	199	(896)	890	0.806	1.005
4554.967	5	$a^6I_{5\frac{1}{2}}-25{,}014$	—	—	—	—	—	—
4552.275	2	$a^6L_{6\frac{1}{2}}-y^6I^\circ_{6\frac{1}{2}}$	—	—	—	—	—	—
4541.269	50	$a^6I_{5\frac{1}{2}}-13^\circ_{5\frac{1}{2}}$	6	(9)	(51)	983	0.974	0.992
4530.328	10	$a^6I_{5\frac{1}{2}}-z^6I^\circ_{4\frac{1}{2}}$	5	96	—	—	1.039	0.943
4506.582	50	$a^6I_{4\frac{1}{2}}-5^\circ_{5\frac{1}{2}}$	5	1626	(82)	1697	0.802	0.965
4505.75	8	$a^6I_{3\frac{1}{2}}-z^6H^\circ_{4\frac{1}{2}}$	—	—	—	—	—	—
4501.808	50	$a^4I_{4\frac{1}{2}}-8^\circ_{4\frac{1}{2}}$	5	250	(124)	2130	0.754	1.004
4491.644	6	$a^6I_{6\frac{1}{2}}-12^\circ_{5\frac{1}{2}}$	5	180	—	2150	1.16	0.98
4485.952	12	$a^4I_{5\frac{1}{2}}-15^\circ_{5\frac{1}{2}}$	6	173	(948)	1059	0.976	1.149
4475.566	12	$a^6I_{4\frac{1}{2}}-z^6I^\circ_{3\frac{1}{2}}$	5	—	(0)	937	(0.803)	0.765
4470.965	8d	$a^6I_{5\frac{1}{2}}-24^\circ_{7\frac{1}{2}}$	—	—	—	—	—	—
4465.601	20	$a^6I_{4\frac{1}{2}}-8^\circ_{4\frac{1}{2}}$	6	(15)	(80)	1000	1.01	0.99
4465.075	20	$a^6I_{3\frac{1}{2}}-3^\circ_{3\frac{1}{2}}$	6	308	(1066)	597	0.443	0.751
4462.985	60	$a^6I_{6\frac{1}{2}}-z^6K^\circ_{7\frac{1}{2}}$	5	—	(0)	1283	(1.109)	1.131
4462.407	30	$a^4I_{4\frac{1}{2}}-9^\circ_{4\frac{1}{2}}$	6	215	(968)	861	0.756	0.971
4457.179	5	$a^6I_{6\frac{1}{2}}-25{,}014$	—	—	—	—	—	—
4456.394	20	$a^4I_{7\frac{1}{2}}-z^6K^\circ_{6\frac{1}{2}}$	7b	—	(0)	1209	1.201	(1.202)
4451.978	50	$a^6I_{3\frac{1}{2}}-4^\circ_{4\frac{1}{2}}$	5	556	—	2948	0.445	1.001
4451.566	100	$a^4I_{5\frac{1}{2}}-z^6K^\circ_{6\frac{1}{2}}$	5	—	(0)	1328	(0.979)	1.033
4446.387	100	$a^4I_{4\frac{1}{2}}-z^6I^\circ_{5\frac{1}{2}}$	5	259	(129)	2184	0.757	1.016
4444.115	5	$a^6I_{6\frac{1}{2}}-13^\circ_{5\frac{1}{2}}$	—	150	(74)	—	(1.148)	0.998
4426.822	12	$a^6I_{5\frac{1}{2}}-9^\circ_{4\frac{1}{2}}$	5	—	(0)	1236	(1.027)	0.982
4414.432	12	$a^6I_{4\frac{1}{2}}-z^6H^\circ_{5\frac{1}{2}}$	5	253	(128)	2195	0.800	1.053
4413.784	5	$a^6I_{6\frac{1}{2}}-25{,}235$	—	—	—	—	—	—
4412.265	40	$a^6I_{4\frac{1}{2}}-23{,}171$	6	278	(1247)	—	0.804	1.082
4411.052	50	$a^6I_{5\frac{1}{2}}-z^6I^\circ_{5\frac{1}{2}}$	7b	(29)	(158)	1019	1.034	1.006
4400.828	50	$a^6I_{4\frac{1}{2}}-z^6K^\circ_{4\frac{1}{2}}$	6	(22)	(98)	794	0.805	0.783
4391.110	10	$a^6I_{6\frac{1}{2}}-15^\circ_{5\frac{1}{2}}$	7b	—	(0)	1159	(1.148)	1.146
4385.663	40	$a^4I_{4\frac{1}{2}}-z^6K^\circ_{3\frac{1}{2}}$	5	(161)	(80)	1645	0.759	0.920
4382.737	15	$a^4I_{5\frac{1}{2}}-17^\circ_{4\frac{1}{2}}$	5	—	(0)	1030	(0.979)	0.968
4381.290	10	$a^4I_{4\frac{1}{2}}-11^\circ_{5\frac{1}{2}}$	—	—	—	—	—	—
4375.039	30	$a^6I_{3\frac{1}{2}}-z^6I^\circ_{3\frac{1}{2}}$	6	309	(1083)	601	0.448	0.757
4374.923	20	$a^6I_{5\frac{1}{2}}-10^\circ_{4\frac{1}{2}}$	5	124	(62)	—	1.028	0.904
4371.069	10	$a^4I_{7\frac{1}{2}}-y^6I^\circ_{7\frac{1}{2}}$	6	(35)	(260)	—	1.196	(1.161)
4368.632	50	$a^6I_{4\frac{1}{2}}-6^\circ_{3\frac{1}{2}}$	4	—	(0)	677	(0.803)	0.839
4366.315	12d	$a^6I_{4\frac{1}{2}}-7^\circ_{4\frac{1}{2}}$	6	211	(947)	—	0.802	1.013
4359.244	15	$a^4I_{4\frac{1}{2}}-24^\circ_{7\frac{1}{2}}$	7b	—	(0)	1112	(1.109)	1.108
4358.699	15	$a^4I_{6\frac{1}{2}}-y^6I^\circ_{6\frac{1}{2}}$	7b	—	(0)	1140	(1.109)	1.171
4358.169	50	$a^6I_{4\frac{1}{2}}-z^6K^\circ_{4\frac{1}{2}}$	6	118	(764)	1092	1.150	1.032
4351.295	30	$a^6I_{3\frac{1}{2}}-z^6K^\circ_{3\frac{1}{2}}$	6	105	(575)	972	1.019	0.914
4342.071	20	$a^6I_{4\frac{1}{2}}-z^6I^\circ_{4\frac{1}{2}}$	6	136	(610)	867	0.800	0.936
4338.697	40	$a^4I_{7\frac{1}{2}}-29{,}027$	7b	—	(0)	1206	(1.199)	1.200
4325.766	100	$a^6I_{7\frac{1}{2}}-z^6K^\circ_{7\frac{1}{2}}$	6	96	(718)	1184	1.233	1.137
4324.89	2h	$a^4I_{5\frac{1}{2}}-26{,}182$	—	—	—	—	—	—
4319.54	15	$a^4I_{5\frac{1}{2}}-18^\circ_{6\frac{1}{2}}$	—	—	—	—	—	—
4316.518	5	$a^4I_{5\frac{1}{2}}-19^\circ_{4\frac{1}{2}}$	—	—	—	—	—	—
4314.511	20	$a^6I_{3\frac{1}{2}}-23{,}171$	5	635	(319)	3300	0.444	1.079
4310.506	20	$a^4I_{4\frac{1}{2}}-12^\circ_{5\frac{1}{2}}$	5	218	—	—	0.742	0.960
4307.778	5	$a^4I_{5\frac{1}{2}}-y^6I^\circ_{5\frac{1}{2}}$	6	(51)	(280)	—	(0.979)	1.030
4303.573	100	$a^6I_{3\frac{1}{2}}-z^6K^\circ_{4\frac{1}{2}}$	5	331	(165)	1936	0.447	0.778
4303.262	3	$a^4I_{6\frac{1}{2}}-27{,}744$	—	—	—	—	—	—
4291.892	3	$a^6K_{4\frac{1}{2}}-29{,}298$	—	—	—	—	—	—
4284.518	25	$a^6I_{5\frac{1}{2}}-z^6K^\circ_{5\frac{1}{2}}$	6	91	(767)	—	1.28	1.19
4282.570	10	$a^6I_{4\frac{1}{2}}-8^\circ_{4\frac{1}{2}}$	5	200	(88)	1908	0.802	1.002
4278.75	5	$a^4I_{4\frac{1}{2}}-25{,}014$	—	—	—	—	—	—
4277.279	20	$a^6I_{4\frac{1}{2}}-12^\circ_{5\frac{1}{2}}$	6	50	(250)	—	(1.027)	0.98
4272.789	15	$a^6I_{3\frac{1}{2}}-6^\circ_{3\frac{1}{2}}$	6	400	(1398)	646	0.445	0.845
4270.565	15	$a^6I_{3\frac{1}{2}}-7^\circ_{4\frac{1}{2}}$	5	561	—	—	0.451	1.012
4266.716	20	$a^4I_{4\frac{1}{2}}-13^\circ_{5\frac{1}{2}}$	5	233	—	—	0.750	0.983
4256.239	10	$a^4I_{4\frac{1}{2}}-25{,}138$	—	—	—	—	—	—
4247.367	50	$a^6I_{3\frac{1}{2}}-z^6I^\circ_{4\frac{1}{2}}$	5	491	(245)	2659	0.449	0.940
4246.879	10	$a^6I_{4\frac{1}{2}}-9^\circ_{4\frac{1}{2}}$	6	165	(740)	—	(0.803)	0.968
4234.196	20	$a^6I_{3\frac{1}{2}}-13^\circ_{5\frac{1}{2}}$	—	—	—	—	—	—

TABLE I. Classified lines of Nd II.—*Continued.*

λ	Int.	Combination	Type	Sep.	p	n	g_1	g_2
4232.378	40	$a^6I_{4\frac{1}{2}}-z^6I^\circ_{5\frac{1}{2}}$	5	210	(105)	1961	0.807	1.017
4228.200	15	$a^6I_{7\frac{1}{2}}-24^\circ_{7\frac{1}{2}}$	—	—	—	—	—	—
4228.025	12	$a^4I_{4\frac{1}{2}}-14^\circ_{3\frac{1}{2}}$	4	283	—	−241	0.749	1.032
4227.719	20	$a^6I_{7\frac{1}{2}}-y^6I^\circ_{6\frac{1}{2}}$	—	—	—	—	—	—
4220.258	10*d*	$a^6I_{6\frac{1}{2}}-y^6I^\circ_{5\frac{1}{2}}$	5	122	(57)	1811	1.147	1.025
4217 282	20	$a^4I_{5\frac{1}{2}}-21^\circ_{5\frac{1}{2}}$	6	(50)	(270)	—	—	—
4211.286	30	$a^4I_{4\frac{1}{2}}-y^6I^\circ_{4\frac{1}{2}}$	6	274	(1233)	897	0.753	1.027
4205.595	20	$a^6I_{5\frac{1}{2}}-y^6I^\circ_{7\frac{1}{2}}$	5	133	(68)	2291	1.293	1.160
4199.099	15	$a^6I_{4\frac{1}{2}}-10^\circ_{4\frac{1}{2}}$	6	93	(426)	—	0.799	0.892
4186.033	8	$a^6I_{5\frac{1}{2}}-15^\circ_{5\frac{1}{2}}$	6	128	(708)	—	1.02	1.15
4179.585	10	$a^6I_{5\frac{1}{2}}-y^6I^\circ_{4\frac{1}{2}}$	4	—	(0)	1004	(1.027)	1.033
4177.321	15	$a^6I_{4\frac{1}{2}}-z^6K^\circ_{5\frac{1}{2}}$	5	112	(57)	1418	0.803	0.915
4175.606	40	$a^6I_{5\frac{1}{2}}-29{,}027$	6	90	(764)	—	1.295	1.205
4173.379	12	$a^6I_{4\frac{1}{2}}-11^\circ_{3\frac{1}{2}}$	4	140	—	290	0.79	0.93
4156.265	5	$a^6I_{3\frac{1}{2}}-9^\circ_{4\frac{1}{2}}$	5	523	(256)	2800	0.443	0 966
4156.083	10	$a^6I_{5\frac{1}{2}}-z^6K^\circ_{6\frac{1}{2}}$	5	—	(0)	1063	(1.027)	1.032
4144.553	10	$a^4I_{4\frac{1}{2}}-16^\circ_{4\frac{1}{2}}$	6	224	(1010)	—	0.753	0.977
4133.361	15	$a^6I_{4\frac{1}{2}}-21^\circ_{5\frac{1}{2}}$	5	133	(68)	—	1.143	1.010
4126.475	1	$a^4I_{4\frac{1}{2}}-17^\circ_{4\frac{1}{2}}$	—	—	—	—	—	—
4123.881	40	$a^4I_{5\frac{1}{2}}-22^\circ_{6\frac{1}{2}}$	5	108	(53)	1681	0.981	1.089
4120.654	6	$a^4I_{7\frac{1}{2}}-y^6I^\circ_{8\frac{1}{2}}$	5	—	(0)	1326	1.204	(1.220)
4113 826	10*d*	$a^6I_{5\frac{1}{2}}-16^\circ_{4\frac{1}{2}}$	5	—	(0)	1173	(1.027)	0.984
4110.472	10	$a^6I_{3\frac{1}{2}}-10^\circ_{4\frac{1}{2}}$	5	452	(223)	2254	0.447	0.899
4109.455	30	$a^6I_{6\frac{1}{2}}-z^6K^\circ_{7\frac{1}{2}}$	5	—	(0)	1059	(1.148)	1.135
4109.073	15	$a^6I_{4\frac{1}{2}}-12^\circ_{3\frac{1}{2}}$	5	167	—	1722	0.802	0.969
4106.582	25	$a^4I_{6\frac{1}{2}}-y^6I^\circ_{7\frac{1}{2}}$	—	—	—	—	—	—
4104.227	10	$a^4I_{5\frac{1}{2}}-23^\circ_{4\frac{1}{2}}$	4	198	—	93	0.984	1.182
4100.240	10	$a^4I_{4\frac{1}{2}}-y^6I^\circ_{6\frac{1}{2}}$	—	185	—	—	(0.979)	1.164
4095.999	1	$a^6I_{5\frac{1}{2}}-17^\circ_{4\frac{1}{2}}$	—	—	—	—	—	—
4085.815	10	$a^6I_{3\frac{1}{2}}-11^\circ_{3\frac{1}{2}}$	6	496	(1746)	700	0.447	0.943
4080 227	20	$a^6I_{4\frac{1}{2}}-25{,}014$	5	317	(157)	2542	0.804	1.121
4075 272	12	$a^6I_{4\frac{1}{2}}-y^6I^\circ_{3\frac{1}{2}}$	4	—	(0)	763	(0.803)	0.814
4075.116	15	$a^4I_{4\frac{1}{2}}-26{,}182$	5	263	—	2199	0.752	1.015
4069.267	15	$a^6I_{4\frac{1}{2}}-13^\circ_{3\frac{1}{2}}$	5	184	(90)	1813	0.805	0 989
4067.727	2*h*	$a^4I_{4\frac{1}{2}}-19^\circ_{4\frac{1}{2}}$	6	291	(1307)	—	(0.754)	1.045
4061.085	40	$a^6I_{7\frac{1}{2}}-z^6K^\circ_{8\frac{1}{2}}$	4	—	(0)	976	1.232	(1.202)
4059.961	20	$a^4I_{4\frac{1}{2}}-y^6I^\circ_{5\frac{1}{2}}$	5	275	(135)	2269	0.757	1.032
4051.145	15	$a^4I_{5\frac{1}{2}}-27{,}744$	5	108	(51)	1683	0.981	1.089
4043.596	15	$a^6I_{6\frac{1}{2}}-22^\circ_{6\frac{1}{2}}$	6	(65)	(425)	—	(1.148)	1.083
4040.796	40	$a^6I_{5\frac{1}{2}}-18^\circ_{5\frac{1}{2}}$	5	76	—	1526	1.031	1.108
4038.124	15	$a^6I_{5\frac{1}{2}}-19^\circ_{4\frac{1}{2}}$	4	—	(0)	949	(1.027)	1.046
4034.012	4	$a^6I_{4\frac{1}{2}}-14^\circ_{3\frac{1}{2}}$	—	—	—	—	—	—
4030.470	20	$a^6I_{5\frac{1}{2}}-y^6I^\circ_{5\frac{1}{2}}$	7*b*	—	(0)	1026	1.026	1.026
4024.785	20	$a^6I_{4\frac{1}{2}}-15^\circ_{5\frac{1}{2}}$	5	346	(175)	2709	0.804	1.150
4021.330	12	$a^6I_{6\frac{1}{2}}-24^\circ_{7\frac{1}{2}}$	4	—	(0)	914	(1.148)	1.117
4020.872	15	$a^6I_{6\frac{1}{2}}-y^6I^\circ_{6\frac{1}{2}}$	6	(20)	(130)	1152	1.142	1.162
4018.826	15	$a^6I_{4\frac{1}{2}}-y^6I^\circ_{4\frac{1}{2}}$	6	225	(988)	926	0.804	1.029
4012.250	80	$a^6I_{3\frac{1}{2}}-z^6K^\circ_{3\frac{1}{2}}$	4	—	(0)	1036	(1.294)	1.267
4000.493	10*d*	$a^4I_{4\frac{1}{2}}-20^\circ_{3\frac{1}{2}}$	4	213	(107)	000	0.751	0.964
3991.743	60	$a^6I_{3\frac{1}{2}}-y^6I^\circ_{3\frac{1}{2}}$	6	372	(1309)	631	0.446	0.818
3990.103	40	$a^6I_{7\frac{1}{2}}-y^6I^\circ_{7\frac{1}{2}}$	6	(76)	(573)	—	(1.231)	1.155
3982 355	20	$a^4I_{5\frac{1}{2}}-28{,}170$	—	—	(0)	950	(0.98)	0.99
3979.479	40	$a^4I_{4\frac{1}{2}}-21^\circ_{3\frac{1}{2}}$	5	265	(131)	2225	0.755	1.020
3976.836	40	$a^6I_{3\frac{1}{2}}-25{,}138$	6	740	(2592)	816	0.445	1.185
3973.650	30	$a^6I_{6\frac{1}{2}}-27{,}744$	6	64	(417)	—	1.148	1.084
3973.269	40	$a^6I_{8\frac{1}{2}}-y^6I^\circ_{8\frac{1}{2}}$	6	(72)	(614)	—	(1.294)	1.222
3963.114	30	$a^6I_{7\frac{1}{2}}-29{,}027$	4	—	(0)	973	(1.231)	1.201
3958.001	30	$a^6I_{4\frac{1}{2}}-16^\circ_{4\frac{1}{2}}$	6	176	(797)	887	0.804	0.980
3952.195	30	$a^6I_{3\frac{1}{2}}-14^\circ_{3\frac{1}{2}}$	6	589	(2060)	—	0.448	1.037
3951.154	40	$a^6I_{5\frac{1}{2}}-21^\circ_{5\frac{1}{2}}$	7*b*	—	—	1020	(1.027)	1.013
3941.512	60	$a^6I_{4\frac{1}{2}}-17^\circ_{4\frac{1}{2}}$	6	154	(690)	722	0.802	0.956
3937.575	20	$a^6I_{3\frac{1}{2}}-y^6I^\circ_{4\frac{1}{2}}$	—	586	(293)	—	(0.447)	1.033
3894.627	20	$a^6I_{4\frac{1}{2}}-26.182$	5	215	(108)	1986	0.807	1.022
3887.866	25	$a^6I_{4\frac{1}{2}}-19^\circ_{4\frac{1}{2}}$	6	243	—	—	0.802	1.045
3880.779	—	$a^6I_{4\frac{1}{2}}-y^6I^\circ_{5\frac{1}{2}}$	5	226	(112)	2052	0.808	1.034
3869.045	20	$a^6I_{5\frac{1}{2}}-22^\circ_{6\frac{1}{2}}$	5	—	(0)	1400	(1.027)	1.084
3863.409	20	$a^6I_{3\frac{1}{2}}-y^6H^\circ_{2\frac{1}{2}}$	4	193	(95)	−56	0.448	0.641
3863.327	10	$a^6I_{3\frac{1}{2}}-17^\circ_{4\frac{1}{2}}$	5	510	(280)	2746	0.451	0.961
3851.748	8	$a^6I_{3\frac{1}{2}}-23^\circ_{4\frac{1}{2}}$	4	152	—	347	1.031	1 183
3848.233	10*d*	$a^6I_{5\frac{1}{2}}-y^6I^\circ_{6\frac{1}{2}}$	—	—	—	—	—	—
3838.981	20	$a^6I_{3\frac{1}{2}}-26{,}041$						
3826.416	10	$a^6I_{4\frac{1}{2}}-20^\circ_{3\frac{1}{2}}$	4	172	(82)	202	0.803	0.975
3811.774	8	$a^6I_{3\frac{1}{2}}-19^\circ_{4\frac{1}{2}}$	5	604	(302)	—	0.43	1.03
3811.073	10	$a^4I_{5\frac{1}{2}}-29{,}298$	5	—	—	1345	(0.979)	0.898
3807.227	15	$a^6I_{4\frac{1}{2}}-21^\circ_{5\frac{1}{2}}$	5	201	(107)	1920	0.803	1.004
3805.359	50	$a^6I_{6\frac{1}{2}}-y^6I^\circ_{7\frac{1}{2}}$	—	—	(0)	1169	(1.148)	1.151
3780.391	20*d*	$a^6I_{7\frac{1}{2}}-y^6I^\circ_{8\frac{1}{2}}$	—	—	(0)	1124	1.233	(1.220)
3769.644	100	$a^4I_{4\frac{1}{2}}-28{,}170$	6	263	(1182)	887	0.757	1.020
3752.679	10	$a^6I_{3\frac{1}{2}}-20^\circ_{3\frac{1}{2}}$	6	530	(1849)	714	0.450	0.980
3714.808	8*d*	$a^6I_{4\frac{1}{2}}-23^\circ_{4\frac{1}{2}}$	6	369	(1661)	995	0.800	1.169
3615.817	20	$a^4I_{4\frac{1}{2}}-29{,}298$	6	149	(672)	826	0.754	0.902
3614.673	8	$a^6I_{4\frac{1}{2}}-28{,}170$	6	214	(960)	—	0.803	1 017
3522.044	12	$a^4I_{5\frac{1}{2}}-25^\circ_{4\frac{1}{2}}$	4	—	(0)	683	(0.979)	1.045
3470.866	10	$a^4I_{4\frac{1}{2}}-30{,}453$	4	236	(114)	—	0.755	0.991
3354.621	10	$a^4I_{4\frac{1}{2}}-25^\circ_{4\frac{1}{2}}$	6	294	(1321)	—	0.74	1.04
3339 063	10	$a^6I_{4\frac{1}{2}}-30{,}453$	4	182	(90)	163	0.799	0.981
3334.471	15	$a^6I_{3\frac{1}{2}}-25^\circ_{4\frac{1}{2}}$	4	—	(0)	948	(1.027)	1.045
3328.270	15	$a^6I_{3\frac{1}{2}}-30{,}037$	4	353	(178)	−195	0.447	0.800
3282.777	8	$a^6I_{3\frac{1}{2}}-30{,}453$	6	547	—	—	0.448	0.995
3231.349	8	$a^6I_{4\frac{1}{2}}-25^\circ_{4\frac{1}{2}}$	6	246	(1106)	—	0.78	1.03

the Bitter electromagnet,[4] we prepared two sets of spectrograms of twenty plates each, containing exposures to an arc between electrodes of neodymium chloride in silver. Field strengths as determined from impurity lines were: set 58, 85,860 oersteds; set 64, 87,180 oersteds. The plates were obtained by using simultaneously several concave gratings of 35-foot radius, with the technique described in previous papers dealing with other elements,[5] and were measured on an automatic comparator.[6]

A quadratic array was first set up by the usual means, and was then extended by means of the interval sorter and interval recorder,[7] using the new wave numbers of Nd II lines obtained in the M.I.T.-W.P.A. wave-length program. This array was then checked and extended by use of the g values obtained from the Zeeman effect work. It was found that incorrect levels could be eliminated quickly when results obtained with both the combination principle and the Zeeman patterns were combined. In this way the intervals provided checks on patterns which had been improperly inter-

[4] G. R. Harrison and F. Bitter, Phys. Rev. **57**, 15 (1940).
[5] G. R. Harrison and J Rand McNally, Jr., Phys. Rev. **58**, 703 (1940).
[6] G. R. Harrison, J. Opt. Soc. Am. **25**, 169 (1935); Rev. Sci. Inst. **9**, 15 (1938); G. R. Harrison and J. P. Molnar, J. Opt. Soc. Am. **30**, 343 (1940).
[7] G. R. Harrison, Rev. Sci. Inst. **4**, 581 (1933); J. Opt. Soc. Am. **28**, 290 (1938).

TABLE II.

Config. $4f^4(^5I)+$	Term	Term Value cm^{-1}	g values *LS*	g values Obs.	No. Lines
		Nd II—low even terms			
$6s$	$a^6I_{3\frac{1}{2}}$	0.00	0.444	0.447	24
$6s$	$a^6I_{4\frac{1}{2}}$	513.33	0.828	0.803	31
$6s$	$a^6I_{5\frac{1}{2}}$	1470.09	1.035	1.027	8
$6s$	$a^4I_{4\frac{1}{2}}$	1650.21	0.727	0.754	26
$6s$	$a^6I_{6\frac{1}{2}}$	2585.46	1.159	1.148	9
$6s$	$a^4I_{5\frac{1}{2}}$	3066.75	0.965	0.979	8
$6s$	$a^6I_{7\frac{1}{2}}$	3801.91	1.239	1.231	1
$5d$	$a^6L_{5\frac{1}{2}}$	4437.52	0.615	0.620	7
$6s$	$a^4I_{6\frac{1}{2}}$	4512.50	1.108	1.109	1
$6s$	$a^6I_{8\frac{1}{2}}$	5085.61	1.294	1.294	4
$5d$	$a^6L_{6\frac{1}{2}}$	5487.66	0.851	0.854	5
$6s$	$a^4I_{7\frac{1}{2}}$	5985.56	1.200	1.199	1
$5d$	$a^6K_{4\frac{1}{2}}$	6005.33	0.546	0.552	11
$5d$	$a^6L_{7\frac{1}{2}}$	6637.48	1.004	0.998	2
$5d$	$a^6K_{5\frac{1}{2}}$	6931.82	0.839	0.842	10
$5d$	$b^6I_{3\frac{1}{2}}$	7524.68	0.444	0.483	12
$5d$	$a^6L_{8\frac{1}{2}}$	7868.73	1.108	1.107	—
$5d$	$a^6K_{6\frac{1}{2}}$	7950.00	1.015	1.015	2
$5d$	$b^6I_{4\frac{1}{2}}$	8420.33	0.828	0.840	9
$5d$	$a^6G_{1\frac{1}{2}}$	8716.51	0.000	0.008	1
$5d$	$a^6K_{7\frac{1}{2}}$	9042.86	1.129	1.127	—
$5d$	$a^6L_{9\frac{1}{2}}$	9166.22	1.183	1.187	—
$5d$	$b^6I_{5\frac{1}{2}}$	9357.83	1.035	1.034	1
$5d$	$a^6H_{2\frac{1}{2}}$	9674.83	0.286	0.453	4
$5d$	$a^6K_{8\frac{1}{2}}$	10,194.70	1.207	1.205	—
$5d$	$b^6I_{6\frac{1}{2}}$	10,337.09	1.159	1.144	—
$5d$	$a^6L_{10\frac{1}{2}}$	10,516.70	1.233	1.247	—
$5d$	$b^6I_{7\frac{1}{2}}$	11,373.38	1.239	1.230	1
$5d$	$a^6K_{9\frac{1}{2}}$	11,392.07	1.263	1.250	—
$5d$	$b^6I_{8\frac{1}{2}}$	12,459.96	1.294	1.284	2

Term or J value	Term Value	g values *LS*	g values Obs.	No. Lines
	Nd II—middle odd terms			
$1°_{4\frac{1}{2}}$	20,672.55		0.788	4
$_{3\frac{1}{2}}$	20,830.03		0.696	3
$2°_{5\frac{1}{2}}$	20,907.33		0.888	4
$z^6H°_{2\frac{1}{2}}$	21,241.11	0.285	0.309	2
$z^6H°_{3\frac{1}{2}}$	21,291.76	0.825	0.826	3
$_{3\frac{1}{2}}$	21,871.53		0.639	2
$z^6H°_{4\frac{1}{2}}$	22,187.63	1.071	0.979	2
$3°_{3\frac{1}{2}}$	22,389.86		0.755	1
$4°_{4\frac{1}{2}}$	22,455.63		1.003	5
$5°_{5\frac{1}{2}}$	22,696.91		0.965	3
$z^6I°_{3\frac{1}{2}}$	22,850.54	0.444	0.755	4
$z^6H°_{5\frac{1}{2}}$	23,159.99	1.203	1.058	3
$_{4\frac{1}{2}}$	23,171.07		1.081	3
$z^6K°_{4\frac{1}{2}}$	23,230.00	0.545	0.778	5
$6°_{2\frac{1}{2}}$	23,397.39		0.845	5
$7°_{4\frac{1}{2}}$	23,409.53		1.012	3
$z^6I°_{4\frac{1}{2}}$	23,537.38	0.828	0.938	6
$8°_{5\frac{1}{2}}$	23,857.27		1.004	7
$9°_{4\frac{1}{2}}$	24,053.36		0.970	5
$z^6I°_{5\frac{1}{2}}$	24,134.08	1.035	1.014	6
$10°_{4\frac{1}{2}}$	24,321.27		0.899	5
$z^6K°_{5\frac{1}{2}}$	24,445.35	0.839	0.917	5
$11°_{5\frac{1}{2}}$	24,467.98		0.946	3
$12°_{5\frac{1}{2}}$	24,842.87		0.970	5
$_{5\frac{1}{2}}$	25,014.91		1.120	1
$y^6I°_{3\frac{1}{2}}$	25,044.65	0.444	0.820	3
$13°_{5\frac{1}{2}}$	25,080.86		0.988	5
$_{3\frac{1}{2}}$	25,138.56		1.187	3
$_{7\frac{1}{2}}$	25,235.62		1.110	1
$14°_{3\frac{1}{2}}$	25,295.26		1.035	4
$15°_{5\frac{1}{2}}$	25,352.37		1.152	3
$y^6I°_{4\frac{1}{2}}$	25,389.21	0.828	1.029	6
$z^6K°_{6\frac{1}{2}}$	25,524.47	1.015	1.030	1
$16°_{4\frac{1}{2}}$	25,771.50		0.980	4
$y^6H°_{2\frac{1}{2}}$	25,876.57	0.286	0.642	4
$17°_{4\frac{1}{2}}$	25,877.18		0.957	4
$_{2\frac{1}{2}}$	26,041.19		—	—
$_{5\frac{1}{2}}$	26,182.49		1.018	2
$18°_{6\frac{1}{2}}$	26,210.75		1.104	4
$19°_{4\frac{1}{2}}$	26,227.09		1.047	5
$y^6I°_{5\frac{1}{2}}$	26,274.08	1.035	1.028	3
$20°_{3\frac{1}{2}}$	26,640.07		0.976	4
$21°_{5\frac{1}{2}}$	26,772.06		1.013	4
$z^6K°_{7\frac{1}{2}}$	26,912.73	1.129	1.133	2
$22°_{6\frac{1}{2}}$	27,308.97		1.087	1
$23°_{4\frac{1}{2}}$	27,425.05		1.177	3
$24°_{7\frac{1}{2}}$	27,445.91		1.112	—
$y^6I°_{6\frac{1}{2}}$	27,448.70	1.159	1.166	2
$_{6\frac{1}{2}}$	27,744.17		1.086	2
$_{4\frac{1}{2}}$	28,170.45		1.017	2
$z^6K°_{8\frac{1}{2}}$	28,418.90	1.207	1.202	1
$y^6I°_{7\frac{1}{2}}$	28,856.78	1.239	1.161	2
$_{8\frac{1}{2}}$	29,027.49		1.203	2
$_{4\frac{1}{2}}$	29,298.60		0.902	1
$z^6K°_{9\frac{1}{2}}$	30,002.26	1.263	1.267	—
$_{2\frac{1}{2}}$	30,037.04		0.800	1
$y^6I°_{8\frac{1}{2}}$	30,246.67	1.294	1.220	1
$_{3\frac{1}{2}}$	30,453.25		0.990	3
$25°_{4\frac{1}{2}}$	31,451.24		1.048	2

preted because of faint or overlapped components, while the g values checked on accidental coincidences of intervals.

RESULTS

Table I contains the lines of Nd II which we have thus far been able to classify. The first two columns contain the wave-length and arc intensity of the line as given in the *M.I.T. Wavelength Tables*, followed by the lower and upper terms from which the line is believed to arise. The fourth column contains the type of Zeeman pattern observed for the line in accordance with the notation described elsewhere.[8] The fifth column, marked "Sep.", contains the fundamental observed separation between lines of the pattern, which is equal to the difference in g values of the lower and upper levels, in terms of 1000 for the normal Lorenz separation. The columns marked p and n contain the displacements from the zero position of the strongest parallel and perpendicularly-polarized components, respectively, expressed in the same units

[8] G. R. Harrison, W. E. Albertson, and N. Hosford, J. Opt. Soc. Am. **31**, 439 (1941).

as column 5. The last two columns contain g values for the lower and upper levels, respectively, as calculated from the observed data. Lines for which no Zeeman data are entered were too weak to observe, or produced incompletely resolved or badly overlapped patterns. Values enclosed in parentheses were assumed from final averages for the level involved, and were then used to calculate a g value for the other level producing the line.

The levels found in the classification are listed in Table II. The first column lists the electron which, added to the configuration $4f^4(^5I)$ of Nd III, is believed responsible for the levels the designations of which are given in column 2, and value in cm^{-1} in column 3. In that part of the table containing the middle odd terms configuration assignments are not given, and in cases where exact term assignments are not known only the inner quantum number J is given. The columns headed *g values* contain respectively the theoretical g values for LS coupling and the g values observed. The final column gives the number of resolved patterns used in arriving at the average measured value of g given in the preceding column.

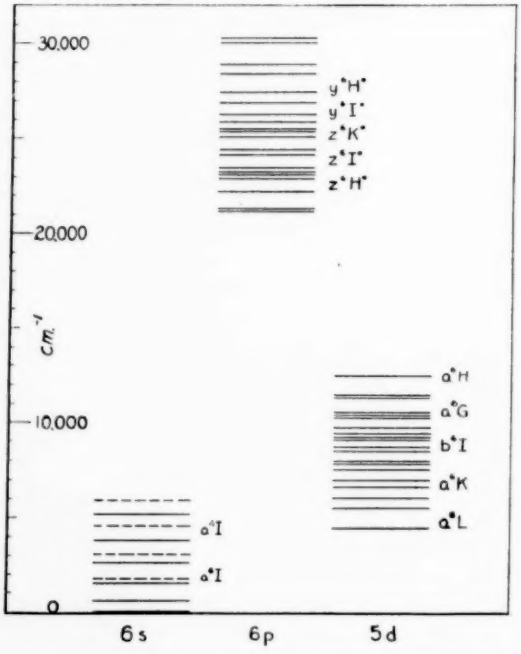

FIG. 1. Identified levels in Nd II to which complete quantum assignments have been made. The strongest lines in the spectrum are those arising from transitions between the upper group of levels and the two lower groups.

LOW CONFIGURATIONS OF SINGLY IONIZED NEODYMIUM

The neutral neodymium atom contains 60 electrons, of which 54 are in closed shells, while 6 are expected to be in the $4f$, $5d$, $6s$, and $6p$ shells. Following the normal order of binding, one might expect the lowest configuration of Nd I to be $4f^4 5d 6s^2$, leading perhaps to a normal configuration in Nd II of $4f^3 5d 6s^2$, $4f^4 6s^2$, or $4f^3 5d 6s$. Instead, the trend observed in Ce II[8] and Pr II[9] is found to continue and $4f^4 6s$ is lowest, with $4f^4 5d$ only slightly higher, both combining strongly with $4f^4 6p$. The terms expected from these configurations are as follows:

$$f^4 s: {}^{6,4}(SDFGI) \quad {}^{4,2}(P_3D_2F_4G_3H_4L_2K_2LM)$$
$$^2(S_2D_4FG_4H_2I_3KL_2N)$$

$$f^4 p: {}^{6,4}(P_2D_2F_3G_2H_2IK)$$
$$^{4,2}(S_3P_5D_9F_9G_{11}H_9I_8K_5L_4M_2N)$$
$$^2(P_6D_5F_9G_7H_9I_6K_6L_3M_3NO)$$

$$f^4 d: {}^{6,4}(SP_2D_4F_3G_4H_3I_2KL)$$
$$^{4,2}(S_5P_9D_{12}F_9G_{11}H_{11}I_8K_6L_6M_4N_2O)$$
$$^2(S_4P_5D_{11}F_{11}G_{14}H_{11}I_{12}K_8L_7M_4N_3OQ).$$

A diagram showing the energy levels of Nd II completely identified thus far is given in Fig. 1. All the low even terms found originate from the $4f^4(^5I)$ term of Nd III by addition of an s or a d electron, while most, if not all, of the upper terms found are believed to rise from addition of a p electron to the same parent configuration.

Table III gives the wave-lengths, estimated arc intensities and temperature classes of identified lines of the fundamental enlarged $s-p$ supermultiplet. Most of the lines in this array check within a few hundredths of a wave number with their calculated values, testifying to the validity of the assignments and the consistency of the wave-length determinations.

The *raies ultimes* of neodymium are usually given as 4303.573A, 3951.154A, and 4177.321A in decreasing intensity. We classify these lines as $a^6I_{3\frac{1}{2}}-z^6K^\circ_{4\frac{1}{2}}$, $a^6I_{5\frac{1}{2}}-21^\circ_{5\frac{1}{2}}$, and $a^6I_{4\frac{1}{2}}-zK^\circ_{5\frac{1}{2}}$. One would expect $a^6I_{8\frac{1}{2}}-z^6K^\circ_{9\frac{1}{2}}$ to be the strongest line in the spectrum and hence the true *raie ultime*,

[9] N. Rosen, G. R. Harrison, and J. R. McNally, Jr., Phys. Rev. **60**, 722 (1941).

TABLE III. Principal supermultiplet of Nd II, (incomplete).*

	$a^6I_{8\frac{1}{2}}$	$a^6I_{7\frac{1}{2}}$	$a^6I_{6\frac{1}{2}}$	$a^6I_{5\frac{1}{2}}$	$a^6I_{4\frac{1}{2}}$	$a^6I_{3\frac{1}{2}}$	$a^4I_{7\frac{1}{2}}$	$a^4I_{6\frac{1}{2}}$	$a^4I_{5\frac{1}{2}}$	$a^4I_{4\frac{1}{2}}$
$z^6K°_{9\frac{1}{2}}$	4012.250 80 III	x	x	x	x	x	x	x	x	x
$z^6K°_{8\frac{1}{2}}$	4284.518 25 IV	4061.085 40 III	x	x	x	x	4456.394 20 IV	x	x	x
$z^6K°_{7\frac{1}{2}}$	—	4325.766 100 IV	4109.455 30 III	x	x	x	—	4462.985 60 IV	x	x
$z^6K°_{6\frac{1}{2}}$	x	4602.242 10 V	4358.169 50 III	4156.083 10 III	x	x	—	—	4451.566 100 III	x
$z^6K°_{5\frac{1}{2}}$	x	x	—	4351.295 30 III	4177.321 15 III	x	x	—	4676.262 2	4385.663 40 III
$z^6K°_{4\frac{1}{2}}$	x	x	x	—	4400.828 50 III	4303.573 100 III	x	x	4958.139 5 V	4632.688 12 V
$y^6I°_{8\frac{1}{2}}$	3973.269 40 IV	3780.391 20*d* IV	x	x	x	x	4120.654 6 IV	x	x	x
$y^6I°_{7\frac{1}{2}}$	4205.595 20 IV	3996.100 40 IV	3805.359 50 III	x	x	x	4371.069 10	4106.582 25 IV	x	x
$y^6I°_{6\frac{1}{2}}$	x	4227.719 20 IV	4020.872 15 III	3848.233 10*d* IV	x	x	—	4358.699 15 IV	4100.240 10 IV	x
$y^6I°_{5\frac{1}{2}}$	x	x	4220.258 10*d* IV	4030.470 20 IV	3880.779 30 IV	x	x	—	4307.778 5 IV	4059.961 20 IV
$y^6I°_{4\frac{1}{2}}$	x	x	x	4179.585 10 IV	4018.826 15 IV	3937.826 20 IV	x	x	—	4211.286 30 IV
$y^6I°_{3\frac{1}{2}}$	x	x	x	x	4075.272 12 IV	3991.743 60 III	x	x	x	—
$z^6H°_{5\frac{1}{2}}$	x	x	4859.030 60 IV	4609.230 5*d*	4414.432 12 IV	x	x	5361.174 3 V	—	4647.759 8 IV
$z^6H°_{4\frac{1}{2}}$	x	x	x	4825.482 100 IV	4612.473 12 IV	4505.741 8	x	x	5228.427 6 V	4867.839 6 V
$z^6H°_{3\frac{1}{2}}$	x	x	x	x	4811.343 60 IV	—	x	x	x	5089.837 10 IV
$z^6H°_{2\frac{1}{2}}$	x	x	x	x	x	4706.542 50 IV	x	x	x	x

* x indicates line forbidden by selection principle for J; lines not found are indicated by —.

but this line, at 4012.250A, though given in our list at intensity 80 and stronger than the two weaker *raies ultimes*, is not usually included in lists of sensitive lines. Intensity anomalies which are similar in character to those found in Pr II[9] will be noted in Table III. The whole matter of the most sensitive lines of Nd and Pr needs re-examination, and exact intensity measurements on these important lines would be well worth making.

Figure 2 shows the shift in binding of levels originating from the configurations f^ns, f^np, and f^nd for the progression La II, Ce II, Pr II, and Nd II; and from f^{n+1} for the first two elements. The lowest f^ns level is taken as zero in each case. This appears to be the actual lowest level of the spectrum except in the case of La II[10] where Russell and Meggers find $5d^2$ and $5d6s$ levels still lower.

No attempt has been made to locate accurately the centers of gravity of the configurations in Fig. 2, but it is obvious that the differences $p-s$ and $p-d$ remain approximately constant through-

[10] H. N. Russell and W. F. Meggers, Bur. Stand. J. Research 9, 625 (1932).

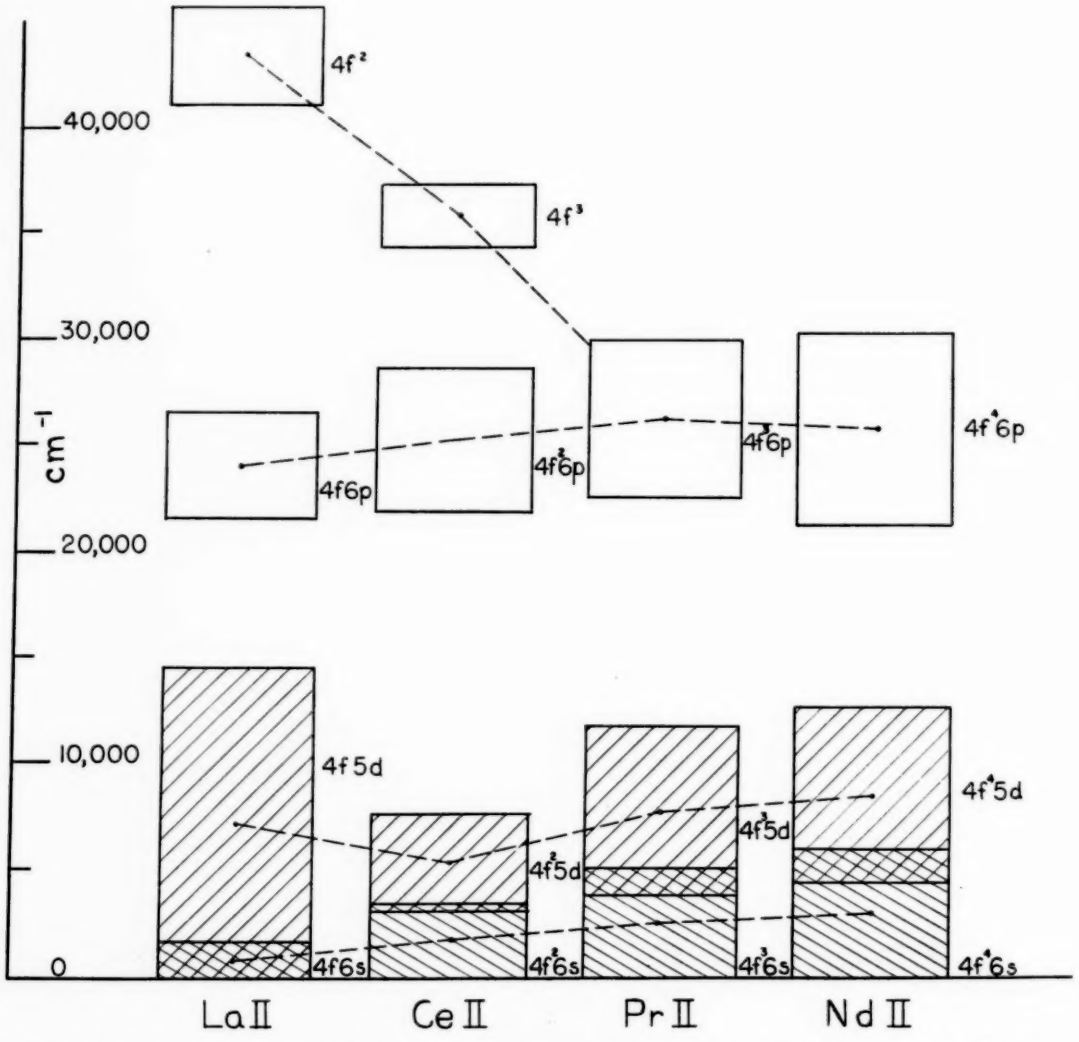

FIG. 2. Variation in the positions of levels due to homologous configurations through the progression La II, Ce II, Pr II, and Nd II, with the lowest level of $f^n s$ set at zero.

out the progression. The f^{n+1} configuration, on the other hand, becomes more closely bound in Ce II than in La II, and it appears that in Pr II many f^4 terms will be found in about the same location as the f^3p terms, while in Nd II they may lie even lower. Figure 2 shows clearly the origin of the great wealth of strong lines emitted by the four elements in and near the violet.

We desire to acknowledge the able assistance of clerical workers on the M.I.T.-W.P.A. Wavelength Project in obtaining the basic data for this analysis, and to express appreciation of a grant from the Rumford Committee of the American Academy of Arts and Sciences in support of the work.

Note added in proof: In every case in this paper the designations $y^6I^\circ_5$ and 21°_5 should be interchanged. This applies to Tables I, II, and III, and simplifies the explanation of the *raies ultimes* anomaly.

Threshold Field Studies of Various Positive Corona Phenomena

K. E. FITZSIMMONS*
Department of Physics, University of California, Berkeley, California
(Received May 19, 1941)

Use of the oscillograph to study the discharge between confocal paraboloid electrodes in air at atmospheric pressure has given the threshold field strength at which the various positive corona phenomena begin. Some effects of humidity and of accumulated oxides in the gap are described. Current-potential curves are given which show the more prominent effects of humidity and accumulated oxides on the discharge after corona onset. From the field data it is possible to verify Meek's theory attending the formation of pre-onset streamers.

INTRODUCTION

PAPERS by Loeb,[1–3] Kip,[4,5] Trichel,[6,7] and others have indicated that streamers are an important aspect of the corona mechanism and of spark breakdown. Loeb pointed out that the streamer mechanism might be an alternative mechanism in the breakdown of plane parallel gaps, and later work of Meek[8] and Loeb[9] has shown it to be the mechanism for values of the product, pressure times gap length, greater than 200 mm×cm in air.

To establish a quantitative theory for streamer formation it was believed that data on the onset fields for corona might be of value. Before the present data were obtained, Meek had postulated a criterion for streamer formation on the basis of spark discharge theory, which was found to predict closely the breakdown potential for plane parallel gaps. It thus became urgent to determine whether or not Meek's criterion applied to streamer formation where the gap geometry gave a non-uniform field, such that streamers initiated corona at much lower potentials than were necessary for breakdown.

To obtain these needed data, it was necessary to measure the onset potentials for streamers in positive point corona with gaps of such geometry that the fields involved could be computed accurately. To this end a series of measurements was carried out with confocal paraboloid electrodes. While making these studies, the fields at which burst pulses, steady burst corona, and breakdown occurred were also measured. In the course of these investigations the first thing that manifested itself was the variabilities introduced by atmospheric conditions, notably humidity and the nitric oxides formed in dry air.

The purpose of these investigations was thus twofold. (1) To give the threshold field strength at which the various positive point corona phenomena begin and to include the newly discovered effects upon these of humidity and accumulations of oxide in the gap. (2) To compare the predictions of Meek's theory with experiment.

APPARATUS

The experiments were performed with air at atmospheric pressure in the gap. Two positive paraboloid points of focal lengths 0.009 cm and 0.019 cm were used, for most of the work, in conjunction with four hollow paraboloid electrodes of focal lengths 1, 2, 3, and 5 cm. The focal lengths of these hollow electrodes gave the effective gap lengths. The points were brass and the hollow electrodes were spun copper.

The high potential source and the method of making oscillographic as well as current and potential observations were very similar to those used by Kip.[4,5] As in Kip's work, a radioactive source was placed in the vicinity of the gap to provide ions to start the various onset phenomena.

When working with dry air in the gap, the entire electrode assembly was placed in a large grounded metal enclosure containing $CaCl_2$ as a

* Now at The State College of Washington, Pullman, Washington.

[1] L. B. Loeb and W. Leigh, Phys. Rev. **51**, 149 (1937).
[2] L. B. Loeb and A. F. Kip, J. App. Phys. **10**, 142 (1939).
[3] Leonard B. Loeb, *Fundamental Processes of Electrical Discharge in Gases* (John Wiley, 1939).
[4] A. F. Kip, Phys. Rev. **54**, 139 (1938).
[5] A. F. Kip, Phys. Rev. **55**, 549 (1939).
[6] G. W. Trichel, Phys. Rev. **54**, 1078 (1938).
[7] G. W. Trichel, Phys. Rev. **55**, 382 (1939).
[8] J. M. Meek, Phys. Rev. **57**, 722 (1940).
[9] L. B. Loeb and J. M. Meek, J. App. Phys. **11**, 438 (1940).

TABLE I. Values for onset of first bursts.

Gap δ (cm)	Potential of point V (volts)	Field at point surface X_A (volts/cm)	Ratio of field to pressure X_A/P (volts/cm/mm)	Distance from point where $\alpha=1$ a (cm)	Average $\int_a^\delta \alpha dx$ for all gaps	Average $\exp[\int_a^\delta \alpha dx]$ for all gaps (ions)
		Dry air—point focal length 0.009 cm				
1	2976	7.0×10^4	92.4	0.0179		
2	3445	7.1×10^4	93.3	0.0181		
3	3660	7.0×10^4	92.0	0.0178	1.31	4.46
5	3890	6.8×10^4	90.0	0.0172		
		Moist air—relative humidity 55 percent at 20°C				
1	2280	5.4×10^4	70.8	0.0116		
2	2840	5.8×10^4	76.8	0.0133		
3	3050	5.8×10^4	76.7	0.0133	0.62	1.86
5	3515	6.2×10^4	81.2	0.0146		

drying agent. A small brushless electric fan fastened above the gap kept the air in circulation. This metal enclosure also served as a limiting space wherein humidity could be controlled and measured when moist air was desired in the gap. Water was introduced into the enclosure by means of a wick from which it was allowed to evaporate until the relative humidity reached the desired value. The relative humidity could be determined by observing a wet and dry bulb thermometer combination through glass windows.

With confocal paraboloids it was possible to calculate the fields, providing the focal lengths of the electrodes and the potential of the point were known. A solution of Laplace's equation, satisfying the boundary conditions involved, leads to the following relation:

$$X=\frac{V}{\log_e(f/F)}\cdot\frac{1}{x+f}. \qquad (1)$$

X is the field in volts/cm at a distance x cm from the end surface of the point electrode along the common axis of the two electrodes, V the potential of the point in volts, f the focal length of the point, and F the focal length of the grounded hollow electrode. It is seen that, once V is determined for a given pair of electrodes, the field at any point in the gap on the common axis can be computed. Furthermore, since $V/\log_e(f/F)$ is a constant for any particular value of V with a given pair of electrodes, the X *vs.* x curve for a given value of V will be a hyperbola. The field will fall in magnitude from a maximum at the point surface to a minimum at the outside electrode surface.

EXPERIMENTAL RESULTS

According to Kip and Trichel we may arrange the phenomena observed in positive point-to-plane corona in the order of their appearance with increasing point potential as follows: (1) small intermittent and irregular pre-onset bursts, (2) pre-onset streamers, (3) steady burst pulse corona of Trichel, (4) breakdown. In essence there is no fundamental difference in the phenomena whether confocal paraboloids or point-to-plane geometry is used. Kip[4] made measurements of fields with confocal paraboloids for the onset of steady burst corona and found the fields to be independent of gap length. He did not, however, extend his observations of this nature to include pre-onset bursts or streamers. In the present work Kip's observations were extensively confirmed, and in addition, a similar independence of gap length and starting fields was found for pre-onset bursts and streamers. This correlates the sequence of the point corona phenomena with the fields for their onset. The observations and discussions attributed to each of these phenomenon will be presented in the order of its onset as the potential of the point was slowly increased.

(1) Pre-Onset Bursts

Burst pulses begin to appear, according to the oscillograph, after the field at the point surface reaches a certain minimum value, depending upon the size of the point and the air pressure.

In the high field region near the point, Townsend's coefficient of electron multiplication α has a value large enough so that an electron which is in this region can produce ions by collision as it moves toward the point. The electrons produced in this process make up an electron avalanche. Townsend's coefficient will depend upon the ratio of field strength to pressure, and since the field increases as the point is approached, the number of positive ions produced by the electron as it moves to the point surface is given by $\int \alpha dx$ taken over the distance x through which the electron moves in reaching the point surface. An electron in a region where the ratio of field to pressure, X/P, is less than 20 volts/cm/mm Hg, contributes very little to ionization by collision as can be seen by reference to Sanders'[10] data on Townsend's coefficient.[11] Loeb and Kip have pointed out that, by use of Sanders' and Townsend's[12] data, the number of ions produced by collision in an electron avalanche can be found by graphical integration of αdx over the distance where α is appreciable and the subsequent evaluation of $\exp[\int \alpha dx]$. This was done for the case of burst onset as well as the other onset phenomena.

Table I gives the values for $\int_0^a \alpha dx$ and for $\exp[\int_0^a \alpha dx]$ for the onset of bursts in both dry and moist air. The relative humidity of the moist air was approximately 55 percent at 20°C. Owing to the rapid decrease of X with distance from the point surface, a was taken[11] as that distance where $\alpha = 1$. Curves in Fig. 1A show the average for all gaps of α *vs.* x at the onset of bursts and streamers in both dry and moist air. Figure 1B shows the corresponding X/P *vs.* x curves. The values of $\exp[\int_0^a \alpha dx]$ for bursts in dry air (4.46 electrons) and in moist air (1.86 electrons) are of the same order of magnitude and are surprisingly small. Each electron coming into the point through a distance a, makes avalanches of only 2 to 4 electrons. Thus, the pulses observed as bursts by Trichel,[6] which numbered in the order of 10^5 or 10^6 ions at least, must consist of a lateral spread of the single small avalanche processes over the point surface. The fact that Trichel observed the burst pulse corona in air at atmospheric pressure to spread over the point as a uniform glow gives confirmation to the idea of the lateral spread. A lateral spread can take place through photoionization of the gas by the photons from the avalanches. Since the high field necessary for avalanche formation exists only near the point; we can expect the glow to first confine itself to the point surface. The burst eventually chokes itself off by positive ion space charge accumulation and by statistical fluctuations.

The reduced value of $\int_0^a \alpha dx$ for the moist air, in comparison to the dry air, with the same criterion for burst pulse detection, can be ascribed only to a much richer yield of photoelectric ionization in contaminated air. This is not surprising since the ionization potentials of O_2 and N_2 are high, and photons capable of exciting them are rare. Water vapor and its dissociation

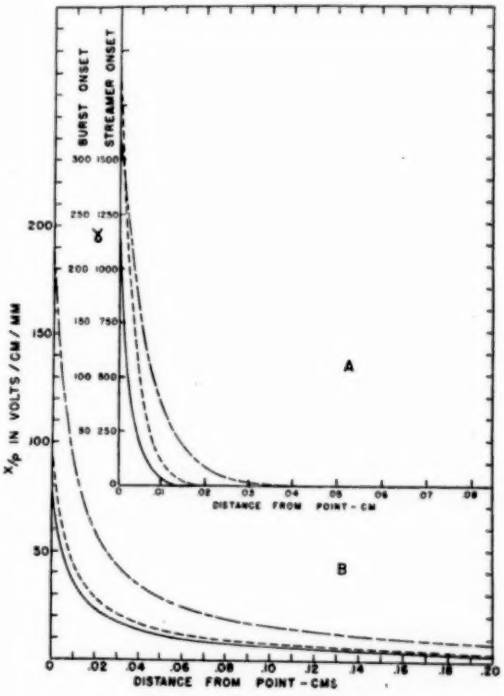

FIG. 1A. Curves showing the variation of Townsend's coefficient α with distance x from the point surface at the onset of first bursts and at the onset of streamers, in moist and dry air. Full curve represents burst onset in dry air; dotted curve represents burst onset in moist air. The dot-dash curve was plotted for streamer onset and was the same for both moist and dry air.

FIG. 1B. X/P *vs.* x curves for the onset of first bursts and for the onset of streamers. The designation given to full, dotted, and dot-dash curves in (A) applies here. Focal length of point for both (A) and (B) was 0.009 cm. Gaps of 1, 2, 3, and 5 cm were used.

[10] Frederick H. Sanders, Phys. Rev. **44**, 1020 (1939).
[11] L. B. Loeb and J. M. Meek, *The Mechanism of the Electric Spark* (Stanford Press, 1941), p. 127.
[12] J. S. Townsend, Phil. Mag. **8**, 738 (1904).

TABLE II. Values for streamer onset.

Gap δ (cm)	f (cm)	V (volts)	X_A (volts/cm)	X_A/P (volts/cm/mm)	a (cm)	Average $\int_0^a \alpha dx$ of all gaps	Average $\exp[\int_0^a \alpha dx]$ of all gaps
			Dry air—focal length of points 0.009 and 0.019 cm				
1	0.009	6124	14.4×10^4	190.0	0.0462		
1	0.019	8010	10.6×10^4	151.0	0.0740	$f=0.009$	$f=0.009$
2	0.009	6809	14.0×10^4	189.0	0.0446	11.00	59,900 ions
2	0.019	9425	10.6×10^4	152.2	0.0740		
3	0.009	7500	14.3×10^4	189.0	0.0459		
3	0.019	10490	10.9×10^4	153.3	0.0750	$f=0.019$	$f=0.019$
5	0.009	8418	14.8×10^4	194.8	0.0476	12.63	306,000 ions
5	0.019	11234	10.6×10^4	151.6	0.0740		
	0.009	Average	14.30×10^4	190.7	0.0467		
	0.019	Average	10.67×10^4	152.2	0.0742		
			Moist air—relative humidity 55 percent at 20°C				
1	0.009	5925	14.0×10^4	184.0	0.0445		
2	0.009	7300	15.0×10^4	197.5	0.0484	11.00	59,900 ions
3	0.009	7485	14.3×10^4	188.3	0.0458		
5	0.009	8000	14.1×10^4	185.1	0.0448		
		Average	14.3×10^4	188.7	0.0464		

products are all readily ionized by photons from O_2 and N_2. The relative efficiency of photo-ionization by radiations from atoms excited by electron impact in moist and dry air is seen from the values of $\int_0^a \alpha dx$ to be of the order of a factor of 2.

(2) Pre-Onset Streamers

Table II gives the quantitative results obtained for this phenomenon. The effect of moist air of 55 percent relative humidity upon streamer onset was tried for the case of the smaller point. Very little difference was found between the values for dry and moist air. The average of the onset fields at the point surface for all four gaps was 14.3×10^4 volts/cm in moist air as well as in dry air. Slightly more variation between values for different gaps was observed in the case of moist air, as can be seen in Table II. It was found that increasing the relative humidity above 60 percent at 20°C brought in more discrepancies for the onset fields of streamers. These discrepancies are doubtless due to the antagonistic actions of the increased photo-ionization following streamer formation and the rapid attachment of electrons to form ions with water vapor. The water vapor ions will have lower mobilities, and this effective lowering of ionic mobility will critically impede streamer formation.

Test of Meek's Theory

According to Meek's theory, the criterion for streamer formation at the positive electrode is that the radial field about the positive space charge in an electron avalanche attains a value X_1, equal to KX_A; X_A is the field at the electrode surface, and K has a value between 0.1 and 1.0. The radial field X_1, in the case of a uniform applied field X, was predicted by Meek to be given by the relation,

$$X_1 = 5.28\times10^{-7}\frac{\alpha \exp[\alpha x]}{(x/P)^{\frac{1}{2}}} \text{ volts/cm.} \quad (2)$$

In the case of confocal paraboloids, however, we are considering a non-uniform applied field, so

TABLE III. Values for pre-onset corona streamers in dry air showing comparison of experimental results with those calculated from Meek's equation.

Gap δ (cm)	f (cm)	L.H.S.	R.H.S.	Difference L.H.S.-R.H.S.	V from Meek's equation (volts)	V Measured (volts)	Deviation* (%)
1	0.009	18.95	19.27	−0.32	6197	6124	+1.20
1	0.019	19.62	19.16	+0.46	7928	8010	−1.03
2	0.009	18.19	19.13	−0.94	7006	6809	+2.90
2	0.019	19.68	19.16	+0.52	9295	9425	−1.40
3	0.009	18.80	19.17	−0.37	7537	7500	+0.50
3	0.019	19.98	19.18	+0.80	10273	10490	−2.10
5	0.009	19.83	19.23	+0.60	8266	8418	−1.80
5	0.019	19.53	19.16	+0.37	11149	11234	−0.80

* (V calculated $-V$ measured)/V measured.

TABLE IV. Values for onset of steady burst corona.

Gap δ (cm)	(cm)	V (volts)	X_A (volts/cm)	X_A/P (volts/cm/mm)	a (cm)	Average $\int_0^a \alpha dx$ for all gaps	Average $\exp[\int_0^a \alpha dx]$ for all gaps
			Dry air—focal length of points 0.009 and 0.019 cm				
1	0.009	6300	14.9×10^4	195.0	0.0474		
1	0.019	9240	12.3×10^4	175.3	0.0855	$f=0.009$	$f=0.009$
2	0.009	7450	15.3×10^4	201.3	0.0496	13.99	1.19×10^6 ions
2	0.019	10902	12.3×10^4	176.0	0.0885		
3	0.009	8300	15.9×10^4	208.8	0.0517		
3	0.019	11958	12.4×10^4	175.0	0.0880	$f=0.019$	$f=0.019$
5	0.009	9650	16.9×10^4	222.4	0.0559	18.87	128.3×10^6 ions
5	0.019	13663	12.8×10^4	183.6	0.0922		
	0.009	Average	15.75×10^4	206.9	0.0512		
	0.019	Average	12.45×10^4	177.5	0.0886		
			Moist air—relative humidity 65 percent at 20°C				
1	0.009	6700	15.8×10^4	207.0			
2	0.009	8030	16.5×10^4	217.0			
3	0.009	8700	16.6×10^4	219.0			
5	0.009	10200	17.9×10^4	235.0			

that α is not constant with distance x from the point. The radial field for this case is given by the equation,

$$X_1 = 5.28\times10^{-7}\frac{\alpha_A \exp\left[\int_0^a \alpha dx\right]}{(a/P)^{\frac{1}{2}}} \text{ volts/cm.} \quad (3)$$

α_A is the value of α at the point electrode surface, and corresponds to the applied field X_A; a is the distance of the point of origin of the avalanche from the point. The point of origin of the avalanche may be taken as that point where $\alpha=1$, for in the highly divergent fields the rate of decline of α is so rapid that there is little contribution[11] to the term $\int \alpha dx$ beyond the point where $\alpha=1$. If we put $X_1=KX_A=0.1X_A$, we obtain the equation

$$\int_0^a \alpha dx + \log_e \alpha_A = 12.16 + \log_e\left(\frac{X_A}{P}\right) + \tfrac{1}{2}\log_e (Pa). \quad (4)$$

With calculations made on the basis of results for streamer onset, it is possible to check the validity of this equation and thus Meek's criterion for streamer formation. The experimental potentials at different gap lengths and from them the values of the fields X_A [by Eq. (1)] at the point surface for streamer onset enable us to determine $\int_0^a \alpha dx$, α_A, and a for each case. It is important to note here that the values of α come from Sanders' and Townsend's independent determinations and not from corona investigations. The method of calculating the potential for streamer onset is to choose some potential as a possible proper value. The value of the field at the point surface and other values of the field associated with finite values of x are then calculated by means of Eq. (1). By use of Sanders' and Townsend's data, a curve relating α and x is plotted and $\int_0^a \alpha dx$ is determined by graphical integration. $\int_0^a \alpha dx$ is then inserted in Eq. (4) together with the corresponding values of X_A, α_A, and a. If the equation is not satisfied, another potential is chosen and the new values of $\int_0^a \alpha dx$, etc., are inserted in the equation. This process is repeated until sufficient values are obtained to plot a curve relating (L.H.S.* − R.H.S.†) with potential V and the value of V is found at which (L.H.S. − R.H.S.) is equal to zero. The values of L.H.S. and R.H.S. for the various gaps and the two points used are given in Table III. The equation is seen to be closely satisfied. In the extreme right-hand column of Table III, a comparison is made between the measured potential and that calculated from Eq. (4).

In his original theory, Meek chose the empirical condition that $K=1.0$. Loeb, in reviewing the

* Left-hand side of Eq. (4).
† Right-hand side of Eq. (4).

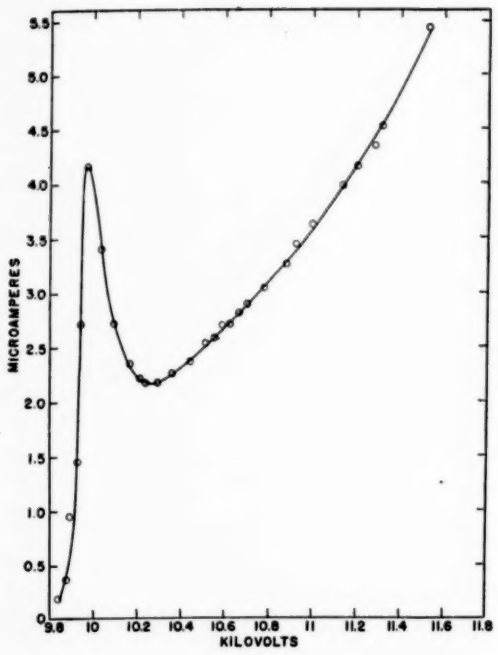

FIG. 2. Corona current-potential curve plotted over the potential range from onset to slightly beyond the linear portion of steady burst corona in air of 65 percent relative humidity at 20°C. Gap length 2 cm; focal length of point 0.0216 cm.

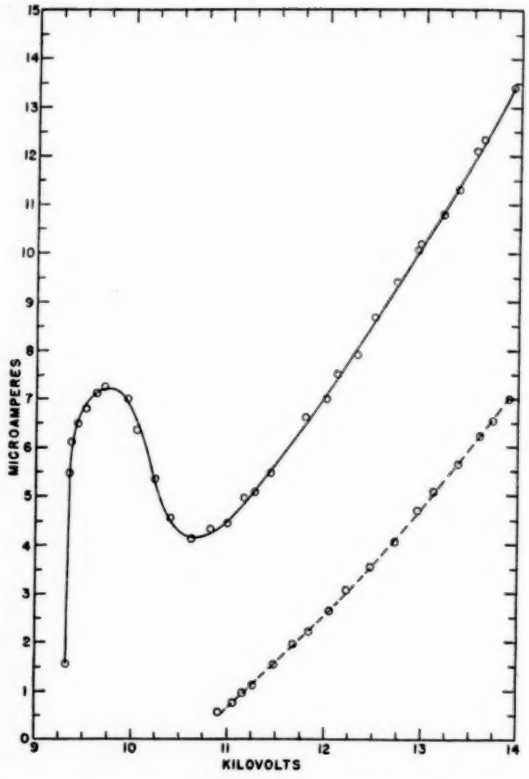

FIG. 3. Corona current-potential curves plotted over the potential range from onset to slightly beyond the linear portion of steady burst corona, showing the effect of gap ventilation. The full curve represents the case of a poorly ventilated gap; the dotted curve was obtained with the same gap well ventilated. Gap length 2 cm; point focal length 0.019 cm.

theory, indicated that K should more likely be less. Meek's calculations with $K=1.0$ gave values of the sparking potential in rough agreement with accepted earlier values. Later studies of the values for breakdown of diverse gaps, as given in the literature, convinced Meek that the value $K=1.0$ was too high, and indicated that a value of $K=0.1$ would be more nearly correct. This became more evident when redeterminations of the sparking potential in air for a 1.0-cm gap by Haseltine[13] yielded the value of 31.6 kilovolts, conforming with some other recent results, in contrast to the older value of 32.2 kilovolts corresponding to $K=1.0$. Because of the accurate determinations of fields possible with confocal paraboloids and the fact that the onset of streamers in corona, as found in the author's investigation, occurred at fields such that Meek's equation yielded the streamers in agreement with theory for $K=0.1$, we must conclude that 0.1 is near the proper value for K.

The fact that we can take values of α from Sanders' data together with the value of K as given by sparking in a plane parallel gap, and predict the streamer onset by Meek's equation, lends strong support to the streamer theory of spark discharge evolved by Loeb and Meek.

(3) Steady Burst Corona

The numerical values associated with the onset of steady burst corona are given in Table IV. Moist air, up to 55 percent relative humidity, had little effect upon the onset fields for steady corona. An interesting result was observed, however, at relative humidities above 60 percent. With a potential on the point corresponding closely to that for the onset of steady burst corona in dry air, there is established a noisy brush corona with the oscillograph showing a rapid succession of very intense streamer pulses. Current measurements, at this part of the observation, indicate a very rapid rise of rather

[13] W. R. Haseltine, Phys. Rev. **58**, 188 (1940).

unsteady current as the potential is increased. Figure 2 illustrates the current-potential relation for this phenomenon. The current soon reaches a peak value and then drops less rapidly toward a minimum with further increase of potential. At the minimum current after onset the oscillograph indicates very few streamers, and with further increase of potential the current begins to rise steadily and linearly with no streamers indicated by the oscillograph. Instead, there is observed the same disturbance as is seen at the onset of steady burst corona in dry air. The data for this curve were taken with a point of 0.0216-cm focal length in conjunction with a 2.0-cm gap; but it is characteristic in general of all the points and gaps that were used. The peak value of current and the potential range from the beginning of any current at all to the start of steady burst corona are very sensitive to changes in humidity. It was impossible to maintain humidity constant enough, with the available apparatus, to get exact reproduction of results. It is to be noted that the potential range, wherein this unsteady brush type corona occurs, is quite limited; consequently, if an observer is changing the potential in steps of 100 volts or more, this unusual part of the curve may be missed entirely. The lower part of Table IV gives the potentials and corresponding approximate fields for the establishment of *steady* burst corona with various gaps; using the 0.009-cm focal length point in moist air of approximately 65 percent relative humidity at 20°C. The fields at the point for the different gaps do not agree with each other as well as in the case of dry air and of course are all higher. This disagreement can be explained by the extreme sensitiveness of the range of brush corona potential to slight humidity changes. The effect of moisture at corona onset is not entirely clear, but a possible explanation is that it increases photoelectric ionization so greatly that streamers can propagate and may take the place of bursts while the current rises rapidly. Furthermore, when the ionization products get loose in moist air, space charges rapidly become very large, and the result of this abnormally rapid space charge fouling is a drop in current until the potential increases to a value where the applied fields can clear out the space charges.

A similar effect upon the current-potential curves in dry air was observed with a poorly ventilated gap. Comparative curves for poor and good ventilation are shown in Fig. 3. This effect is undoubtedly due to the formation of nitric oxides, which are produced in considerable quantities, and have ionization thresholds in the ultraviolet around 1200 angstroms and above. Thus, as in the case of moist air, increased photoelectric ionization may allow streamers to propagate and take the place of bursts with a resulting abnormal rise in current, but, in addition, the oxides can produce very large space charge effects through attaching electrons and slowing both positive and negative ions; so that the current eventually drops until sufficient fields are applied to remove the space charges. With dry air and a well ventilated gap, the current-potential curves have the same general characteristics as those obtained by Kip[4] with point-to-plane corona.

(4) Spark Breakdown

The breakdown potentials and the corresponding but approximate fields calculated from them are tabulated in Table V. Field curves, obtained by assuming no space charge effects, are shown in Fig. 4. These curves, of course, do not represent the exact state of affairs because of the field distorting charges which, with heavy currents, must exist in the gap. Nevertheless, it is easy to see that the gap length has a decided effect upon the fields for breakdown.[4] Pre-onset

TABLE V. Values for breakdown potentials and approximate fields.

Gap δ (cm)	f (cm)	V (volts)	X (volts/cm)	X/P (volts/cm/mm)
		Dry air		
1	0.009	12000	28.3×10^4	372
1	0.019	13220	17.6×10^4	252
2	0.009	17500	36.0×10^4	474
2	0.019	22889	25.9×10^4	370
3	0.009	23400	44.7×10^4	588
3	0.019	29053	30.2×10^4	425
5	0.009	35000	61.3×10^4	807
5	0.019	42092	39.7×10^4	567
		Moist air—relative humidity 55 percent at 20°C		
1	0.009	11200	26.4×10^4	347
2	0.009	18000	37.0×10^4	487
3	0.009	23340	44.6×10^4	587
5	0.009	35000	61.3×10^4	807

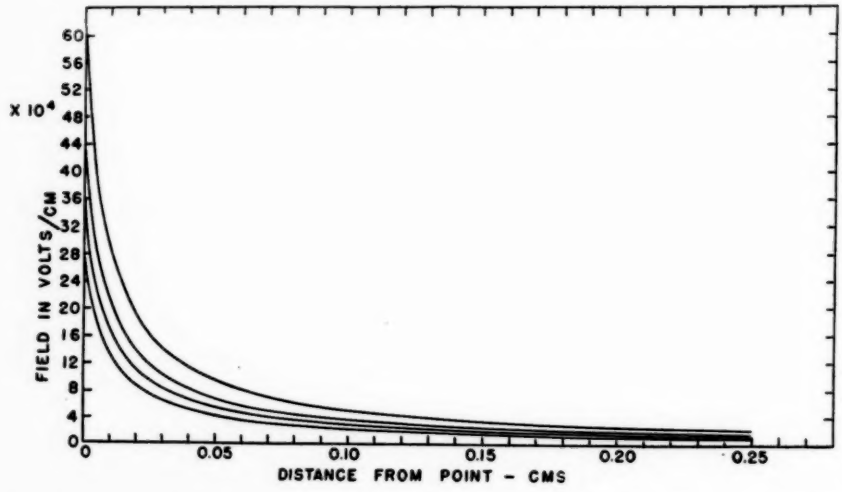

FIG. 4. Breakdown field *vs.* distance from point for various gaps. Beginning with the bottom curve for the 1-cm gap, the curves for the 2-, 3-, and 5-cm gaps follow above in the order of the gap lengths.

bursts, streamers, and steady burst corona each start, for a given point, when the field at its surface reaches a value unique for the phenomenon. Furthermore, the field throughout the gap for any gap is the same within the limits of the gap. There is thus one value of $\int_0^a \alpha dx$ for each phenomenon and each point at which the phenomenon begins. $\int_0^a \alpha dx$ is independent of gap length because the lower limit ($\alpha = 1$) occurs too near the point (i.e. $a < 1$ cm). The field for breakdown, with a given gap, is not independent of gap length since streamers must cross the gap for breakdown to occur; and the shorter it is the more easily do streamers cross because, (1) space charges are cleared more readily, (2) the streamers do not have so far to go.

From Table V it is seen that the effect of moist air is of no consequence except for the shortest gap. With relative humidities above 65 percent, however, breakdown may occur at lower potentials and the results are less reproducible. It was found that poor circulation of air in the gap had a more profound effect upon the breakdown potential than did water vapor; and it is quite likely that the experimental difficulty in properly ventilating the 1.0-cm gap resulted in the comparatively low value for breakdown potential when air of 55 percent relative humidity was used. It was observed consistently that, with either moist or dry air, breakdown would occur at lower potentials when the gap was poorly ventilated. For example, in the case of a 2.0-cm gap with a point of 0.019-cm focal length, breakdown occurred at 16,678 volts with poor ventilation, but increased to 22,889 volts with good ventilation.

In conclusion, the writer takes this opportunity to express his gratitude to Professor Leonard B. Loeb at whose suggestion this work was undertaken, and whose hearty support in guidance and interpretation of results have been most helpful.

Resistivity of Antimony-Tin Single Crystals at Low Temperatures

C. T. LANE AND W. A. DODD
Sloane Physics Laboratory, Yale University
(Received December 17, 1941)

The electrical resistivity of single crystals of pure antimony and alloys of antimony containing small amounts of tin has been determined in the temperature range from 300°K to 4.2°K. In all cases the crystals were orientated such that [111] was perpendicular to the electric field, and various amounts of tin up to about three atomic percent were employed. All the alloys showed normal metallic properties, i.e., the resistivity decreased as the temperature was lowered. However, the average temperature coefficient of resistance between 4.2°K and 77.3°K decreases sharply with increasing tin content and assumes a small constant value at three atomic percent tin. While the addition of tin at room temperature changes the resistivity only slightly, the effect at liquid helium temperature is very large. This "residual" resistivity is approximately a parabolic function of the tin concentration. Qualitative comparison of these results with the Bloch theory of metals is made.

THE three metals, arsenic, antimony, and bismuth are well known to be relatively poor conductors of electricity and are among the few metals whose resistance in the liquid state is less than that for the solid. It has been shown that a Brillouin zone characteristic of the crystal structure of these metals will contain just five electronic states per atom, and the atoms of these metals contain just five electrons beyond the closed *d* shells (valency electrons). Since, however, these metals are not insulators, the inference is that some electrons overlap into a higher zone leaving an equal number of vacant states or positive holes in the first-mentioned zone. Since, as has been mentioned, the conductivity is small, the number of such overlapping electrons must likewise be small, and when the zone structure is destroyed by melting the lattice, the conductivity becomes comparable with that of the divalent metals.

In particular, if small amounts of tin are added to pure antimony, we should expect that the number of overlapping electrons would be reduced for the following reasons. First, tin, in small amounts, forms a simple substitutional solid solution with antimony, and hence the crystal parameters of the alloys are essentially the same as those for pure antimony. Hence, the antimony zone structure is preserved in the alloys. Second, due to the fact that tin has a valency of four, each added atom of this metal will remove one electron from the antimony structure.

Previously S. H. Browne and one of us have reported the effect on the magnetic properties of antimony of variation in the electron concentration by the above means.[1] The results of this investigation indicated that the overlap in antimony was approximately 10^{-2} electron per atom. In the present investigation the effect of varying the overlap on the temperature dependence of the electrical resistivity has been studied.

EXPERIMENTAL DETAILS

The single crystals were produced from the same materials and in the same manner as those used in the previous work referred to in reference 1. In some instances the same crystals were used again. As previously, no chemical analysis was made of the crystals, and the ingredients were accurately weighed and thoroughly mixed in a quartz crucible, under a hydrogen atmosphere, well above the melting point of antimony. The crystals averaged about three inches in length and one-eighth inch in diameter.

Current and potential leads of No. 40 copper wire were spot welded to each crystal. This was done by placing the crystal, the wire, and a ballast resistor of about 25 ohms in series with a d.c. source of potential of 24 volts and touching the wire momentarily to the crystal. Under a low power microscope the wire was seen to have melted into the crystal at the point of contact. In this way and because of the fineness of the wires,

[1] S. H. Browne and C. T. Lane, Phys. Rev. **60**, 899 (1941).

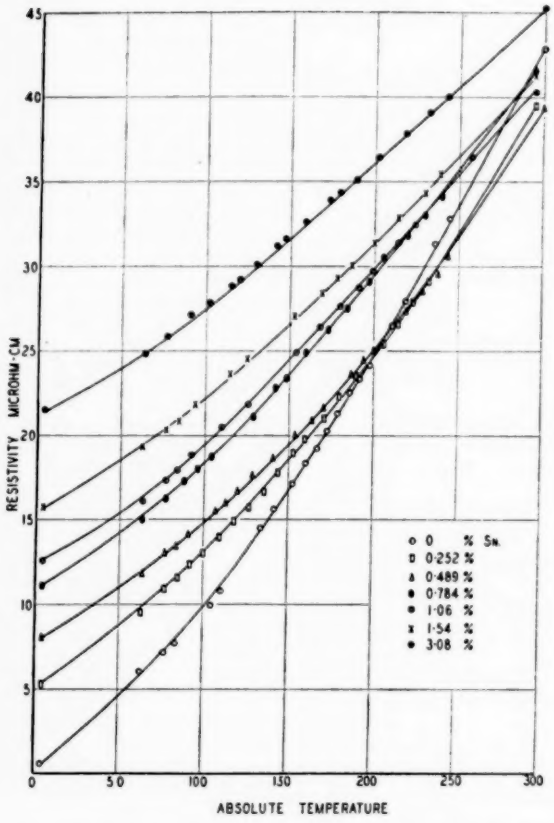

FIG. 1. Resistivity of antimony-tin single crystals from room temperature to 4.2°K.

electrical connection was established with as little disturbance as possible to the specimens.

The resistance of the specimens was determined potentiometrically by comparison with a one-thousandth ohm standard resistance. The current through the crystals, in most cases, was about 70 ma. Since thermoelectric effects in antimony, especially when different parts of the circuit are at widely different temperatures, are likely to be large, a standard type K potentiometer was adapted to the circuit described by Kapitza and Milner.[2] In this type of arrangement any unbalanced thermoelectric potential produces only a steady deflection of the galvanometer while actual e.m.f.'s are balanced dynamically, i.e., by observing the absence of galvanometer "kick."

This circuit proved very useful for our purposes, since not only were any spurious thermoelectric effects automatically eliminated, but in addition the magnitude of the steady galvanometer deflection was a very sensitive measure of any temperature gradients along the specimen.

The specimens were mounted in a hard rubber holder at the bottom of a long narrow dewar flask of soft glass. The resistance was measured at room temperature and at the following fixed points: sublimation point of CO_2 (195°K), boiling point of ethylene (103°K), boiling point of pure oxygen (90.2°K), boiling point of pure nitrogen (77.3°K), near the triple point of nitrogen (ca. 64°K), and finally at the normal boiling point of liquid helium (4.2°K). All the above gases were liquefied by the use of liquid air with the exception of the last one, which was produced by the Kapitza helium liquefier in our laboratory.[3]

In order to obtain observations at a number of temperatures above that of liquid nitrogen, the dewar flask was allowed to warm up gradually from this temperature, the temperature of the specimen being determined by means of a copper-constantan thermocouple whose junction was cemented to the middle of the specimen. Since the warming-up period was of the order of several hours, a large number of resistance determinations at various temperatures could readily be made. If long (14 inches) and narrow ($1\frac{1}{4}$ inches) dewar flasks were used it was found that the temperature change along the specimens never exceeded 1°C at any time. The determinations made in this way were found to be in good agreement with those made at the oxygen, ethylene, and CO_2 fixed points.

In every case the crystallographic orientation of the specimens was such that [111] was perpendicular to the axis of the rod to within one degree. Hence in all instances the current was very approximately perpendicular to [111].

The cross-sectional area of the crystals was determined by observing the height to which a liquid (CCl_4) rose in a fine tube when a known length of crystal was immersed in a wider connecting tube. The apparatus was calibrated by observations on a piece of $\frac{1}{8}$-inch drill rod. The distance between the potential leads was determined with a traveling microscope. The individual resistivities are probably accurate to about two percent.

[2] P. Kapitza and C. Milner, J. Sci. Inst. **14**, 165 (1937).

[3] C. T. Lane, Rev. Sci. Inst. **12**, 326 (1941).

RESULTS AND DISCUSSION

Figure 1 is a plot of the resistivity in microhm cm in the whole temperature range for pure antimony and various alloys. Figure 2 shows the relation between the "residual" resistivity of the alloys as a function of the amount of contained tin. (Curve I). The residual resistance is taken to be equal to the resistance at 4.2°K.[4] Curve II, Fig. 2, is a plot of the mean temperature coefficient of resistance (θ_{Av}) in the range 4.2°K to 77.3°K, as a function of alloy composition. In this case θ_{Av} is defined as the difference between the resistance at 77.3°K and 4.2°K divided by the resistance at 77.3°K.

An inspection of Fig. 1 shows that all the alloys behave as "normal" metals, that is, the resistance decreases more or less linearly as the absolute temperature is reduced. No negative temperature coefficient, such as has been reported in bismuth alloys,[5] is observed even though in the last alloy all the overlapping electrons have been removed, if the previous estimate of overlap is correct as we believe it to be. On the model which we are using we should expect an antimony alloy in which the overlap has disappeared to behave more like a semi-conductor than a metal. This is brought out more clearly by the plot in Curve II, Fig. 2. A true semi-conductor should have a negative temperature coefficient. For these alloys, however, the mean temperature coefficient appears to approach a small constant value at the higher percentages of tin and gives no indication of becoming negative anywhere up to the solubility limit for the solid solution (about 6 percent tin).

The case of the residual resistivity, Curve I, Fig. 2, is of some interest. For the case of random solid solutions of monovalent metals Nordheim[6] has shown that the part of the residual resistivity due to scattering of the electron waves by foreign atoms is given by

$$\rho_0=\frac{h}{2e^2\Omega_0 N^{\frac{1}{3}}}\left(\frac{3}{\pi}\right)^{\frac{1}{3}}Q,$$

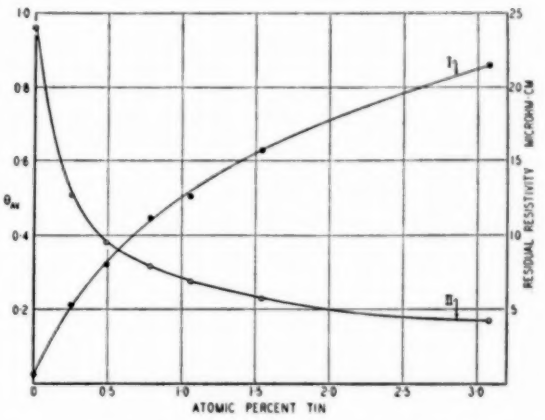

FIG. 2. Curve I—Residual resistivity of antimony-tin single crystals as a function of tin content. Curve II—Mean temperature coefficient between 4.2°K and 77.3°K as a function of tin content.

where N is the effective number of free electrons per cc and Ω_0 is the atomic volume. In the case of a binary alloy the quantity Q is given by

$$Q=\tfrac{1}{2}(1-Z)ZQ_{12},$$

where Z is the atomic fraction of the solute and Q_{12} may be thought of as the effective scattering cross section of each atom of the solute.

In the present experiment Z is always a very small quantity and therefore Q and hence ρ_0 should be a linear function of Z. This, however, is not the case. The residual resistivity is roughly a parabolic function of Z. Two possible reasons for this discrepancy suggest themselves. First, tin may not form a true random solid solution with antimony. This seems unlikely except for extremely small values of Z (around 0.01 percent) where there is some evidence that groups of foreign atoms segregate in the (111) planes of the crystal, at least in the allied element bismuth.[7]

A second more likely possibility lies in the fact that as Z is increased the effective number of free electrons is reduced. It is difficult, however, to form an estimate of this effect since some of the conduction in antimony is undoubtedly due to positive holes.[8]

While the numbers of overlapping electrons and positive holes are equal in pure antimony, this is no longer true when a tetravalent impurity

[4] Some rough measurements on pure antimony indicated that the resistivity was substantially constant between 4.2°K and 1.6°K.

[5] N. Thompson, Proc. Roy. Soc. **A155**, 111 (1936).

[6] L. Nordheim, Ann. d. Physik **9**, 641 (1931).

[7] A. B. Focke, Phys. Rev. **46**, 623 (1934).

[8] The Hall coefficient in polycrystalline antimony is positive.

is added. The difference is[9]

$$N^{(+)}-N^{(-)}=Z/\Omega_0. \quad (1)$$

Further, Jones has shown that, if one assumes complete circular symmetry about [111] (actually it is trigonal) then the conductivity perpendicular to the principal axis (our case) is given by

$$\sigma_\perp=\sigma_\perp{}^{(-)}+\sigma_\perp{}^{(+)}, \quad (2)$$

where

$$\sigma_\perp{}^{(-)}=\frac{e^2}{c^2}\frac{\tau^{(-)}N^{(-)}}{m^{(-)}},$$

$$\sigma_\perp{}^{(+)}=\frac{e^2}{c^2}\frac{\tau^{(+)}N^{(+)}}{m^{(+)}}.$$

Here τ is the relaxation time and m the reduced mass.

It appears from (1) combined with (2) that the effect of reducing the overlap would be to add an additional term to ρ_0 over and above the linear term due to the random atomic scattering. The experimental results, however, indicate just the opposite effect. It appears, therefore, that one must suppose that the low temperature conductivity is due mainly to positive holes, and further that as the overlap is reduced the density of such holes sharply increases.

In conclusion we should like to express our thanks to Dr. S. H. Browne for providing some of the crystals used in this experiment. This work was supported, in part, by a grant from the George Sheffield Fund.

[9] H. Jones, Proc. Roy. Soc. **A155**, 653 (1936).

FEBRUARY 1 AND 15, 1942 PHYSICAL REVIEW VOLUME 61

Theory of Complex Spectra. I

GIULIO RACAH
The Hebrew University, Jerusalem, Palestine

(Received November 14, 1941)

This paper gives a closed formula which entirely replaces for the two-electron spectra the previous lengthy calculations with the diagonal-sum method. Applications are also made to some configurations with three or more electrons and to the p'' configurations of the nuclei.

§1. INTRODUCTION

THE first-order perturbation energy for the terms of a given configuration was calculated at first by Slater.[1] In his classical paper he showed that the electrostatic interaction between two electrons depends on a very few integrals F^k and G^k, and he developed the diagonal-sum procedure for calculating the coefficients of these integrals; with this procedure he obtained numerical tables of coefficients for the two-electron configurations involving s, p, or d electrons. These tables were extended by several authors[2] to f electrons and to some configurations with three or more electrons.

But the diagonal-sum procedure has some deficiencies. Firstly, when two terms of a kind occur in a given configuration, this procedure will determine only the sum of their energies, and they can be separated only by other methods. Secondly, this method does not give general formulas, but only numerical tables; it is therefore impossible to make generalizations, and one must begin again for each new case with new and more complex calculations.[3]

It is the purpose of this paper to substitute for the numerical methods of Chapters VI and VII of TAS more general methods and more conformable to Chapter III of the same book.

[1] J. C. Slater, Phys. Rev. **34**, 1293 (1929).
[2] See E. U. Condon and G. H. Shortley, *Theory of Atomic Spectra* (Cambridge 1935), (which we shall denote by TAS), Chapters VI and VII, for definitions, notations and bibliographical indications.
[3] G. H. Shortley and B. Fried, Phys. Rev. **54**, 739 (1938).

§2. TWO-ELECTRON CONFIGURATIONS

If ω is the angle between the radii vectors of the two electrons, the coefficients f_k of F^k are[4] the eigenvalues of the matrix

$$(l_1 l_2 m_1 m_2 | P_k(\cos\omega) | l_1 l_2 m_1' m_2'); \tag{1}$$

here P_k is the Legendre polynomial of the order k. The transformation which diagonalizes this matrix is $(l_1 l_2 LM | l_1 l_2 m_1 m_2)$, and therefore

$$f_k(l_1 l_2 L) = \sum_{m_1 m_2 m_1' m_2'} (l_1 l_2 LM | l_1 l_2 m_1 m_2)(l_1 l_2 m_1 m_2 | P_k(\cos\omega) | l_1 l_2 m_1' m_2')(l_1 l_2 m_1' m_2' | l_1 l_2 LM), \tag{2}$$

or

$$f_k(l_1 l_2 L) = (l_1 l_2 LM | P_k(\cos\omega) | l_1 l_2 LM). \tag{3}$$

In the same way, if $\pm g_k$ are the coefficients of G^k for the singlet and for the triplet terms, we have

$$g_k(l_1 l_2 L) = \sum_{m_1 m_2 m'_1 m'_2} (l_1 l_2 LM | l_1 l_2 m_1 m_2)(l_1 l_2 m_1 m_2 | P_k(\cos\omega) | l_2 l_1 m'_2 m'_1)(l_1 l_2 m'_1 m'_2 | l_1 l_2 LM), \tag{4}$$

and in view of[5]

$$(l_1 l_2 m'_1 m'_2 | l_1 l_2 LM) = (-1)^{l_1 + l_2 - L}(l_2 l_1 m'_2 m'_1 | l_2 l_1 LM), \tag{5}$$

this becomes

$$g_k(l_1 l_2 L) = (-1)^{l_1 + l_2 - L}(l_1 l_2 LM | P_k(\cos\omega) | l_2 l_1 LM). \tag{6}$$

Slater calculated the matrix elements of $P_k(\cos\omega)$ in the $l_1 l_2 m_1 m_2$ scheme, and then obtained the eigenvalues of this operator by means of the diagonal-sum procedure; we will calculate the matrix elements of $\cos\omega$ directly in the $l_1 l_2 LM$ scheme by the method of Güttinger and Pauli,[6] and then calculate f_k and g_k with the ordinary methods of matrix calculations.

If $\mathbf{u}_i$ is the unit vector in the direction from the origin to the electron i, by comparing TAS $4^3 21$ with TAS $9^3 11$, we have

$$(l_i \| u_i \| l_i) = 0, \quad (l_i \| u_i \| l_i - 1) = (l_i - 1 \| u_i \| l_i) = \frac{1}{[(2l_i - 1)(2l_i + 1)]^{\frac{1}{2}}}; \tag{7}$$

and since

$$\cos\omega = (\mathbf{u}_1 \cdot \mathbf{u}_2), \tag{8}$$

introducing (7) in TAS $12^3 2$ we find that the only non-vanishing elements of $(l_1 l_2 LM | \cos\omega | l_1' l_2' LM)$ are

$$\begin{aligned}
(l_1 l_2 LM | \cos\omega | l_1 - 1\ l_2 - 1\ LM) &= -\frac{[(l_1 + l_2 + L + 1)(l_1 + l_2 + L)(l_1 + l_2 - L)(l_1 + l_2 - L - 1)]^{\frac{1}{2}}}{2[(2l_1 - 1)(2l_1 + 1)(2l_2 - 1)(2l_2 + 1)]^{\frac{1}{2}}}, \\
(l_1 l_2 LM | \cos\omega | l_1 + 1\ l_2 - 1\ LM) &= \frac{[(L + l_1 - l_2 + 2)(L + l_1 - l_2 + 1)(L + l_2 - l_1)(L + l_2 - l_1 - 1)]^{\frac{1}{2}}}{2[(2l_1 + 1)(2l_1 + 3)(2l_2 - 1)(2l_2 + 1)]^{\frac{1}{2}}}, \\
(l_1 l_2 LM | \cos\omega | l_1 - 1\ l_2 + 1\ LM) &= \frac{[(L + l_1 - l_2)(L + l_1 - l_2 - 1)(L + l_2 - l_1 + 2)(L + l_2 - l_1 + 1)]^{\frac{1}{2}}}{2[(2l_1 - 1)(2l_1 + 1)(2l_2 + 1)(2l_2 + 3)]^{\frac{1}{2}}}, \\
(l_1 l_2 LM | \cos\omega | l_1 + 1\ l_2 + 1\ LM) &= -\frac{[(l_1 + l_2 + L + 3)(l_1 + l_2 + L + 2)(l_1 + l_2 - L + 2)(l_1 + l_2 - L + 1)]^{\frac{1}{2}}}{2[(2l_1 + 1)(2l_1 + 3)(2l_2 + 1)(2l_2 + 3)]^{\frac{1}{2}}}.
\end{aligned} \tag{9}$$

From these formulas it is possible to calculate the matrix elements of $P_k(\cos\omega)$ with the ordinary methods of matrix calculations; in order that these elements may have a value different from zero, k must satisfy the conditions

$$k + l_1 + l'_1 = 2g_1, \quad k + l_2 + l'_2 = 2g_2 \tag{10}$$

[4] TAS §8[6].
[5] TAS 14^3 7.
[6] Güttinger and Pauli, Zeits. f. Physik **67**, 743 (1931); TAS §10^3 *et seq.*

(g_1 and g_2 are integers), and the so-called triangular conditions

$$|l_1-l'_1| \leqslant k \leqslant l_1+l'_1, \quad |l_2-l'_2| \leqslant k \leqslant l_2+l'_2; \tag{11}$$

if these conditions are satisfied, the final result is

$$(l_1l_2LM|P_k(\cos\omega)|l'_1l'_2LM) = \frac{(-1)^{g_1+g_2-k}(2g_1-2l_1)!(2g_2-2l'_2)!g_1!g_2!}{(g_1-k)!(g_1-l_1)!(g_1-l'_1)!(g_2-k)!(g_2-l_2)!(g_2-l'_2)!(2g_1+1)!(2g_2+1)!}$$

$$\cdot\left[\frac{(2l_1+1)(2l'_1+1)(2l_2+1)(2l'_2+1)(l_1+l_2+L+1)!(l'_1+l'_2+L+1)!}{\times(l_1+l_2-L)!(l'_1+l'_2-L)!(L+l_1-l_2)!(L+l'_2-l'_1)!}\right]^{\frac{1}{2}}$$

$$\cdot\sum_u (-1)^u \frac{(u+l'_1-l'_2)!(u+l_2-l_1)!(k+l_1+l'_2-u)!}{(u+L+1)!(u-L)!(l_1+l_2-u)!(l'_1+l'_2-u)!(k-l_1-l'_2+u)!}, \tag{12}$$

where, in the summation, u takes on all integral values consistent with the factorial notation, the factorial of a negative number being meaningless.

In order to demonstrate this formula, it suffices to verify that (12) reduces to $\delta(l_1l'_1)\delta(l_2l'_2)$ for $k=0$ and to (9) for $k=1$ and that, introducing (12) for $k=n-1$ and $k=n-2$ in the formula[7]

$$P_n(\cos\omega) = \frac{2n-1}{n}\cos\omega P_{n-1}(\cos\omega) - \frac{n-1}{n}P_{n-2}(\cos\omega) \tag{13}$$

written in matrix form, we obtain again (12) for $k=n$. These verifications are somewhat long, but they are not difficult and will be omitted for brevity.

It is remarkable that (12) has an unsymmetrical aspect: it is however possible (as is shown in the appendix) to transform this formula by means of algebraic identities and to replace it with[8]

$$(l_1l_2LM|P_k(\cos\omega)|l'_1l'_2LM)$$

$$= \frac{(-1)^{g_1+g_2-k-L}(l_1+l'_1-k-1)!!(k+l_1-l'_1-1)!!(k+l'_1-l_1-1)!!}{\times(l_2+l'_2-k-1)!!(k+l_2-l'_2-1)!!(k+l'_2-l_2-1)!!}$$

$$\cdot\left[\frac{(2l_1+1)(2l_2+1)(2l'_1+1)(2l'_2+1)(l_1+l_2-L)!(l'_1+l'_2-L)!}{\times(L+l_1-l_2)!(L+l'_1-l'_2)!(L+l_2-l_1)!(L+l'_2-l'_1)!}\right]^{\frac{1}{2}}$$

$$\cdot\sum_v (-1)^v \frac{(l_1+l_2+l'_1+l'_2+1-v)!}{(l_1+l_2-L-v)!(l'_1+l'_2-L-v)!(l_1+l'_1-k-v)!(l_2+l'_2-k-v)!v!} \tag{12'}$$

$$\times(k+L-l_1-l'_2+v)!(k+L-l'_1-l_2+v)!$$

Introducing (12′) in (3) and (6), and putting

$$v = l_1+l_2-L-w,$$

[7] Courant and Hilbert, *Methoden der Mathematischen Physik* (Springer, 1931), p. 73, Eq. (19).

[8] With the symbol $n!!$ we indicate the *semifactorial* of n, that is the product 1.3.5 . . . n if n is odd, and the product 2.4.6 . . . n if n is even.

we obtain

$$f_k(l_1l_2L)=\frac{(k-1)!!^4(2l_1-k-1)!!(2l_2-k-1)!!(2l_1+1)(2l_2+1)}{(2l_1+k+1)!!(2l_2+k+1)!!}$$
$$\times\sum_w(-1)^w\binom{l_1+l_2+L+1+w}{w}\binom{l_1+l_2-L}{w}\binom{L+l_1-l_2}{k-w}\binom{L+l_2-l_1}{k-w} \quad (14)$$

and

$$g_k(l_1l_2L)=(-1)^{l_1+l_2-L}\frac{(k+l_1-l_2-1)!!^2(k+l_2-l_1-1)!!^2(l_1+l_2-k-1)!!^2(2l_1+1)(2l_2+1)}{(l_1+l_2+k+1)!!^2}$$
$$\times\sum_w(-1)^w\binom{l_1+l_2+L+1+w}{w}\binom{l_1+l_2-L}{w}\binom{L+l_1-l_2}{k+l_1-l_2-w}\binom{L+l_2-l_1}{k+l_2-l_1-w}. \quad (15)$$

The dependence on L of such formulas was already given by Kramers[9] for f_k and by Brinkman[10] for g_k by means of a group-theoretical procedure, but it was impossible, by such a general method, to give the first factor.

Putting

$$p=l_1(l_1+1)l_2(l_2+1),\quad s=l_1(l_1+1)+l_2(l_2+1),\quad \Lambda=L(L+1),\quad \lambda=\frac{\Lambda-s}{2}=(\mathbf{l}_1\cdot\mathbf{l}_2),\quad q=(l_1+l_2+1)^2, \quad (16)$$

we obtain, for the most common and important cases:

$$f_0=1,$$
$$f_2=\frac{6\lambda^2+3\lambda-2p}{(2l_1-1)(2l_1+3)(2l_2-1)(2l_2+3)}, \quad (17)$$
$$f_4=9\frac{70\lambda^4+350\lambda^3-10(6p-5s-39)\lambda^2-10(17p-6s-9)\lambda+3p(2p-4s-27)}{4(2l_1-3)(2l_1-1)(2l_1+3)(2l_1+5)(2l_2-3)(2l_2-1)(2l_2+3)(2l_2+5)},$$

and

$$g_{l_1-l_2}(l_1l_2L)=\frac{(-1)^{l_1+l_2-L}}{2^{2k}}\binom{2k}{k}\frac{\Lambda(\Lambda-2)(\Lambda-6)\cdots[\Lambda-(k-1)k]}{(2l_2+1)(2l_2+3)^2(2l_2+5)^2\cdots(2l_1-1)^2(2l_1+1)},$$

$$g_{l_1-l_2+2}(l_1l_2L)=\frac{(-1)^{l_1+l_2-L}}{2^{2k-1}}\binom{2k-2}{k-1}\Lambda(\Lambda-2)(\Lambda-6)\cdots[\Lambda-(k-3)(k-2)]. \quad (18)$$
$$\cdot\frac{k(2k-1)\Lambda^2-2(k-1)(2k-1)(q-k)\Lambda+(k-1)[(2k-3)q^2-(4k^2-6k-1)q+(k-1)k^2]}{(2l_2-1)^2(2l_2+1)(2l_2+3)^2(2l_2+5)^2\cdots(2l_1-1)^2(2l_1+1)(2l_1+3)^2}.$$

By means of these formulas all results of TAS and of Shortley and Fried[3] were checked, and a sole mistake was found: the coefficient of F_2 and of G_2 in the F terms of the configuration ff is not $+10$, as reported in TAS (p. 207), but -10, as given in the original paper of Condon and Shortley.[11]

§3. CONFIGURATIONS WITH THREE OR MORE ELECTRONS

The expression of the electrostatic interaction of two electrons as function of λ is not only important for a more rapid calculation of the two-electron terms: in the case of three or more electrons the methods of Chapter III of TAS give us the possibility of calculating the matrix elements of

[9] Kramers, Proc. Amst. Acad. **34**, 965 (1931).
[10] Brinkman, Zeits. f. Physik **79**, 753 (1932).
[11] Condon and Shortley, Phys. Rev. **37**, 1030 (1931).

$\lambda_{ij}=(\mathbf{l}_i\cdot\mathbf{l}_j)$ in every complex case of vector coupling; and it is therefore possible to calculate the terms of more complex configurations, even if two or more terms of the same kind occur.

We will at first pay attention to some particular applications to atomic and nuclear spectra, that can be treated without matrix calculations; then we shall treat in detail the p^2p configuration, and give the results for the p^2l configuration. For other important configurations and for the cases of (jj) coupling the calculations are more complex, and a new general procedure for this purpose will therefore be developed in a later paper.

The first application was already made to the p^n configurations by Van Vleck,[12] who found empirically the formula of f_2 for p electrons, and expressed λ^2_{ij} as a linear function of λ_{ij} and of $(\mathbf{s}_i\mathbf{s}_j)$ by means of Dirac's vector model; but, as Van Vleck himself pointed out, such a procedure is not generally sufficient for d^n configurations.

This procedure suffices however for the terms of d^n with higher multiplicity. In these states all spins are parallel, and it follows therefore from the principle of antisymmetry that the possible values of each λ are 0 or -5 (F or P resultant); from this we have that

$$\lambda^2+5\lambda=0; \tag{19}$$

introducing this relation into the expressions

$$f_2(dd)=\frac{2\lambda^2+\lambda-24}{147}, \quad f_4(dd)=\frac{35\lambda^4+175\lambda^3-585\lambda^2-2655\lambda-162}{7938}, \tag{20}$$

we obtain

$$f_2=-(3\lambda+8)/49, \quad f_4=(15\lambda-9)/441, \tag{21}$$

and therefore

$$E=\sum_{i<j}\left(F^0-\frac{3\lambda_{ij}+8}{49}F^2+\frac{15\lambda_{ij}-9}{441}F^4\right);$$

since for a d^n term

$$L(L+1)=6n+2\sum_{i<j}\lambda_{ij}, \tag{22}$$

we obtain that for all d^n configurations with $S=n/2$

$$E=\frac{n(n-1)}{2}F^0-\frac{3\tfrac{1}{2}L(L+1)+n(4n-13)}{49}F^2+\frac{15\tfrac{1}{2}L(L+1)-9\tfrac{1}{2}n(n+9)}{441}F^4. \tag{23}$$

§4. THE NUCLEAR CONFIGURATIONS p^n

The calculation of the energy levels of a nuclear configuration p^n with symmetrical forces was made by Hund[13] with the diagonal-sum procedure. After very long calculations he obtained a numerical table for the energies of such configurations, and from this table he deduced empirical formulas for the interactions of Wigner and of Majorana. The direct calculation of such formulas is a remarkable application of the above developed methods.

Putting, as customary in order to avoid fractional coefficients,

$$F_0=F^0, \quad F_2=F^2/25, \tag{24}$$

we obtain from (17) that the normal (Wigner) interaction between two particles is

$$V_{ij}=F_0+(6\lambda_{ij}^2+3\lambda_{ij}-8)F_2; \tag{25}$$

[12] J. H. Van Vleck, Phys. Rev. **45**, 412 (1934).
[13] Hund, Zeits. f. Physik **105**, 202 (1937).

hence the Wigner interaction between all particles of the configuration is

$$V_W=\frac{n(n-1)}{2}F_0+\sum_{i<j}(6\lambda_{ij}^2+3\lambda_{ij}-8)F_2. \tag{26}$$

In order to calculate this sum, we cannot use Dirac's vector model, because the exclusion principle does not hold for a proton and a neutron; but we can observe that for p particles the operator

$$M_{ij}=\lambda_{ij}^2+\lambda_{ij}-1 \tag{27}$$

is Majorana's operator of position exchange, since it has the eigenvalue 1 for the symmetrical states S and D, and the eigenvalue -1 for the antisymmetrical state P: from (26) and (27) we obtain

$$V_W=\frac{n(n-1)}{2}F_0+\sum_{i<j}(6M_{ij}-3\lambda_{ij}-2)F_2. \tag{28}$$

The sum

$$\mathfrak{M}=\sum_{i<j}M_{ij} \tag{29}$$

is Hund's $(\alpha-\beta)$ and depends only from the symmetry character of the positional eigenfunction of the level: it is the difference between the number of symmetrically connected couples and the number of antisymmetrically connected couples. From (29) and from

$$\sum_{i<j}\lambda_{ij}=\tfrac{1}{2}L(L+1)-n, \tag{30}$$

we obtain

$$V_W=\frac{n(n-1)}{2}F_0+[6\mathfrak{M}-\tfrac{3}{2}L(L+1)-n(n-4)]F_2. \tag{31}$$

The Majorana interaction is

$$V_M=\sum_{i<j}M_{ij}V_{ij}=\mathfrak{M}F_0+\sum_{i<j}(\lambda_{ij}^2+\lambda_{ij}-1)(6\lambda_{ij}^2+3\lambda_{ij}-8)F_2 \tag{32}$$

and reduces to

$$V_M=\mathfrak{M}F_0+\sum_{i<j}(M_{ij}-3\lambda_{ij}+3)F_2 \tag{33}$$

in virtue of

$$\lambda_{ij}^3+2\lambda_{ij}^2-\lambda_{ij}-2=0 \tag{34}$$

(which expresses the fact that λ_{ij} has only the eigenvalues 1, -1, and -2) and of (27). In view of (29) and (30), (33) becomes

$$V_M=\mathfrak{M}F_0+[\mathfrak{M}-\tfrac{3}{2}L(L+1)+\tfrac{3}{2}n(n+1)]F_2. \tag{35}$$

Putting

$$F_0=A-\tfrac{1}{3}B \quad \text{and} \quad F_2=\tfrac{1}{3}B$$

in (31) and (35), we obtain Hund's formulas.

When two terms with the same L, R, S and $\mathfrak{M}$ occur, Hund could only calculate their sum, and said that his formulas hold for their mean values; since our method gives the energies of all terms separately, we can say that in the later case the first-order energies are the same, and that Hund's formulas hold for each term separately.

§5. THE CONFIGURATION p^2p

It follows from §2 that the interaction between two non-equivalent p electrons is

$$W_{pp}=F^0(np,n'p)+\frac{6\lambda^2+3\lambda-8}{25}F^2(np,n'p)\pm(-1)^L\left[G^0(np,n'p)+\frac{6\lambda^2+3\lambda-8}{25}G^2(np,n'p)\right], \tag{36}$$

where the upper sign holds when the spins are antiparallel, and the lower sign when the spins are parallel.

Following Dirac's vector model[14] we can substitute the operator

$$-\frac{1+4(\mathbf{s}\cdot\mathbf{s}')}{2}=-\frac{1+\mu}{2} \tag{37}$$

for the double sign. For $(-1)^L$ we can substitute the operator (27).

Considering that λ satisfies the Eq. (34), we have that

$$W_{pp}=F^0(np,n'p)+\frac{6\lambda^2+3\lambda-8}{25}F^2(np,n'p) \\ -\frac{1+\mu}{2}\left[(\lambda^2+\lambda-1)G^0(np,n'p)+\frac{\lambda^2-2\lambda+2}{25}G^2(np,n'p)\right]. \tag{38}$$

Putting

$$F_0=F^0(np,np)+2F^0(np,n'p),\quad F_2=\tfrac{1}{25}F^2(np,np),\quad F'_2=\tfrac{1}{25}F^2(np,n'p),$$
$$G_0=G^0(np,n'p),\quad G_2=\tfrac{1}{25}G^2(np,n'p),$$

and marking by 1 and 2 the two np electrons, and by 3 the $n'p$ electron, we obtain for the electrostatic interaction of the $np^2n'p$ configuration:

$$E=F_0+(6\lambda_{12}^2+3\lambda_{12}-8)F_2+\sum_1^2{}_i(6\lambda_{i3}^2+3\lambda_{i3}-8)F'_2 \\ -\sum_1^2{}_i\frac{1+\mu_{i3}}{2}[(\lambda_{i3}^2+\lambda_{i3}-1)G_0+(\lambda_{i3}^2-2\lambda_{i3}+2)G_2]. \tag{39}$$

The most convenient scheme for calculating this energy operator is the LS scheme of the parent ion np^2. In this scheme λ_{12} is diagonal, and the coefficient of F_2 is therefore the diagonal matrix

$$\|(\mathrm{L}|6\lambda_{12}^2+3\lambda_{12}-8|\mathrm{L}')\|=\begin{array}{c|ccc} & \mathrm{D} & \mathrm{P} & \mathrm{S} \\ \mathrm{D} & 1 & 0 & 0 \\ \mathrm{P} & 0 & -5 & 0 \\ \mathrm{S} & 0 & 0 & 10 \end{array}. \tag{40}$$

In order to calculate the coefficients of F'_2, G_0 and G_2 we must at first calculate the matrices of λ_{i3}. From TAS 10[3]2 we have

$$\|(\mathrm{L}\vdots l_i\vdots\mathrm{L}')\|=\begin{array}{c|ccc} & \mathrm{D} & \mathrm{P} & \mathrm{S} \\ \mathrm{D} & \frac{1}{2} & \pm\frac{1}{2\sqrt{3}} & 0 \\ \mathrm{P} & \pm\frac{1}{2\sqrt{3}} & \frac{1}{2} & \pm\left(\frac{2}{3}\right)^{\frac{1}{2}} \\ \mathrm{S} & 0 & \pm\left(\frac{2}{3}\right)^{\frac{1}{2}} & \frac{1}{2} \end{array}, \tag{41}$$

[14] Dirac, Proc. Roy. Soc. **A123**, 714 (1929) and *Quantum Mechanics* (Oxford, 1930), Chapter 11.

the upper sign holding for $i=1$ and the lower for $i=2$; from this table and from TAS $12^{3}2$ we obtain

$$\|(\mathrm{L}L\,|\,\lambda_{i3}\,|\,\mathrm{L}'L)\|=\begin{array}{c|ccc} & \mathrm{D} & \mathrm{P} & \mathrm{S} \\ \mathrm{D} & \dfrac{\Lambda-8}{4} & \mp\dfrac{[\Lambda(12-\Lambda)]^{\frac{1}{2}}}{4\sqrt{3}} & 0 \\ \mathrm{P} & \mp\dfrac{[\Lambda(12-\Lambda)]^{\frac{1}{2}}}{4\sqrt{3}} & \dfrac{\Lambda-4}{4} & \mp\dfrac{[\Lambda(6-\Lambda)]^{\frac{1}{2}}}{\sqrt{6}} \\ \mathrm{S} & 0 & \mp\dfrac{[\Lambda(6-\Lambda)]^{\frac{1}{2}}}{\sqrt{6}} & \dfrac{\Lambda-2}{4} \end{array}, \tag{42}$$

Λ having the meaning of (16); and this matrix gives us easily the coefficient of F'_2:

$$\|(\mathrm{L}L\,|\,\sum_{1}^{2}{}_i\,(6\lambda_{i3}^{2}+3\lambda_{i3}-8)\,|\,\mathrm{L}'L)\|=\begin{array}{c|ccc} & \mathrm{D} & \mathrm{P} & \mathrm{S} \\ \mathrm{D} & \dfrac{\Lambda^2-15\Lambda+40}{2} & 0 & \dfrac{\Lambda[(12-\Lambda)(6-\Lambda)]^{\frac{1}{2}}}{\sqrt{2}} \\ \mathrm{P} & 0 & \dfrac{-3\Lambda^2+21\Lambda-20}{2} & 0 \\ \mathrm{S} & \dfrac{\Lambda[(12-\Lambda)(6-\Lambda)]^{\frac{1}{2}}}{\sqrt{2}} & 0 & \dfrac{-5\Lambda^2+42\Lambda-64}{4} \end{array}. \tag{43}$$

In order to calculate the coefficients of G_0 and G_2 we must also calculate the matrices of $\mu_{i3}=4(\mathbf{s}_i\cdot\mathbf{s}_3)$. From TAS $10^{3}2$ and $12^{3}2$ we obtain in the same way

$$\|(\mathrm{s}S\,|\,\mu_{i3}\,|\,\mathrm{s}'S)\|=\begin{array}{c|cc} & \mathrm{s}=1 & \mathrm{s}=0 \\ \mathrm{s}=1 & S(S+1)-1\tfrac{1}{4} & \mp[[S(S+1)+\tfrac{1}{4}][1\tfrac{5}{4}-S(S+1)]]^{\frac{1}{2}} \\ \mathrm{s}=0 & \mp[[S(S+1)+\tfrac{1}{4}][1\tfrac{5}{4}-S(S+1)]]^{\frac{1}{2}} & S(S+1)-\tfrac{3}{4} \end{array} \tag{44}$$

and therefore

$$\left\|\left(\,{}^{m}\mathrm{L}\;{}^{2}L\left|\frac{1+\mu_{i3}}{2}\right|{}^{m'}\mathrm{L}\;{}^{2}L\right)\right\|=\begin{array}{c|cc} & {}^{3}\mathrm{L} & {}^{1}\mathrm{L} \\ {}^{3}\mathrm{L} & \dfrac{1}{2} & \mp\dfrac{\sqrt{3}}{2} \\ {}^{1}\mathrm{L} & \mp\dfrac{\sqrt{3}}{2} & \dfrac{1}{2} \end{array} \tag{45}$$

and

$$\left({}^{3}\mathrm{L}\;{}^{4}L\left|\frac{1+\mu_{i3}}{2}\right|{}^{3}\mathrm{L}\;{}^{4}L\right)=1. \tag{45'}$$

TABLE I.

Atom	Configuration	$(^4P-{}^4D)/(^4D-{}^2S)$
Theory	$np^2n'p$	0.667
N I	$2p^23p$	0.521
N I	$2p^24p$	0.504
O II	$2p^23p$	0.520
S II	$3p^24p$	0.604

From (42) and (45) we get

$$\left\|\left(\alpha L\ {}^2L\left|\sum_1^2{}_i\frac{1+\mu_{i3}}{2}(\lambda_{i3}{}^2+\lambda_{i3}-1)\right|\alpha' L'\ {}^2L\right)\right\|$$

$$= \begin{array}{c|ccc} & {}^1D & {}^3P & {}^1S \\ {}^1D & \dfrac{\Lambda^2-12\Lambda+24}{24} & \dfrac{(\Lambda-4)[\Lambda(12-\Lambda)]^{\frac12}}{8} & \dfrac{\Lambda[(12-\Lambda)(6-\Lambda)]^{\frac12}}{12\sqrt2} \\ {}^3P & \dfrac{(\Lambda-4)[\Lambda(12-\Lambda)]^{\frac12}}{8} & \dfrac{\Lambda^2-8\Lambda+8}{8} & \dfrac{(\Lambda-1)[\Lambda(6-\Lambda)]^{\frac12}}{2\sqrt2} \\ {}^1S & \dfrac{\Lambda[(12-\Lambda)(6-\Lambda)]^{\frac12}}{12\sqrt2} & \dfrac{(\Lambda-1)[\Lambda(6-\Lambda)]^{\frac12}}{2\sqrt2} & \dfrac{-5\Lambda^2+48\Lambda-60}{48} \end{array} \tag{46}$$

and

$$\left\|\left(\alpha L\ {}^2L\left|\sum_1^2{}_i\frac{1+\mu_{i3}}{2}(\lambda_{i3}{}^2-2\lambda_{i3}+2)\right|\alpha' L'\ {}^2L\right)\right\|$$

$$= \begin{array}{c|ccc} & {}^1D & {}^3P & {}^1S \\ {}^1D & \dfrac{\Lambda^2-30\Lambda+240}{24} & \dfrac{(\Lambda-10)[\Lambda(12-\Lambda)]^{\frac12}}{8} & \dfrac{\Lambda[(12-\Lambda)(6-\Lambda)]^{\frac12}}{12\sqrt2} \\ {}^3P & \dfrac{(\Lambda-10)[\Lambda(12-\Lambda)]^{\frac12}}{8} & \dfrac{\Lambda^2-2\Lambda-40}{8} & \dfrac{(\Lambda-7)[\Lambda(6-\Lambda)]^{\frac12}}{2\sqrt2} \\ {}^1S & \dfrac{\Lambda[(12-\Lambda)(6-\Lambda)]^{\frac12}}{12\sqrt2} & \dfrac{(\Lambda-7)[\Lambda(6-\Lambda)]^{\frac12}}{2\sqrt2} & \dfrac{-5\Lambda^2+12\Lambda+156}{48} \end{array} . \tag{47}$$

From (42) and (45′) we get

$$\left({}^3P\ {}^4L\left|\sum_1^2{}_i\frac{1+\mu_{i3}}{2}(\lambda_{i3}{}^2+\lambda_{i3}-1)\right|{}^3P\ {}^4L\right)=-\frac{\Lambda^2-8\Lambda+8}{4} \tag{46′}$$

and

$$\left({}^3P\ {}^4L\left|\sum_1^2{}_i\frac{1+\mu_{i3}}{2}(\lambda_{i3}{}^2-2\lambda_{i3}+2)\right|{}^3P\ {}^4L\right)=-\frac{\Lambda^2-2\Lambda-40}{4}. \tag{47′}$$

Introducing our results into (39) we obtain

$$^4D=F_0-5F_2-F'_2-G_0-4G_2,$$

$$^4P=F_0-5F_2+5F'_2-G_0-10G_2,$$

$$^4S=F_0-5F_2-10F'_2+2G_0-10G_2,$$

$$^2S = F_0 - 5F_2 - 10F'_2 - G_0 + 5G_2,$$

$$^2F = F_0 + F_2 + 2F'_2 - G_0 - G_2.$$

The energy matrix for the ^2D terms is

	^1D	^3P
^1D	$F_0+F_2-7F'_2+\frac{1}{2}G_0-4G_2$	$-\frac{3}{2}G_0+3G_2$
^3P	$-\frac{3}{2}G_0+3G_2$	$F_0-5F_2-F'_2+\frac{1}{2}G_0+2G_2$

and has the eigenvalues

$$^2D = F_0 - 2F_2 - 4F'_2 + \tfrac{1}{2}G_0 - G_2 \pm 3[(F_2 - F'_2 - G_2)^2 + \tfrac{1}{4}(G_0 - 2G_2)^2]^{\frac{1}{2}}.$$

The energy matrix for the ^2P terms is

(46)

	^1D	^3P	^1S
^1D	$F_0+F_2+7F'_2-\frac{1}{6}G_0-\frac{2}{3}\frac{3}{3}G_2$	$(-G_0+2G_2)\sqrt{5}$	$(4F'_2-\frac{1}{3}G_0-\frac{1}{3}G_2)\sqrt{5}$
^3P	$(-G_0+2G_2)\sqrt{5}$	$F_0-5F_2+5F'_2+\frac{1}{2}G_0+5G_2$	$-G_0+5G_2$
^1S	$(4F'_2-\frac{1}{3}G_0-\frac{1}{3}G_2)\sqrt{5}$	$-G_0+5G_2$	$F_0+10F_2-\frac{1}{3}G_0-\frac{1}{3}\frac{0}{3}G_2$

It follows from our results that the ratio $(^1P - {}^3P)/(^1D - {}^3S)$ has the theoretical value of $\frac{2}{3}$. The comparison with the experimental ratios[15] is given in Table I.

The deviations are of the same order as those of the np^3 configurations of the same elements.[16]

§6. THE CONFIGURATION p^2l

The terms of the configuration $np^2n'l$ can be calculated in the same way as those of $np^2n'p$. The only difference is that the coefficients of G^{l-1} and G^{l+2} in W_{pl} are polynomials of higher degree in λ, and must be reduced to the second degree by means of the equation

(47)

$$\lambda^3 + 2\lambda^2 - (l^2 + l - 1)\lambda - l(l+1) = 0, \tag{48}$$

which corresponds to the Eq. (34) of the pp case. This reduction cannot be carried out without specifying the value of l; it is possible however to avoid such direct reduction, by calculating at first the single values of $g_{l-1}(l1L)$ and $g_{l+1}(l1L)$ for the three possible values of L by means of (15), and then determining the polynomials of the second degree which assume these values for the values l, -1, and $-(l+1)$ of the variable λ. By this procedure we find that the electrostatic interaction between a p and a l electron can be expressed by means of the formula

(46′)

$$W_{pl} = F^0(np, n'l) + [6\lambda^2 + 3\lambda - 4l(l+1)]F'_2 - \frac{1+\mu}{2}[(\lambda^2 + l\lambda - l)G_{l-1} + (\lambda^2 - (l+1)\lambda + l + 1)G_{l+1}], \tag{49}$$

where[17]

(47′)

$$F'_2 = \frac{F^2(np, n'l)}{5(2l-1)(2l+3)}, \quad G_{l-1} = \frac{3G^{l-1}(np, n'l)}{(2l+1)(2l-1)^2}, \quad G_{l+1} = \frac{3G^{l+1}(np, n'l)}{(2l+1)(2l+3)^2}. \tag{50}$$

From this point the calculations were carried out exactly in the same way as for p^2p, and give the following results

[15] See Bacher and Goudsmit, *Atomic Energy States* (McGraw-Hill, 1932).
[16] TAS, p. 198.
[17] Our definitions (50) differ in some cases by a factor 3 from the definitions of TAS, p. 177.

Quartets:

$$L=l+1: \quad F_0-5F_2-l(2l-1)F'_2-l(2l-1)G_{l-1}-2(l+1)G_{l+1},$$

$$L=l: \quad F_0-5F_2+(2l-1)(2l+3)F'_2-l(2l-1)G_{l-1}-(l+1)(2l+3)G_{l+1},$$

$$L=l-1: \quad F_0-5F_2-(l+1)(2l+3)F'_2+2lG_{l-1}-(l+1)(2l+3)G_{l+1}.$$

Doublets:

$$L=l+2: \quad F_0+F_2+2l(2l-1)F'_2-l(2l-1)G_{l-1}-G_{l+1},$$

$$L=l-2: \quad F_0+F_2+2(l+1)(2l+3)F'_2-G_{l-1}-(l+1)(2l+3)G_{l+1},$$

$$L=l+1: \quad F_0-2F_2-(l+3)(2l-1)F'_2+\tfrac{1}{2}(2l-1)G_{l-1}-G_{l+1}$$
$$\pm[[3F_2-3(2l-1)F'_2-\tfrac{1}{2}(l-1)(2l-1)G_{l-1}-(l+2)G_{l+1}]^2+3l(l+2)[\tfrac{1}{2}(2l-1)G_{l-1}-G_{l+1}]^2]^{\frac{1}{2}},$$

$$L=l-1: \quad F_0-2F_2-(l-2)(2l+3)F'_2-G_{l-1}-\tfrac{1}{2}(2l+3)G_{l+1}$$
$$\pm[[3F_2+3(2l+3)F'_2+(l-1)G_{l-1}-\tfrac{1}{2}(l+2)(2l+3)G_{l+1}]^2+3(l^2-1)[G_{l-1}+\tfrac{1}{2}(2l+3)G_{l+1}]^2]^{\frac{1}{2}}.$$

The energy matrix for the doublets with $L=l$ is of the third order and has the elements:

$$(^1D|E|^1D)=F_0+F_2-(2l-3)(2l+5)F'_2-\frac{2l^2-13l+12}{6}G_{l-1}-\frac{2l^2+17l+27}{6}G_{l+1},$$

$$(^3P|E|^3P)=F_0-5F_2+(2l-1)(2l+3)F'_2+\tfrac{1}{2}l(2l-1)G_{l-1}+\tfrac{1}{2}(l+1)(2l+3)G_{l+1},$$

$$(^1S|E|^1S)=F_0+10F_2-\tfrac{1}{3}l(2l-1)G_{l-1}-\tfrac{1}{3}(l+1)(2l+3)G_{l+1},$$

$$(^1D|E|^3P)=\tfrac{1}{2}[(2-l)G_{l-1}+(l+3)G_{l+1}][(2l-1)(2l+3)]^{\frac{1}{2}},$$

$$(^3P|E|^1S)=\tfrac{1}{2}[-(2l-1)G_{l-1}+(2l+3)G_{l+1}][2l(l+1)]^{\frac{1}{2}},$$

$$(^1D|E|^1S)=(2F'_2-\tfrac{1}{6}G_{l-1}-\tfrac{1}{6}G_{l+1})[2l(l+1)(2l-1)(2l+3)]^{\frac{1}{2}}.$$

APPENDIX

From the addition theorem for binomial coefficients

$$\sum_s \binom{x}{s}\binom{y}{z-s}=\binom{x+y}{z}, \tag{51}$$

putting $x=a-b$, $y=b$, $z=a-c$, we have

$$\frac{a!}{b!c!}=\sum_s \frac{(a-b)!(a-c)!}{(a-b-s)!(a-c-s)!(b+c-a+s)!s!}. \tag{52}$$

If y is negative, we can transform (51) by means of

$$\binom{y}{z-s}=(-1)^{z-s}\binom{z-s-y-1}{z-s} \tag{53}$$

and obtain

$$\sum_s (-1)^s\binom{x}{s}\binom{z-s-y-1}{z-s}=(-1)^z\binom{x+y}{z} \tag{54}$$

or

$$\sum_s (-1)^s\binom{x}{s}\binom{z-s-y-1}{z-s}=\binom{z-x-y-1}{z}; \tag{54'}$$

putting $y=z-t-1$ we have from (54)

$$\sum_s (-1)^s \frac{(t-s)!}{s!(x-s)!(z-s)!} = (-1)^z \frac{(t-z)!(x+z-t-1)!}{x!z!(x-t-1)!} \quad \text{if} \quad x>t\geqslant z\geqslant 0, \tag{55}$$

and from (54′)

$$\sum_s (-1)^s \frac{(t-s)!}{s!(x-s)!(z-s)!} = \frac{(t-x)!(t-z)!}{x!z!(t-x-z)!} \quad \text{if} \quad t\geqslant x\geqslant 0,\ t\geqslant z\geqslant 0. \tag{55'}$$

Using repeatedly (52), and also (55) and (55′), we can transform the sum in (12) as follows:

$$\begin{aligned}
&\sum_u (-1)^u \frac{(u+l'_1-l'_2)!}{(u+L+1)!}\cdot\frac{(u+l_2-l_1)!}{(u-L)!(k-l_1-l'_2+u)!}\cdot\frac{(k+l_1+l'_2-u)!}{(l_1+l_2-u)!(l_1'+l'_2-u)!}\\
&\quad=\sum_{\alpha\beta u}(-1)^u\frac{(u+l'_1-l'_2)!}{(u+L+1)!}\cdot\frac{(L+l_2-l_1)!(l_2+l'_2-k)!}{(L+l_2-l_1-\alpha)!(l_2+l_2'-k-\alpha)!(k-l_2-l'_2-L+u+\alpha)!\alpha!}\\
&\qquad\cdot\frac{(k+l'_2-l_2)!(k+l_1-l'_1)!}{(k+l'_2-l_2-\beta)!(k+l_1-l'_1-\beta)!(l'_1+l_2-k-u+\beta)!\beta!}\\
&\quad=\sum_{\alpha\beta}(-1)^{k-l_2-l'_2-L+\alpha}\frac{(L+l_2-l_1)!(l_2+l'_2-k)!(k+l'_2-l_2)!(k+l_1-l'_1)!}{(L+l_2-l_1-\alpha)!(l_2+l'_2-k-\alpha)!(k+l'_2-l_2-\beta)!(k+l_1-l'_1-\beta)!}\\
&\qquad\cdot\frac{(l'_1+l_2+L-k-\alpha)!}{(l'_1+l_2+L+1-k+\beta)!}\cdot\frac{(\alpha+\beta)!}{(l'_1-l'_2-L+\alpha+\beta)!(L+l'_2-l'_1)!\alpha!\beta!}\\
&\quad=\sum_{\alpha\beta\gamma}(-1)^{k-l_2-l'_2-L+\alpha}\frac{(L+l_2-l_1)!(l_2+l'_2-k)!(k+l'_2-l_2)!(k+l_1-l'_1)!(l'_1+l_2+L-k-\alpha)!}{(L+l_2-l_1-\alpha)!(l_2+l'_2-k-\alpha)!(k+l'_2-l_2-\beta)!}\\
&\qquad\times(k+l_1-l'_1-\beta)!(l'_1+l_2+L+1-k+\beta)!\\
&\qquad\cdot\frac{1}{(L+l'_2-l'_1-\gamma)!(\alpha-\gamma)!(l'_1-l'_2-L+\beta+\gamma)!\gamma!}\\
&\quad=\sum_\gamma(-1)^{k-l_2-l'_2-L+\gamma}\frac{(L+l_2-l_1)!(l_2+l'_2-k)!(k+l'_2-l_2)!(k+l_1-l'_1)!}{(L+l'_2-l'_1-\gamma)!\gamma!}\\
&\qquad\cdot\frac{(l_1+l'_1-k)!(L+l'_1-l'_2)!}{(L+l_2-l_1-\gamma)!(l_2+l'_2-k-\gamma)!(l_1+l'_1-l_2-l'_2+\gamma)!}\\
&\qquad\cdot\frac{(k+l_1+l'_1+1+\gamma)!}{(l'_1+l'_2+L+1)!(l_1+l_2+L+1)!(k+l_1-l'_2-L+\gamma)!(k+l'_1-l_2-L+\gamma)!}.
\end{aligned}$$

Putting $\gamma=l_2+l'_2-k-v$, this expression becomes

$$\sum_v (-1)^{v-L}\frac{\begin{array}{r}(L+l_2-l_1)!(l_2+l'_2-k)!(k+l'_2-l_2)!(k+l_1-l'_1)!\\ \times(l_1+l'_1-k)!(L+l'_1-l'_2)!(l_1+l_2+l'_1+l'_2+1-v)!\end{array}}{\begin{array}{r}(k+L-l'_1-l_2+v)!(l_2+l'_2-k-v)!(k+L-l_1-l'_2+v)!v!(l_1+l'_1-k-v)!\\ \times(l_1+l_2-L-v)!(l'_1+l'_2-L-v)!(l'_1+l'_2+L+1)!(l_1+l_2+L+1)!\end{array}};$$

introducing this result into (12) we obtain (12′).

Letters to the Editor

PROMPT publication of brief reports of important discoveries in physics may be secured by addressing them to this department. The closing date for this department is the third of the month. Because of the late closing date for the section no proof can be shown to authors. The Board of Editors does not hold itself responsible for the opinions expressed by the correspondents. Communications should not in general exceed 600 words in length.

Electron Polarization

C. G. SHULL*
New York University, University Heights, New York, New York
February 1, 1942

ACCORDING to the Mott calculations[1] based on the Dirac electron theory, under suitable conditions electron polarization should become observable in a doubly-scattered beam of fast electrons. Several previous experiments in this field have yielded contradictory results. Dymond's experiment[2] showed no definite effect within his experimental error of 1 percent. Kikuchi[3] has obtained agreement with the theory, but his results have been questioned because of his use of thick scattering foils with their consequent depolarizing action.[4]

Briefly, the present experiment consisted in studying the number of electrons scattered in the two directions, parallel and anti-parallel to the incident beam, as shown in Fig. 1. Electrons of 400-kev energy were scattered through angles of 90° by gold foils sufficiently thin to insure single scattering (four times thinner than required by Wentzel's criterion). Simultaneous counting was performed at the two positions by Geiger-Müller counters. In the design of the equipment, provision was made for the evaluation of other asymmetries which might mask the true polarization. The asymmetries considered were those caused by (1) geometrical differences, (2) counter dissimilarities, and (3) differences in the "reflection" and transmission intensities (cf. below). Electron polarization will cause a greater number of electrons to be scattered in the anti-parallel direction than in the parallel direction.

With both foils of gold and the first one set in the transmission orientation (as shown in Fig. 1), a residual asymmetry of 8 percent was found. To test the correctness of this asymmetry, an aluminum foil was substituted for the second gold scattering foil, thereby making the expected polarization asymmetry much smaller. The asymmetry then found was 1 percent in the opposite direction, confirming the reality of the above effect. A total of nearly one million and a half electrons have been counted and tabulated into the results listed here.

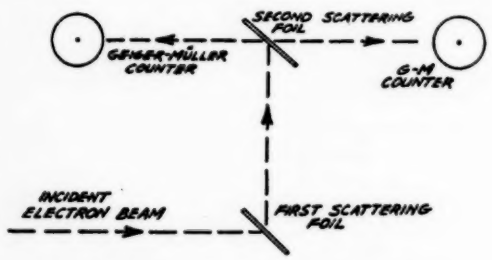

FIG. 1. Schematic diagram of experiment.

The reflection-transmission asymmetry found by Chase and Cox[5] appears to play an important role in polarization experiments. A difference in the number of electrons scattered through the "reflection" side of the foil, the one on which the beam is incident, and the number scattered at the same angle through the other side, the side of transmission, has been observed. This reflection-transmission ratio for the gold foils used amounted to 1.56. There is the possibility then that a reflection polarization asymmetry (in which only electrons "reflected from" the foils are studied) exists as distinct from a transmission polarization asymmetry (in which only electrons scattered through the foil are studied). This difference has been established from the experimental data. The transmission polarization asymmetry is about 2 percent larger than the 8 percent asymmetry given above, while the reflection polarization asymmetry is much smaller than either. Bartlett and Watson[6] have published recalculations of the equations in Mott's treatment and have found for the polarization asymmetry corresponding to 400-kev electron energy, a value of 11 percent.

Since Dymond's experiment, from the figure given in his publication, is of the "reflection" type, the expected asymmetry should be considerably smaller than that predicted by the original theory.

Further experiments on this problem are being carried out with coincidence counters in place of single counters; a complete discussion of this as well as the present work will be published in the near future.

* Now with The Texas Company, Beacon, New York.
[1] Mott, Proc. Roy. Soc. **135**, 429 (1932).
[2] Dymond, Proc. Roy. Soc. **145**, 657 (1934).
[3] Kikuchi, Proc. Phys. Math. Soc. Japan **22**, 805 (1940).
[4] M. E. Rose and H. A. Bethe, Phys. Rev. **55**, 277 (1939).
[5] C. T. Chase and R. T. Cox, Phys. Rev. **58**, 243 (1940).
[6] J. H. Bartlett and R. E. Watson, Phys. Rev. **56**, 612 (1939).

The Behavior of Proportional Counter Amplification at Low Voltages

M. E. ROSE AND W. E. RAMSEY
Bartol Research Foundation of the Franklin Institute, Swarthmore, Pennsylvania
January 10, 1942

IN a recent paper[1] an investigation of the general character of gas amplification in proportional counters was described. This work was confined to the measurement of high amplification factors as a function of counter voltage, counter geometry, nature of gas filler, and gas pressure. Instrumental limitations prevented the pursuit of these studies into the region of low gas amplification where the transition to ionization chamber behavior is to be expected. In order to explore this region and to verify the essential correctness of the ideas previously presented the measurements have been extended by a radically different method.

The principle of the method is based on the comparison of currents in a counter measured at potentials above and below the threshold voltage (voltage at which gas amplification factor begins to depart from unity). The amplification factor at any voltage is then directly obtained as the ratio of these currents.

A tube has been designed which serves equally well for measuring ionization currents in the chamber with and without gas amplification. While the customary counter geometry was preserved all the constructional refinements necessary for the measurement of small ionization currents were incorporated. Since the smallest currents involved are less than 10^{-14} ampere, the need for this care is apparent. A description of the apparatus is given in the caption to Fig. 1(A).

In Fig. 1(B) the amplification factor as a function of counter voltage is given for an argon-oxygen mixture and for two pressures of commercial methane. The voltage region over which the tube is operating as an ionization chamber is immediately evident from these curves. While a threshold voltage is apparent in the present results, this is not to be identified with the threshold voltage as defined in the previous work.[1] According to the theory there developed [cf. Eq. (14)], the amplification curves should show a sharp cut-off at voltages considerably above those observed here. This disagreement is only apparent and is to be explained by the fact that the theory referred to is based on a model which neglects fluctuations in ionization and energy loss of the secondary electrons. These fluctuations are most important at low amplification and the observed behavior is readily interpreted in terms of an energy distribution of the electrons arising in the avalanche process. As a result of the finite width of this distribution the multiplication process, at a given counter voltage, does not start at a fixed point, as previously assumed, but there will be a distribution of such points. Finally, the essentially exponential behavior of the amplification factor, as evidenced by the linear portions of the curves in Fig. 1(B), is in complete agreement with the prediction of the theory.

A more detailed discussion of the present experiment will appear in a forthcoming issue of the *Journal of the Franklin Institute*.

[1] M. E. Rose and S. A. Korff, Phys. Rev. **59**, 850 (1941).

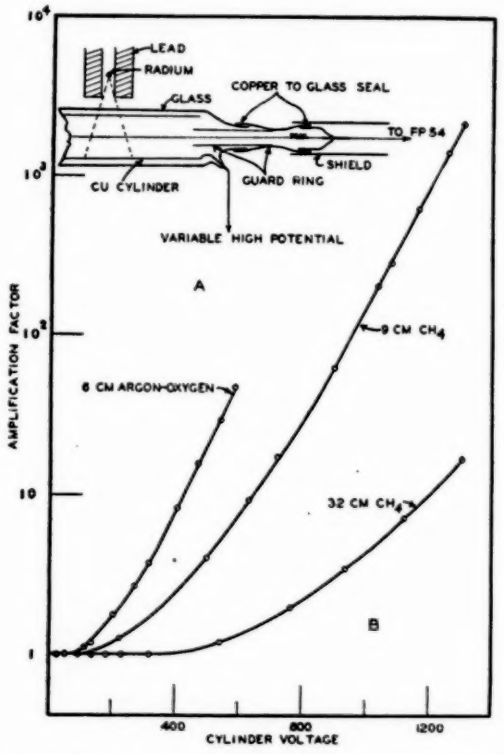

FIG. 1. A. One end (other of similar construction) of the ionization chamber-counter. The central wire connected to the floating grid of FP54 electrometer tube, grid current 10^{-15} amp. Grid of tube maintained at constant potential by compensating inductively for flow of charge to the wire. These known induced potentials provide a measurement of the charge on the wire. Range of measurement extended over wide limits by adding capacity to wire system. Shield and holder for FP54 tube evacuated to eliminate spurious ionization currents. Elimination of leakage currents by guard rings demonstrated by complete run with radium source removed. B. Amplification factor (logarithmic scale) against cylinder voltage for 6-cm argon-oxygen ($0.94A$-$0.06O_2$) and two pressures of CH_4.

Electric Strength of Dielectrics

A. E. W. AUSTEN AND S. WHITEHEAD
The British Electrical and Allied Industries Research Association (E.R.A.)
November 17, 1941

IN a recent paper[1] von Hippel and Maurer have described measurements of the electric strength of a number of dielectrics and its dependence on temperature. They expressed the intention of affording a basis of comparison of their measurements (particularly on KBr) and ours, between which there is a fairly serious discrepancy at low temperatures. We should like to make the following observations in reply.

Edge discharges have received considerable study in these laboratories. When using plane specimens, an immersion medium has not generally been considered suitable unless it has been possible to show either that the product of strength and conductivity of the liquid has been higher than for the test material, or that a substantial increase of conductivity of the immersion medium has produced no change in apparent electric strength. Such conditions were found difficult to satisfy at low temperatures, hence the recessed specimen was preferred. A comparison of the various techniques in the difficult case of mica is given in some detail by Thomas and Hackett[2] and gives us some confidence in thinking that our method of recessed specimens is free from the effects of edge discharge.

In the work of Thomas and Hackett[2] and Standring,[3] we find impulse electric strengths are consistently equal to or greater than values for sustained voltages. At the other end of the scale, we know no exceptions to the rule that an insulator will support only a reduced voltage if the electric stress is indefinitely maintained. Accordingly, we feel that the suggestion by von Hippel and Maurer that a slower application of voltage can give a more valid result requires more evidence.

One unsatisfactory feature of our results remains, i.e., low and erratic values were obtained with polished specimens of KBr. There was some evidence that the rather crude method of polishing used, by means of alumina in oil on a chamois leather covered tool, *produced*, not merely failed to remove, fairly large surface defects. It is therefore our opinion that these specimens were unsatisfactory for this reason and that the results with ground specimens of KBr are valid. Ground specimens for quartz gave the same values as polished specimens, while ground specimens of KBr gave consistent and normal values at room temperatures and above. Irreversible changes due to reduction of temperature were shown to be absent. If, therefore, the discrepancy between von Hippel and Maurer's results and ours is due to the ground surface of our tests, the effect must be masked at room temperature, presumably by a space charge, and manifest itself with some rapidity as the temperature is reduced from about $+10°C$ to $-20°C$. The change in conduction phenomena which might be expected to be associated with such an effect would be a novel hypothesis and, in this connection, an exposition of the variation of conductivity with stress at different temperatures, which was measured but not described by von Hippel and Maurer, would be of great interest.

It would also be of interest to know why von Hippel and Maurer consider their present results to be superior to those reported by von Hippel and Buehl,[4] which were obtained by an apparently similar method. The later results are lower by an amount corresponding to an error of some 40 percent in thickness or 100°C in temperature. An improvement in technique generally produces an *increase* in the values of electric strength obtained rather than a decrease. It would also be useful to know how many tests an individual point on von Hippel and Maurer's curves represents.

[1] A. von Hippel and R. J. Maurer, Phys. Rev. **59**, 820 (1941).
[2] Thomas and Hackett, I.E.E.J. **88**, Pt. I, 295 (1941).
[3] Standring, I.E.E.J. **88**, Pt. II, 360 (1941).
[4] A. von Hippel and R. C. Buehl, Phys. Rev. **56**, 941 (1939).

Remarks on the Letter of A. E. W. Austen and S. Whitehead

Electric Strength of Dielectrics

A. VON HIPPEL, R. J. MAURER, AND G. M. LEE
Massachusetts Institute of Technology, Cambridge, Massachusetts
January 19, 1942

WE should like to give very briefly the information desired.

A point in our breakdown characteristics corresponds, in general, to several independent measurements on different samples. A breakdown experiment, to be considered valid, must fulfill the requirement that the current-voltage characteristic up to the breakdown point shows no disturbance by discharges, and that the microscopic examination of the sample after the test confirms that the breakdown path lies well inside the area of contact between electrode and sample. For example, the revised point for KBr at $T=-158°C$ is the result of three independent measurements yielding values of 366, 338, and 352 kv/cm. The revised point of the breakdown strength at $-73°C$ is based upon a single observation, but it does not differ much from the previous value.

Our new apparatus has been designed for the purpose of giving more accurate data at low temperatures. The old arrangement, in which the high voltage was introduced from below, gave difficulties in the humid summer months on account of condensation of moisture. We feel that the new measurements are reliable.

Electric Breakdown of Ionic Crystals

H. FRÖHLICH
H. H. Wills Physical Laboratory, University of Bristol, England
November 17, 1941

IN two recent papers in this Journal, von Hippel and Maurer[1] and von Hippel and Lee[2] reported some very interesting new experiments on the dielectric strength of ionic crystals. I should like to point out here that these experiments, especially the measurements of the behavior of mixed crystals, provide valuable new confirmation of the author's theory of this effect.[3,4] In this theory the breakdown strength F is calculated from the condition that electrons with a critical energy E gain in the external field F as much energy as they lose to the lattice. Denoting the latter by $B(E)$ we may write

$$e^2F^2\tau(E)/m=B(E), \tag{1}$$

where $\tau(E)$ is the time of relaxation of electrons with the energy E. It is an essential point in the theory that the energy E is of the same order of magnitude as the energy of the conductive electrons in metals (some ev) because this allows us to calculate τ and B in a similar way as in the theory of metals. In a crystal with a small admixture c of foreign atoms, this means that B does neither depend on the temperature T nor appreciably on c whereas[5]

$$1/\tau=1/\tau_p(T)+1/\tau_f, \quad c\ll 1. \tag{2}$$

Here $\tau_p(T)$ is the time of relaxation of the pure crystal, which decreases with increasing T, but does not depend on c; τ_f is independent of T, but

$$1/\tau_f\sim c, \quad c\ll 1. \tag{3}$$

Thus an admixture of foreign atoms always decreases τ similarly as in metals.

Both an admixture of foreign atoms, or an increase of temperature will, therefore, increase the breakdown strength F, as has also been found experimentally up to a certain temperature T_0 where a different type of breakdown sets in. It was formerly thought that this was the beginning of breakdown through thermal instability but von Hippel and Lee[2] suggest other reasons. In any case our theory is valid only below T_0. For KBr which shows a particularly great temperature effect, von Hippel and Maurer[1] give corrected data for F at low temperatures which if correct[6] will give a closer agreement with the theoretically predicted ones than do the previous experimental data.[7–9] Nevertheless, as mentioned before,[4] a complete *quantitative* agree-

TABLE I.

T	$c=0.4$	1.7	4.6%
−150°C	18	20	(13)
−100°C	25	21	(14)
− 50°C	28	24	(16)
0°C	30	23	(13)

ment with the theoretical formula cannot be expected owing to too great simplification of the theoretical treatment of the lattice vibrations.

It thus seemed desirable to derive a relation which allows a check on the fundamental assumptions of the theory independent of the special way in which the absolute values of τ and B were calculated. Such a relation follows[4] at once from Eqs. (1), (2), and (3):

$$F^2(c, T)-F^2(0, T)=cl, \quad c\ll 1, \tag{4}$$

where l depends neither on c nor on T. $F(c, T)$ is the breakdown strength of a crystal at temperature T with an admixture of $100c$ atomic percent foreign atoms. The characteristic point in the relation (4) is the appearance of F^2 and not of F. It is true, if in addition to $c\ll 1$ also $cl\ll F^2(0, T)$, Eq. (4) turns into the more trivial

$$F(c, T)-F(0, T)=cD, \tag{5}$$

if $cD\ll F(0, T)$, and $c\ll 1$, where D is independent of c and T. Therefore, in order to find a real check on (4) an admixture is required which, although $c\ll 1$, changes F considerably, so that no longer $cl\ll F^2(0, T)$.

It is fortunate to find that von Hippel and Lee provide just the required kind of experiments. They find that an admixture of about 4 percent of AgCl to a NaCl crystal increases F by a factor 2. Through their experimental points they draw $F-T$ curves for various values of c. From these curves the quantity

$$l_{\text{exp}}=\{F^2(c, T)-F^2(0, T)\}/c \tag{6}$$

can be deduced which, according to (4), should be a constant (for $T\lesssim T_0\sim 0$°C). Table I gives the results in arbitrary units. For $c=4.6$ percent the extrapolation seems to be very unsafe; a curve giving much better theoretical agreement could easily be drawn through the (only two) experimental points. This has to be considered in judging the result. In view of the fact that F^2, from which l_{exp} is calculated, varies by more than a factor 10, the experiments discussed here seem to provide fair evidence for the correctness of relation (4).

[1] A. von Hippel and R. J. Maurer, Phys. Rev. **59**, 820 (1941).
[2] A. von Hippel and Lee, Phys. Rev. **59**, 824 (1941).
[3] H. Fröhlich, Proc. Roy. Soc. **A160**, 230 (1937); **172**, 94 (1939); Phys. Rev. **56**, 349 (1939).
[4] H. Fröhlich, Proc. Roy. Soc. **A178**, 493 (1941).
[5] Equation (2) has never been derived for slow (thermal) electrons, and it seems doubtful whether it holds in this case. It therefore seems to be doubtful whether a theory of electric breakdown based on the action of slow electrons could account for the observed effect of the admixture of foreign atoms.
[6] A. E. W. Austen and S. Whitehead, Phys. Rev. **61**, 200 (1942).
[7] R. C. Buehl and A. von Hippel, Phys. Rev. **56**, 941 (1939).
[8] A. E. W. Austen and Hackett, Nature **143**, 637 (1939).
[9] A. E. W. Austen and S. Whitehead, Proc. Roy. Soc. **A176**, 33 (1940).

Proceedings of The American Physical Society

DECEMBER 1941 MEETING HELD AT STANFORD UNIVERSITY, CALIFORNIA

THE 245th regular meeting of the American Physical Society was held at Stanford University, California, on December 19, 1941. There were about sixty persons in attendance. The program consisted of the 22 contributed papers, abstracts of which are subjoined.

PAUL KIRKPATRICK
Local Secretary for the Pacific Coast

ABSTRACTS OF CONTRIBUTED PAPERS

1. Efficiency of Positive and Negative Ions as Condensation Nuclei in the Wilson Cloud Chamber. CARL E. NIELSEN, *University of California.*—It is necessary to know the correlation between droplets formed and ions present if the count of droplets in the cloud chamber is used to determine ionization. The droplet to ion ratio f is dependent upon the expansion ratio x, the sign of the ions, and the composition of the vapor. Curves representing the dependence of f upon x have been obtained experimentally for ions of both signs for three different ethyl-alcohol and water mixtures. The experimental results are well represented by the relation $\ln(1-f)=-te^{bx}$, in which t and b are constants related to the sensitive time of the chamber and the properties of the gas and vapor used. With mixtures not too far from 70 percent ethyl alcohol, all positive ions serve as condensation nuclei when negative ions begin to be effective. If a field is used to separate positive and negative ions, the presence of a negative track is evidence that all positive ions are represented by drops in the positive track.

2. Electrons and Heavier Particles at 14,125 Feet. WILSON M. POWELL,* *Kenyon College, Gambier, Ohio.*—In 200 cloud-chamber photographs under 1.27 cm of iron and 1 cm of lead there appear 985 tracks when the chamber is operated at random. Two hundred seventy-nine tracks could not be identified. Of 706 tracks 565 or 80 percent were electrons and the remainder were heavy particles. If the number of electrons is assumed to be increased by a factor of ten in passing through the lead and iron this indicates that 29 percent of the incoming rays are electrons. Fourteen particles show heavy ionization. Thirty photon produced pairs and 10 electron produced pairs appear. A possible explanation for this large number of photon pairs may lie in the stronger absorption of the electrons at this energy.

* Guggenheim Fellow at the University of California.

3. An Efficient Green Line Source. J. KAPLAN, *University of California at Los Angeles.*—A preliminary report of the most intense green line tube to be discovered so far was made by the author at the Pasadena meeting. The tube contains 100 mm N_2 and small amounts of oxygen generated by heating $KMnO_4$. The beautiful green color of this afterglow shows how great the efficiency of green line excitation is. The change in the spectrum of the afterglow with time, reported earlier by the author for the 3466 line of nitrogen, can be observed visually, by noting the change in the color of the glow, or through a direct vision spectroscope. The first positive bands practically disappear in about three seconds, while the green line persists for about 20 seconds. The forbidden lines of oxygen λ5577 and λ2972 appear to last longer than does the λ3466 line of nitrogen. After the first two or three seconds the tube becomes a monochromatic source of λ5577 in the visible and practically a dichromatic source of λ3466 and λ2972 in the near ultraviolet. The tremendous efficiency of the green line excitation is shown also by the strong green line excitation even when most of the oxygen has been cleaned up.

4. Pair Theories of Meson Scattering. E. NELSON AND J. R. OPPENHEIMER, *University of California.*—With a theory of the interaction of spin one-half mesotrons with nuclei in which the nuclear particle, treated as an extended source of mesotrons, is strongly coupled to the mesotron field, both nuclear scattering of low energy mesotrons and the range of nuclear forces were found to be independent of the spin dependence of the coupling and to be given by the size of the source. Thus the scattering cross section for spin dependent coupling is the same as that calculated by Weinberg for scalar coupling. If one uses the observed scattering cross section of cosmic-ray mesotrons, which is of the order of the square of the Compton wave-length of the proton, to fix the size of the source, one obtains a range of nuclear forces only one-tenth of the observed range, which is of the order of the Compton wave-length of the mesotron. Similar results hold when more than one pair are simultaneously created by the nuclear particle. These results show that it is not possible to reconcile small scattering of mesotrons with the observed range of nuclear forces in a theory involving coupling energies non-linear in the mesotron field.

5. The Primary and Probable Ionization of Helium by Cosmic Rays. WAYNE E. HAZEN, *University of California.*—A cylindrical cloud chamber (30 cm×30 cm) was ex-

panded at random. A magnetic field of about 1000 gauss made possible a determination of momentum. The illumination was at an angle of 45° with the chamber axis and photographs were taken at $f10$ and 1/200 sec. with a stereoscopic camera. The tracks of ionizing radiation which passed through the chamber within 1/10 sec. after completion of the expansion were photographed as well as the diffuse tracks of pre-expansion radiation. The sensitive time was checked after every four or five expansions with a shuttered x-ray beam and was always greater than 3/10 sec. Under such conditions each dot appearing along the image of a post-expansion track represented a primary ionization event. Since the clearing field of 40 volts per cm was not shorted out, the columns of positive and negative ions in diffuse tracks were well separated and the probable ionization could also be determined.

6. High Energy Scattering of Deuterons by Protons. D. J. BOHM AND ROY THOMAS, *University of California.* (*Introduced by J. R. Oppenheimer.*)—The scattering of high energy protons on deuterons has been investigated for the range 3–6 Mev of relative kinetic energy using the Born approximation. A complete analytic treatment is possible if the wave functions and potentials are approximated by Gauss functions whose parameters are chosen to give the best fit to available information on the deuteron. It has been found that the tensor forces contribute to the scattering at high angles, and that exchange terms are small but appreciable. Experimental study of the deuteron-proton scattering in this range, especially with regard to angular dependence, would be very desirable because considerable information on the form of the potential well and the types of force present may be obtained by comparison with the calculated values.

7. Further Results on Magnetic Scattering of Neutrons. F. BLOCH AND M. HAMERMESH, *Stanford University, California.*—The scattering and polarization of neutrons passing through iron have been studied using, for the $3d$ shell, a form factor calculated from the tabulated Fe wave-functions of Manning and Goldberg. For the experiment of Alvarez and Bloch, a theoretical effect of 5.1 percent is obtained, in sufficiently good agreement with the experimental result of 6 percent. Extremely large polarization effects are predicted for neutrons of wave-length between 3 and 4A. The effect of the purely magnetic term in the scattering has been examined. The presence of this term leads to a noticeable difference between the scattering of neutrons by specimens at room temperature and above the Curie point, assuming that there the magnetic scattering disappears. Also, this magnetic term is different for unmagnetized and completely demagnetized specimens at any given temperature; it should result in a 25 percent effect in the transmission of neutrons of 4A wave-length through a 4-cm specimen.

8. Angular Distribution in Deuteron Disintegration by Electrons. C. RICHMAN, *University of California.* (*Introduced by J. R. Oppenheimer.*)—In the disintegration of deuterons by electrons, the two effects, corresponding to electric dipole and magnetic dipole photodisintegration of the deuteron, produce their characteristic angular distributions. The electric effect gives approximately a $\sin^2\vartheta$ distribution where ϑ is the angle between the direction of the incident electron and the direction of motion of the proton produced by the collision; the magnetic effect gives a uniform distribution. The complete angular distribution is then of the form $A+B\sin^2\vartheta$, A and B constants for a given energy of electrons. Verification of magnetic disintegration may therefore be obtained through observations of angular distribution. The results of some calculations of A and B for energies not far from the threshold 2.17 Mev are given in the table below. A and B are in units of $10^{-32}d\Omega/4\pi$ cm^2.

Kinetic Energy of Electrons Mev	2.32	2.40	2.50	2.60
A	5.00	9.69	16.6	24.2
B	.877	2.95	8.02	16.4

The range corrections included in these numbers were made on the assumption of a Majorana interaction and a range of $2.80\cdot10^{-13}$ cm.

9. Artificial Radioactivity of Some Rare Earths. C. S. WU AND E. SEGRÈ, *University of California.*—About one year ago we started an investigation of the artificial radioactivity of praseodymium, neodymium and samarium (prepared by Professor Rolla) with a special regard to the possibility of forming radioactive isotopes of element 61. Results were obtained in substantial agreement with those reported by the Ohio group using rare earths of a different author. Some additional assignments were made as follows:

Pr^{140} 3.5 min. β^+ $Pr^{141}(n,2n)$,
Pr^{142} 18.7 hr. β^-, β^- end point 2 Mev no γ.

For the Nd 47 hr. β^-, β^- end point of 0.95 Mev was found in disagreement with the 2.9 Mev found by the Ohio group. $Pr+\alpha$ gives an activity with an apparent half-life of about $200d$. This is probably the same activity as that found by the Ohio group with a period >100 days. It may reasonably be assigned to an isotope of element 61. The high γ to β ratio suggests K-capture or isomeric transition. Absorption measurements give an energy of roughly 670 Kev for the γ-ray. Similar long life rays are shown by deuteron bombarded neodymium. We could not find the 19 hr. activity induced by α on Pr reported by the Ohio group. Samarium bombarded with neutrons shows a 47 hr. period due to an isomeric transition as shown by the characteristic x-rays of Sm emitted.

10. Radiations from Radioactive Gold, Tungsten and Dysprosium. ARNOLD F. CLARK, *University of Indiana.**—By use of a Geiger-Mueller tube counter, both beta-gamma and gamma-gamma coincidences were found associated with the 2.7 day Au^{198}, the 24 hr. W^{187} and the 2.5 hr. Dy^{165} activities. The results show that the beta-ray spectrum of gold is simple, with an absorption end point of 0.78 Mev. The efficiency of the gamma counter indicates that this decay is followed by the 0.44 and 0.28 Mev gamma-rays in cascade.[1,2] Tungsten beta-rays with energies greater than 0.5 Mev give no beta-gamma coincidences, which shows that the beta spectrum is complex. The high

energy beta group, with a maximum energy of 1.4 Mev,[3] evidently leaves the residual nucleus in the ground state. Roughly 40 percent of the beta-rays belong to the low energy group. The maximum energy gamma-ray measures 0.9 Mev; however, the gamma-gamma coincidences indicate that there are other gamma-rays in parallel with the 0.9 Mev transition. The maximum energy gamma-ray from the dysprosium activity is 1.1 Mev. In this case the coincidence results were only qualitative.

* Now at the Radiation Laboratory, University of California, Berkeley.
[1] J. R. Richardson, Phys. Rev. **55**, 609 (1939).
[2] Folke Norling, Arkiv for Mat., Astr. och Fysik **27**, B. 9 (1941).
[3] Fajans and Sullivan, Phys. Rev. **58**, 276 (1940).

11. Gamma-Rays from Radioactive Mercury. A. C. HELMHOLZ, *Department of Physics, Radiation Laboratory, University of California, Berkeley.*—The electron lines from radioactive mercury formed by the deuteron bombardment of gold have been investigated with a β-ray spectrograph. The activities have been studied by Wu and Friedlander,[1] and the samples were kindly supplied by them. K, L, and M conversion lines from two γ-rays, and L and M from a third have been observed. Successive exposures showed the first two to follow the 25 hr. period, the third the 64 hr. period. The energies are 161, 130, and 75 kev, in fair agreement with lines previously reported by Valley.[2] In the case of the first two γ-rays the L conversion is more intense than the K. This may indicate γ-rays of high multipole order. The fact that Wu and Friedlander found that all three of these γ-rays are emitted by Au^{197}, to which both the 25 hr. and 64 hr. periods decay, also indicates large possible spin changes.

[1] C. S. Wu, G. Friedlander, Phys. Rev. **60**, 747 (1941).
[2] G. E. Valley, Phys. Rev. **60**, 167 (1941).

12. Theory of Intensity and Polarization of Continuous X-Radiation. ROBERT WEINSTOCK, *Stanford University.* (*Introduced by F. Bloch.*)—One computes the probability that an electron moving toward an atom with velocity v_1 be deflected through a given angle θ with asymptotic velocity v_2, having experienced an energy loss $h\nu$. These dipole matrix elements of the single process have been rigorously computed by Sommerfeld,[1] but the necessary incoherent integration over all polar angles (θ, ϕ) of scattering of the incident electron has not in general been calculated in closed form. This is carried out by means of a series expansion; the resulting integrated series converges with sufficient rapidity to be suitable for numerical computation of any order of accuracy. One is thereby able to answer principal questions as to intensity and polarization of continuous x-radiation. The assumptions of an infinitely thin target, negligible retardation and relativity, and a pure Coulomb field as seen by the incident electron during emission, are made. Comparison with the absolute intensity measurement of Smick and Kirkpatrick[2] was good only as to order of magnitude, the disagreement being by a factor of 2.8. The agreement with the relative intensity measurements of Harworth and Kirkpatrick[2] is completely satisfactory.

[1] Ann. d. Physik **11**, 257 (1931).
[2] Phys. Rev. **60**, 162–163 (1941).

13. The Value of the Faraday. RAYMOND T. BIRGE, *University of California.*—The best voltameter value of the Faraday F appears to be $96{,}488 \pm 10$ abs. coul. (chemical scale), but many persons distrust this result, because of the numerous sources of systematic error (known and unknown) inherent in all voltameter work. One may, however, obtain a number of values of F, completely independent of voltameter work, since certain $f(e, m, h)$ involve F, and others do not. A systematic treatment of all such data now leads to new weighted average values of F ranging from 96,502 to 96,516, depending on the weightings adopted. The probable error of the weighted average, in each case, is approximately 12 coulombs. An assumed value $F = 96{,}516$ abs. coul. almost completely eliminates the present small discrepancies between certain types of determination of e/m, and leads to $1.7595_6 \pm 0.0001_6$ as the new weighted average. It raises e only from 4.8025 to 4.8039 ($\times 10^{-10}$), with no change in the probable error of ± 0.001 (see Abstract No. 21). This new evidence thus shows that the present voltameter value of F is unlikely to be in error by more than 30 coulombs, although an increase in value of roughly this amount would significantly improve the consistency of certain $f(e, m, h)$.

14. Regulated Voltage Supplies. L. MARTON, *Stanford University.*—The requirements for constancy of voltage supplies of magnetic electron microscopes are very high (1 part in 10,000 or better). These requirements have been satisfied up to now either (1) by the use of large capacitors on the high voltage side, (2) by the use of special power supplies for the primary (motor generators or saturated core regulators), and (3) by regulated circuits operating on the feedback principle. In principle a regulation of the power supply can be avoided by sending the electron beam through a very stable magnetic analyzer (monochromator) and using the exit aperture as a new source of electrons. Experience shows however that secondary effects (variable charges on different parts of the microscope, etc.) may prevent stable operation, if the beam current is varying too much. Such effects can be avoided by using non-regulated power supplies for the acceleration of the electrons to almost the full value of their speed and adding a last stage of acceleration compensating the fluctuations of the previous stages. Such a last stage can be made, for instance, by sending the accelerated beam itself through a magnetic analyzer and using the deviations from a pre-set value to operate the last stage through an amplifier.

15. Non-Laue Reflections from Various Crystals. DONALD S. TEAGUE, *Stanford University.* (*Introduced by Paul Kirkpatrick.*)—With a photographic spectrometer attempts were made to observe reflections of molybdenum K radiation at incidence angles near but not identical to the Bragg angles (modified reflection, diffuse reflection), using crystals of iron, zinc blende, barite, calcite, Rochelle salt, and quartz. The order given is one of increasing crystal perfection. As crystal perfection increased, the range of angles of incidence over which line reflection could be observed decreased steadily from several degrees to about two

minutes. With the most imperfect crystals, iron and zinc blende, no evidence of inconstancy in the angle of deviation of a monochromatic reflection was observed. With barite, calcite and Rochelle salt the inconstancy was readily observed, while with quartz, the most perfect crystal used, the usable range of angles of incidence was so short as to prevent observation of the shift, if it existed. In all observed cases, this shift was in the sense required by the theory of diffuse scattering,[1] and had magnitudes in agreement with the theory or somewhat higher.

[1] S. Siegel and W. H. Zachariasen, Phys. Rev. **57**, 795 (1940).

16. Quantization of the Wave Field for Particles with Spin 3/2. S. KUSAKA AND J. WEINBERG, *University of California.*—Using the formulation of the theory of particles with spin 3/2 developed by Rarita and Schwinger,[1] we have quantized the wave field in the presence of static external electromagnetic field. The quantization was carried out according to Fermi-Dirac statistics by the method of Snyder and Weinberg,[2] i.e., by demanding that the occupation numbers of the normal modes of the wave field have eigenvalues 0 and 1. It is shown that the commutator of the wave field and its canonical conjugate, taken at the same time, is equal to the projection operator which restricts the wave field to a function satisfying the supplementary conditions. This projection operator has been calculated and found to be a point operator containing the delta function and its first and second derivatives, and to be a gauge invariant function of the electromagnetic field. It follows from this that the charge densities at two points outside each others' light-cone commute. The problem for spin 2 and the general theory for higher spins are now being investigated.

[1] W. Rarita and J. Schwinger, Phys. Rev. **60**, 61 (1941).
[2] H. Snyder and J. Weinberg, Phys. Rev. **57**, 307 (1940).

17. Applications of the Multiharmonograph to the Graphical Solution of Physical and Mathematical Equations. S. LEROY BROWN, *The University of Texas.*—A multiharmonograph with thirty harmonic elements has been found to have a great variety of applications ranging from simple synthesis and harmonic analysis to the graphing of Legendre polynomials and the solution of thirtieth-degree equations. The machine is essentially a synthesizer with fifteen sine components and fifteen cosine components, but so arranged that either the sum of all the components may be plotted against the angle or one set of components may be plotted at right angles to the other set. In addition, the epoch angle of each component is adjustable as well as its amplitude. In general, the function to be graphed or equation to be solved is transformed into a harmonic form by trigonometric substitution, DeMoivre's theorem, or expansion into a power series and then transformed to the harmonic form. The machine has practical application to harmonic synthesis, harmonic analysis, determination of the real and complex roots of polynomials, representation of polar equations, solution of certain types of non-linear simultaneous equations, solution of transcendental functions, graphing of Legendre's polynomials (and associated Legendre's functions), and the graphing of certain types of trigonometric equations encountered in the determination of parameters in crystal structure.

18. Negative Point-to-Plane Corona in Air. GILBERT G. HUDSON, *Department of Physics, University of California.*—The regular relaxation oscillator-like pulses observed by Trichel[1] in room air could not be obtained with clean, smooth points until the discharge had been run for thirty minutes or so. Microscopic examination of the point showed that a few dust specks (about 0.01 mm diameter) had been collected near the tip. A clean point dusted with MgO powder was then found to give regular pulses at once. Even in dry air, where the irregular pulses were first observed, the Trichel pulses were produced for the short time during which the specks remained on the point. The electrons emitted from these particles by a process such as the Paetow[2] effect initiate a new pulse as soon as the inhibiting negative ions have been swept out of the region near the point. These triggering electrons thus insure the periodicity of the pulses. Pitting of the Pt point was observed, and the formation of oxide deposits by the discharge was also indicated. A pre-onset discharge was seen to take place from larger oxide particles favorably located near the tip.

[1] G. W. Trichel, Phys. Rev. **54**, 1078 (1938).
[2] H. Paetow, Zeits. f. Physik **111**, 770 (1939). See also L. B. Loeb, *Fundamental Processes of Electrical Discharge*, p. 498.

19. Properties of Coronas in Pure and Impure H_2, N_2 and A. GERHARD L. WEISSLER, *University of California.*—Studies were made on very pure Hg free electron free gases H_2 and N_2, and on A which differs from these by having metastable states. Streamer formation requires adequate photo-ionization. Either burst pulses in positive corona or Trichel pulses in negative corona require respectively heavy positive and negative space charges. In H_2, N_2 and A negative ions cannot form and negative Trichel pulses are not observed. Photo-ionization is weak in N_2 and H_2 and streamer formation occurs only at higher fields; burst pulses are not observed. Pure argon shows no corona but gives sparks on positive and arcs on negative points, owing to intense photo-ionization of metastables. Addition of N_2 or H_2 destroying metastables permits streamers and burst pulses to form on the positive point. It changes the arc to a corona on the negative point but gives no Trichel pulses. Less than 0.1 percent O_2 in all gases restores Trichel pulses, preonset and onset streamers and burst pulses. Clean-up by negative corona discovered by W. H. Bennett[1] is shown to be caused by formation and adsorption of water vapor. The etching of points reported by W. H. Bennett occurs in pure gases and appears to be some sort of a sputtering process.

[1] W. H. Bennett, Phys. Rev. **58**, 992 (1940)

20. Regulated Power Supplies. L. MARTON AND R. G. E. HUTTER, *Stanford University.*—For different branches of physics regulated power supplies are becoming more and more important. Many designs have been proposed in the last few years, some of them operated by means of negative

feedback.[1,2] By a mathematical analysis of such circuits the limitation of regulation (current or voltage-regulation) can be located to some elements of the circuit. As a result of such analysis a better design is proposed with very much improved constancy for normal line fluctuations and load variations. The improved circuit uses a single stage of negative feedback and a special voltage regulation in the screen grid circuit of the d.c. amplifier. The influence of the changes in input can be completely compensated for any arbitrary setting of the output. The experiments show excellent agreement with the calculations.

[1] H. S. Black, Bell Sys. Tech. J. **13**, 1 (1934).
[2] A. W. Vance, RCA Rev. **5**, 293 (1941).

21. The Value of the Electronic Charge. RAYMOND T. BIRGE, *University of California.*—(1) The present best weighted average for the viscosity of air is $\eta_{23}=(1832.5\pm1.0)\times10^{-7}$. This value, combined with a weighted average of all oil-drop work, gives $e=(4.8117\pm0.0057)\times10^{-10}$. (2) From the properties of calcite and grating wave-lengths of x-rays, $N_0=(6.0228_3\pm0.0011)\times10^{23}$, and $e=F/N_0=4.8025\pm0.0010$. (3) The possibility of large unsuspected errors in the adopted voltameter value of F seems to be excluded by the results of Abstract No. 13. The new *independent* values of F give $e=4.8034$ to 4.8039, with a probable error of ±0.0011. (4) From a least squares solution of *all* $f(e, m, h)$ *not* involving F, one obtains $e=4.80376$ to 4.80386, according to the weighting, with a probable error of ±0.002. Since this last evaluation is completely independent of the properties of calcite, as well as of F, it appears to eliminate the possibility of any significant error in e due to imperfect crystal structure of calcite, in agreement with DuMond and Bollman's 1936 results. A probable error of ±0.002, applied to some value of e between 4.8025 and 4.8035, should thus represent adequate allowance for these suggested sources of systematic error.

22. Production of Mesotrons, "Stars," Cascade Showers Produced by Penetrating Rays, Slow Protons, Evidence for the Disintegration Electron. WILSON M. POWELL,* *Kenyon College, Gambier, Ohio.*—In 2512 cloud-chamber photographs made at random at 14,125 feet there appear 1,085 particles that penetrate 2 cm or more of lead without producing secondaries. There are 458 particles that show heavy ionization, 35 protons that stop in the chamber, 19 mesotrons stopping in the chamber, 10 of which show an accompanying track that can be interpreted as the disintegration electron. Nine particles in addition give questionable evidence of being mesotrons with accompanying disintegration electrons. Six particles might be interpreted as protons. Three showers appear to be produced by heavy particles. Two mesotrons are produced in the chamber. Ninety-seven showers of more than 6 particles appear.

* Guggenheim Fellow at the University of California.